Technical Letter Report

TLR-RES/DE/REB-2021-14-R1

Probabilistic Leak-Before-Break Evaluations of Pressurized-Water Reactor Piping Systems using the Extremely Low Probability of Rupture Code

Date:

April 2022

Prepared in response to Task 4 of User Need Request NRR-2014-004, by:

C. J. Sallaberry
Engineering Mechanics Corporation of Columbus

R. Kurth
Engineering Mechanics Corporation of Columbus

E. Kurth-Twombly
Engineering Mechanics Corporation of Columbus

F. W. Brust
Engineering Mechanics Corporation of Columbus

NRC Project Managers:

Matthew Homiack
Materials Engineer
Component Integrity Branch

Shah Malik
Sr. Materials Engineer
Component Integrity Branch

Division of Engineering
Office of Nuclear Regulatory Research
U.S. Nuclear Regulatory Commission
Washington, DC 20555–0001

DISCLAIMER

This report was prepared as an account of work sponsored by an agency of the U.S. Government. Neither the U.S. Government nor any agency thereof, nor any employee, makes any warranty, expressed or implied, or assumes any legal liability or responsibility for any third party's use, or the results of such use, of any information, apparatus, product, or process disclosed in this publication, or represents that its use by such third party complies with applicable law.

This report does not contain or imply legally binding requirements. Nor does this report establish or modify any regulatory guidance or positions of the U.S. Nuclear Regulatory Commission and is not binding on the Commission.

EXECUTIVE SUMMARY

This study used the Extremely Low Probability of Rupture (xLPR) probabilistic fracture mechanics code to demonstrate that pressurized-water reactor (PWR) piping systems previously approved for leak-before-break (LBB) continue to exhibit an extremely low probability of rupture consistent with the requirements of Title 10 of the *Code of Federal Regulations*, Part 50, Appendix A, General Design Criterion (GDC) 4, when subject to the effects of primary water stress-corrosion cracking (PWSCC). The U.S. Nuclear Regulatory Commission (NRC) Office of Nuclear Regulatory Research conducted this study at the request of the Office of Nuclear Reactor Regulation to complete the evaluation of such systems after initially demonstrating that a subset indeed continue to demonstrate an extremely low probability of rupture.

This study included an expanded scope of piping systems beyond the typical Westinghouse four-loop PWR designs considered in an initial study. All piping systems which have received prior LBB approvals from the NRC staff and which contain Alloy 82/182 dissimilar metal welds (DMWs) that are susceptible to PWSCC were binned for this study as follows:

- Westinghouse 4-loop reactor vessel inlet and outlet nozzle DMWs
- Westinghouse pressurizer surge line nozzle DMWs
- Combustion Engineering and Babcock and Wilcox reactor coolant pump nozzle DMWs
- Westinghouse steam generator nozzle DMWs
- Combustion Engineering hot leg branch line nozzle DMWs
- Combustion Engineering cold leg branch line nozzle DMWs
- Westinghouse two- and three-loop reactor vessel inlet and outlet nozzle DMWs

For each bin, a representative weld was analyzed using actual plant data when available and engineering judgement when not. Probability distributions were used to represent the material variability, inherent uncertainties associated with the weld residual stress (WRS) profiles, and other uncertainties. Deterministic inputs for the analyses of each bin were selected such that they would bound all inservice DMWs represented by the bin. Based on previous analytical experience, the highest normal operating loads, temperatures, and pressures were selected, along with the largest outer diameters and thinnest pipe wall thicknesses.

Several cases were used to analyze the piping in each bin. A base case included the effects of PWSCC initiation and growth for both circumferential and axial cracks with leak rate detection, inservice inspection, and safe shutdown earthquake events. These cases were used to estimate the base probabilities of rupture with a 1 gallon per minute leak rate detection capability. Since these probabilities were typically zero even with a large sample size, additional quantities of interest (QoIs), such as the time-dependent probabilities of first crack, first leak, and rupture both with and without a 10-year inspection frequency were also estimated. The base case was supplemented with a sensitivity study case where each realization begins with one axial and one circumferential crack at top dead center of the weld. As outlined in the prior study, the LBB ratio and LBB time lapse QoIs are not impacted by the crack initiation

models; therefore, estimates for these two QoIs were more accurately calculated using this approach. In addition, prior studies have highlighted the importance of WRS and the associated uncertainties. Thus, an additional sensitivity study case that considered a more severe WRS profile was also included for each bin. Other sensitivity studies were included to analyze the impacts of fatigue and mechanical mitigation, as appropriate.

The xLPR code analyzes the risks associated with a single weld; however, GDC 4 requires an aggregation of results at the system-level. Therefore, a piping system-level analysis was necessary to combine the individual bin results and estimate the total probability of rupture for the various PWR piping systems of interest. Consistent with the prior study, the probability of rupture with a 1 gallon per minute leak rate detection capability served as the QoI used to assess whether such piping systems demonstrate an extremely low probability of rupture consistent with the requirements of GDC 4. The estimated probabilities using this QoI were zero with exceptions studied and explained, so aggregation of the results at the system-level was also zero. The system-level results are thus below the acceptance criterion of 1×10^{-6} ruptures per reactor-year and, therefore, all the piping systems considered continue to meet the requirements of GDC 4.

To illustrate the contributions of the various welds at the system-level, estimates were prepared for the probabilities of first crack, first leak, and rupture with and without a 10-year inspection frequency for three representative piping systems that bound the various configurations in the operating PWRs. The representative piping systems were previously approved for LBB in Westinghouse four-loop PWRs, Westinghouse two- and three-loop PWRs, and CE and B&W PWRs. The aggregation method considered all the welds to be independent consistent with the prior study. The largest contributing components were shown to vary depending on the QoI under consideration.

Successful application of the xLPR code in this study to demonstrate that the rupture probabilities of PWR piping systems that contain DMWs and were previously approved for LBB remain extremely low when subject to PWSCC reinforces the role of probabilistic fracture mechanics in making the demonstrations required by GDC 4 as originally envisioned by the Commission. Accordingly, the Office of Nuclear Regulatory Research recommends no changes to the GDC 4 regulations. Additionally, in the absence of a strong industry interest in future LBB applications, the Office of Nuclear Regulatory Research recommends no changes to NUREG-0800, “Standard Review Plan for the Review of Safety Analysis Reports for Nuclear Power Plants: LWR Edition,” Section 3.6.3, “Leak-Before-Break Evaluation Procedures,” Revision 1, issued March 2007, to support probabilistic LBB applications. Should a demand for probabilistic LBB guidance arise in the future, an expansion of the deterministic review procedures may be pursued based on the results of this study.

Revision 1 of the report clarifies in Sections 2.2.3 and 2.2.4 that the LBB time lapse and LBB ratio QoIs calculate rupture based on the combined normal operating and non-probabilistically treated seismic loads. The threshold values for these QoIs where ruptures are precluded under certain conditions have also been included. In addition, Revision 1 includes updated analyses for the Westinghouse steam generator nozzle DMWs. Specifically, the DMW configurations

with no mechanical mitigation and with overlays for PWSCC mitigation were re-analyzed using updated WRS and other inputs that more accurately represent conditions in the PWR fleet. Sections 3.5.4 and 3.5.5 document the updated inputs and results. Because the updated results had potential ruptures before leak rate detection under combined normal operating and non-probabilistically treated seismic loads, supplemental analyses were conducted to estimate the probabilities of rupture with leak rate detection and probabilistically treated seismic events. The results, which are summarized in newly added Sections 3.5.4.2.6 and 3.5.5.2.6, indicate that seismic events are not a significant contributor to the probabilities of rupture in these cases. The report's prior conclusions and recommendations were not impacted by any of the updated analysis results.

ACKNOWLEDGEMENTS

This study was facilitated in part through a collaborative effort between the NRC Office of Nuclear Regulatory Research and the Electric Power Research Institute (EPRI) under an addendum to their Memorandum of Understanding on cooperative nuclear safety research. The authors benefited from the experience, knowledge, and work of many individuals supporting both organizations. The authors would particularly like to thank Mr. Matthew Homiack of the NRC staff and Dr. Craig Harrington of EPRI for their guidance in leading these efforts. The authors also thank Mr. Markus Burkardt of Dominion Engineering, Inc. as he was a major force in gathering input data and reviewing various documents. All the fruitful discussions and exchanges with him over the course of the project were much appreciated. The authors also thank Nathan Glunt of EPRI for his valuable assistance in developing specific inputs using his experience and knowledge. The authors would also like to thank Mr. Bruce Bishop from Phoenix Engineering Associates, Inc., who was a constant and reliable source of historical information on both deterministic and probabilistic approaches and associated rationales. He reviewed most of the analyses performed and his insights led to many improvements. Finally, the authors wish to thank John Broussard of Dominion Engineering, Inc. for his help in identifying key information for some of the welds of interest so that the associated weld residual stress profiles could be developed.

TABLE OF CONTENTS

LIST OF TABLES

LIST OF FIGURES

ACRONYMS

cc	cubic centimeters
CDF	cumulative distribution function
CE	Combustion Engineering
CFR	*Code of Federal Regulations*
COV	coefficient of variation
DM1	Direct Model 1
DMW	dissimilar metal weld
DW	deadweight
EFPY	effective full-power years
EPRI	Electric Power Research Institute
FOI	factor of improvement
GDC	general design criterion
gpm	gallons per minute
ID	inner diameter
ISI	in-service inspection
kg	kilogram
LBB	leak-before-break
LHS	Latin hypercube sampling
mon	month
MPa	megapascal
MSIP®	Mechanical Stress Improvement Process®
NLKH	non-linear kinematic hardening
NRC	Nuclear Regulatory Commission
PDI	Performance Demonstration Initiative
PFM	probabilistic fracture mechanics
POD	probability of detection
PWHT	post-weld heat treatment
PWR	pressurized-water reactor
PWSCC	primary water stress-corrosion cracking
RCP	reactor coolant pump
RVIN	reactor vessel inlet nozzle
RVON	reactor vessel outlet nozzle
SRP	standard review plan
SS	stainless steel
SSE	safe shutdown earthquake
TWC	through-wall crack
WRS	weld residual stress
xLPR	Extremely Low Probability of Rupture

1 INTRODUCTION

1.1 Summary of Prior Probabilistic LBB Study

NUREG-2247, "Extremely Low Probability of Rupture Version 2 Probabilistic Fracture Mechanics Code," issued August 2021 [1], describes the Extremely Low Probability of Rupture (xLPR) code. In a prior study, as documented in U.S. Nuclear Regulatory Commission (NRC) Technical Letter Report, TLR-RES/DE/REB-2021-09, "Probabilistic Leak-Before-Break Evaluation of Westinghouse Four-Loop Pressurized-Water Reactor Primary Coolant Loop Piping using the Extremely Low Probability of Rupture Code," issued August 13, 2021 [2], the xLPR code was used to demonstrate that a selected pressurized-water reactor (PWR) piping system exhibits an extremely low probability of rupture consistent with the requirements of Title 10 of the *Code of Federal Regulations* (10 CFR), Part 50, Appendix A, General Design Criterion (GDC) 4 [3], when subject to the effects of primary water stress-corrosion cracking (PWSCC). The piping system selected for that study was the primary or main loop piping in a Westinghouse four-loop PWR design. This configuration was selected because it is the predominant piping system for which the NRC staff has granted prior leak-before-break (LBB) approvals. This design also has multiple dissimilar metal welds (DMWs), which supported the second objective of the study to combine the estimates from multiple welds to generate an annual, piping system-level failure frequency. Finally, most of the input data needed to analyze the piping system were already available and conveniently assembled in the required xLPR input set format.

The primary objectives of the prior study were twofold:

1. use the xLPR code to generate numerical failure frequency estimates with uncertainties for welds in a representative PWR piping system considering the effects of PWSCC, fatigue, leak rate detection, in-service inspection (ISI), mitigation, and seismic events
2. combine the estimates from multiple welds to generate an annual, piping system-level failure frequency to determine whether the requirements of GDC 4 were met

Several quantities of interest (QoIs) were defined and calculated in the prior study to support the desired safety conclusions. These metrics were the probabilities of rupture with leak rate detection, leak rate jump, LBB time lapse, and LBB ratio. The analyses for the reactor vessel outlet nozzle (RVON) and reactor vessel inlet nozzle (RVIN) DMWs included base cases and sensitivity study cases to investigate the effects of specific analysis parameters and assumptions.

Some important observations were made based on all the cases that were analyzed in the prior study. First, the probability of a rupture occurring before a leak is detected (i.e., a break-before-leak scenario) is extremely low and should not be an issue for either the RVON or RVIN welds considering the inputs used in the simulations. Also, the WRS profile and its uncertainty was found to be one of the most influential inputs. In addition, axial cracks only impacted the probability of first leak, but the predicted leak rates were so low that the associated cracks

would only be detected through ISI. Furthermore, the likelihood of having both an axial crack and a circumferential crack was so low that it did not affect the results. Therefore, it would be appropriate to exclude axial cracks under similar analysis conditions.

A system-level analysis was performed to aggregate the results from the multiple RVON and RVIN welds in the main loop piping. Only the results for the four RVON welds were combined, however, as the RVIN weld results were too low to have an impact. The approach considered each weld to be independent, which is reasonably conservative. Since the individual weld probabilities were low, the aggregated probabilities were only increased by roughly a factor four, which corresponds with the number of RVON welds in the system. Thus, the system-level results did not affect the conclusions drawn on an individual weld basis and remain below 1×10^{-6} ruptures per reactor-year consistent with the basis for the GDC 4 rulemaking. In conclusion, the prior study demonstrated that, for a typical primary loop piping system in a Westinghouse four-loop PWR, the probability of rupture with consideration of the active degradation mechanism PWSCC is extremely low consistent with the requirements of GDC 4.

1.2 Objectives of the Present Study

The present study builds on the results from the prior study by using the xLPR code to analyze the remaining PWR piping systems that contain DMWs and were previously approved for LBB to determine whether the rupture probabilities remain extremely low when subject to PWSCC as required by GDC 4. The primary objectives of the present study are the same as in the prior study. An additional objective of the present study is to assess NRC's regulatory framework with respect to LBB to determine if any changes are necessary.

As in the prior study, the following set of QoIs were considered:

- Rupture with Detection – This QoI directly estimates the occurrence of ruptures with consideration of a 1 gallon per minute (gpm) leak rate detection capability and ISI, if necessary. It is represented as a cumulative probability over the simulated period of plant operation.

- Leak Rate Jump – This QoI estimates the probability of a sudden jump in leakage from below a lower leak rate threshold value to above an upper leak rate threshold value from one simulation time step to the subsequent time step. The probabilistic result is expressed as a time-dependent probability over the simulated period of plant operation. It is based directly on the recommendations in the technical basis document on acceptance criteria [4].

- LBB Time Lapse – This QoI estimates the time between a detectable leak rate and a rupture. The probabilistic result is a cumulative distribution of the LBB time lapse over the simulated period of plant operation conditional on having cracks that both leak and rupture the pipe. It provides useful insights by capturing the time-dependent behavior of the system, which cannot be captured in a deterministic LBB analysis.

- LBB Ratio – This QoI estimates the ratio between the critical crack length at rupture and the length of a crack that results in detectable leakage. It is the probabilistic analog to

the deterministic LBB acceptance criterion from NUREG-0800, “Standard Review Plan for the Review of Safety Analysis Reports for Nuclear Power Plants: LWR Edition” (SRP), Section 3.6.3, “Leak-Before-Break Evaluation Procedures,” Revision 1, issued March 2007 [5]. The probabilistic result is a cumulative distribution of the LBB ratio over the simulated period of plant operation conditional on having cracks that both leak and rupture the pipe.

These QoIs are only impacted by circumferential cracks because: (a) the axial crack leak rates are too small to impact the leak rate jump event when multiple axial cracks are present, and (b) the remaining QoIs depend on ruptures, which are caused only by circumferential cracks. For some of the cases considered, the QoIs may be zero or not applicable (e.g., without leakage, the LBB time lapse and LBB ratio cannot be calculated). Thus, as in the prior study, the time-dependent probabilities of first crack, first leak, and rupture without leak rate detection and ISI were also analyzed for each case. These QoIs are the standard indicator outputs from the xLPR code.

2 ANALYSIS APPROACH

2.1 Piping Systems of Interest

The piping systems of interest in this study are ones that that contain Alloy 82/182 DMWs and were previously approved for LBB by the NRC staff. The scope includes the main coolant loop piping in most Westinghouse, Combustion Engineering (CE), and Babcock and Wilcox (B&W) PWRs. The scope also includes the pressurizer surge line piping in some Westinghouse and CE PWRs. Additionally, at one CE PWR, the scope also includes the high-pressure injection and shutdown coolant system branch line piping. For reference, Figure 2-1, Figure 2-2, and Figure 2-3 illustrate the typical reactor coolant system piping arrangements for Westinghouse, CE, and B&W PWRs, respectively.

Table 2-1 identifies the applicable operating PWRs, piping systems, and locations of the DMWs in each system. Although licensed to operate when this study was conducted, Diablo Canyon Nuclear Power Plant, Units 1 and 2, and Indian Point Nuclear Generating, Units 2 and 3 were not explicitly included because their owners had announced plans to cease operations. Some of the DMWs have been mechanically mitigated against PWSCC, and the table also identifies the type of mechanical mitigation, if applicable.

For the purposes of this study, the piping systems were organized into bins to optimize the number of analyses that were performed. The bins were determined primarily based on the plant designs, piping systems, and locations of the PWSCC-susceptible welds. The six bins were as follows:

1. Westinghouse four-loop reactor vessel inlet and outlet nozzle DMWs
2. Westinghouse pressurizer surge line piping to pressurizer nozzle DMWs
3. CE and B&W reactor coolant pump (RCP) inlet and outlet nozzle DMWs
4. Westinghouse steam generator nozzle DMWs
5. CE hot leg branch connection DMWs and CE high-pressure injection system DMWs
6. Westinghouse two- and three-loop reactor vessel inlet and outlet nozzle DMWs

Some of the unique aspects of each bin are as follows:

- Although Westinghouse four-loop reactor vessel outlet nozzle (RVON) DMWs were included in the prior study, new reference cases were developed for the present study in Bin 1. The new reference cases are largely based on Case 1.1.6 from the prior study, but with the inclusion of axial cracks and a bounding value for the hydrogen concentration in the reactor coolant for consistency with cases defined for the other bins. These settings were determined to be the most appropriate based on the sensitivity study results from the prior study.

- No welding residual stress (WRS) profiles had previously been developed for Bin 2. In addition, the operating temperatures are higher, and the diameters and thicknesses are smaller as compared to the Westinghouse RVON DMWs. Further, all the welds have been subject to mechanical mitigation, thus requiring more cases to cover the different sensitivities.
- Bin 3 has a relatively low WRS value at the inside diameter, so even with uncertainty in the WRS profile, the values are comparable to the normal operating stresses and thus the probabilities of crack initiation and rupture were expected to be quite low.
- The welds in Bin 4 all have a double-vee groove configuration, which has a significantly different WRS profile that needed to be developed.
- Bin 5 has smaller diameters and higher operating temperatures as compared to the Westinghouse RVON DMWs. It also includes auxiliary lines not previously studied. The second set of Bin 5 cases operate at cold leg temperatures; therefore, a substantially lower rupture frequency as compared to components that operate at hot leg temperatures was expected based on the results from the prior study.
- The welds in Bin 6 grouped RVONs in Westinghouse 2-loop and 3-loop PWRs because Westinghouse 4-loop PWRs were the focus of the prior study. These systems are like the previously studied Westinghouse four-loop systems, so no significant differences were expected.

As PWSCC is the primary degradation mechanism of interest, only the Alloy 82/182 DMWs were analyzed.

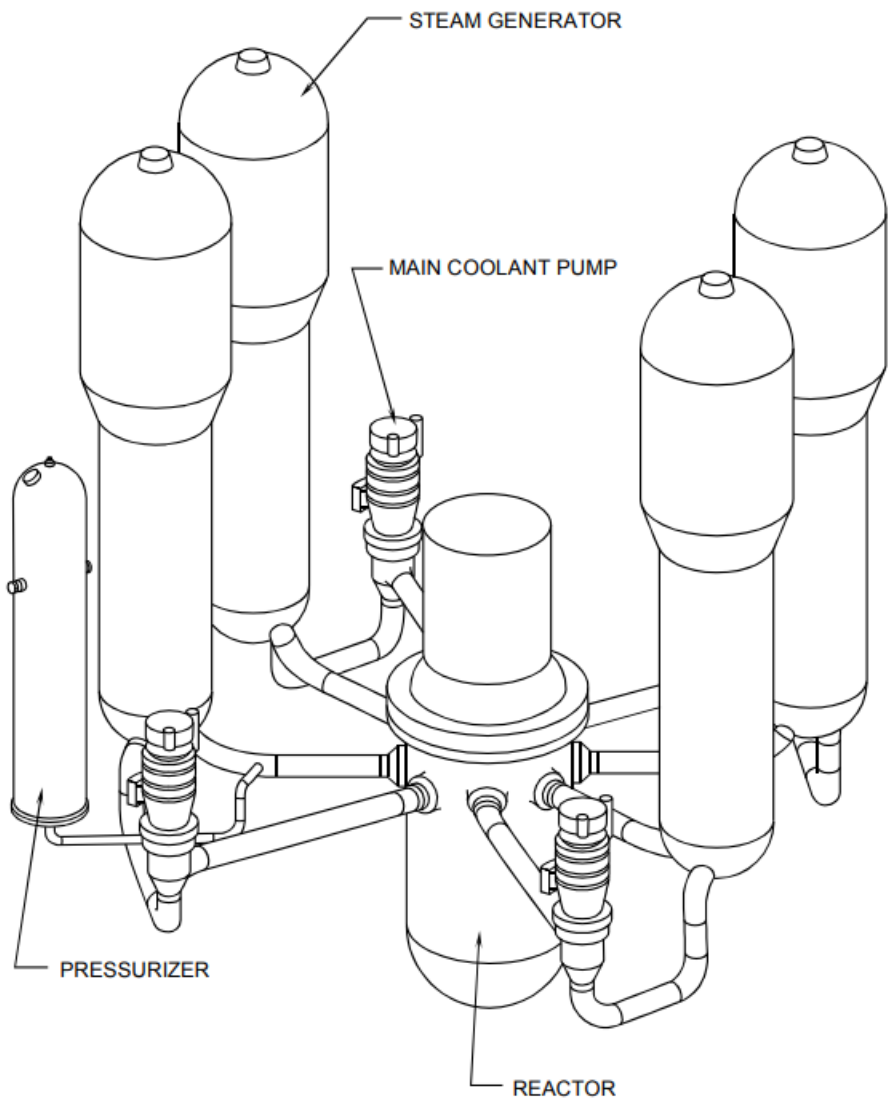

Figure 2-1 Typical Westinghouse four-loop PWR nuclear steam supply system piping arrangement

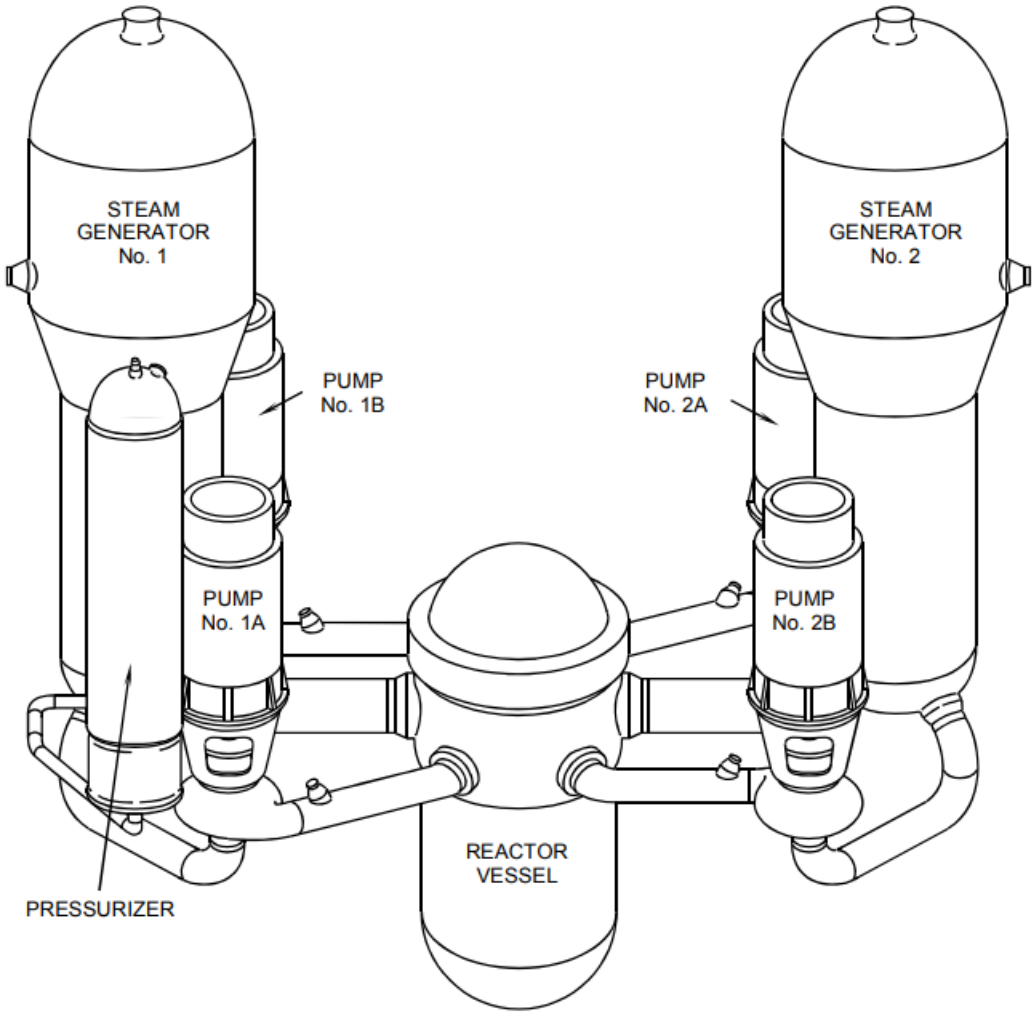

Figure 2-2 Typical CE PWR nuclear steam supply system piping arrangement

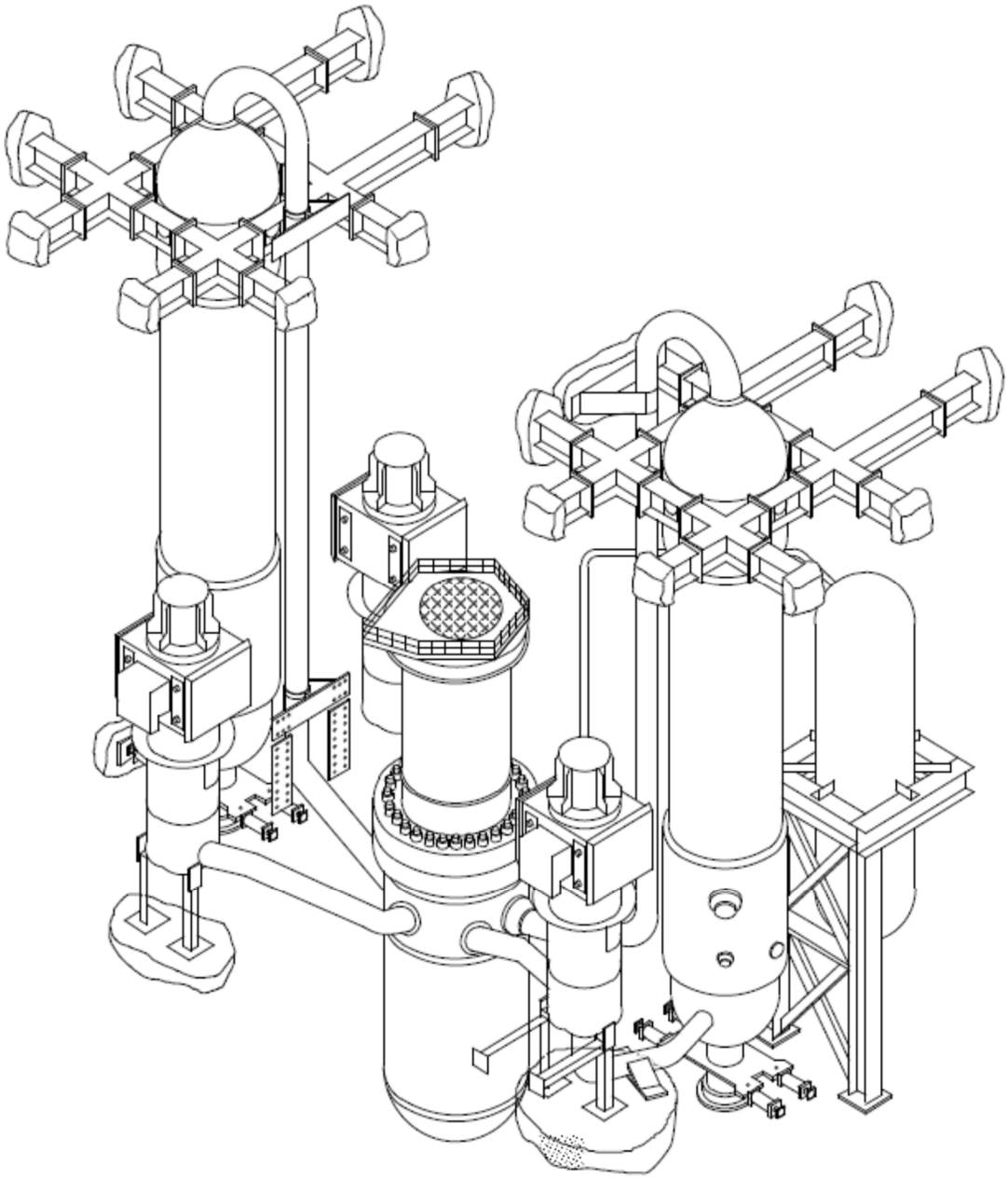

Figure 2-3 Typical B&W PWR nuclear steam supply system piping arrangement

Table 2-1 Scope of piping systems analyzed

Plant	Design	Piping System(s) Approved for LBB	Location of Welds Susceptible to PWSCC	Mechanical Mitigation
Arkansas Nuclear One, Unit 1	B&W	Reactor Coolant Piping [6]	RCP Inlet and Outlet Nozzles	None
Arkansas Nuclear One, Unit 2	CE	Reactor Coolant Piping [7]	RCP Inlet and Outlet Nozzles	None
Beaver Valley, Unit 2	Westinghouse 3-loop	Hot and Cold Legs [8], Pressurizer Surge Line [9]	RVONs, RVINs, and Pressurizer Surge Line Nozzle	None for the RVON and RVIN DMWs; Overlay for the Pressurizer Surge Line Nozzle DMW
Braidwood, Units 1 and 2	Westinghouse 4-loop	Hot and Cold Legs [10]	RVONs and RVINs	MSIP®
Byron, Units 1 and 2	Westinghouse 4-loop	Hot and Cold Legs [10]	RVONs and RVINs	MSIP®
Callaway, Unit 1	Westinghouse 4-loop	Hot and Cold Legs [11]	RVONs and RVINs	None*
Calvert Cliffs, Units 1 and 2	CE	Reactor Coolant Piping [7]	RCP Inlet and Outlet Nozzles	None
Catawba, Unit 2	Westinghouse 4-loop	Hot and Cold Legs [12]	RVONs and RVINs	None
Comanche Peak, Units 1 and 2	Westinghouse 4-loop	Hot and Cold Legs [13], Pressurizer Surge Line [14], [15]	RVONs, RVINs, and Pressurizer Surge Line Nozzle	None for the RVON and RVIN DMWs; Overlay for the Pressurizer Surge Line Nozzle DMWs

* The Callaway, Unit 1 RVON and RVIN DMWs have been peened, but the impacts of peening were not considered in this study.

Plant	Design	Piping System(s) Approved for LBB	Location of Welds Susceptible to PWSCC	Mechanical Mitigation
D.C. Cook, Units 1 and 2	Westinghouse 4-loop	Hot and Cold Legs [16], Pressurizer Surge Line [17]	RVONs, RVINs, and Pressurizer Surge Line Nozzle	MSIP® for the Unit 1 RVON and RVIN DMWs; None for the Unit 2 RVON and RVIN DMWs; Overlay for the Units 1 and 2 Pressurizer Surge Line Nozzle DMWs
Davis-Besse, Unit 1	B&W	Reactor Coolant Piping [6]	RCP Inlet and Outlet Nozzles	Overlay
Farley, Units 1 and 2	Westinghouse 3-loop	Hot and Cold Legs [18], Pressurizer Surge Line [19]	RVONs, RVINs, and Pressurizer Surge Line Nozzle	None for the RVON and RVIN DMWs; Overlay for the Pressurizer Surge Line Nozzle DMWs
McGuire, Unit 1	Westinghouse 4-loop	Hot and Cold Legs [20]	RVONs and RVINs	None
Millstone, Unit 2	CE	Reactor Coolant Piping [7], Pressurizer Surge Line [21], Shutdown Cooling Line [22], Safety Injection Line [23]	RCP Inlet and Outlet Nozzles, Hot Leg Surge Line Nozzle, Hot Leg Shutdown Cooling Nozzle, Cold Leg High Pressure Injection Nozzle	None for the RCP Inlet and Outlet Nozzle DMWs; Overlay for the Hot Leg Surge Line Nozzle, Hot Leg Shutdown Cooling Nozzle, and Cold Leg High Pressure Injection Nozzle DMWs
Millstone, Unit 3	Westinghouse 4-loop	Hot and Cold Legs [24]	RVONs and RVINs	None

Plant	Design	Piping System(s) Approved for LBB	Location of Welds Susceptible to PWSCC	Mechanical Mitigation
North Anna, Units 1 and 2	Westinghouse 3-loop	Hot and Cold Legs [25]	Steam Generator Inlet and Outlet Nozzles	Overlay for Unit 1 Steam Generator Inlet Nozzle DMWs; None for Unit 1 Stem Generator Outlet Nozzle DMWs; Inlay for Unit 2 Steam Generator Inlet and Outlet Nozzle DMWs
Oconee, Units 1, 2, and 3	B&W	Reactor Coolant Piping [6]	RCP Inlet and Outlet Nozzles	None
Palisades	CE	Reactor Coolant Piping [7]	RCP Inlet and Outlet Nozzles	None
Point Beach, Units 1 and 2	Westinghouse 2-loop	Hot and Cold Legs [26], Pressurizer Surge Line [27]	Steam Generator Inlet and Outlet Nozzles	Inlay for Steam Generator Inlet and Outlet Nozzle DMWs
Prairie Island Units 1 and 2	Westinghouse 2-loop	Hot and Cold Legs [28], Pressurizer Surge Line [29]	Pressurizer Surge Line Nozzle	Overlay
Robinson, Unit 2	Westinghouse 3-loop	Hot and Cold Legs [30]	RVONs and RVINs	None
Salem, Units 1 and 2	Westinghouse 4-loop	Hot and Cold Legs [31]	RVONs and RVINs	MSIP® for Unit 1 RVON and RVIN DMWs; MSIP® for Unit 2 RVON DMWs; None for Unit 2 RVIN DMWs
Seabrook, Unit 1	Westinghouse 4-loop	Hot and Cold Legs [32]	RVONs and RVINs	MSIP®
Sequoyah, Units 1 and 2	Westinghouse 4-loop	Hot and Cold Legs [33], Pressurizer Surge Line [34]	Pressurizer Surge Line Nozzle	Overlay

Plant	Design	Piping System(s) Approved for LBB	Location of Welds Susceptible to PWSCC	Mechanical Mitigation
Shearon Harris, Unit 1	Westinghouse 3-loop	Hot and Cold Legs [35]	RVONs and RVINs	MSIP® for RVON DMWs; None for RVIN DMWs
South Texas, Units 1 and 2	Westinghouse 4-loop	Hot and Cold Legs [36], Pressurizer Surge Line [37], [38]	RVONs, RVINs, and Pressurizer Surge Line Nozzle	MSIP® for Unit 1 RVON and RVIN DMWs; None for Unit 2 RVON and RVIN DMWs; Overlay for Units 1 and 2 Pressurizer Surge Line Nozzle DMWs
St. Lucie, Units 1 and 2	CE	Reactor Coolant Piping [7]	RCP Inlet and Outlet Nozzles	None
V.C. Summer, Unit 1	Westinghouse 3-loop	Hot and Cold Legs [39], [40]	RVONs, RVINs, and Steam Generator Inlet and Outlet Nozzles	None for the Hot Leg “A” RVON DMW, which was Replaced with Alloy 52; MSIP® for the Hot Leg “B” and “C” RVON DMWs; None for RVIN DMWs; Inlay for Steam Generator Inlet and Outlet Nozzle DMWs
Vogtle, Units 1 and 2	Westinghouse 4-loop	Hot and Cold Legs [41], Pressurizer Surge Line [42]	RVONs, RVINs, and Pressurizer Surge Line Nozzle	MSIP® for Units 1 and 2 RVON DMWs; None for Units 1 and 2 RVIN DMWs; Overlay for Units 1 and 2 Pressurizer Surge Line Nozzle DMWs

Plant	Design	Piping System(s) Approved for LBB	Location of Welds Susceptible to PWSCC	Mechanical Mitigation
Waterford, Unit 3	CE	Reactor Coolant Piping [7], Pressurizer Surge Line [43]	RCP Inlet and Outlet Nozzles, Pressurizer Surge Line Nozzle, and Hot Leg Surge Line Nozzle	None for the RCP Inlet and Outlet Nozzle DMWs; Overlay for the Pressurizer Surge Line Nozzle and Hot Leg Surge Line Nozzle DMWs
Watts Bar, Units 1 and 2	Westinghouse 4-loop	Hot and Cold Legs [44], Pressurizer Surge Line [45]	RVONs, RVINs, and Pressurizer Surge Line Nozzle	MSIP®
Wolf Creek, Unit 1	Westinghouse 4-loop	Hot and Cold Legs [11]	RVONs and RVINs	None*

2.2 Quantities of Interest

The QoIs considered in this study were selected on the basis that they could provide information to a decisionmaker to determine whether a piping system has an extremely low probability of rupture consistent with the requirements of GDC 4. The evaluation period for all the QoIs was 80 effective full-power years (EFPY) to bound plant operation as would be authorized by an original 40-year operating license and up to two renewed operating licenses. The 80-EFPY evaluation period assumes a plant capacity factor of 100 percent throughout the entire period of licensed operation. Thus, as presented in this report, 80 EFPY is equivalent to 80 calendar years of operation. This assumption is conservative as it subjects the piping components to the most amount of degradation in a simulation.

Sections 2.2.1 through 2.2.4 describe the primary QoIs in detail (i.e., probability of rupture with detection, leak rate jump, LBB time lapse, and LBB ratio). Two leak rate detection capabilities were considered in this study for the LBB time lapse and LBB ratio calculations: 1 and 10 gpm. The latter was chosen because many licensees had demonstrated a 1 gpm leak rate detection capability for approval of their original, deterministic LBB analyses. However, per SRP Section 3.6.3, a safety factor of 10 was applied, which results the 10 gpm value. This safety factor was meant to address many of the uncertainties that the xLPR code addresses directly; therefore, the former 1 gpm leak rate detection capability was also examined. The other QoIs considered included the probabilities of first crack, first leak, and rupture without detection.

* The Wolf Creek, Unit 1 RVON and RVIN DMWs have been peened, but the impacts of peening were not considered in this study.

These QoIs were considered for informational purposes to support the general LBB concept, and because they can be more useful when analyzing results from sensitivity studies.

2.2.1 Probability of Rupture with Detection

The probability of rupture is one of the standard xLPR indicator results. With consideration of the offsetting effects of leak rate detection, it was used in this study as the decisionmaking QoI for probabilistic LBB assessment because it directly addresses the language in GDC 4 (i.e., "demonstrate that … piping rupture is extremely low"). The probability of rupture with leak rate detection is the average of an indicator function that takes on: (a) a value of zero for each realization without rupture and for each realization that had a leak rate greater than the leak rate detection threshold before rupture, and (b) a value of one for each realization that ruptured before the leak was detected. A 1 gpm leak rate detection capability was considered, and when the probability of rupture with leak rate detection was nonzero, the impact of a 10-year inspection frequency was also considered. The probabilistic result is expressed as a time-dependent probability of occurrence over the 80-EFPY evaluation period.

2.2.2 Leak Rate Jump

The leak rate jump and associated thresholds are based directly on the recommendations in the technical basis document on acceptance criteria [4]. It was considered as an informative QoI in this study because it estimates the probability of a sudden jump in leakage from below a lower threshold value (defined as 10 gpm) to above an upper threshold value (defined as 50 gpm) from one simulation time step to the subsequent time step (defined as 1 month). Several conservatisms are present in this approach as detailed in [4]. This QoI can be used to support probabilistic LBB assessment because a quickly increasing leak rate would indicate fast and potentially unstable crack growth that could lead to rupture or a loss of coolant accident. Ruptures are also counted in the leak rate jump results if they occur before the lower leak rate jump threshold is reached. An advantage of this QoI is that it accounts for the temporal aspects of the problem. As such, it provides greater insights as compared to deterministic LBB analyses prepared following the guidance in SRP Section 3.6.3, which does not account for such aspects. Additionally, as explained in [4], this QoI is tied to the NRC's risk-informed decisionmaking framework. The main factors that affect the leak rate jump are the crack growth rate and crack opening displacement. The probabilistic result is expressed as a time-dependent probability of occurrence over the 80-EFPY evaluation period.

2.2.3 LBB Time Lapse

The LBB time lapse estimates the time between a detectable leak rate under normal operating loads and a rupture under combined normal operating and non-probabilistically treated seismic loads. It was considered as an informative QoI in this study because, when a through-wall crack (TWC) is experiencing subcritical crack growth, the time between when the TWC is detected by a plant's leakage detection system and when the TWC becomes unstable and leads to rupture provides insights into the time-dependent behavior of the system. The main factors that affect the LBB time lapse are the crack growth rate and uncertainties in the leak rate models. The probabilistic result is a distribution of the LBB time lapse conditional on having

cracks that leak and a seismic event that ruptures the pipe. It is expressed as a cumulative distribution function (CDF) based on the 80-EFPY evaluation period. Because it assumes that the seismic loads are applied in every time step, an LBB time lapse greater than zero indicates that leak rate detection precludes seismic rupture. Additionally, since the combined normal operating and seismic loads are greater than the normal operating loads by themselves, rupture under normal operating loads is also precluded when the LBB time lapse is greater than zero.

2.2.4 LBB Ratio

The LBB ratio estimates the ratio between (a) the critical crack length at rupture under combined normal operating and non-probabilistically treated seismic loads, and (b) the length of a crack that results in detectable leakage under the normal operating loads. It was considered as an informative QoI in this study because it is the probabilistic analog to the current deterministic LBB acceptance criterion. In accordance with SRP Section 3.6.3, the deterministic LBB analysis should demonstrate that there is a margin of at least two between the leakage crack size and the critical crack size. The leakage crack size represents the size of the TWC under normal operating loads that will produce a leak rate 10 times greater than the reactor coolant system leak rate detection capability. The critical crack size represents the size of the crack at the onset of instability under normal operating plus safe shutdown earthquake (SSE) loads. Both 1 and 10 gpm leak rate detection capabilities were chosen to define the LBB ratio in this study, however. The main factors that affect the LBB ratio are the crack size, crack opening displacement, leak rate, and crack stability models. The probabilistic result is a distribution of the LBB ratio conditional on having cracks that leak and a seismic event that ruptures the pipe. It is expressed as a CDF based on the 80-EFPY evaluation period. Because it assumes that the seismic loads are applied in every time step, an LBB ratio greater than one indicates that leak rate detection precludes seismic rupture. Additionally, since the combined normal operating and seismic loads are greater than the normal operating loads by themselves, rupture under normal operating loads is also precluded when the LBB ratio is greater than one.

2.3 Statistical Approach

2.3.1 Sample Size

An annual failure frequency of less than 1 x 10^{-6} was used as the acceptance criterion in this study. Such a threshold is consistent with the basis for the GDC 4 rulemaking. Considering that the evaluation period is 80 EFPY consistent with the prior study, it was estimated that a sample size of 100,000 is necessary to guarantee that any undesirable event will not be missed in the analysis.

The probability of having at least one unwanted outcome, O (e.g., pipe rupture), with an annual frequency, λ, occurring over a period of τ years is shown as follows:

$$P(O_{\lambda,\tau} \geq 1) = 1 - e^{-\lambda\tau} \qquad \text{Equation 1}$$

Using Equation 1, the probability of an event with an annual frequency of 1 x 10^{-6} to occur over 80 EPFY is roughly $P\left(O_{10^{-6},80} \geq 1\right) = 8 \times 10^{-5}$. Further, a sample size of n for an event, E, with a probability of occurrence, p, leads to np expected events. The probability of not generating a single event (i.e., missing the likelihood of an event whose probability of occurrence is p) can be estimated as follows:

$$P(E = 0)_n = \binom{n}{0} p^0 (1-p)^{n-0} = (1-p)^n \qquad \text{Equation 2}$$

Then, let E_0 represent an event with an unwanted outcome of annual frequency $\lambda = 10^{-6}$ occurring over a period of $\tau = 80$ years. The expected number of E_0 events and probabilities of not generating any events for sample sizes of 10,000; 50,000; 70,000; and 100,000 are respectively as follows:

$$\overline{E_0}(n = 10K) = 0.8;\ P(E_0)_{10K} \cong 0.45\ (44.93\%)$$

$$\overline{E_0}(n = 50K) = 4;\ P(E_0)_{50K} \cong 0.018\ (1.83\%)$$

$$\overline{E_0}(n = 70K) = 5.6;\ P(E_0)_{70K} \cong 0.0037\ (0.37\%)$$

$$\overline{E_0}(n = 100K) = 8;\ P(E_0)_{100K} \cong 0.0003\ (0.03\%)$$

Considering these estimates, a sample size of 10,000 is not enough to confidently capture events with an annual frequency of 1 x 10^{-6}, and a sample size of at least 50,000 would be necessary to have a 98 percent confidence level (i.e., only a 2 percent error).

Alternatively, if some margin is desired over the annual frequency and, for instance, the sample size is expected to capture events with an annual frequency of 5 x 10^{-7}, then let E_1 represent an event with an unwanted outcome of annual frequency $\lambda = 10^{-7}$ occurring over a period of $\tau = 80$ years. The expected number of E_1 events and probabilities of not generating any events considering the same sample sizes as before are respectively as follows:

$$\overline{E_1}(n = 10K) = 0.4\ ;\ P(E_1)_{10K} \cong 0.67\ (67.03\%)$$

$$\overline{E_1}(n = 50K) = 2\ ;\ P(E_1)_{50K} \cong 0.14\ (13.53\%)$$

$$\overline{E_1}(n = 70K) = 2.8\ ;\ P(E_1)_{70K} \cong 0.06\ (6.08\%)$$

$$\overline{E_1}(n = 100K) = 4;\ P(E_1)_{100K} \cong 0.02\ (1.83\%)$$

Under these conditions, a sample size of 100,000 would be necessary to have a 98 percent confidence level. A traditional threshold in statistics is to use a 95 percent confidence level (i.e., only a 5 percent error). Accordingly, a sample size of 100,000 was determined to be the most appropriate for the desired level of accuracy in this study.

Furthermore, due to the age of the piping systems under consideration and the fact that most welds have not experienced any detectable PWSCC, it is possible that estimation of the annual

frequency will not be based on the entire 80-EFPY evaluation period, but rather on the final years of plant operation as a predictive frequency. Since mechanistically there are periods of time between crack initiation, leakage, and rupture, such a predictive frequency is expected to be higher than a frequency based on the entire 80-EFPY evaluation period.

With a shorter simulation time, a larger sample size is required to confirm that an event with an unwanted outcome and an annual frequency of 1 x 10^{-6} does not occur. Suppose, for instance, that E_2 represents an event with an unwanted outcome of annual frequency $\lambda = 10^{-6}$ occurring over a period of $\tau = 30$ years. The expected number of E_2 events and probabilities of not generating any events considering the same sample sizes as before are respectively as follows:

$$\overline{E_2}(n = 10K) = 0.3 \; ; P(E_2)_{10K} \cong 0.74 \; (74.08\%)$$

$$\overline{E_2}(n = 50K) = 1.5 \; ; \; P(E_2)_{50K} \cong 0.22 \; (22.31\%)$$

$$\overline{E_2}(n = 70K) = 2.1 \; ; \; P(E_2)_{70K} \cong 0.13 \; (12.25\%)$$

$$\overline{E_2}(n = 100K) = 3.0 \; ; P(E_2)_{100K} \cong 0.05 \; (4.98\%)$$

Under these conditions, any sample size below 100,000 would lead to a confidence level lower than 95 percent.

In conclusion, a sample size of 100,000 is appropriate to confidently demonstrate that events with unwanted outcomes have annual frequencies of occurrence lower than 1 x 10^{-6}. This sample size was used for all the simulations in this study that used Direct Model 1 for crack initiation. The adequacy of this PWSCC initiation model was demonstrated through the sensitivity studies performed in the prior study. A sample of size 5,000 was used for all simulations that used the initial flaw density option (i.e., pre-existing cracks) conditional on the assumption that the probability of having a circumferential crack occurring over the 80-EFPY evaluation period will be at most 0.05 (i.e., 5,000 occurrences of crack out of 100,000 samples).

2.3.2 Sampling Loop and Random Seed

As demonstrated in the prior study [2], using a single loop consisting entirely of either the aleatory (inner) or epistemic (outer) loop produced statistically equivalent results. As a result, 7 separate simulations with 15,000 realizations on the epistemic (outer) loop were generally used to produce a 105,000-realization composite simulation. Latin hypercube sampling (LHS) was used to take advantage of its denser stratification of each uncertain input distribution. A similar approach was used for the present study, except that the number of realizations was reduced to 10,000 and the number of replicate simulations was increased to 10. Such an approach produced 100,000-realization composite simulations when Direct Model 1 was used. A single, 5,000-realization simulation was used again for simulations that used the initial flaw density option.

The GoldSim® random number generator has been tested extensively, and these tests confirmed that the choice of random seeds does not affect the statistical results, even when

consecutive random seeds are selected. While only the epistemic (outer) loop was used, and the quasi-totality* of the uncertain parameters was set to epistemic, both the epistemic and aleatory random seeds were changed for each replicate simulation. The random seeds used in each simulation are recorded in Appendix B.

2.4 Computational Platforms and Simulation Execution Strategy

All the analyses were executed on the computational platforms described in Table 2-2. Nearly all the simulations used GoldSim Pro with its parallel processing capabilities to decrease code run times.

Table 2-2 Computational platforms

	Platform 1	Platform 2	Platform 3
Random-Access Memory	32 GB	32 GB	16GB
Central Processing Unit	Intel® Core™ i9-9920X @ 3.5GHz	Intel® Core™ i9-10920X @ 3.5GHz	Intel® Core™ i7-4790X @ 3.6GHz
Operating System	Microsoft Windows 10 Pro	Microsoft Windows 10 Pro	Microsoft Windows 10 Pro
Disk Drive	Solid State Drive	Solid State Drive	Hard Disk Drive
GoldSim License	GoldSim Pro	GoldSim Pro	GoldSim Pro
GoldSim Version	11.1.7	11.1.7	11.1.7

2.5 Project Team

This study was facilitated in part through a collaborative effort between the NRC's Office of Nuclear Regulatory Research and EPRI under an addendum to their general memorandum of understanding on cooperative nuclear safety research [46]. Separate NRC and EPRI analysis teams were formed, which included NRC staff, EPRI staff, and their contractors. Case definition and data collection activities necessary to gather sources for inputs were largely a cooperative effort. The teams were then left to independently complete the agreed upon scope of analyses. All results were shared between the teams, but their ultimate presentation and the conclusions drawn were strictly an independent exercise. This report presents the NRC team's results and conclusions.

* The xLPR code only supports an aleatory uncertainty type for the fatigue crack initiation model parameter C_o (Global ID 2528).

2.6 Necessary Code Corrections and Modifications

Several xLPR code problems were corrected and improvements were implemented for the prior study. In summary, these changes were as follows:

- Corrected a problem that led to double counting the pressure in the circumferential crack opening displacement calculations.
- Corrected a problem that led to double counting the pressure in the circumferential surface crack and circumferential TWC stability calculations.
- Extended the range of validity of the axial crack opening displacement module to provide more accurate calculations for low values of ρ, which represents the ratio between the half-crack length and the square root of the median radius multiplied by the thickness (i.e., $\rho = c/\sqrt{R_m \times t}$).
- Corrected a problem that affected the results conditional on ISI when a rupture occurred in the same time step as an inspection.
- Corrected a problem that affected the ISI results when the option to consider only the deepest surface crack was selected (Global ID 0820).

All these changes have been included in the version of the xLPR code used for the runs in the present study. The major version including all these changes was xLPR v2.0d, and the minor version was xLPR v2.0d_002. The minor version removes unused output results to reduce the final file size and includes additional outputs relevant to the present study. These version designations are specific to this study.

3 ANALYSES

3.1 Scope

The scope of analyses performed is summarized in the case matrix shown in Table 3-1. The bins and cases were selected and defined by the NRC and EPRI project teams. Appendix A summarizes the results for each case. The analysis inputs are listed in Appendix B. Sections 3.1.1 through 3.1.5 describe the cases selected for each bin. Sections 3.2 through 3.8 provide the results for each bin.

3.1.1 Bases Cases with PWSCC Initiation and Growth

A base case analysis was performed for all bins to assess the likelihood of failure due to PWSCC initiation and growth for both circumferential and axial cracks. The effects of leak detection, ISI, and SSE events were also assessed in these analyses.

3.1.2 Initial Flaw Sensitivity Study Cases

A sensitivity study was performed for all bins where, instead of Direct Model 1 for crack initiation, pre-existing flaws were assumed in both the axial and circumferential orientations and subject to PWSCC growth. These cases were included so that the impact of having a crack in the weld could be more accurately assessed from a larger number of realizations with cracks. Note that all these probabilities are conditional on having a crack at the beginning of the simulation, and they should not be interpreted without correction from a risk standpoint. The effects of leak rate detection, ISI, and seismic events were also assessed in these analyses. The LBB time lapse and LBB ratio QoIs are conditional on having a crack occurring and are not affected by crack initiation. As a result, it was expected that the resulting CDFs would be similar between the base case and the initial flaw sensitivity study case, with the latter providing a finer representation because of more realizations with ruptures.

3.1.3 More Severe WRS Sensitivity Study Cases

A sensitivity study was performed considering a more severe, yet plausible, WRS profile for Bins 2, 3, 4 and 5. The definition of severity was based on factors that would more likely lead to rupture using engineering judgement and operating experience. In all cases, to ensure plausibility, the more severe WRS profile was based on either another modeler's results for the same weld geometry or from another location in the weld (i.e., in the butter rather than the weld centerline). The WRS profiles used in for each bin are documented and summarized in Appendix C.

3.1.4 Mechanical Mitigation Sensitivity Study Cases

Sensitivity studies were performed applying mechanical mitigation for Bins 2 and 4. These analyses simulated the effects of overlays and the mechanical stress improvement process (MSIP®). Data on overlays applied to existing operating plants were assessed to determine an

average time of application and overlay thickness. MSIP® mitigation used the rules from the xLPR WRS Subgroup report [47] to develop a post-mitigation WRS profile, and the time of application was determined from the operating plant records. Additionally, a sensitivity study was performed for Bin 4 (i.e., for Westinghouse steam generator nozzle DMWs), where an inlay was applied in the first month of operation to represent DMWs in this bin that were placed into service with the inlay already applied. Finite element analysis (FEA) was performed to generate the WRS profile for this case as detailed in Appendix C.

3.1.5 Fatigue Sensitivity Study Cases

A sensitivity study was performed for Bin 2 to consider the impacts of fatigue crack initiation and growth. The pressurizer surge line experiences thermal stratification transients and insurge-outsurge transients that are not present in the primary coolant loop piping. Therefore, this analysis assessed the impact of these transients on the resulting probabilities. Fatigue sensitivity study cases were not included for the other bins based on the findings from the prior study.

Table 3-1 Summary of analysis cases

Weld Bin	Case No.	Report Section	Crack Orientations	Crack Initiation Method	Crack Growth Mechanism	Objective
Bin 1: Westinghouse 4-loop RVON and RVIN DMWs	1.1.6a and 1.1.6c	3.2.1	Circumferential and Axial	PWSCC (Direct Model 1)	PWSCC	Assess the base likelihood of failure caused by PWSCC initiation and growth without mechanical mitigation
	1.1.6b	3.2.2	Circumferential and Axial	Initial Flaw Density (1 Axial and 1 Circ. Crack)	PWSCC	Assess the base likelihood of failure with pre-existing flaws and subsequent PWSCC growth of circumferential and axial cracks without mechanical mitigation
Bin 2: Westinghouse Pressurizer Surge Line Nozzle DMWs	2.1.0	3.3.1	Circumferential and Axial	PWSCC (Direct Model 1)	PWSCC	Assess the base likelihood of failure caused by PWSCC initiation and growth without mechanical mitigation
	2.1.1	3.3.2	Circumferential and Axial	Initial Flaw Density (1 Axial and 1 Circ. Crack)	PWSCC	Assess the base likelihood of failure with pre-existing flaws and subsequent PWSCC growth of circumferential and axial cracks without mechanical mitigation
	2.1.2	3.3.3	Circumferential and Axial	PWSCC (Direct Model 1)	PWSCC	Sensitivity study of Case 2.1.0 considering a more severe WRS profile
	2.1.3	3.3.4	Circumferential and Axial	PWSCC (Direct Model 1)	PWSCC	Sensitivity study of Case 2.1.0 considering overlay mitigation
	2.1.4	3.3.5	Circumferential and Axial	PWSCC (Direct Model 1) & Fatigue	PWSCC & Fatigue	Assess the base likelihood of failure caused by fatigue initiation and growth without mechanical mitigation
	2.1.5	3.3.6	Circumferential and Axial	PWSCC (Direct Model 1)	PWSCC	Sensitivity study of Case 2.1.0 considering MSIP® mitigation

Weld Bin	Case No.	Report Section	Crack Orientations	Crack Initiation Method	Crack Growth Mechanism	Objective
Bin 3: CE and B&W RCP Nozzle DMWs	3.1.0	3.4.1	Circumferential and Axial	PWSCC (Direct Model 1)	PWSCC	Assess the base likelihood of failure caused by PWSCC initiation and growth without mechanical mitigation
	3.1.1	3.4.2	Circumferential and Axial	Initial Flaw Density (1 Axial and 1 Circ. Crack)	PWSCC	Assess the base likelihood of failure with pre-existing flaws and subsequent PWSCC growth of circumferential and axial cracks without mechanical mitigation
	3.1.2	3.4.3	Circumferential and Axial	PWSCC (Direct Model 1)	PWSCC	Sensitivity study of Case 3.1.0 considering a more severe WRS profile
Bin 4: Westinghouse Steam Generator Nozzle DMWs	4.1.0	3.5.1	Circumferential and Axial	PWSCC (Direct Model 1)	PWSCC	Assess the base likelihood of failure caused by PWSCC initiation and growth with inlay mitigation
	4.1.1	3.5.2	Circumferential and Axial	Initial Flaw Density (1 Axial and 1 Circ. Crack)	PWSCC	Assess the base likelihood of failure with pre-existing flaws and subsequent PWSCC growth of circumferential and axial cracks with inlay mitigation
	4.1.2	3.5.3	Circumferential and Axial	PWSCC (Direct Model 1)	PWSCC	Sensitivity study of Case 4.1.0 considering a more severe WRS profile
	4.1.3	3.5.4	Circumferential and Axial	PWSCC (Direct Model 1)	PWSCC	Sensitivity study of Case 4.1.0 considering overlay instead of inlay mitigation
	4.1.4	3.5.5	Circumferential and Axial	PWSCC (Direct Model 1)	PWSCC	Sensitivity study of Case 4.1.0 without mechanical mitigation

Weld Bin	Case No.	Report Section	Crack Orientations	Crack Initiation Method	Crack Growth Mechanism	Objective
Bin 5a: CE Hot Leg Branch Line Nozzle DMWs	5.1.0	3.6.1	Circumferential and Axial	PWSCC (Direct Model 1)	PWSCC	Assess the base likelihood of failure caused by PWSCC initiation and growth without mechanical mitigation
	5.1.1	3.6.2	Circumferential and Axial	Initial Flaw Density (1 Axial and 1 Circ. Crack)	PWSCC	Assess the base likelihood of failure with pre-existing flaws and subsequent PWSCC growth of circumferential and axial cracks without mechanical mitigation
	5.1.2	3.6.3	Circumferential and Axial	PWSCC (Direct Model 1)	PWSCC	Sensitivity study of Case 5.1.0 considering a more severe WRS profile
Bin 5b: CE Cold Leg Branch Line Nozzle DMWs	5.2.0	3.7.1	Circumferential and Axial	PWSCC (Direct Model 1)	PWSCC	Assess the base likelihood of failure caused by PWSCC initiation and growth without mechanical mitigation
	5.2.1	3.7.2	Circumferential and Axial	Initial Flaw Density (1 Axial and 1 Circ. Crack)	PWSCC	Assess the base likelihood of failure with pre-existing flaws and subsequent PWSCC growth of circumferential and axial cracks without mechanical mitigation
Bin 6: Westinghouse 2- and 3-loop RVON and RVIN DMWs	1.3.0	3.8.1	Circumferential and Axial	PWSCC (Direct Model 1)	PWSCC	Assess the base likelihood of failure caused by PWSCC initiation and growth without mechanical mitigation
	1.3.1	3.8.2	Circumferential and Axial	Initial Flaw Density (1 Axial and 1 Circ. Crack)	PWSCC	Assess the base likelihood of failure with pre-existing flaws and subsequent PWSCC growth of circumferential and axial cracks without mechanical mitigation

3.2 Bin 1: Westinghouse Four-Loop RVON and RVIN DMWs

Westinghouse four-loop RVON and RVIN DMWs were analyzed in the prior study [2]. Cases 1.1.6a, 1.1.6b, and 1.1.6c were created to represent these welds in the present study. They are equivalent to the base case (i.e., Case 1.1.0) in the prior study with the inclusion of axial cracks and with the hydrogen concentration in the reactor coolant reduced from 37 cubic centimeters per kilogram (cc/kg) to 25 cc/kg. Using the reduced hydrogen concentration is a bounding approach as it increases crack growth rates and represents the lower bound of the PWR operating conditions as described in EPRI Technical Report 1022852, "Materials Reliability Program: Probabilistic Assessment of Chemical Mitigation of Primary Water Stress Corrosion Cracking in Nickel-Base Alloys (MRP-307)," issued June 29, 2011 [48].

The Westinghouse four-loop RVON base cases for this study (i.e., Cases 1.1.6a and 1.1.6c), and the corresponding initial flaw sensitivity study case (i.e., Case 1.1.6b), are described in Sections 3.2.1 and 3.2.2, respectively. Cases 1.1.6a and 1.1.6c are equivalent, except that the former uses a 10-year inspection frequency, and the latter uses a 5-year inspection frequency. The different inspection frequencies were considered to assess the impact of the length of time between inspections.

3.2.1 Base Case

3.2.1.1 Case Description

The objective of Case 1.1.6a was to generate a new reference case for Westinghouse four-loop RVON DMWs to establish a point of comparison for all the cases in the present study that use Direct Model 1 for crack initiation. Case 1.1.6a is based on Cases 1.1.6 and 1.1.14 from the prior study, which were sensitivity studies on the effects of axial cracks and dissolved hydrogen concentration, respectively. Figure 3-1 shows the WRS profiles used to analyze Case 1.1.6a. They are the same WRS profiles that were used in Case 1.1.0 from the prior study and are described in Section C6.1. Section B1 describes the specific inputs and other simulation details used to analyze the case.

Case 1.1.6c is like Case 1.1.6a only with a different inspection frequency to assess the impact of the length of time between inspections. The inspection frequency in Case 1.1.6a was set to 1 every 10 years; whereas, in Case 1.1.6c it was set to 1 every 5 years consistent with American Society of Mechanical Engineers (ASME) Code Case N-770-5, "Alternative Examination Requirements and Acceptance Standards for Class 1 PWR Piping and Vessel Nozzle Butt Welds Fabricated With UNS N06082 or UNS W86182 Weld Filler Material With or Without Application of Listed Mitigation Activities," approved November 7, 2016 [49]. This code case is mandated by the NRC in 10 CFR 50.55a(g)(6)(ii)(F). The outputs affected by this change are the time-dependent probabilities of leakage with ISI and rupture with ISI.

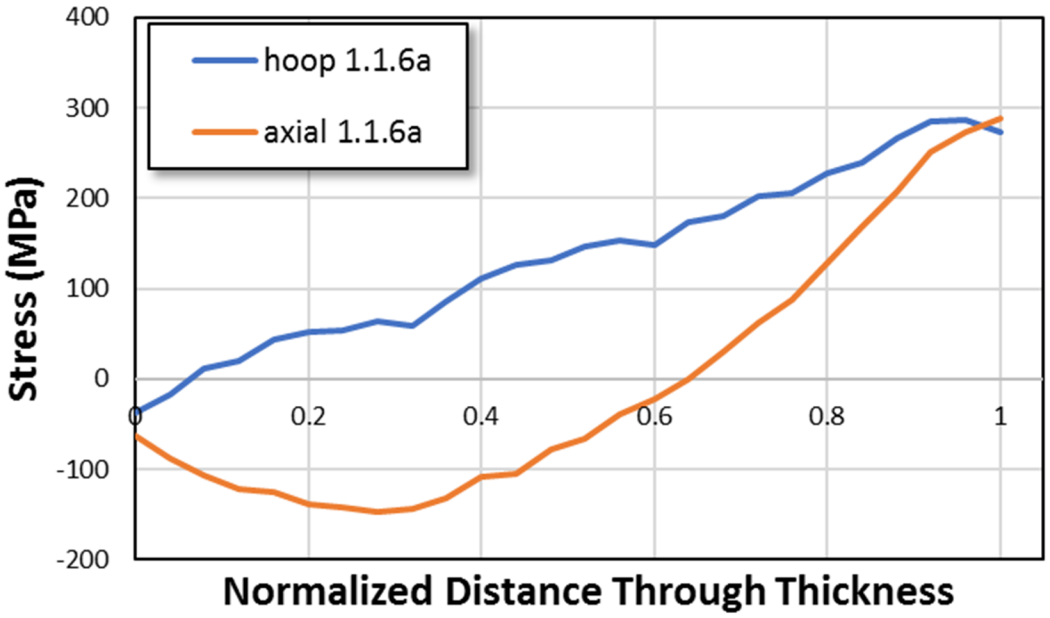

Figure 3-1 Cases 1.1.6a and 1.1.6c WRS profiles

3.2.1.2 Results and Analysis

3.2.1.2.1 Probability of Rupture with Detection

There were no ruptures with a 1 gpm leak rate detection capability for this case.

3.2.1.2.2 Leak Rate Jump

There were no leak rate jump events for this case.

3.2.1.2.3 LBB Time Lapse

The mean LBB time lapses and standard errors with 1 and 10 gpm leak rate detection capabilities were respectively as follows:

- 36.6 ± 1.2 months (minimum observed: 14 months)
- 25.1 ± 0.9 months (minimum observed: 9 months)

All LBB time lapses beyond 12 EFPY were conservatively excluded as they were found to strongly influence the mean. Such a long period of time is also not of practical interest. For example, if the LBB time lapse is greater than 12 EFPY, it is typically due to a slow-growing crack, an arrested crack, or a crack that has been mechanically mitigated, if applied.

Figure 3-2 shows the LBB time lapse CDFs for Case 1.1.6a compared with Case 1.1.0 from the prior study. The leftward shift for the Case 1.1.6a results is due to the bounding hydrogen concentration used in the analysis.

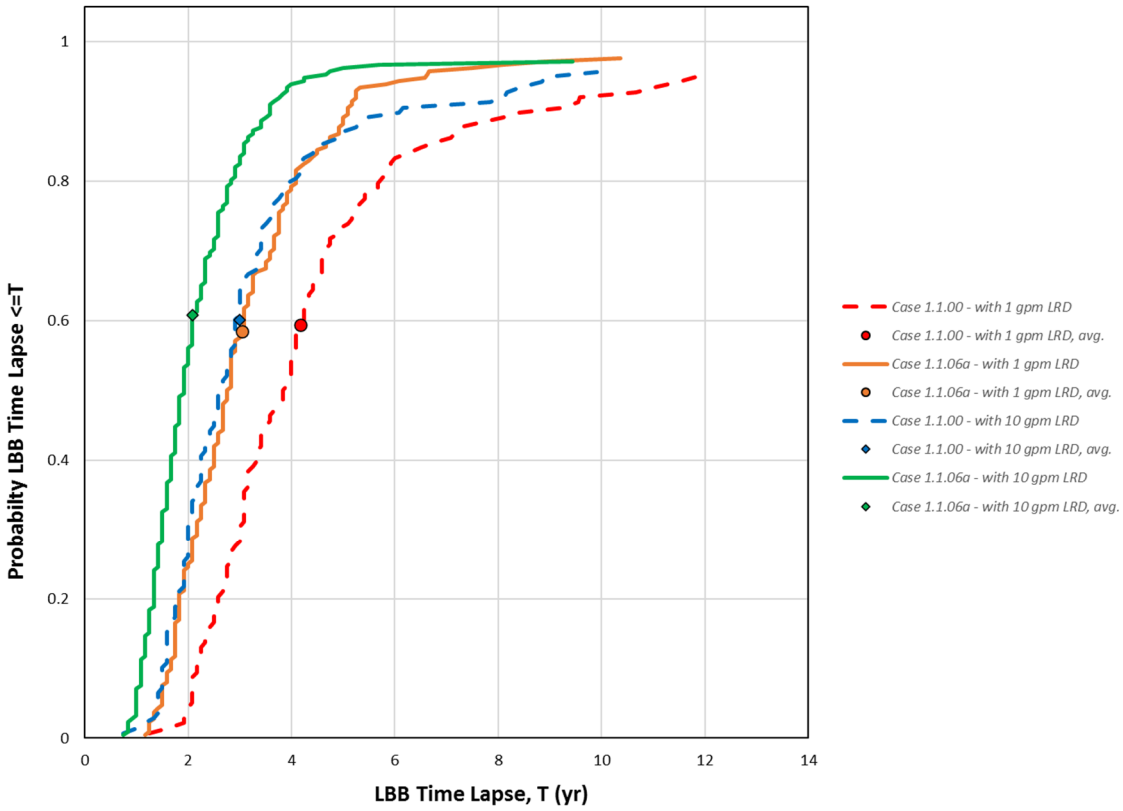

Figure 3-2 Case 1.1.6a LBB time lapse results

3.2.1.2.4 LBB Ratio

The mean LBB ratios and standard errors with 1 and 10 gpm leak rate detection capabilities were respectively as follows:

- 9.64 ± 0.07 (minimum observed: 1.66)
- 4.58 ± 0.02 (minimum observed: 1.56)

Figure 3-3 shows the LBB ratio CDFs for Case 1.1.6a compared with Case 1.1.0 from the prior study. As can be observed, the LBB ratio distributions are not affected by the hydrogen concentration, and thus the Case 1.1.6a results lie on top of the results for Case 1.1.0.

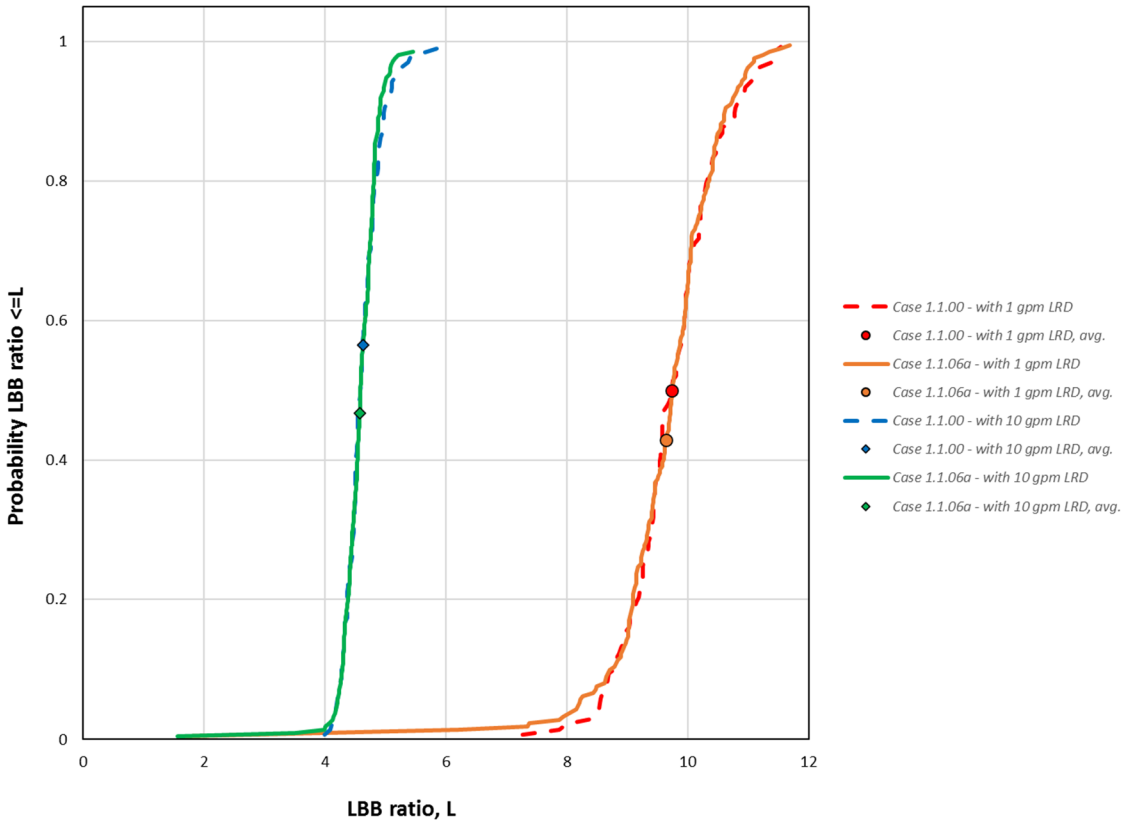

Figure 3-3 Case 1.1.6a LBB ratio results

3.2.1.2.5 Standard Indicators

Figure 3-4 shows the probabilities of first crack and first circumferential crack for Case 1.1.6a. The probabilities are consistent with the values reported for Case 1.1.6 in the prior study [2].

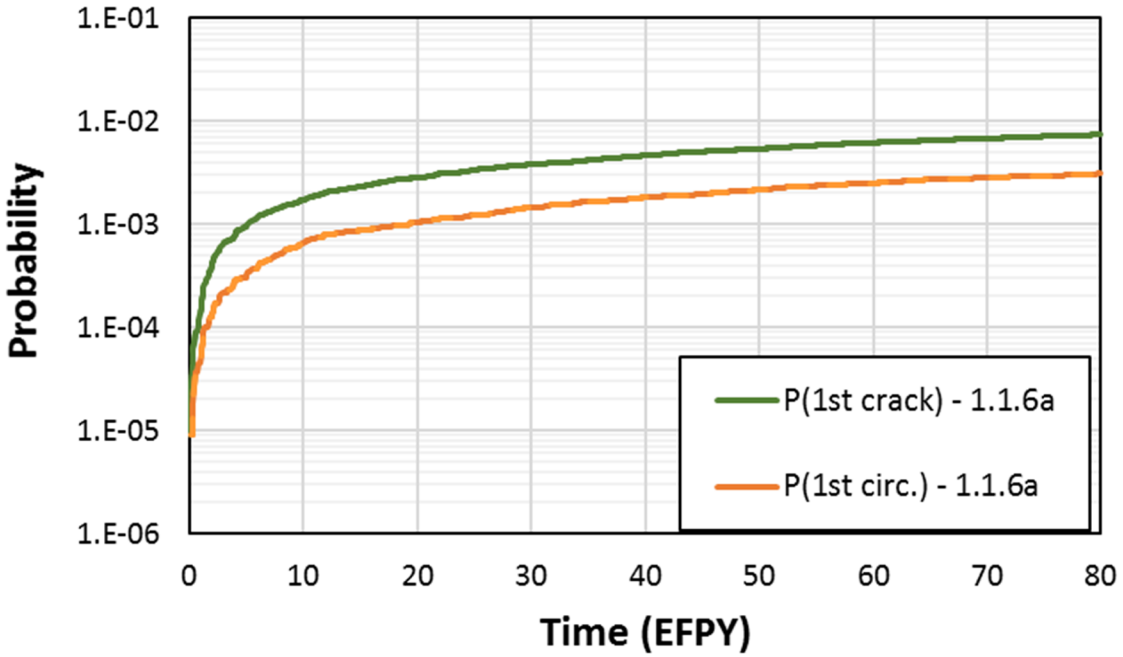

Figure 3-4 Case 1.1.6a time-dependent probabilities of first crack

Figure 3-5 shows the probabilities of first leak, first circumferential crack leak, and first leak with ISI for Case 1.1.6a with a 10-year inspection frequency. The values are slightly higher than the ones reported in the prior study because of the bounding hydrogen concentration, which leads to increased crack growth rates.

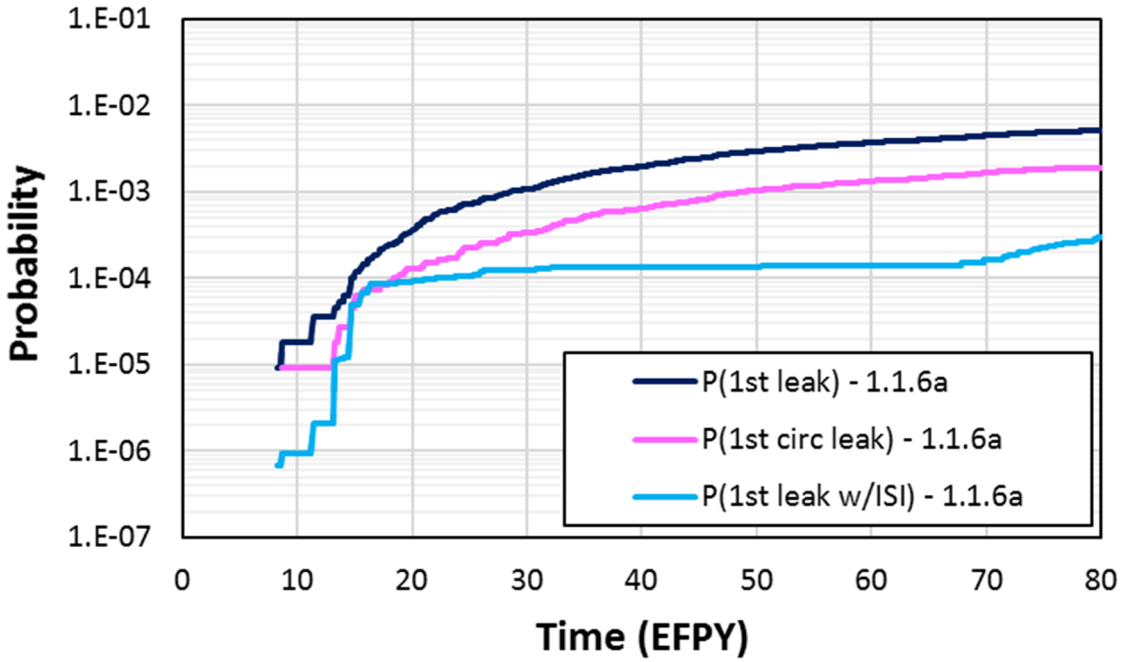

Figure 3-5 Case 1.1.6a time-dependent probabilities of first leak with a 10-year inspection frequency

Figure 3-6 shows the probabilities of first leak, first circumferential crack leak, and first leak with ISI for Cases 1.1.6a and 1.1.6c, which considered 10- and 5-year inspection frequencies, respectively. As expected, only the probability of first leak with ISI is affected. The more frequent inspections in Case 1.1.6c reduce the probability of first leak to 2.92 x 10^{-5} over 80 EFPY, which corresponds to an annual frequency of 3.65 x 10^{-7}.

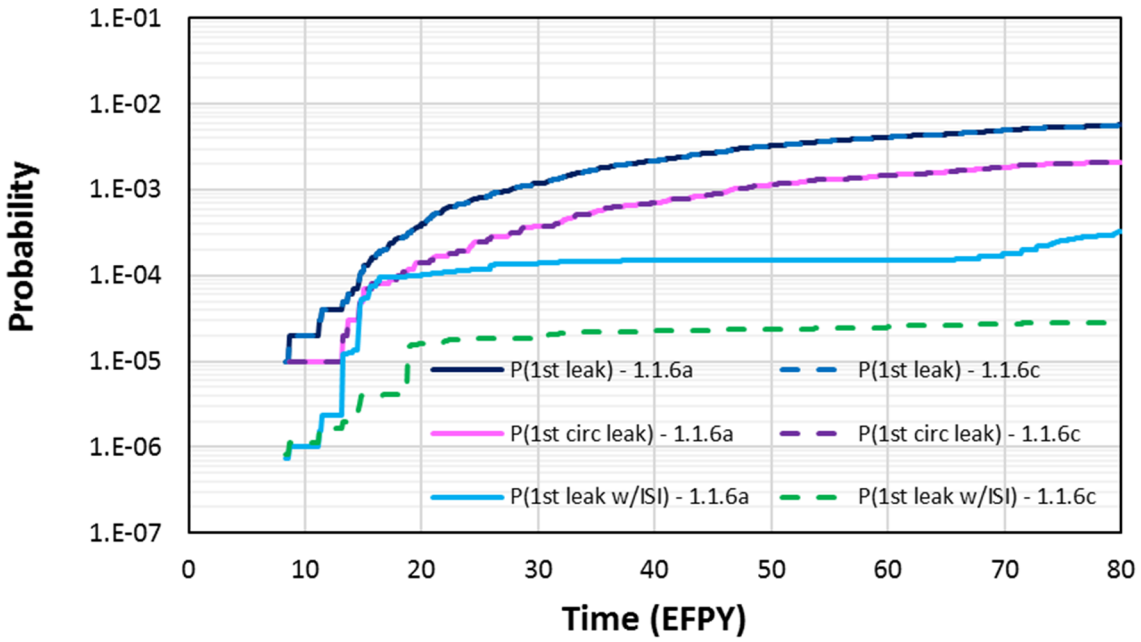

Figure 3-6 Comparison of Case 1.1.6c time-dependent probabilities of first leak, first circumferential leak, and first leak with ISI with Case 1.1.6a

Figure 3-7 shows the probabilities of rupture, rupture with SSE, and rupture with ISI for Case 1.1.6a, which considered a 10-year inspection frequency. There were no occurrences of rupture over 80 EFPY when leak detection is considered.

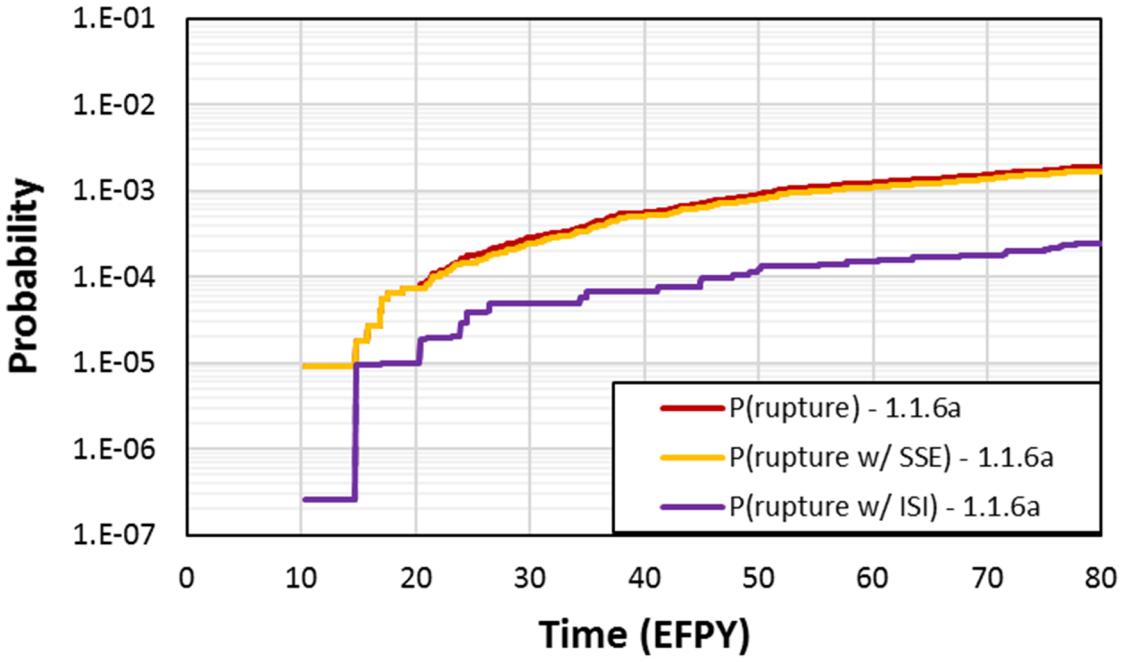

Figure 3-7 Case 1.1.6a time-dependent probabilities of rupture with a 10-year inspection frequency

Figure 3-8 shows the probabilities of rupture and rupture with ISI for Cases 1.1.6a and 1.1.6c, which considered 10- and 5-year inspection frequencies, respectively. As expected, only the probability of rupture with ISI is affected. The more frequent inspections in Case 1.1.6c reduce the probability of rupture with ISI to 1.71×10^{-6} over 80 EFPY, which corresponds to an annual frequency of 2.14×10^{-8}.

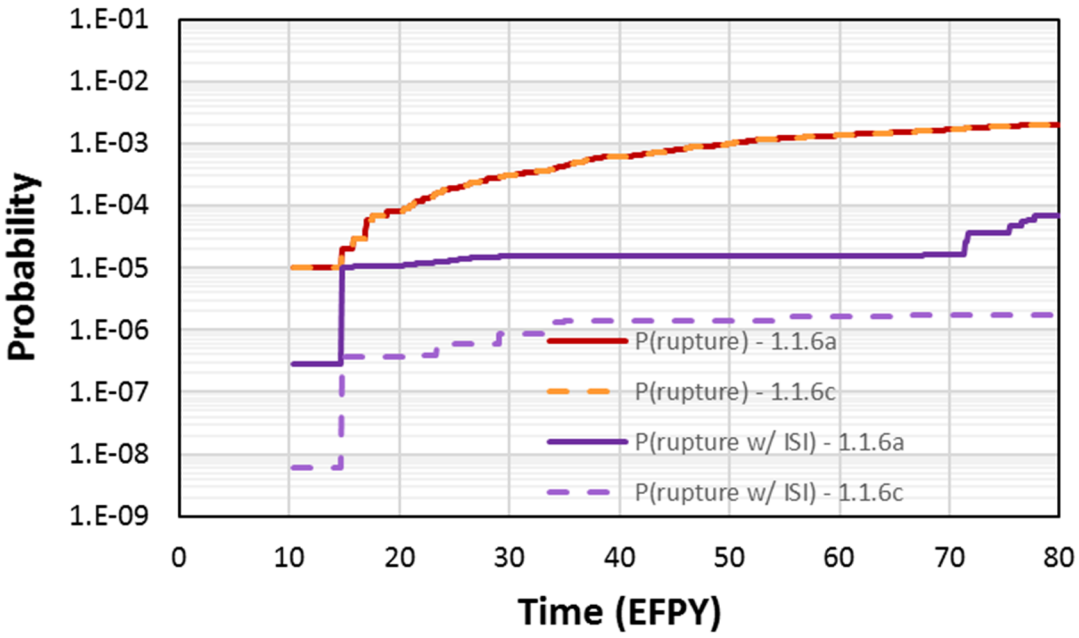

Figure 3-8 Comparison of Case 1.1.6c time-dependent probabilities of rupture and rupture with ISI with Case 1.1.6a

3.2.2 Initial Flaws

3.2.2.1 Case Description

The objective of Case 1.1.6b was to generate a new reference case for Westinghouse four-loop RVON DMWs to establish a point of comparison for all the cases in the present study that consider pre-existing flaws. This case uses the same inputs as Case 1.1.6a except that, instead of Direct Model 1 for crack initiation, it uses pre-existing axial and circumferential flaws. Section B2 describes the specific inputs and other simulation details used to analyze the case.

3.2.2.2 Results and Analysis

3.2.2.2.1 Probability of Rupture with Detection

There were no ruptures with a 1 gpm leak rate detection capability for this case.

3.2.2.2.2 Leak Rate Jump

There were no leak rate jump events for this case.

3.2.2.2.3 LBB Time Lapse

The mean LBB time lapses and standard errors with 1 and 10 gpm leak rate detection capabilities were respectively as follows:

- 38.66 ± 0.26 months (minimum observed: 10 months)
- 26.43 ± 0.18 months (minimum observed: 7 months)

Note that all results beyond 12 EFPY have been excluded for the reasons explained in Section 3.2.1.2.3.

Figure 3-9 shows the LBB time lapse CDFs for Case 1.1.6b as compared to Case 1.1.6a. The results lie on top of each other, which indicates that starting with an existing crack does not affect this QoI.

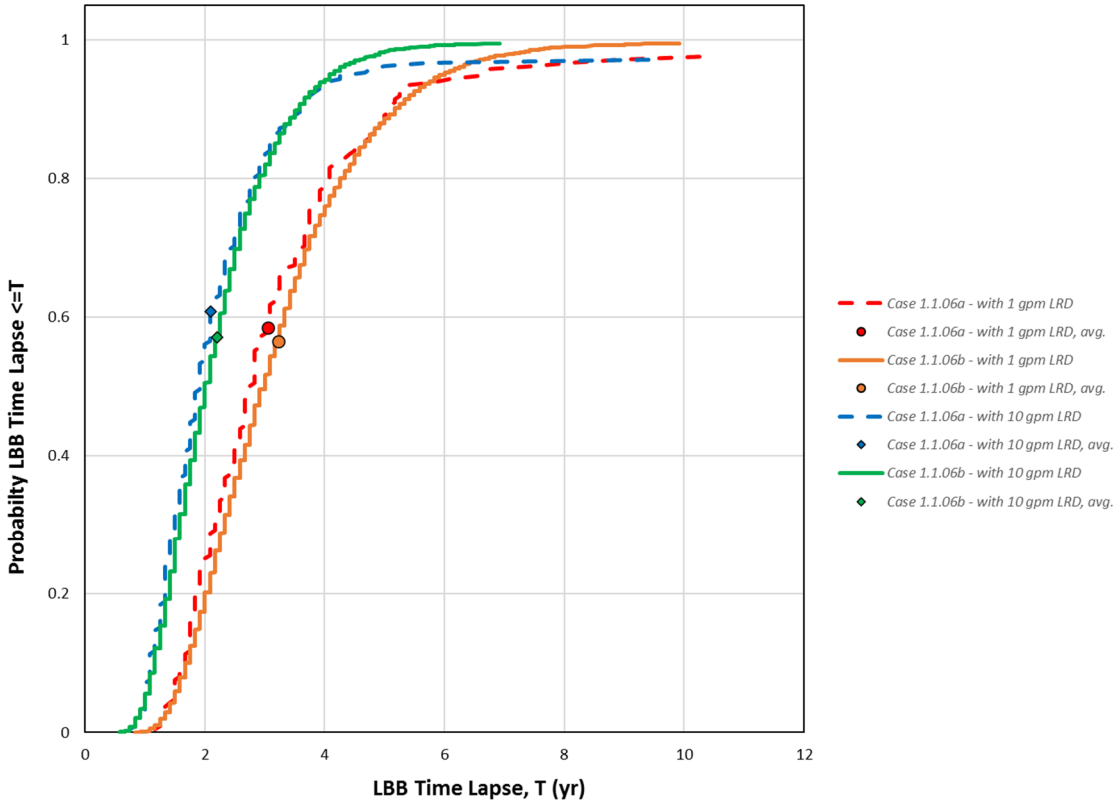

Figure 3-9 Case 1.1.6b LBB time lapse results

3.2.2.2.4 LBB Ratio

The mean LBB ratios and standard errors with 1 and 10 gpm leak rate detection capabilities were respectively as follows:

- 9.86 ± 0.01 (minimum observed: 7.71)
- 4.64 ± 0.00* (minimum observed: 3.99)

Figure 3-10 shows the LBB ratio CDF plots for Cases 1.1.6a and 1.1.6b. There is good agreement between the results of the two cases.

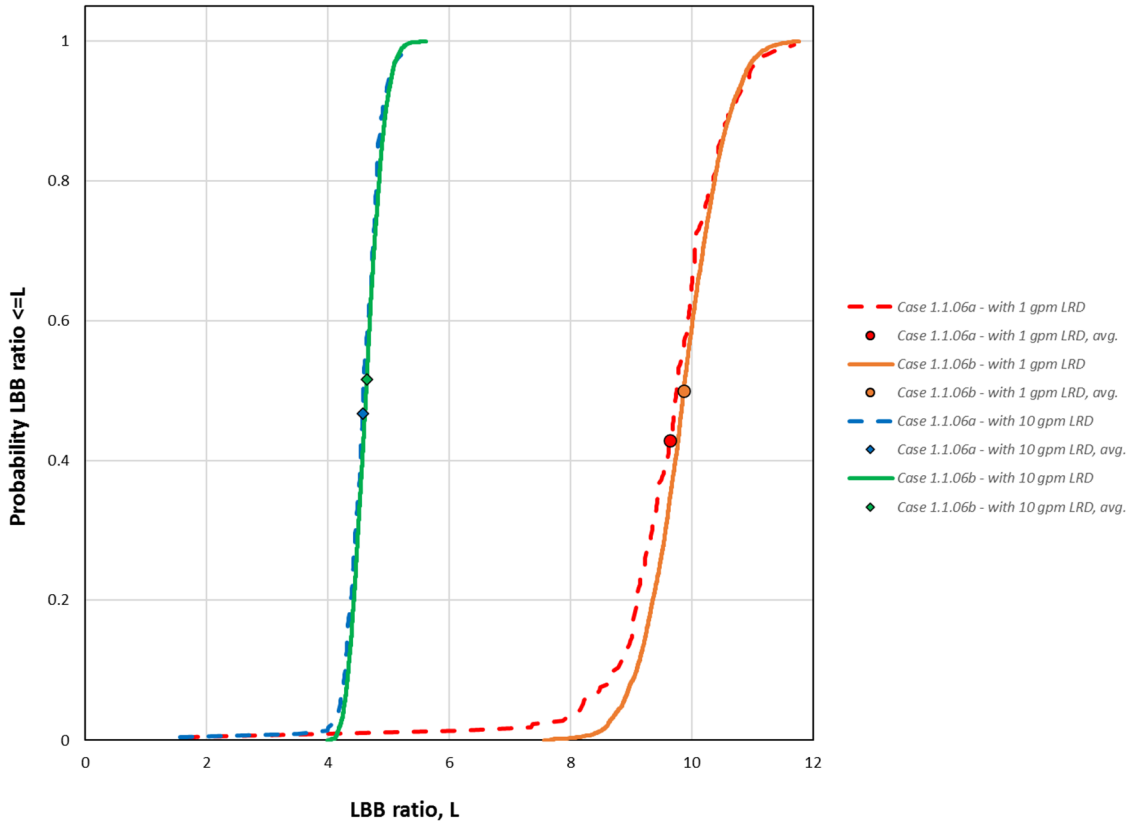

Figure 3-10 Case 1.1.6b LBB ratio results

3.2.2.2.5 Standard Indicators

Figure 3-11 shows the probabilities of first leak for Case 1.1.6b. The results for the circumferential cracks are consistent with the observations from the Case 1.1.14 sensitivity study on the hydrogen concentration from the prior study. The 10-year inspection frequency reduces the probability by about one order of magnitude after 80 EFPY.

* The standard errors are reported with 2-digit accuracy. A standard error of 0.00 is lower than 0.01.

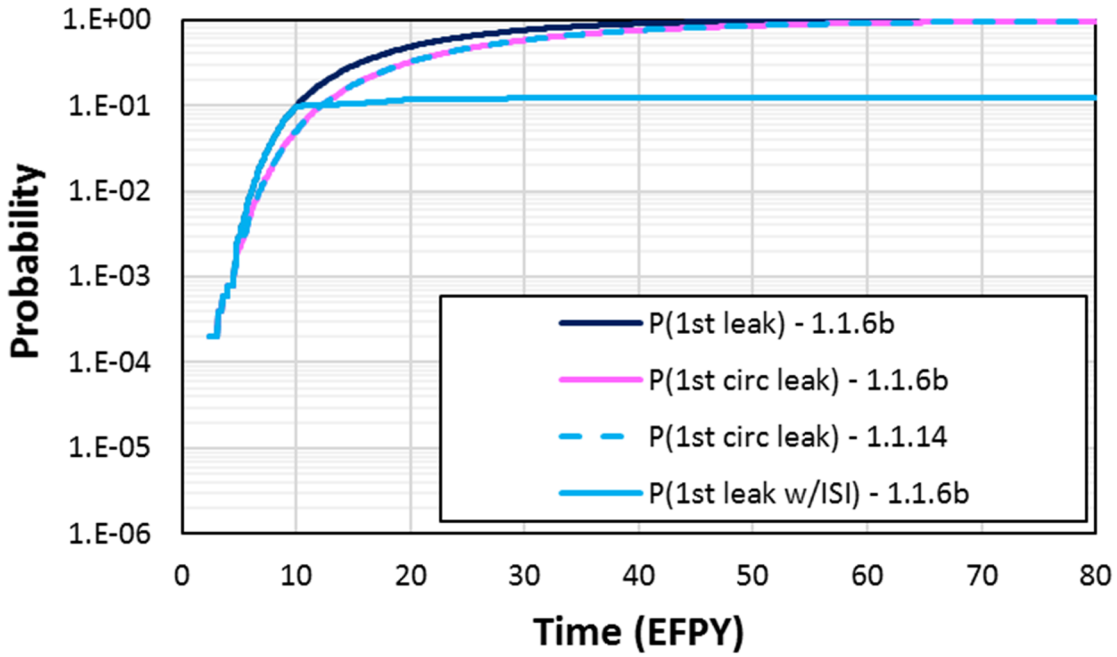

Figure 3-11 Case 1.1.6b time-dependent probabilities of first leak

Figure 3-12 shows the probabilities of rupture for Case 1.1.6b. There were no occurrences of rupture over 80 EFPY when leak detection is considered.

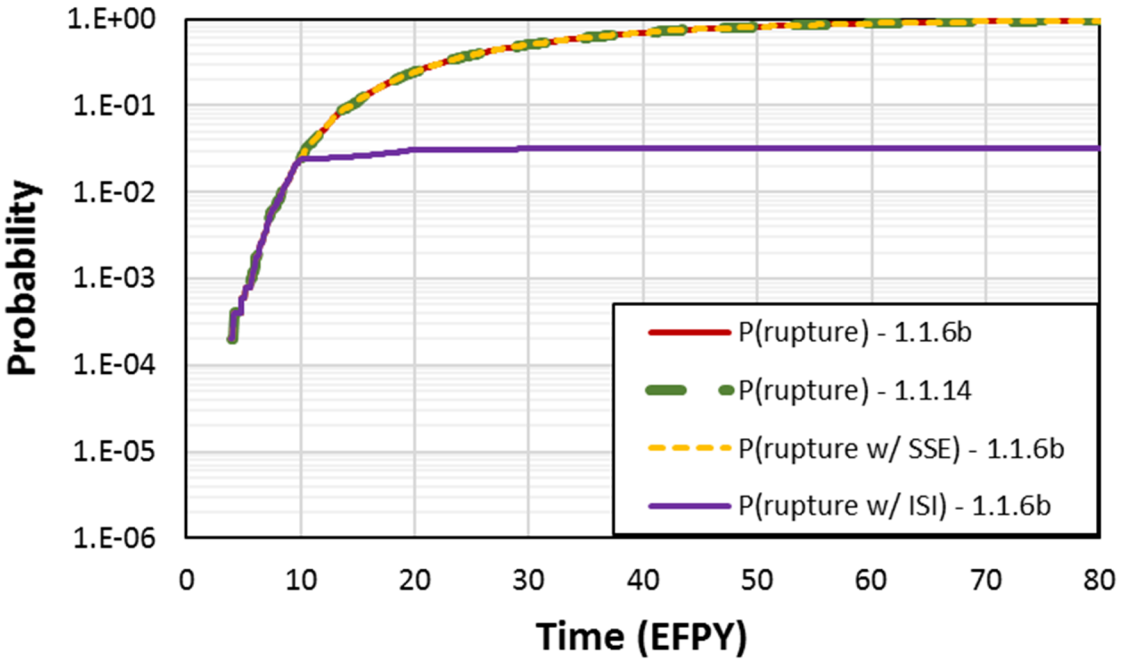

Figure 3-12 Case 1.1.6b time-dependent probabilities of rupture

3.3 Bin 2: Westinghouse Pressurizer Surge Line Nozzle DMWs

The following cases were used to analyze the Westinghouse pressurizer surge line nozzle DMWs represented by Bin 2:

- Case 2.1.0: base case
- Case 2.1.1: initial flaws
- Case 2.1.2: more severe WRS
- Case 2.1.3: overlay mitigation
- Case 2.1.4: fatigue
- Case 2.1.5: MSIP® mitigation

The cases and associated analyses are described in Sections 3.3.1 through 3.3.6, respectively.

3.3.1 Base Case

3.3.1.1 Case Description

The objective of Case 2.1.0 was to assess the base likelihood of failure caused by PWSCC initiation and growth without mechanical mitigation. The effects of leak detection, ISI, and SSE were also assessed. This case used bounding values for the geometry and loading, both normal operating and SSE stresses, based on the information from the applicable references in Table 2-1. The ISI parameters are from the xLPR ISI module validation report [50]. Figure 3-13 shows the mean WRS profiles used to analyze the case. They were developed using FEA for a representative pressurizer surge line nozzle with a fill-in type weld geometry. Figure C-1 illustrates the geometry in detail, and further details on the development of the WRS profiles are in Section C2.1. Section B4 describes the specific inputs and other simulation details used to analyze the case.

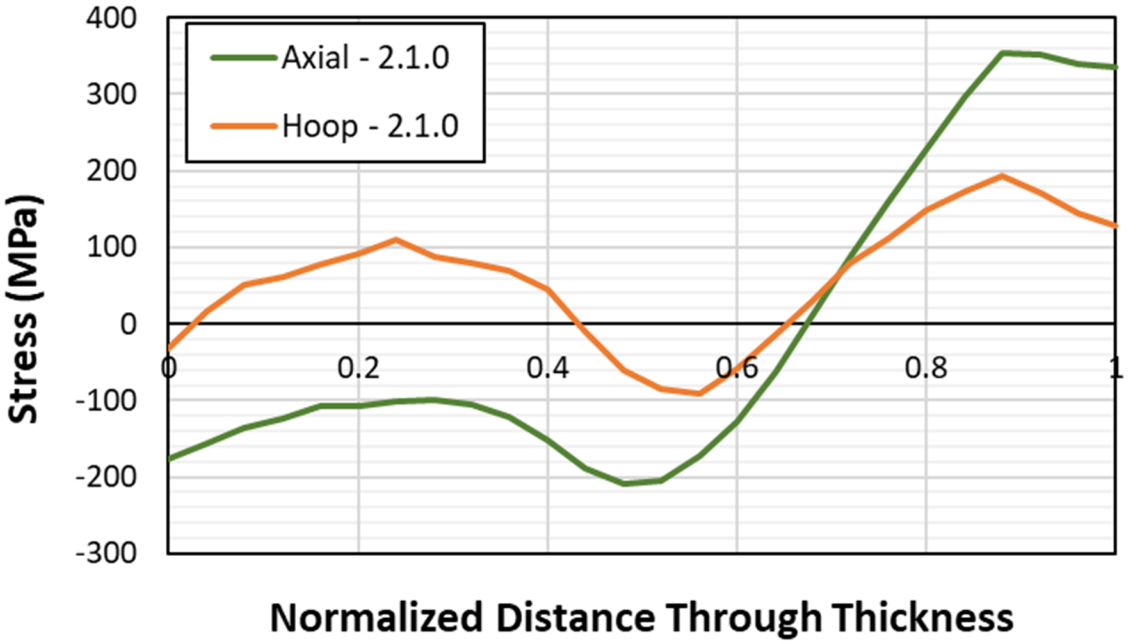

Figure 3-13 Case 2.1.0 WRS profiles

3.3.1.2 Results and Analysis

3.3.1.2.1 Probability of Rupture with Detection

There were no ruptures with a 1 gpm leak rate detection capability for this case.

3.3.1.2.2 Leak Rate Jump

There were no leak rate jump events for this case.

3.3.1.2.3 LBB Time Lapse

The mean LBB time lapses and standard errors with 1 and 10 gpm leak rate detection capabilities were respectively as follows:

- 6.50 ± 0.67 months (minimum observed: 4 months)
- 1.08 ± 0.08 months (minimum observed: 1 month)

Note that all results beyond 12 EFPY have been excluded for the reasons explained in Section 3.2.1.2.3.

Figure 3-14 shows the LBB time lapse CDFs for Case 2.1.0. The values are a lot lower as compared with Case 1.1.6a, which indicate shorter times from detectable leakage to rupture in the case of the pressurizer surge line nozzle DMWs. This result is because of the smaller diameter of the pressurizer surge line, which leads to larger crack sizes in proportion to the circumference to reach 1 or 10 gpm leak rates. The proportionally larger crack sizes are closer

both in time and size to the critical crack size, as shown in the supplemental analysis in Section 3.3.2.3. The result can also be attributed to the higher operating temperature of the pressurizer surge line.

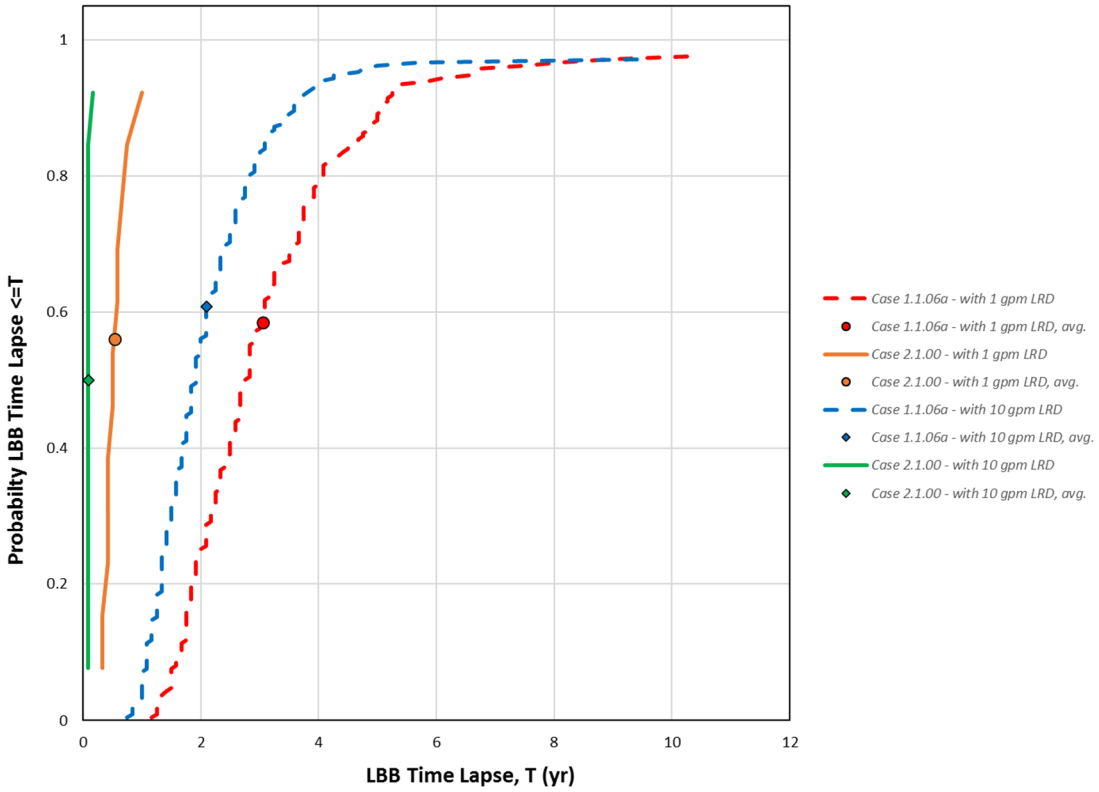

Figure 3-14 Case 2.1.0 LBB time lapse results

3.3.1.2.4 LBB Ratio

The mean LBB ratios and standard errors with 1 and 10 gpm leak rate detection capabilities were respectively as follows:

- 4.42 ± 0.12 (minimum observed: 3.73)
- 1.99 ± 0.07 (minimum observed: 1.62)

Figure 3-15 shows the LBB ratio CDFs for Case 2.1.0. As for the LBB time lapse CDFs, the values are lower than Case 1.1.6a due to the smaller diameter of the pressurizer surge line.

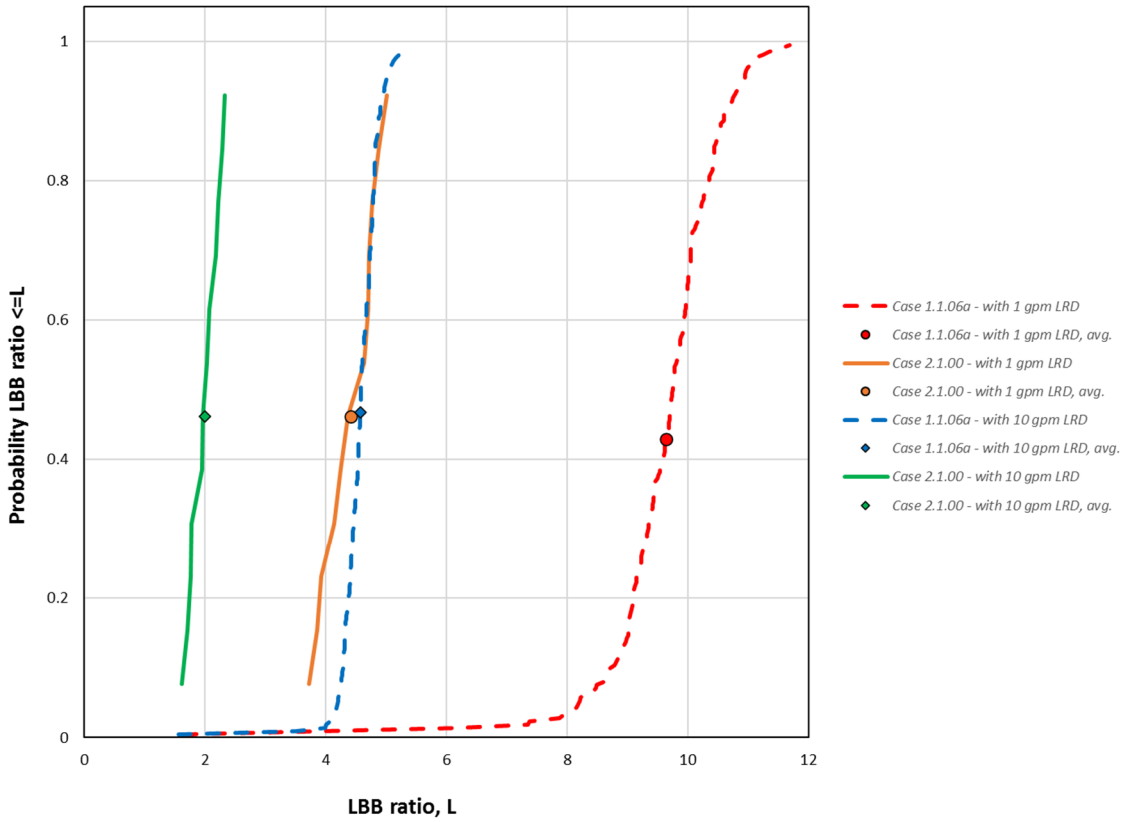

Figure 3-15 Case 2.1.0 LBB ratio results

3.3.1.2.5 Standard Indicators

Figure 3-16 shows the probabilities of first crack for Case 2.1.0 as compared with Case 1.1.6a. The probability of first crack is higher by a factor of 2 due to axial cracks; however, the probability of circumferential crack is lower by one order of magnitude.

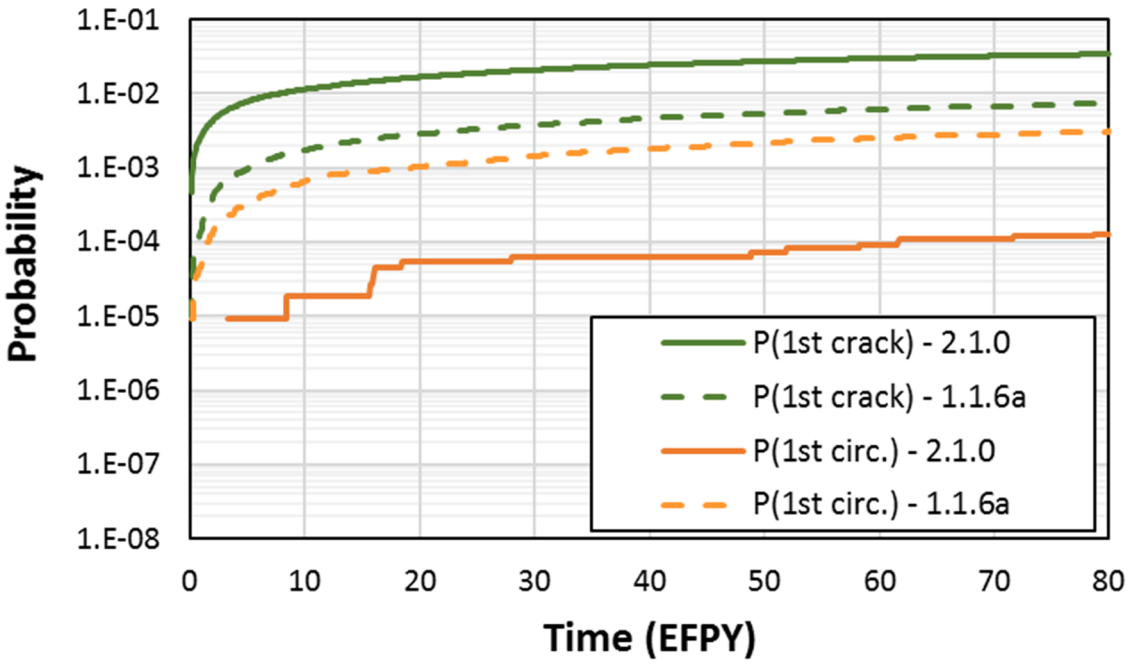

Figure 3-16 Case 2.1.0 time-dependent probabilities of first crack

Figure 3-17 shows the probabilities of first leak for Case 2.1.0 as compared with Case 1.1.6a. As with the probability of first crack, the probability of leakage is higher due to the inclusion of axial cracks. The impact of a 10-year inspection frequency is reduced due to a sharp rise in probability during the first 10 EFPY. With an increased inspection frequency for the surge line as is currently required by ASME Code Case N-770-5, which is mandated by 10 CFR 50.55a(g)(6)(ii)(F), the impact of ISI would be more pronounced. However, since the main concern is rupture and not leakage, it is not necessary to revisit the 10-year inspection frequency used for the analysis. The probability of leakage due to only circumferential cracks is lower by more than one order of magnitude, which is consistent with the probability of first leak results. This reduction is attributed, in part, to the difference between the mean axial and hoop WRS at the inside diameter of the weld.

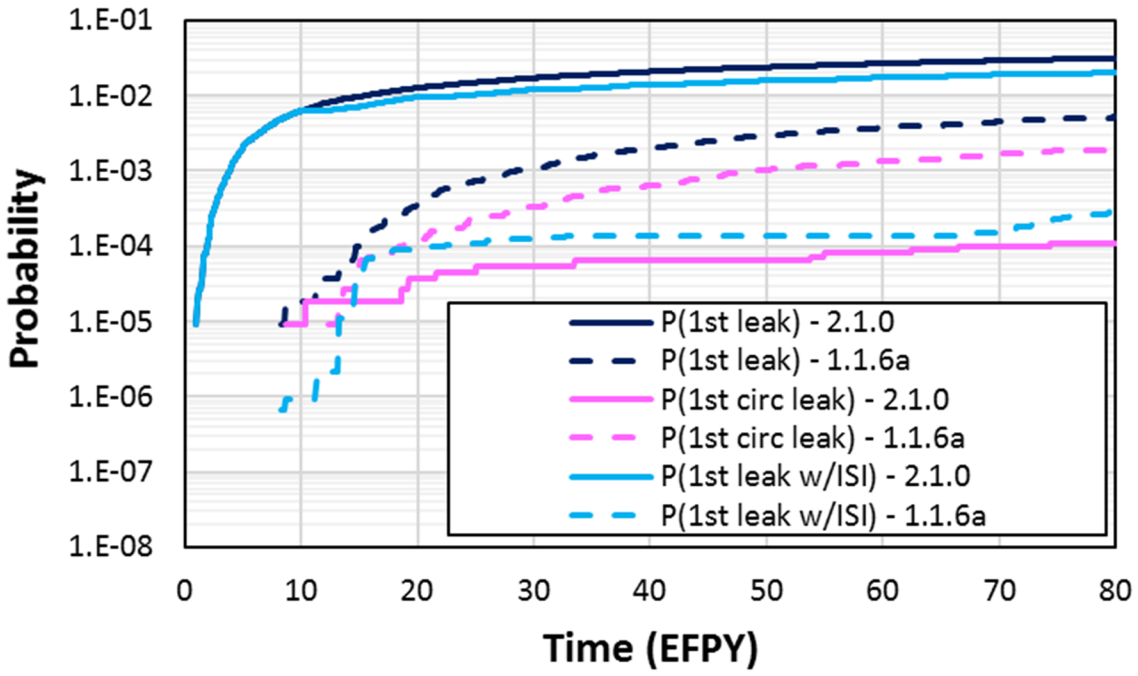

Figure 3-17 Case 2.1.0 time-dependent probabilities of first leak

Figure 3-18 shows the probabilities of rupture for Case 2.1.0 as compared to Case 1.1.6a. These probabilities are more than one order of magnitude lower for Case 2.1.0. It should be noted that the inspection frequency was set to one inspection every 10 years to give a consistent comparison for all the welds in this study, and currently the pressurizer surge line welds are required by 10 CFR 50.55a(g)(6)(ii)(F) to be inspected more frequently (i.e., every other refueling outage, which is approximately every 3 to 4 years). The probability of rupture when ISI is considered is lower than 1 x 10^{-6} ruptures per year with the 10-year inspection frequency, and it is expected to be even lower with the current NRC inspection requirements.

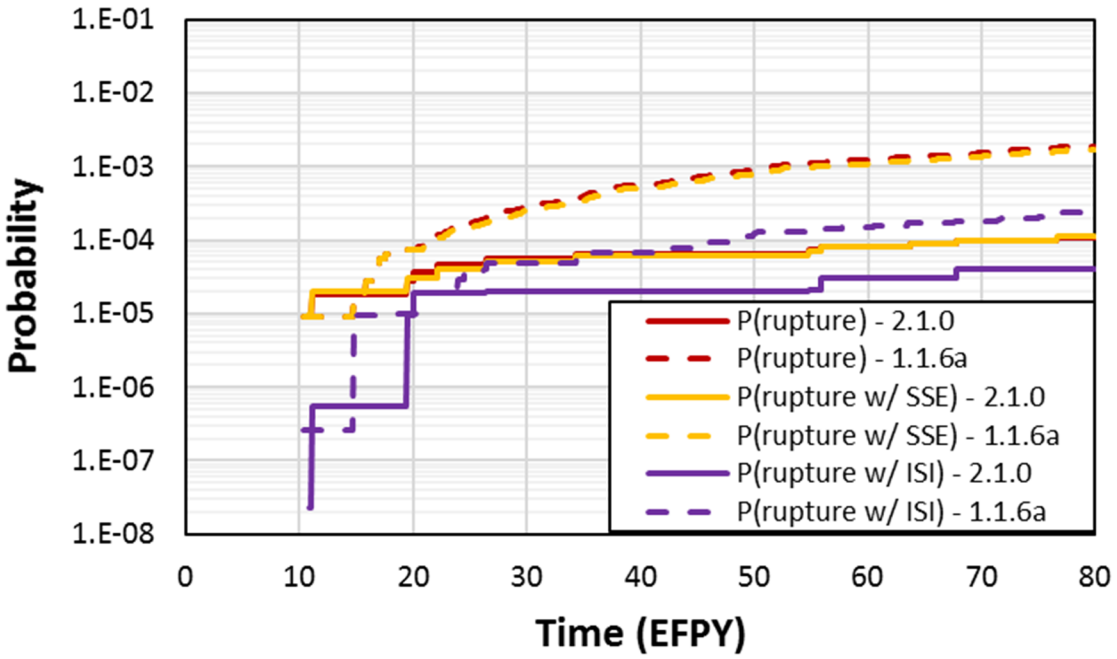

Figure 3-18 Case 2.1.0 time-dependent probabilities of rupture

3.3.2 Initial Flaws

3.3.2.1 Case Description

The objective of Case 2.1.1 was to assess the base likelihood of failure with pre-existing flaws and subsequent PWSCC growth of circumferential and axial cracks without mechanical mitigation. This case uses the same inputs as Case 2.1.0 except that, instead of Direct Model 1 for crack initiation, it uses pre-existing axial and circumferential flaws. The WRS profiles were the same as in the Case 2.1.0 analysis. Section B5 describes the specific inputs and other simulation details used to analyze the case.

3.3.2.2 Results and Analysis

3.3.2.2.1 Probability of Rupture with Detection

There were no ruptures with a 1 gpm leak rate detection capability for this case.

3.3.2.2.2 Leak Rate Jump

There were no leak rate jump events for this case.

3.3.2.2.3 LBB Time Lapse

The mean LBB time lapses and standard errors with 1 and 10 gpm leak rate detection capabilities were respectively as follows:

- 6.59 ± 0.07 months (minimum observed: 2 months)
- 1.28 ± 0.02 months (minimum observed: 0 month)

Note that all results beyond 12 EFPY have been excluded for the reasons explained in Section 3.2.1.2.3.

Figure 3-19 shows the LBB time lapse CDFs from Case 2.1.1 as compared to Case 2.1.0. Consistent with the expectations described in Section 3.1.2, the CDFs are similar. The reason for the low LBB time lapses is described in Section 3.3.2.3.

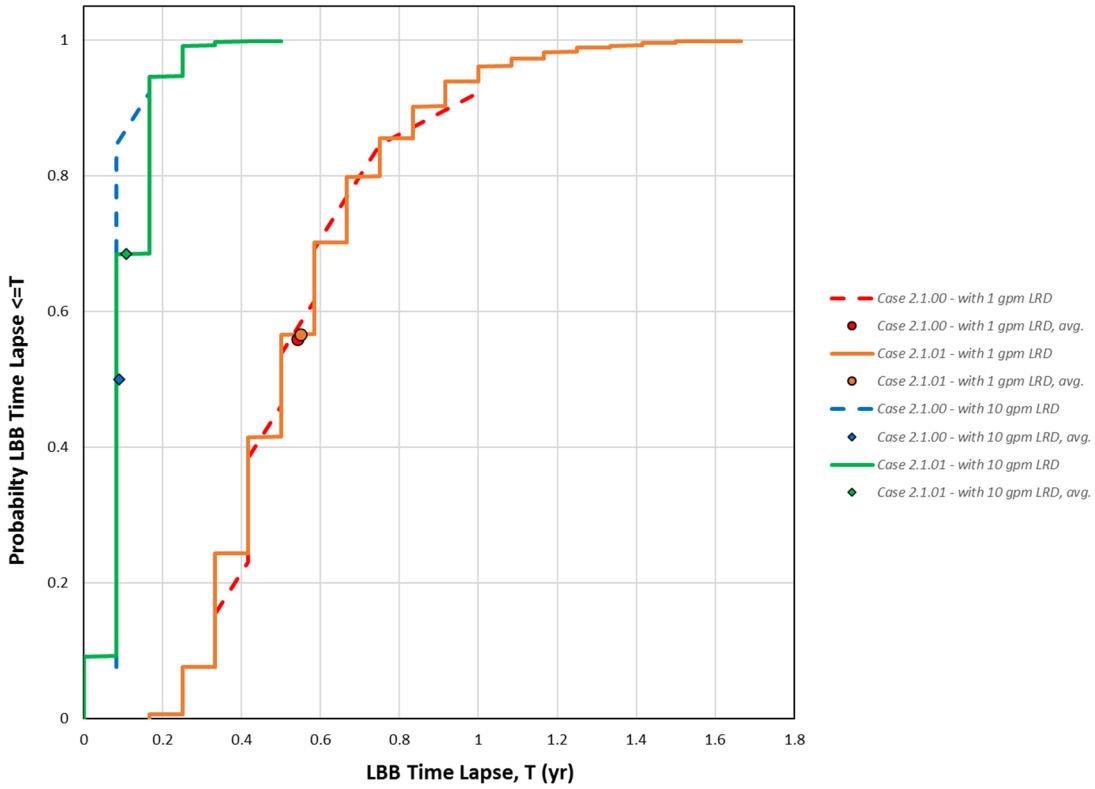

Figure 3-19 Case 2.1.1 LBB time lapse results

3.3.2.2.4 LBB Ratio

The mean LBB ratios and standard errors with 1 and 10 gpm leak rate detection capabilities were respectively as follows:

- 4.49 ± 0.02 (minimum observed: 2.48)
- 1.99 ± 0.01 (minimum observed: 1.26)

Figure 3-20 shows the LBB ratio CDF plots for Case 2.1.1. As expected, there is good agreement with the results from Case 2.1.0.

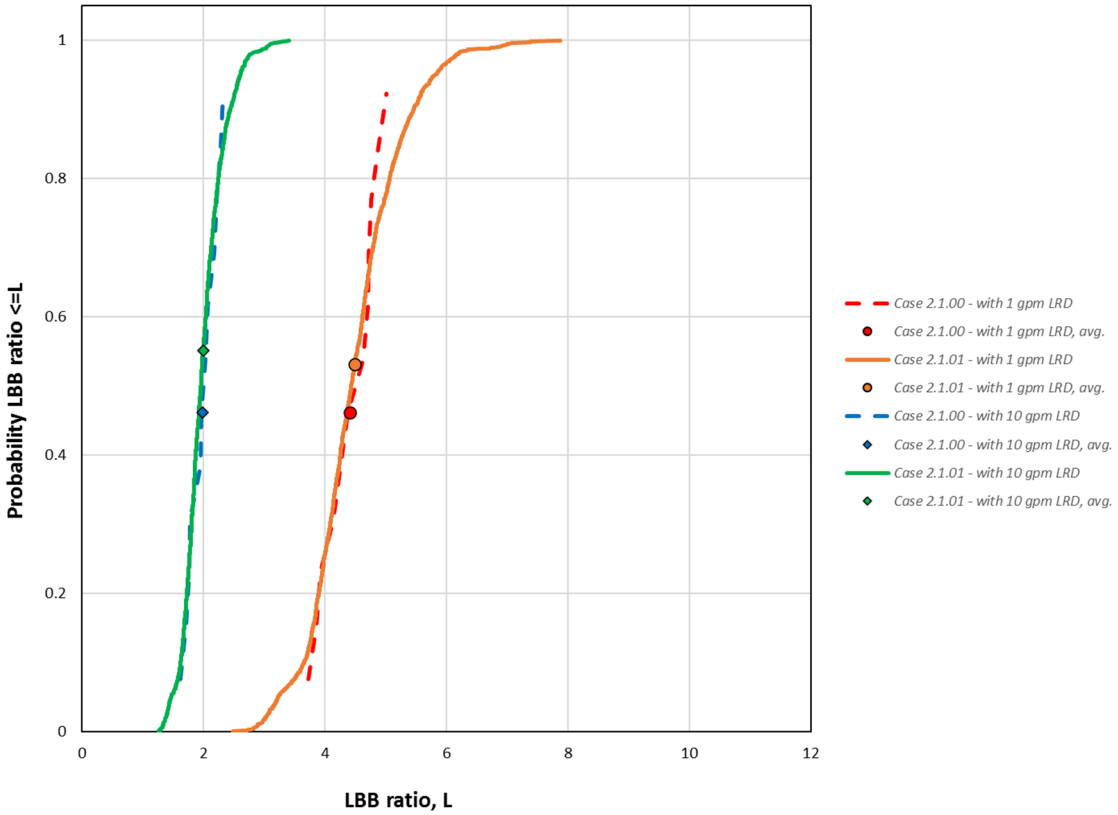

Figure 3-20 Case 2.1.1 LBB ratio results

3.3.2.2.5 Standard Indicators

Figure 3-21 shows the probabilities of first leak for Case 2.1.1 as compared with Case 1.1.6b. The rapid crack growth over the first 10 EPFY greatly reduces the impact of inspections when conducted every 10 years. More frequent inspections, as are currently required by 10 CFR 50.55a(g)(6)(ii)(F), would show a greater incidence on the results.

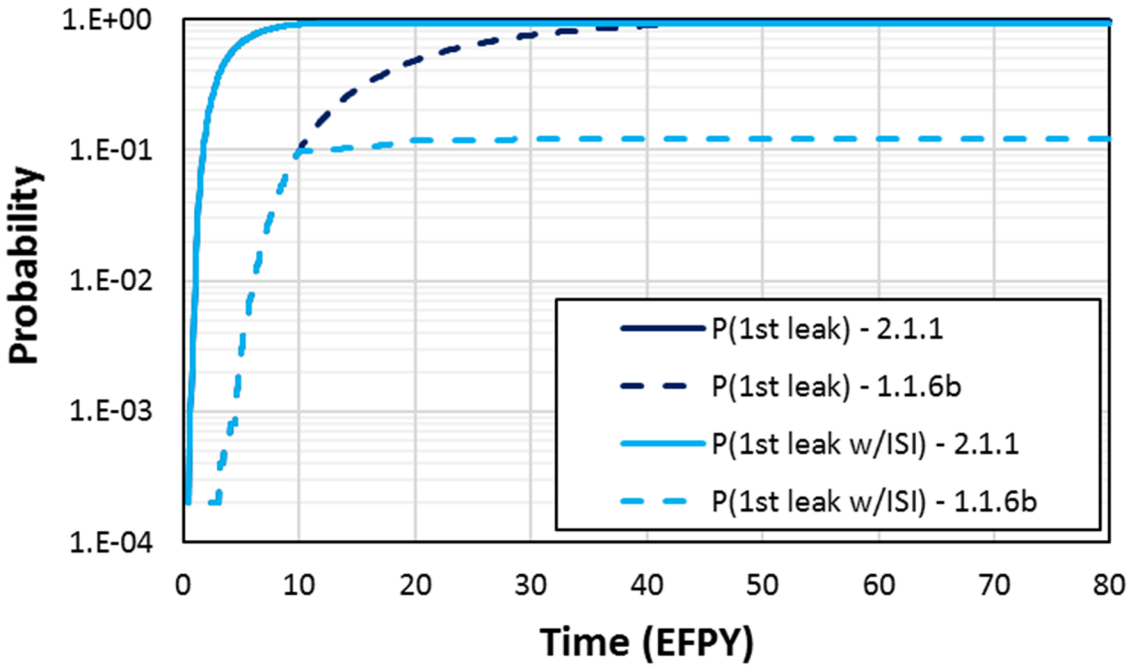

Figure 3-21 Case 2.1.1 time-dependent probabilities of first leak

Figure 3-22 shows the probabilities of rupture for Case 2.1.1 as compared with Case 1.1.6b. In smaller diameter piping, circumferential cracks take less time to reach the critical crack size, which leads to higher probabilities of rupture at earlier times as compared to larger diameter piping, such as the Westinghouse RVON DMW, when every realization starts with an existing circumferential crack. As a result, the probability of rupture with ISI is also higher in Case 2.1.1.

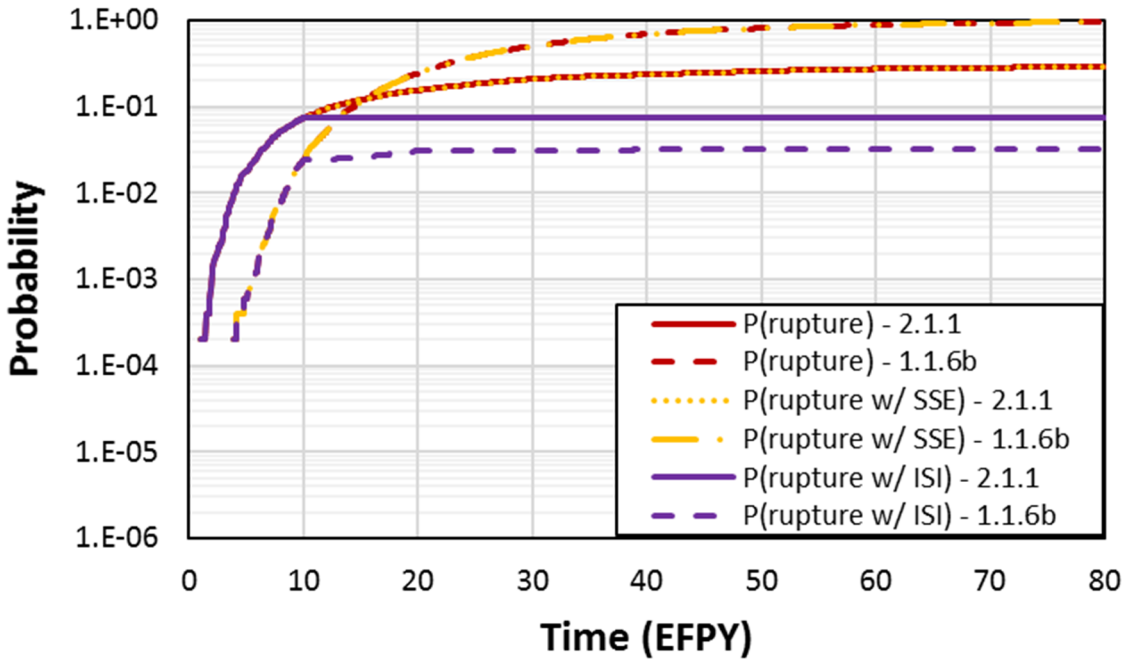

Figure 3-22 Case 2.1.1 time-dependent probabilities of rupture

3.3.2.3 Supplemental Analyses

To illustrate the impact of the pipe diameter on the leak rate, distributions of the circumferential crack leak rates at (a) the time of first circumferential leak occurrence, and (b) the time step before rupture, were estimated and compared to similar distributions from Case 1.1.6b. The Case 2.1.1 results were used instead of the results from Case 2.1.0 because more instances of leakage were generated, and both Figure 3-19 and Figure 3-20 confirm that the two cases lead to similar results. Figure 3-23 shows the distribution of leak rate at the time of first circumferential leak for both Cases 2.1.1 and 1.1.6b. The leak rates for the larger diameter pipe are, on average, about 3 times greater.

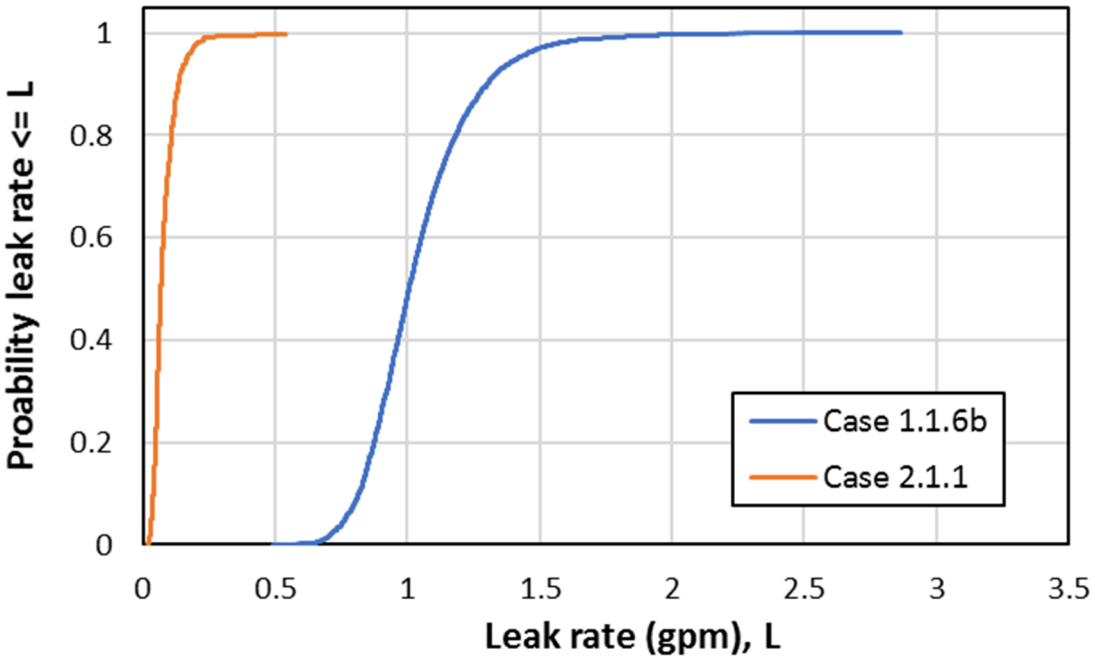

Figure 3-23 Comparison of Cases 2.1.1 and 1.1.6b first circumferential leak rates

Figure 3-24 shows the distribution of leak rate one month before rupture for both Cases 2.1.1 and 1.1.6b. A logarithmic scale is used on the horizontal axis denoting that the difference between the two cases is about two orders of magnitude. This analysis shows that smaller diameter pipes are more sensitive to the detectable leak rate.

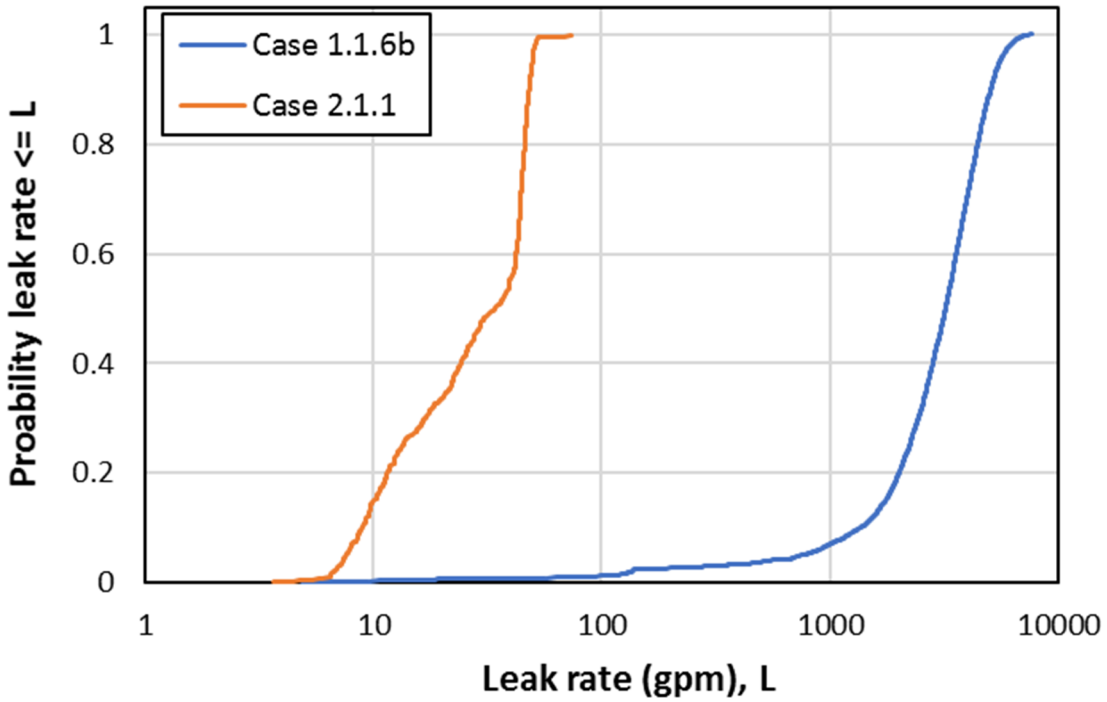

Figure 3-24 Comparison of Cases 2.1.1 and 1.1.6b leak rates one month before rupture

3.3.3 More Severe WRS

3.3.3.1 Case Description

Case 2.1.2 was a sensitivity study of Case 2.1.0 considering a more severe WRS profile. This case used the same inputs as Case 2.1.0 but with a change to the mean hoop and axial WRS profiles. The standard deviations used to represent uncertainties in the WRS profiles were the same as in Case 2.1.0. Figure 3-25 shows the WRS profiles used to analyze the case. These profiles were developed using the same FEA that was used to develop the WRS profiles for Case 2.1.0; however, for Case 2.1.2, the WRS profiles were extracted from the weld butter rather than from the weld centerline. The WRS profile is considered more severe because the higher inside diameter stress favors PWSCC initiation, which has been shown through prior sensitivity analyses to have a large influence on the probability of rupture as documented in TLR-RES/DE/CIB-2021-11, "Sensitivity Studies and Analyses Involving the Extremely Low Probability of Rupture Code," issued May 14, 2021 [51]. Additional details on development of the WRS profiles are in Section C2.2. Section B6 describes the specific inputs and other simulation details used to analyze the case.

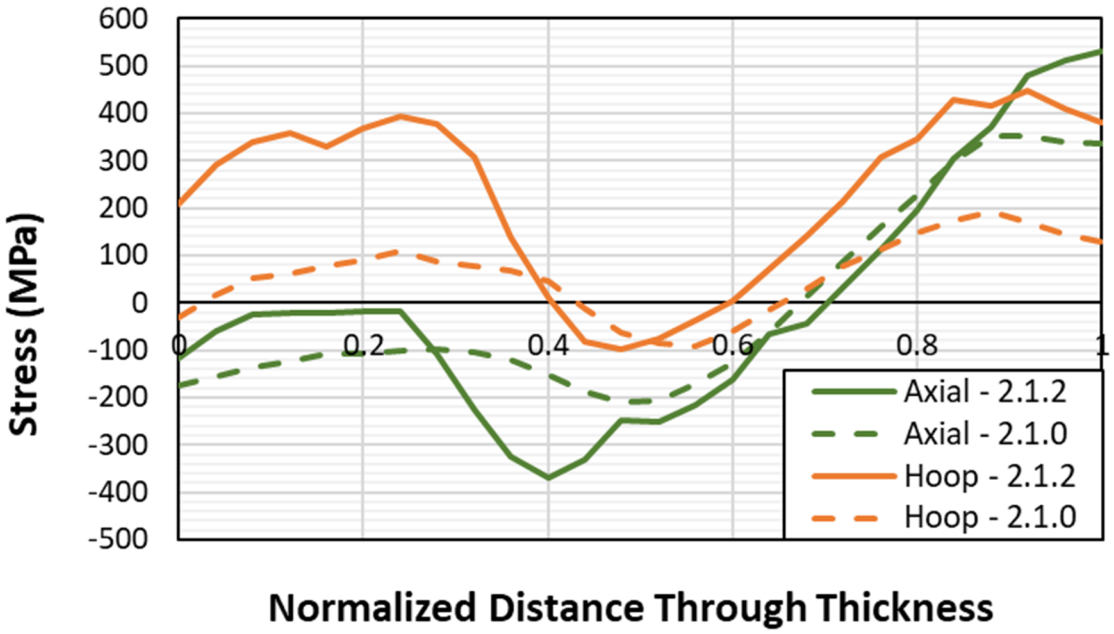

Figure 3-25 Case 2.1.2 WRS Profiles

3.3.3.2 Results and Analysis

3.3.3.2.1 Probability of Rupture with Detection

There were no ruptures with a 1 gpm leak rate detection capability for this case.

3.3.3.2.2 Leak Rate Jump

There were no leak rate jump events for this case.

3.3.3.2.3 LBB Time Lapse

The mean LBB time lapses and standard errors with 1 and 10 gpm leak rate detection capabilities were respectively as follows:

- 4.58 ± 0.22 months (minimum observed: 1 month)
- 1.30 ± 0.08 months (minimum observed: 0 month)

Note that all results beyond 12 EFPY have been excluded for the reasons explained in Section 3.2.1.2.3.

Figure 3-26 shows the LBB time lapse CDF plots for Case 2.1.2. As compared to the Case 2.1.1 results, the LBB time lapse is reduced when the more severe WRS profile is used, especially for a 1 gpm leak rate detection capability.

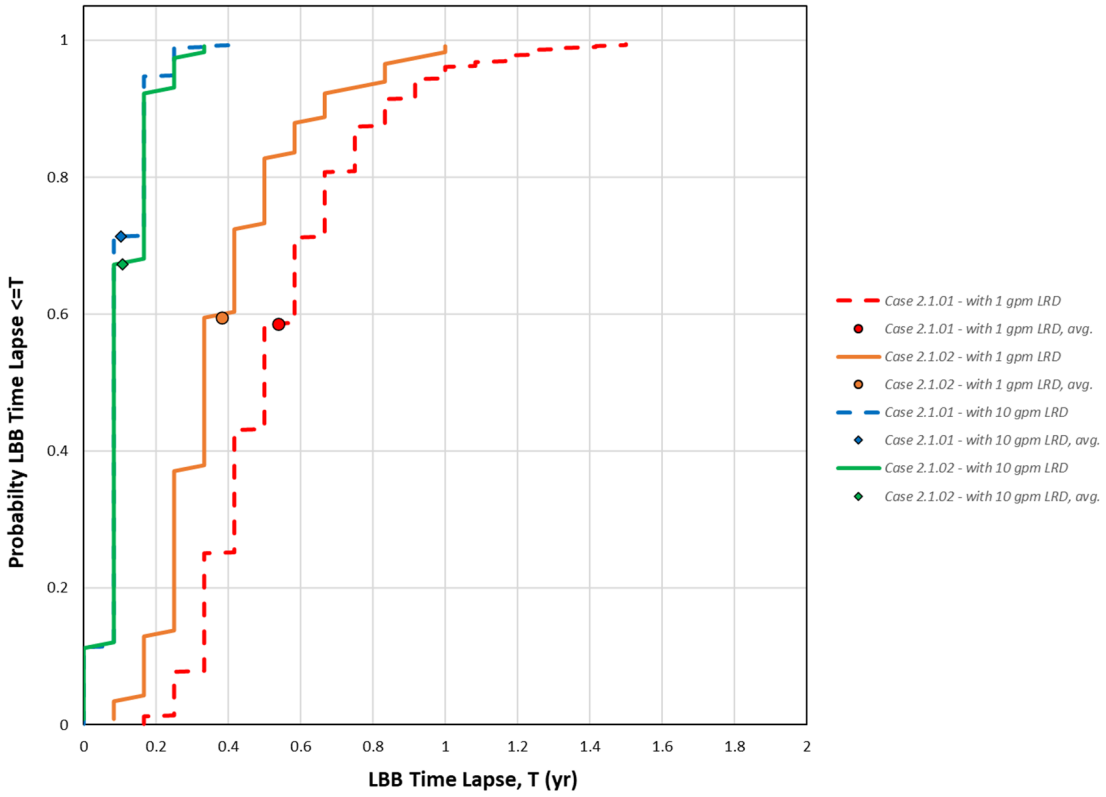

Figure 3-26 Case 2.1.2 LBB lapse time results

3.3.3.2.4 LBB Ratio

The mean LBB ratios and standard errors with 1 and 10 gpm leak rate detection capabilities were respectively as follows:

- 3.70 ± 0.07 (minimum observed: 1.95)
- 2.01 ± 0.03 (minimum observed: 1.43)

Figure 3-27 shows the LBB ratio CDF plots for Case 2.1.2. As compared to the Case 2.1.1 results, the LBB ratios for a 1 gpm leak rate detection capability are lower with the more severe WRS profile.

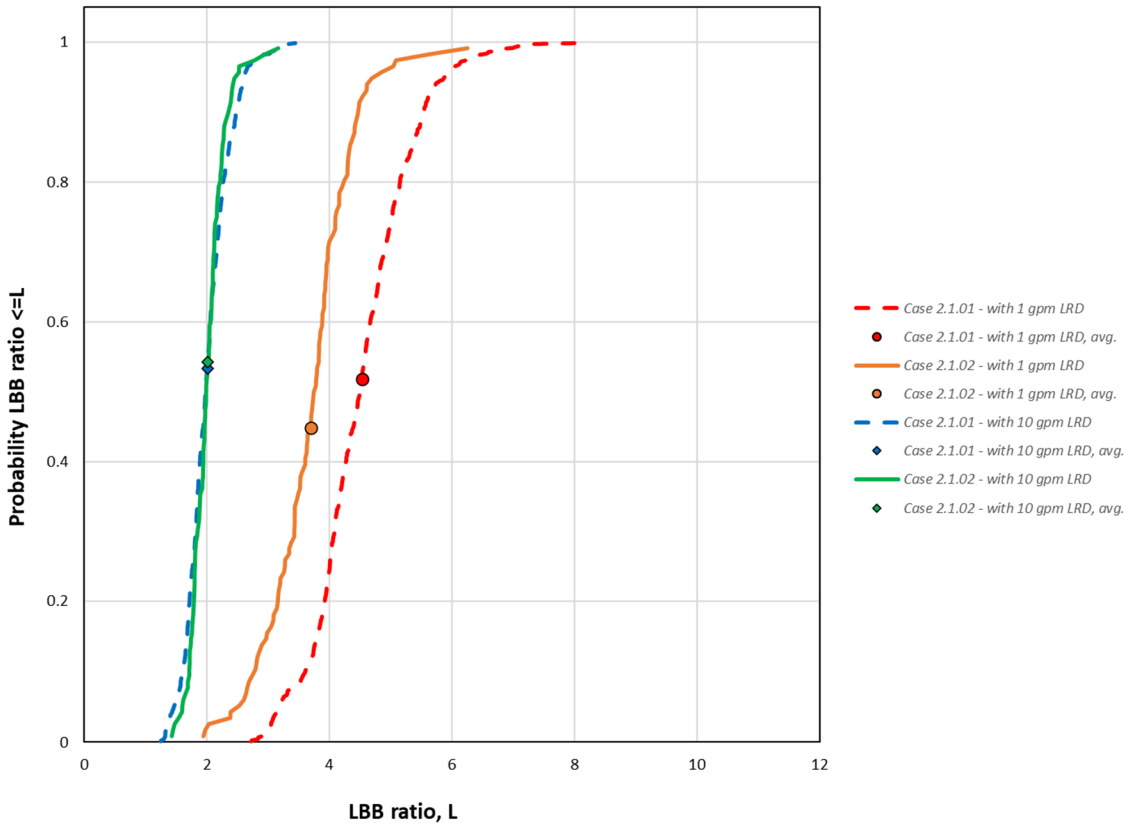

Figure 3-27 Case 2.1.2 LBB ratio results

3.3.3.2.5 Standard Indicators

Figure 3-28 shows the probabilities of first crack for Case 2.1.2 as compared with Case 2.1.0. The more severe WRS profile in Case 2.1.2 leads to increases in both the probabilities of first crack and first circumferential crack.

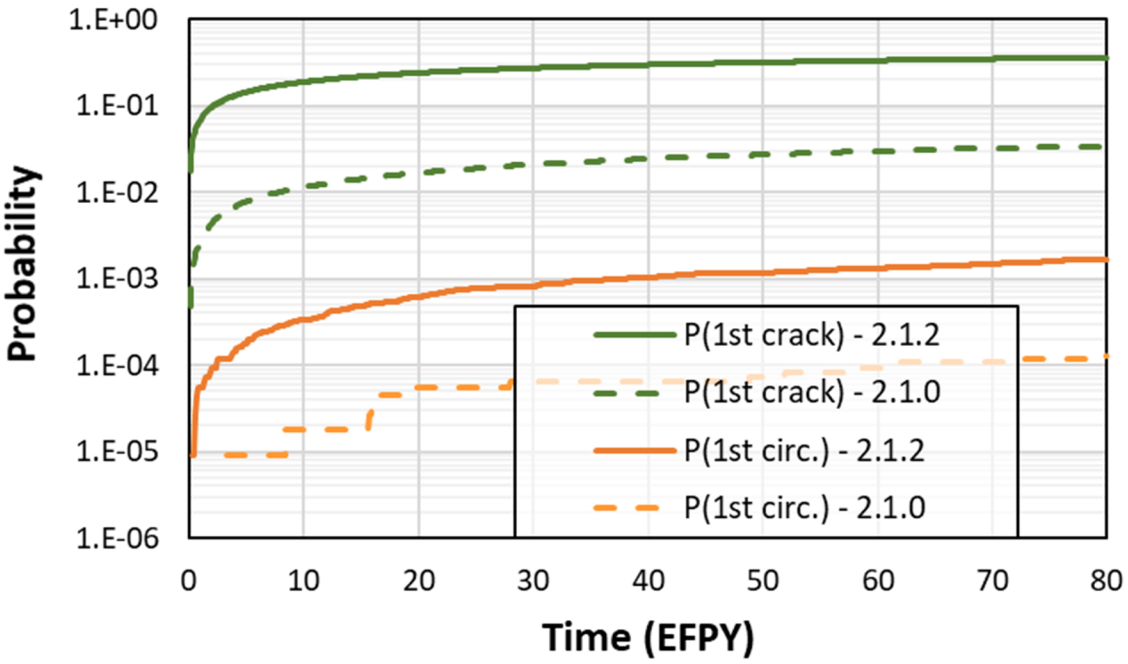

Figure 3-28 Case 2.1.2 time-dependent probabilities of first crack

Figure 3-29 shows the probabilities of first leak for Case 2.1.2 as compared with Case 2.1.0. As with the probabilities of first crack, the probabilities of first leak are greater by roughly one order of magnitude.

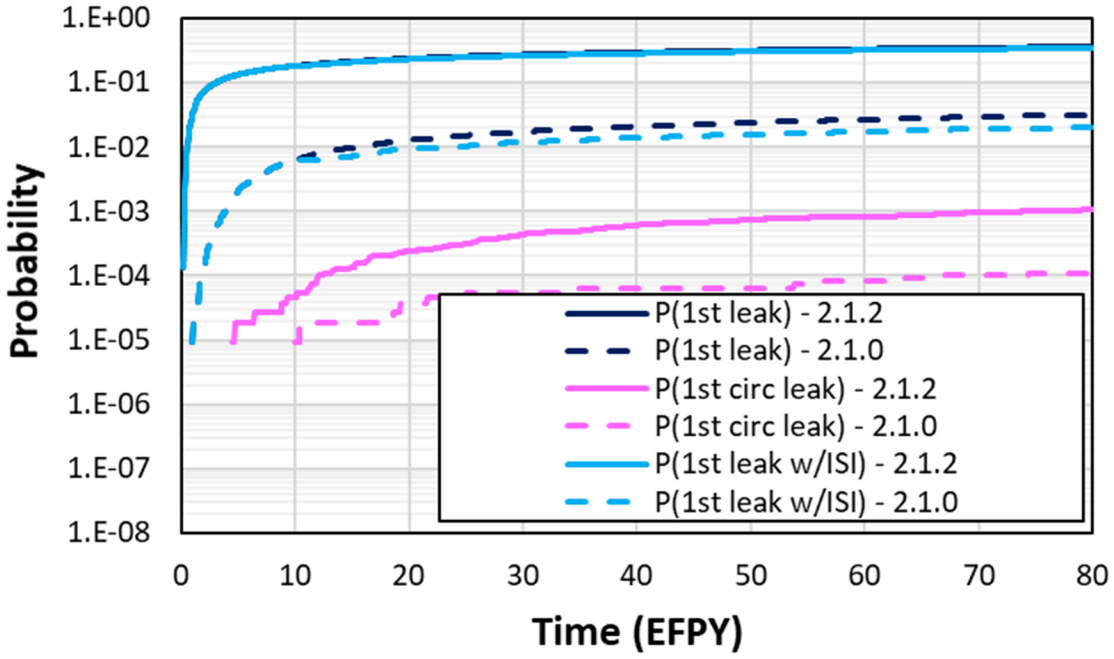

Figure 3-29 Case 2.1.2 time-dependent probabilities of first leak

Figure 3-30 shows the probabilities of rupture for Case 2.1.2 as compared with Case 2.1.0. The probabilities for Case 2.1.2 are more than one order of magnitude lower.

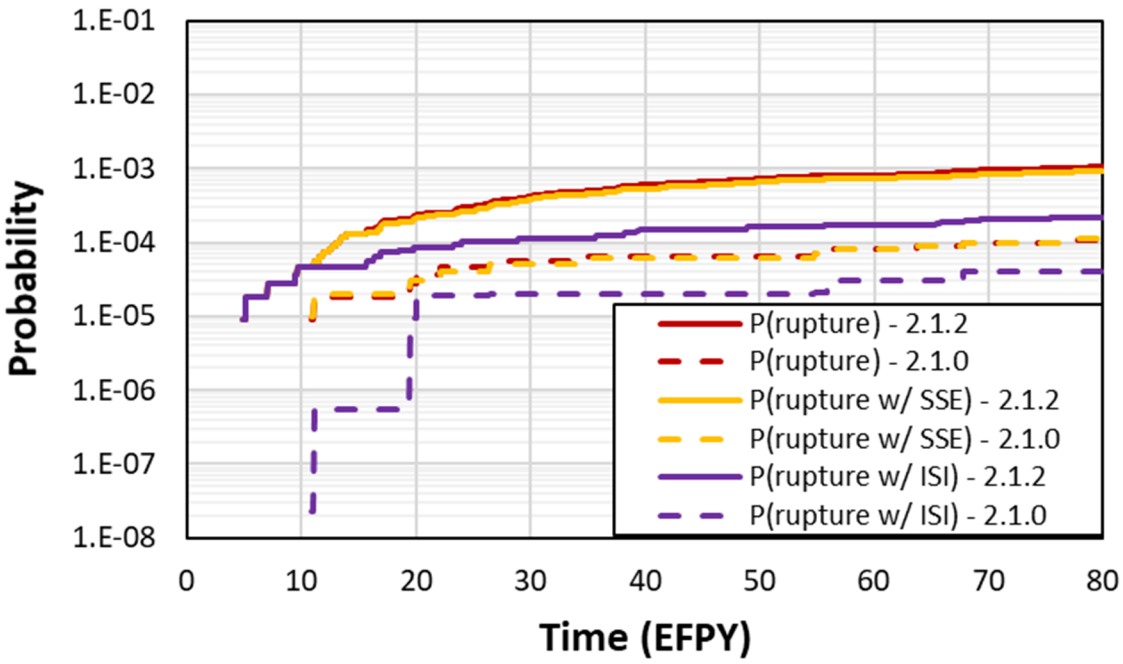

Figure 3-30 Case 2.1.2 time-dependent probabilities of rupture

3.3.4 Overlay Mitigation

3.3.4.1 Case Description

Case 2.1.3 was a sensitivity study of Case 2.1.0 considering overlay mitigation. Most of the pressurizer surge line nozzle DMWs represented by Bin 2 have overlays. In the analysis, the overlay was applied at 25 EFPY based on the average application time for the DMWs represented by Bin 2. The overlay thickness was set to 12.5 centimeters (cm), which was the minimum thickness of all welds represented by the bin. Figure 3-31 shows the WRS profiles used to analyze the case. They were developed by applying the mechanical mitigation rules from the xLPR WRS Subgroup report [47] to the WRS profiles used for Case 2.1.0. Section B7 describes the specific inputs and other simulation details used to analyze the case.

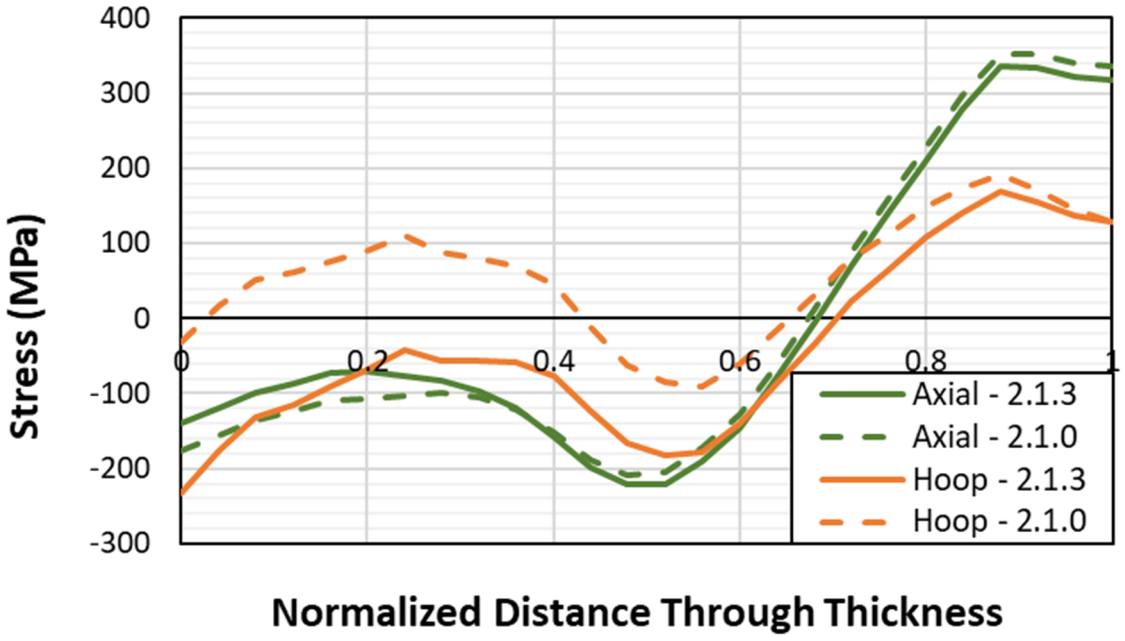

Figure 3-31 Case 2.1.3 WRS profiles

3.3.4.2 Results and Analysis

3.3.4.2.1 Probability of Rupture with Detection

Two out of 100,000 realizations had ruptures with a 1 gpm leak rate detection capability in Case 2.1.3. While it may seem counterintuitive, the application of the overlay is the cause of these ruptures. As modeled in the xLPR code, any existing crack in the original weld material will continue to grow through the weld thickness, and it will not be stopped at the interface between the original weld and the overlay. Thus, the cracks can grow through the PWSCC-susceptible Alloy 82/182 weld to the more PWSCC-resistant Alloy 52/152 overlay. At this point, crack growth in the depth direction slows in the overlay because of the PWSCC growth factor of improvement (FOI), which was set to 324 (i.e., PWSCC growth in the Alloy 52/152 overlay was modeled to occur 324 times more slowly than PWSCC growth in the Alloy 82/182 original weld metal). The FOI of 324 represents the 75th percentile FOI as recommended in EPRI Technical Report 3002010756, "Materials Reliability Program: Recommended Factors of Improvement for Evaluating Primary Water Stress Corrosion Cracking (PWSCC) Growth Rates of Thick-Wall Alloy 690 Materials and Alloy 52, 152, and Variants Welds (MRP 386)," issued December 22, 2017 [52]. However, the faster PWSCC growth continues in the Alloy 82/182 weld around the circumference, and eventually the cracks become unstable when they grow large enough. One of the two cases was because of a surface crack rupture. In the other case, rupture occurred as soon as the crack grew through-wall.

The associated annual frequency of rupture is 2.5 x 10^{-7}, which is below the 1 x 10^{-6} acceptance threshold considered in this study. When the effects of a 10-year inspection frequency are considered, the annual frequency is reduced to 1.25 x 10^{-9} (i.e., essentially zero) after 80 EFPY.

The probability of surface crack rupture when a 10-year inspection frequency is considered is lower than 1.0 x 10^{-10} (i.e., essentially zero). More frequent inspections per ASME Code Case N-770-5, which is currently mandated by 10 CFR 50.55a(g)(6)(ii)(F), would further reduce the probability of surface crack rupture.

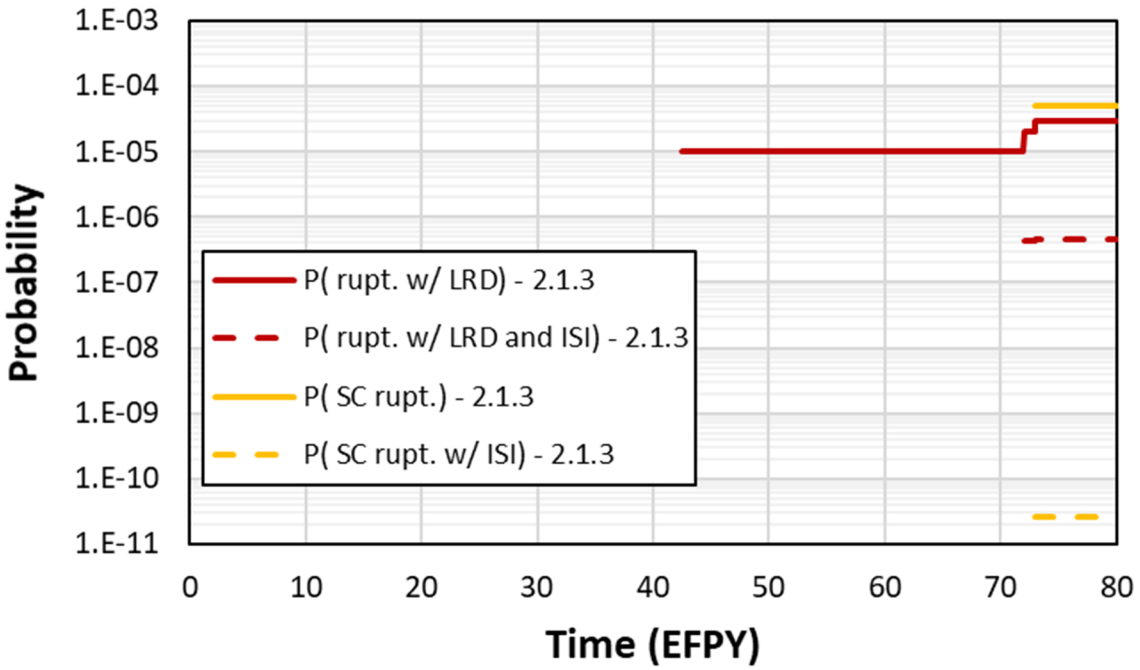

Figure 3-32 Case 2.1.3 time-dependent probabilities of rupture with leak rate detection and ISI

3.3.4.2.2 Leak Rate Jump

Two realizations out of 100,000 had a leak rate jump, giving a probability of leak rate jump of 2 x 10^{-5}. These correspond with the two realizations that had ruptures with leak rate detection as discussed in Section 3.3.4.2.1.

3.3.4.2.3 LBB Time Lapse

The mean LBB time lapses and standard errors with 1 and 10 gpm leak rate detection capabilities were respectively as follows:

- 10.8 ± 5.7 months (minimum observed: 0 month)
- 8.6 ± 4.9 months (minimum observed: 0 month)

Note that all results beyond 12 EFPY have been excluded for the reasons explained in Section 3.2.1.2.3.

Figure 3-33 shows the LBB time lapse CDF plots for Case 2.1.3. The low number of ruptures does not allow for an accurate representation of the CDF. However, the tendencies are to have

(a) a shorter LBB time lapse when the rupture occurs before 25 EFPY when the overlay is applied, and (b) a longer LBB time lapse for the few ruptures that occur after 25 EFPY.

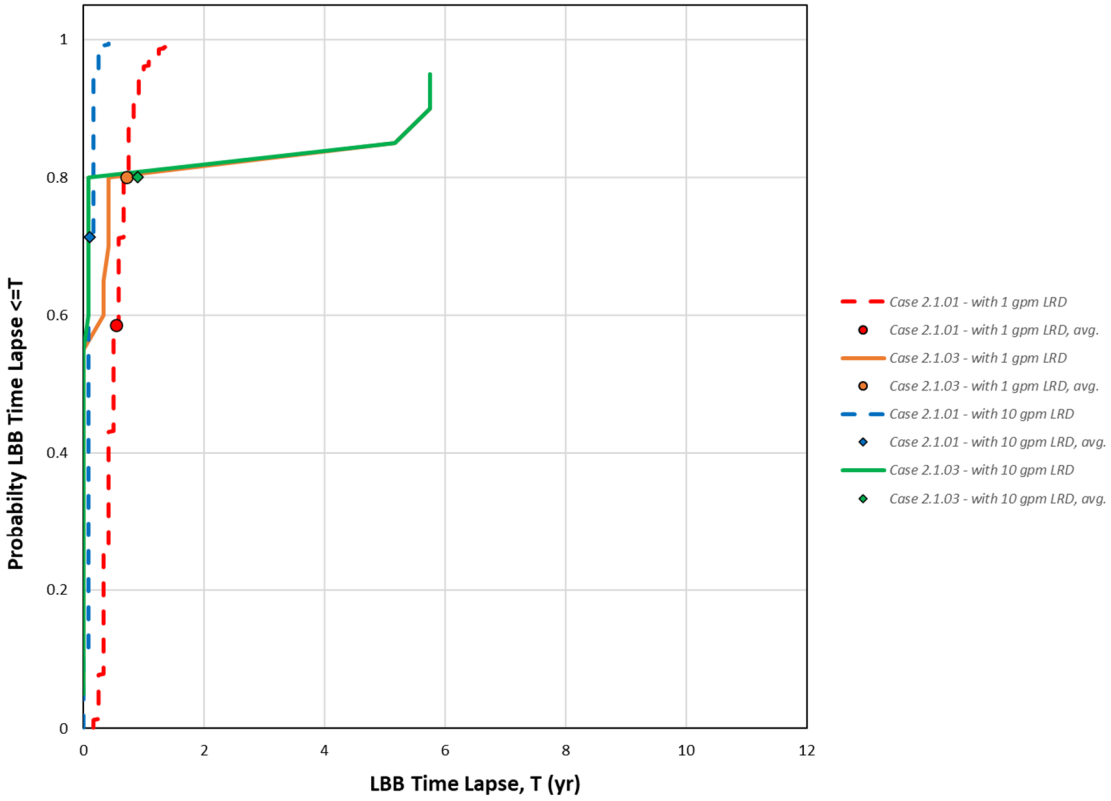

Figure 3-33 Case 2.1.3 LBB time lapse results

3.3.4.2.4 LBB Ratio

The mean LBB ratios and standard errors with 1 and 10 gpm leak rate detection capabilities were respectively as follows:

- 2.06 ± 0.35 (minimum observed: 0.85)
- 1.39 ± 0.11 (minimum observed: 0.85)

Figure 3-34 shows the LBB ratio CDF plots for Case 2.1.3. The low number of ruptures does not provide an accurate representation of the CDF. The distributions are lower as compared to Case 2.1.0 because most of the higher LBB ratios in Case 2.1.0 happen at later times.

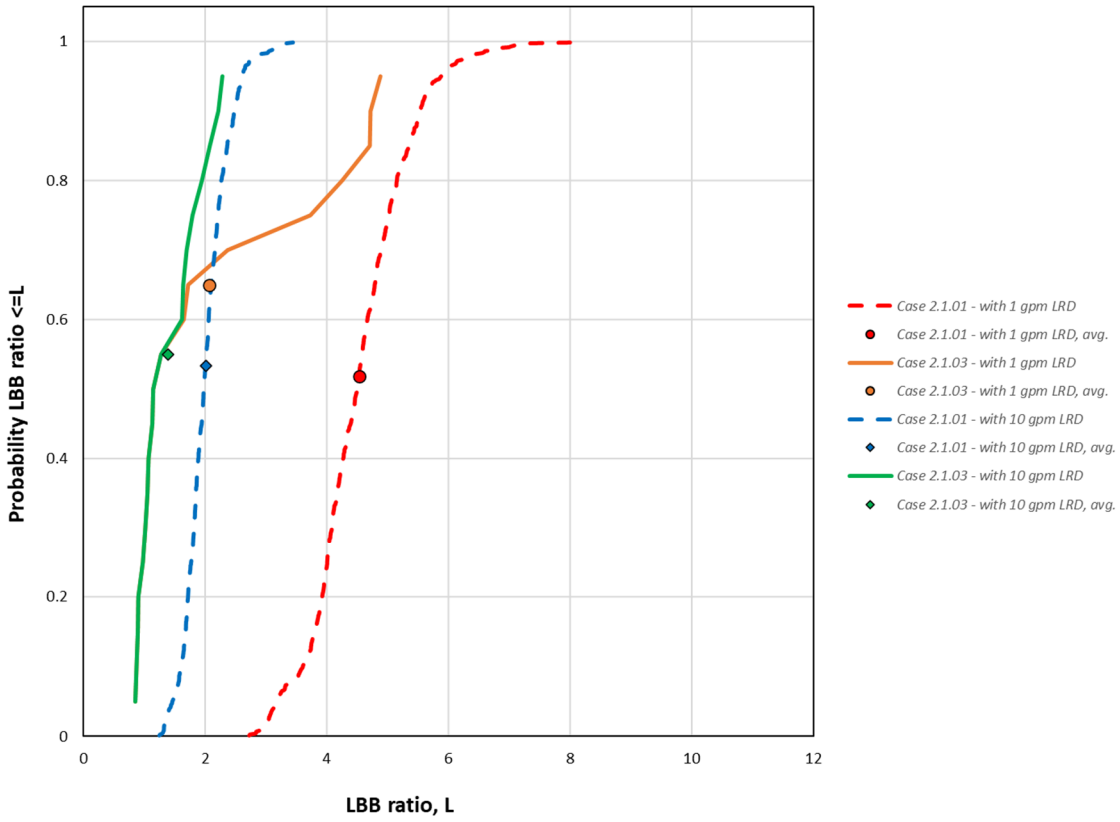

Figure 3-34 Case 2.1.3 LBB ratio results

3.3.4.2.5 Standard Indicators

Figure 3-35 shows the probabilities of first crack for Case 2.1.3 as compared to Case 2.1.0. The overlay applied at 25 EFPY is too late to have much effect on the overall probability of first crack, whereas it leads to an increase in the probability of first circumferential crack.

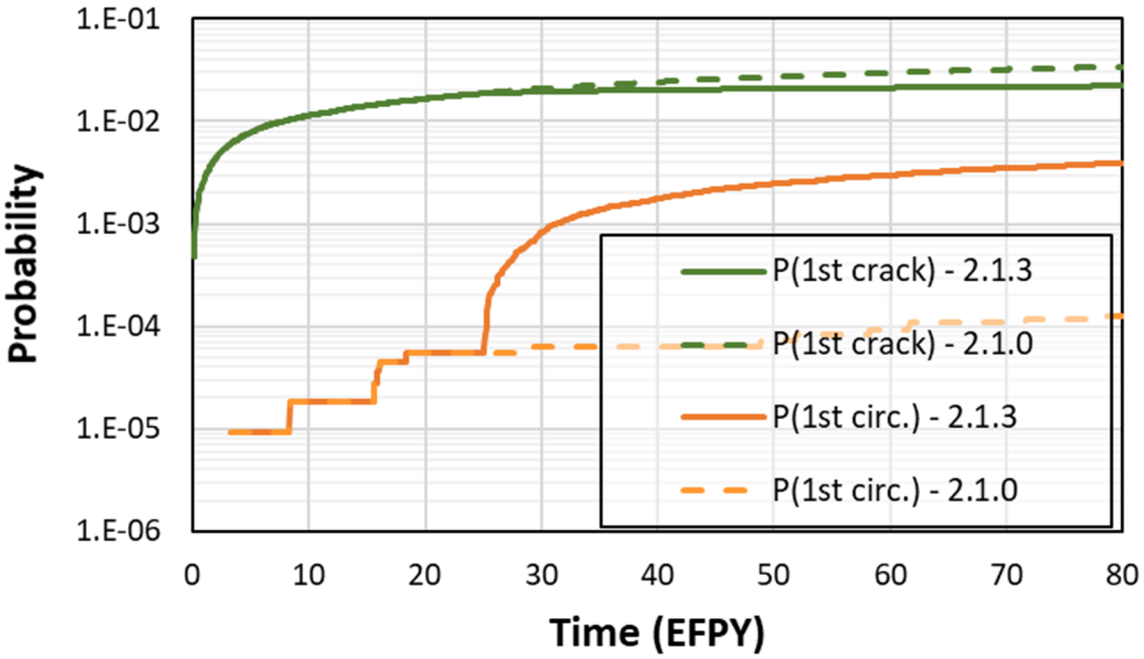

Figure 3-35 Case 2.1.3 time-dependent probabilities of first crack

Figure 3-36 shows the probabilities of first leak for Case 2.1.3 as compared with Case 2.1.0. The impact of the overlay on the probability of first leak is strong, which leads to a strong delay for the increase in crack size. The decrease in probability is because of the repair of any TWCs when the overlay is applied. The increase in circumferential crack leakage is consistent with the increase in circumferential crack initiation. However, the overlay delays the occurrence of leakage because of slower crack growth in the depth direction when cracks reach the overlay. As a result, even though there is a factor of 40 difference in circumferential crack initiation, there is only a factor of 3 difference in circumferential crack leak.

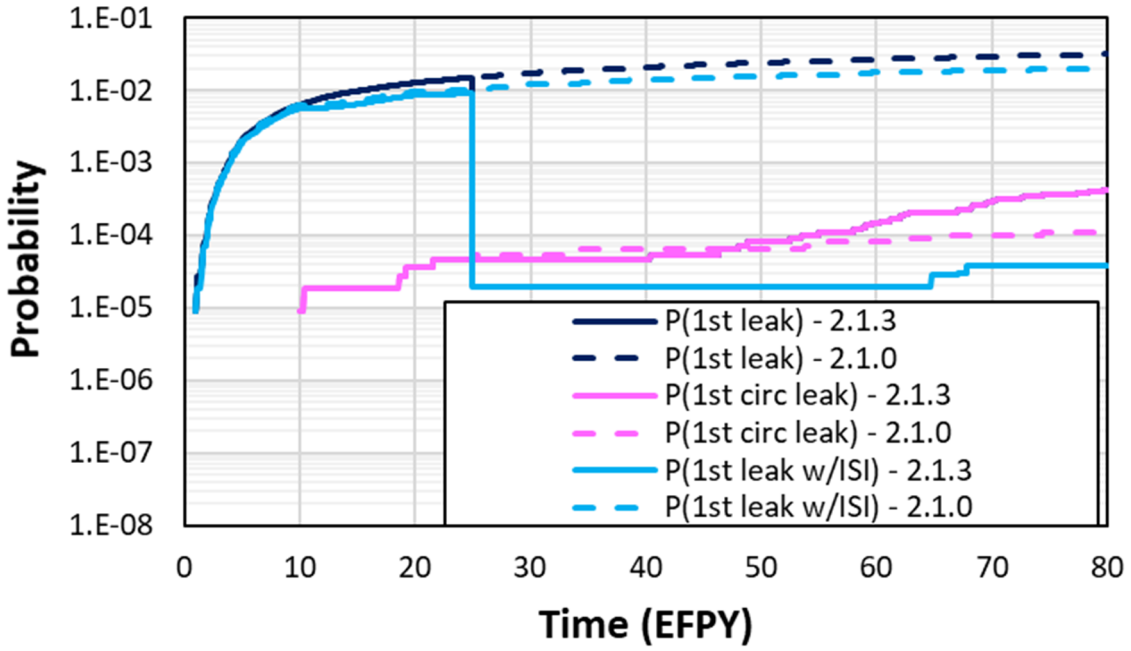

Figure 3-36 Case 2.1.3 time-dependent probabilities of first leak

Figure 3-37 shows the probabilities of rupture for Case 2.1.3 as compared to Case 2.1.0. The probabilities increase slightly for Case 2.1.3, but they remain low.

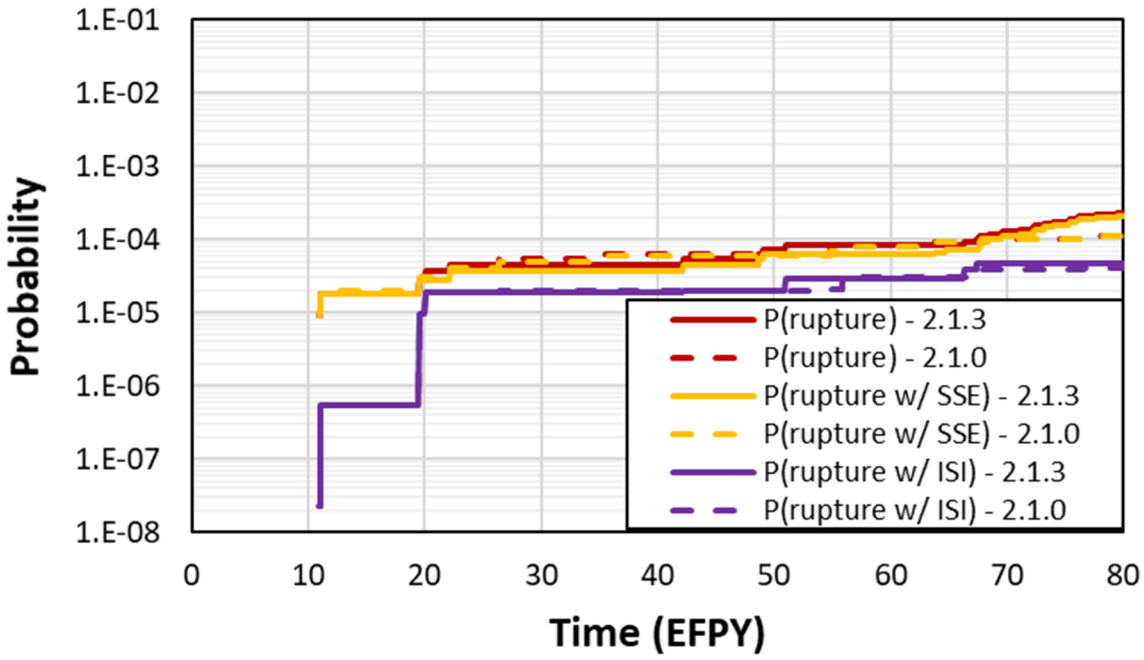

Figure 3-37 Case 2.1.3 time-dependent probabilities of rupture

3.3.5 Fatigue

3.3.5.1 Case Description

The objective of Case 2.1.4 was to assess the base likelihood of failure caused by fatigue initiation and growth without mechanical mitigation. The fatigue crack initiation and growth parameters used for the analysis were from the xLPR Inputs Group report [53]. The transient definitions were developed based on information from the following reports:

- Structural Integrity Associates, Inc., SIR-98-096, "Pressurizer Surge Line Leak-Before-Break Evaluation Millstone Nuclear Power Station, Unit 2," issued October 1998 [21]
- Structural Integrity Associates, Inc., Report No. 1301103.401, "Flaw Tolerance Evaluation of St. Lucie Surge Line Welds Using ASME Code Section XI, Appendix L," issued May 2015 [54]
- Structural Integrity Associates, Inc., Report No. 1100756.401, Revision 1, "Flaw Tolerance Evaluation of Turkey Point Surge Line Welds Using ASME Code Section XI, Appendix L," issued May 2012 [55]

Based on conversations with EPRI and Westinghouse Electric Company personnel, it was concluded that these transients would be sufficient to gain an understanding of the effects of fatigue on Westinghouse pressurizer surge line nozzle DMWs. The WRS profiles were the same as in the Case 2.1.0 analysis. Section B8 describes the specific inputs and other simulation details used to analyze the case.

3.3.5.2 Results and Analysis

3.3.5.2.1 Probability of Rupture with Detection

There were no ruptures with a 1 gpm leak rate detection capability for this case.

3.3.5.2.2 Leak Rate Jump

There were no leak rate jump events for this case.

3.3.5.2.3 LBB Time Lapse

The mean LBB time lapses and standard errors with 1 and 10 gpm leak rate detection capabilities were respectively as follows:

- 2.45 ± 0.28 months (minimum observed: 1 month)
- 0.73 ± 0.14 months (minimum observed: 0 month)

Note that all results beyond 12 EFPY have been excluded for the reasons explained in Section 3.2.1.2.3.

Figure 3-38 shows the LBB time lapse CDF plots for Case 2.1.4. As observed for the fatigue and PWSCC sensitivity study case in the prior study (i.e., Case 1.1.15), fatigue accelerates

crack growth especially for deep surface cracks or TWCs. Thus, the time from detectable leak to rupture is reduced.

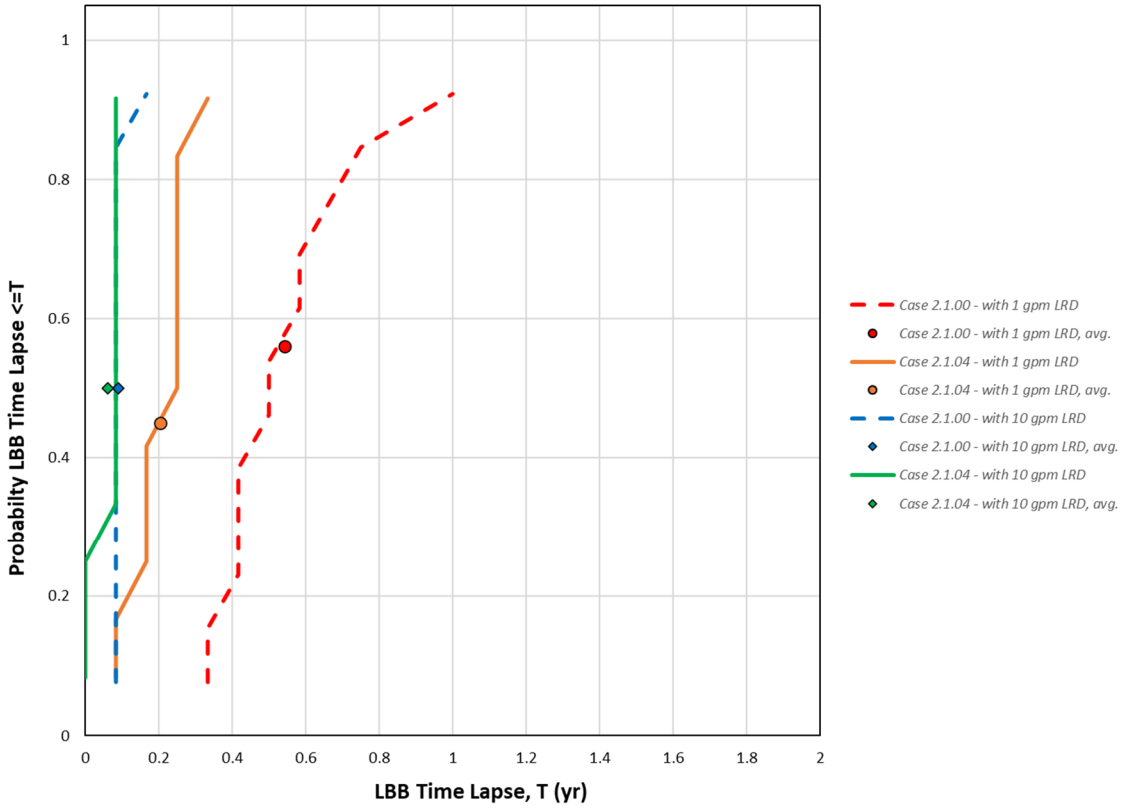

Figure 3-38 Case 2.1.4 LBB lapse time results

3.3.5.2.4 LBB Ratio

The mean LBB ratios and standard errors with 1 and 10 gpm leak rate detection capabilities were respectively as follows:

- 4.85 ± 0.67 (minimum observed: 3.28)
- 2.49 ± 0.48 (minimum observed: 1.33)

Figure 3-39 shows the LBB ratio CDF plots for Case 2.1.4. Fatigue does not affect the crack size required for a given leak rate, nor does it impact the critical crack size for rupture; therefore, the LBB ratio is not affected. The change in LBB ratio is simply due to the larger size of the crack when it ruptures due to faster crack growth. This leads to inaccuracy in the calculation of the critical crack size, which affects the LBB ratio calculation.

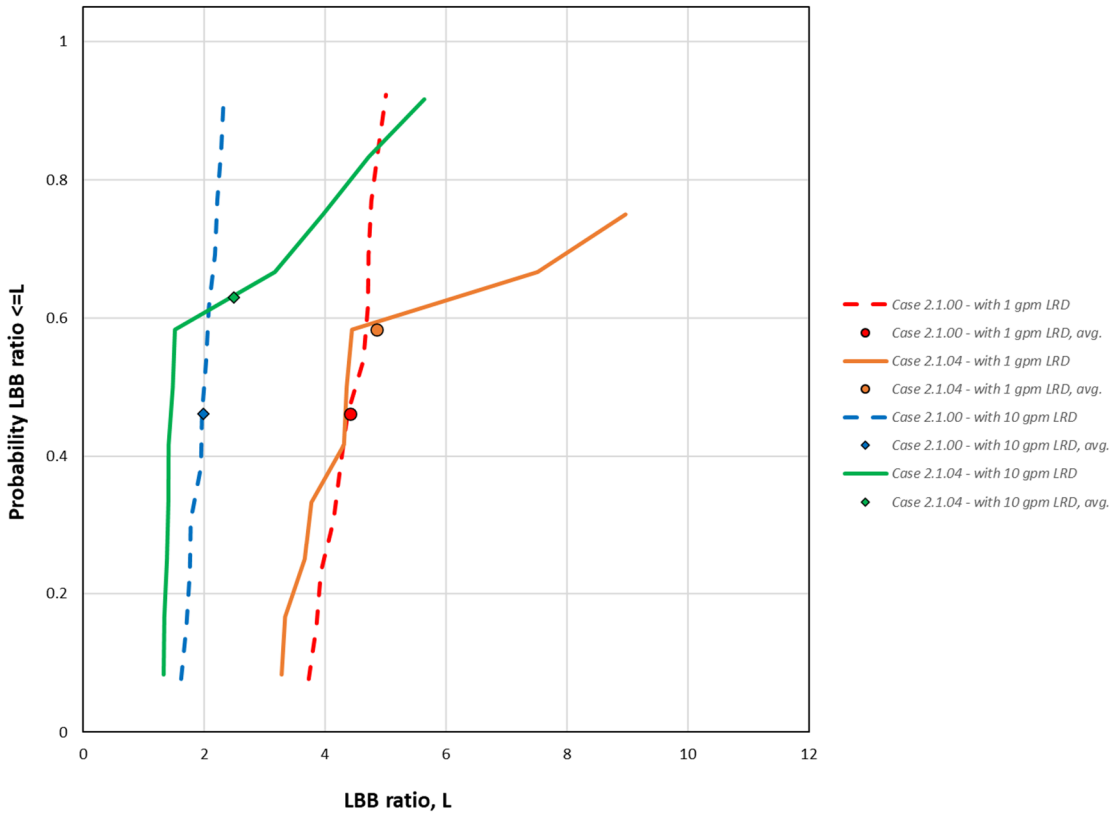

Figure 3-39 Case 2.1.4 LBB ratio results

3.3.5.2.5 Standard Indicators

Figure 3-40 shows the probabilities of first crack from Case 2.1.4. The results are essentially identical to Case 2.1.0, which indicates that fatigue does not cause additional crack initiations. All the crack initiations are because of PWSCC.

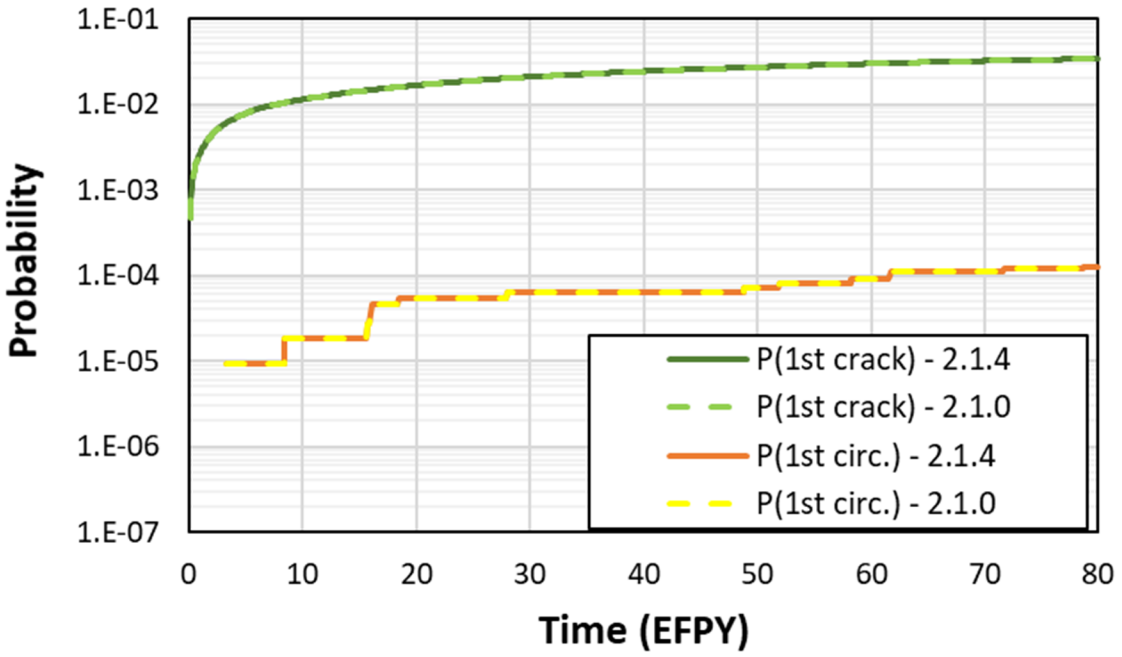

Figure 3-40 Case 2.1.4 time-dependent probabilities of first crack

Figure 3-41 shows the probabilities of first leak for Case 2.1.4. These results are virtually identical to Case 2.1.0, which indicates that fatigue does not impact the probabilities of first leak.

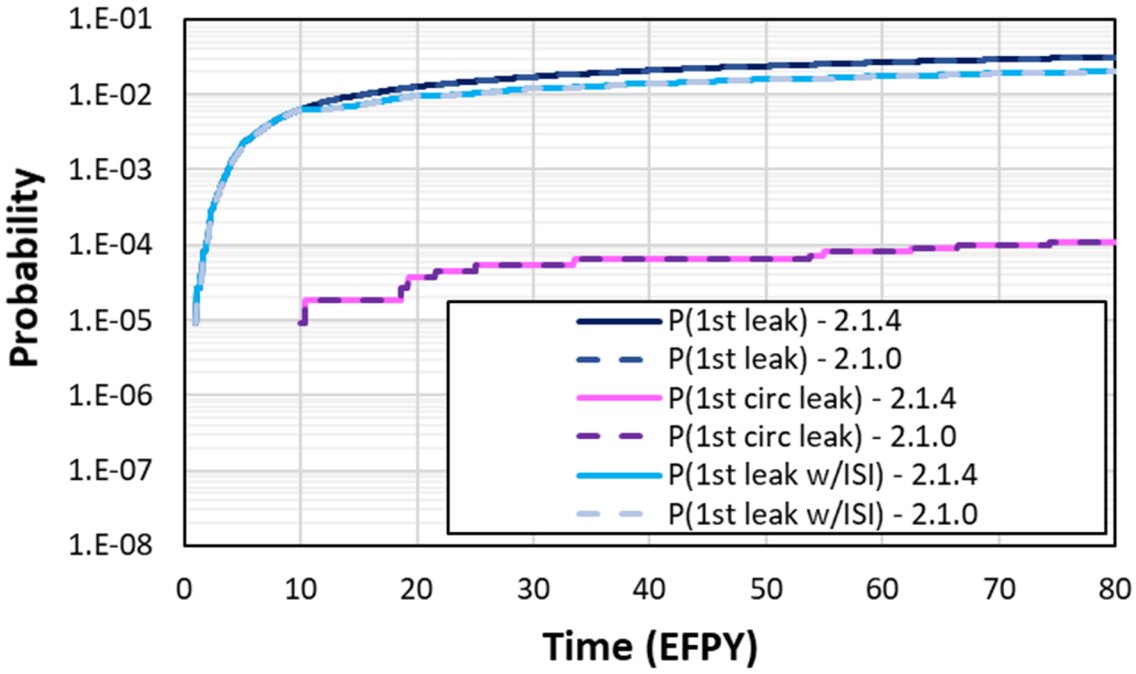

Figure 3-41 Case 2.1.4 time-dependent probabilities of first leak

Figure 3-42 shows the probabilities of rupture for Case 2.1.4. The addition of fatigue should only increase the probability of rupture. One realization was counted as an SSE rupture when

fatigue was added. A close examination of the results revealed that the normalized outer half-length had a value of 2 or more, as if the outer crack length was twice the circumference, which is not physically possible. It appears from these results that the fatigue mechanisms cause crack growth that is not expected by the xLPR code. This issue was referred to the maintenance process for further investigation and correction.

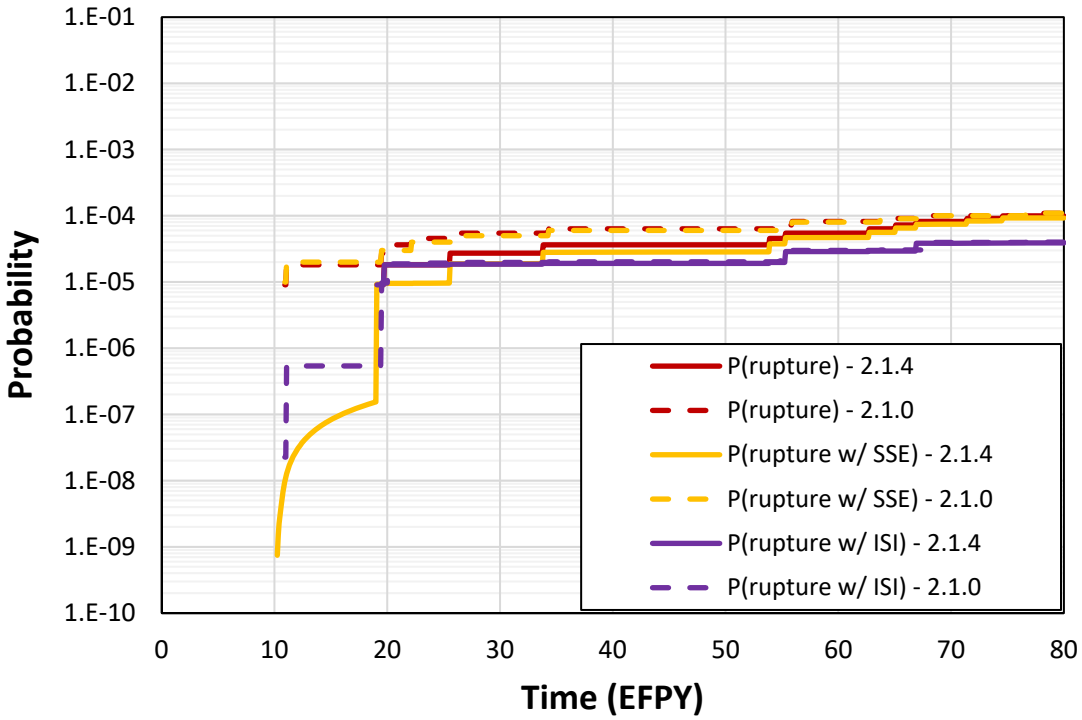

Figure 3-42 Case 2.1.4 time-dependent probabilities of rupture

3.3.6 MSIP® Mitigation

3.3.6.1 Case Description

Case 2.1.5 was a sensitivity study of Case 2.1.0 considering MSIP® mitigation. MSIP® was applied at 12 EFPY, which was the latest time of MSIP® application for the welds represented by the bin. Figure 3-43 shows the WRS profiles used to analyze the case. They were developed using rules from the xLPR WRS Subgroup report [47] and applied to the WRS profile used for the Case 2.1.0 analysis. Section B9 describes the specific inputs and other simulation details used to analyze the case.

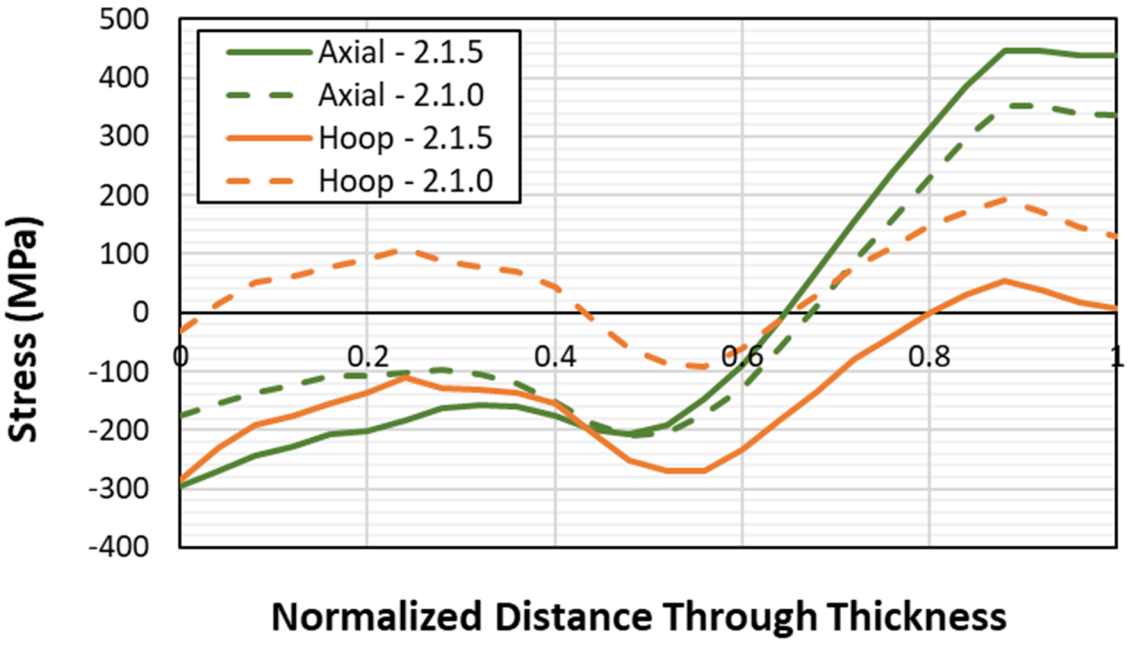

Figure 3-43 Case 2.1.5 WRS profiles

3.3.6.2 Results and Analysis

3.3.6.2.1 Probability of Rupture with Detection

There were no ruptures with a 1 gpm leak rate detection capability for this case

3.3.6.2.2 Leak Rate Jump

There were no leak rate jump events for this case.

3.3.6.2.3 LBB Time Lapse

The mean LBB time lapses and standard errors with 1 and 10 gpm leak rate detection. capabilities were respectively as follows:

- 4.5 ± 0.5 months (minimum observed: 4 months)
- 1.0 ± 0.0 month (minimum observed: 1 month)

Since only 2 out of 100,000 realizations led to rupture in this case, these numbers are included for completeness but should not be used to draw any conclusions.

Figure 3-44 shows the LBB time lapse CDF plots for Case 2.1.5. Due to the limited number of ruptures before MSIP® application, the CDFs are linear and rough; however, they follow the same trends as in Case 2.1.1.

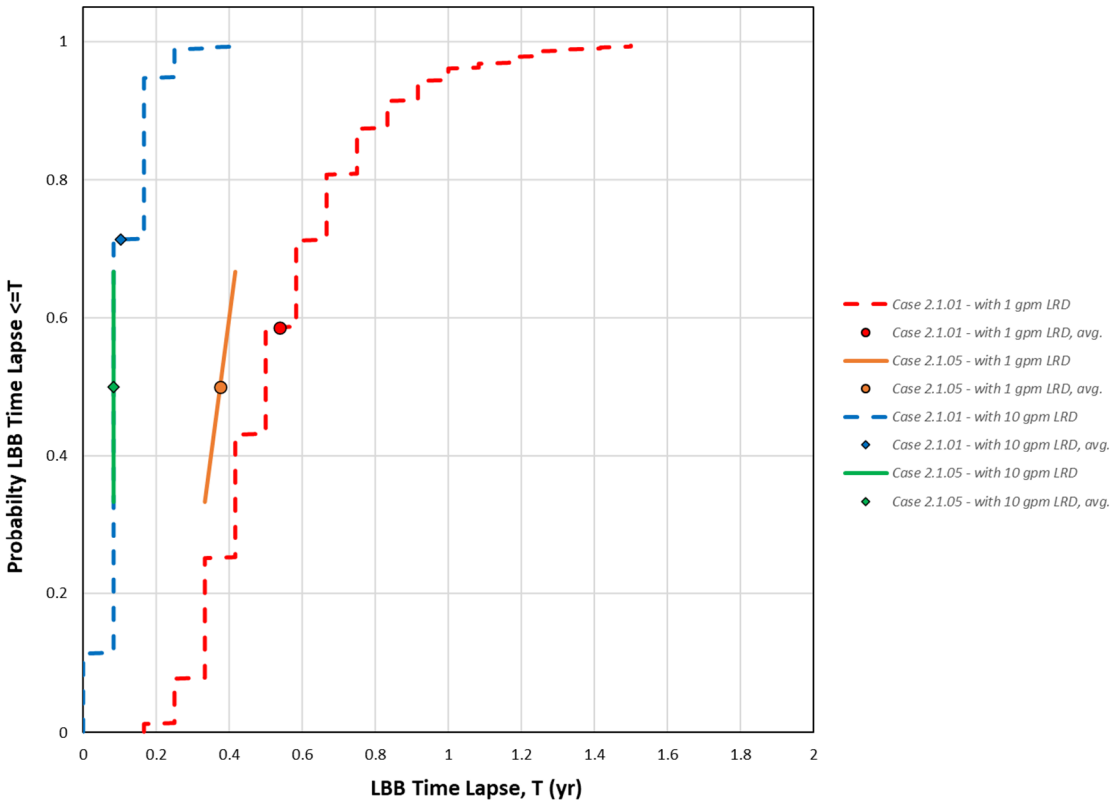

Figure 3-44 Case 2.1.5 LBB time lapse results

3.3.6.2.4 LBB Ratio

The mean LBB ratios and standard errors with 1 and 10 gpm leak rate detection capabilities were respectively as follows:

- 4.49 ± 0.23 (minimum observed: 4.25)
- 2.12 ± 0.17 (minimum observed: 1.95)

Like the LBB time lapse results, the mean LBB ratios and CDFs are based on only 2 realizations and are included for completeness only; they should not be used to draw any conclusions. Figure 3-45 shows the LBB ratio CDF plots for Case 2.1.5. As for the LBB lapse time results, the CDFs follow the same trends as Case 2.1.1.

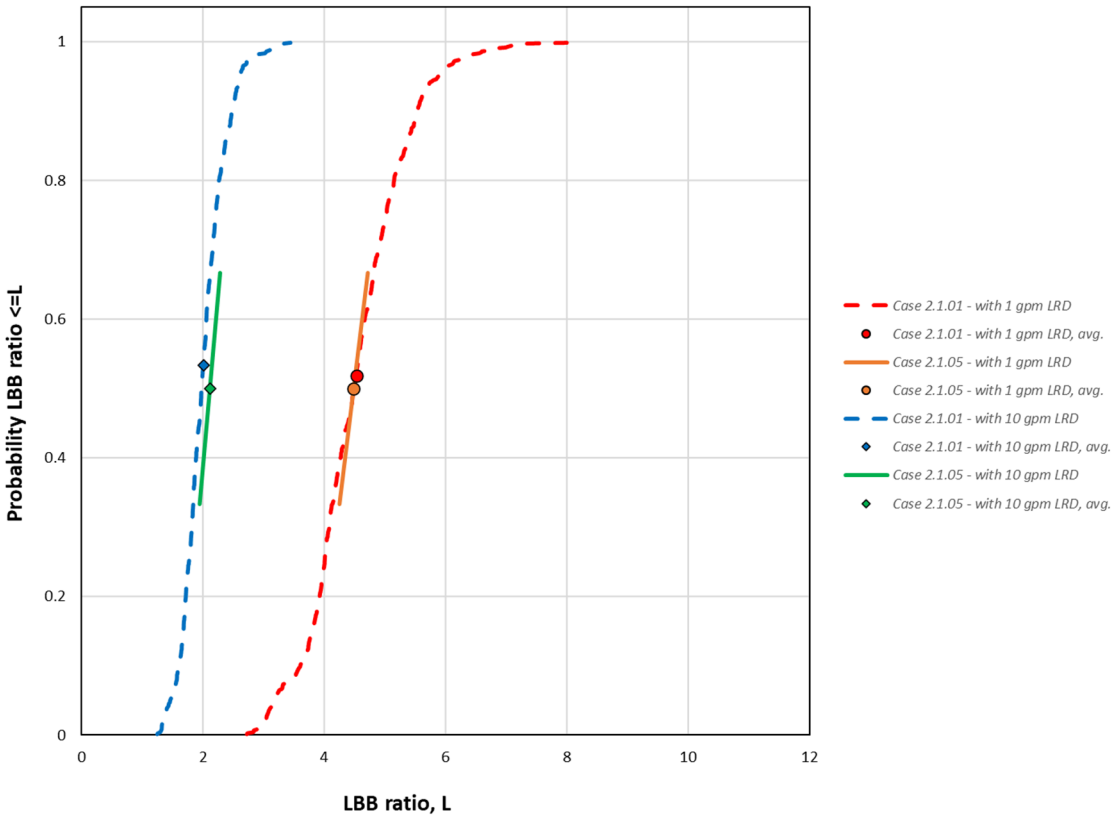

Figure 3-45 Case 2.1.5 LBB ratio results

3.3.6.2.5 Standard Indicators

Figure 3-46 shows the probabilities of first crack for Case 2.1.5 as compared with Case 2.1.0. The MSIP® application at 12 EFPY stops any additional occurrences of both axial and circumferential cracks.

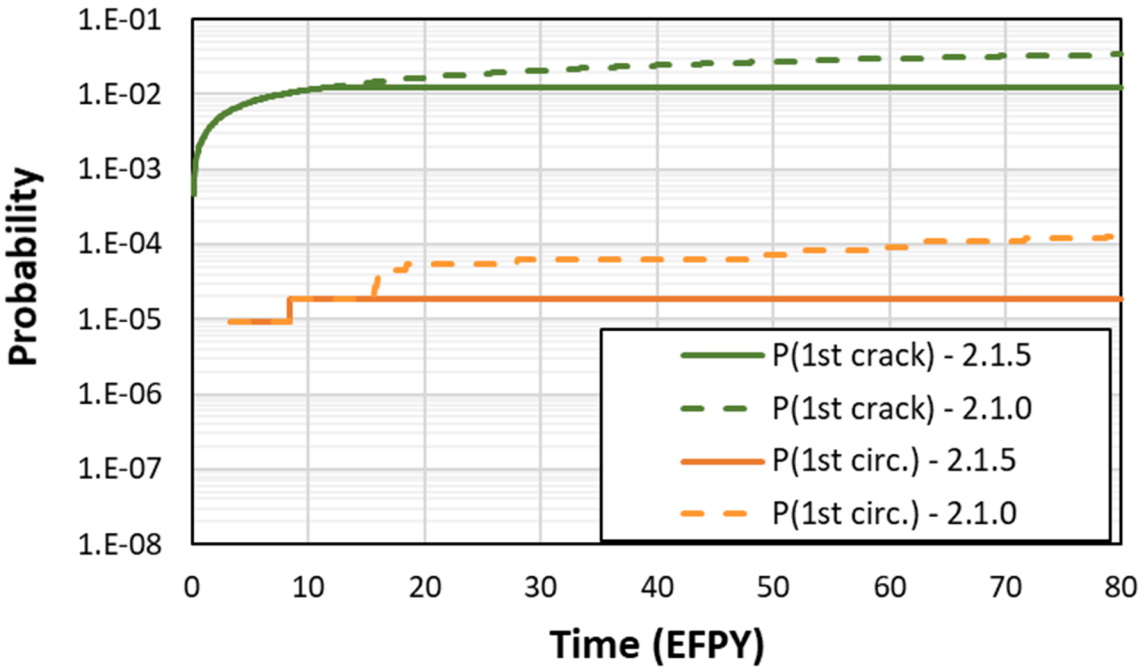

Figure 3-46 Case 2.1.5 time-dependent probabilities of first crack

Figure 3-47 shows the probabilities of first leak for Case 2.1.5 as compared with Case 2.1.0. Like the probabilities of crack initiation, the probabilities of first leak do not increase after the MSIP® is applied at 12 EFPY.

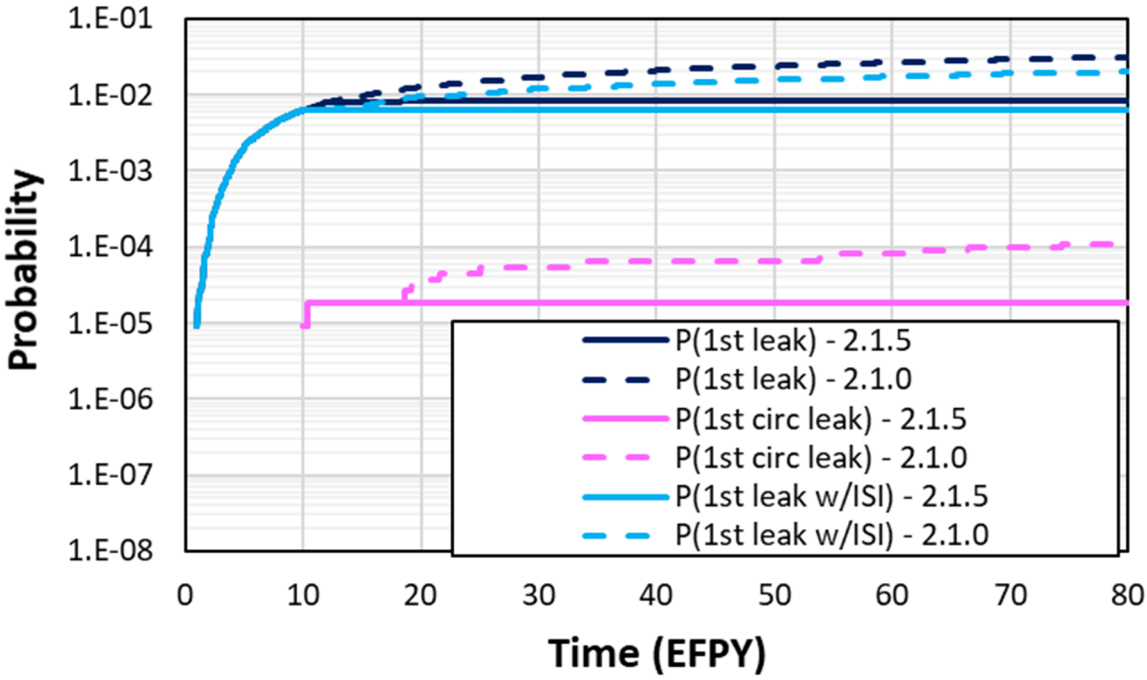

Figure 3-47 Case 2.1.5 time-dependent probabilities of first leak

Figure 3-48 shows the probabilities of rupture from Case 2.1.5 as compared with Case 2.1.0. Again, these probabilities stop increasing when the MSIP® is applied at 12 EFPY.

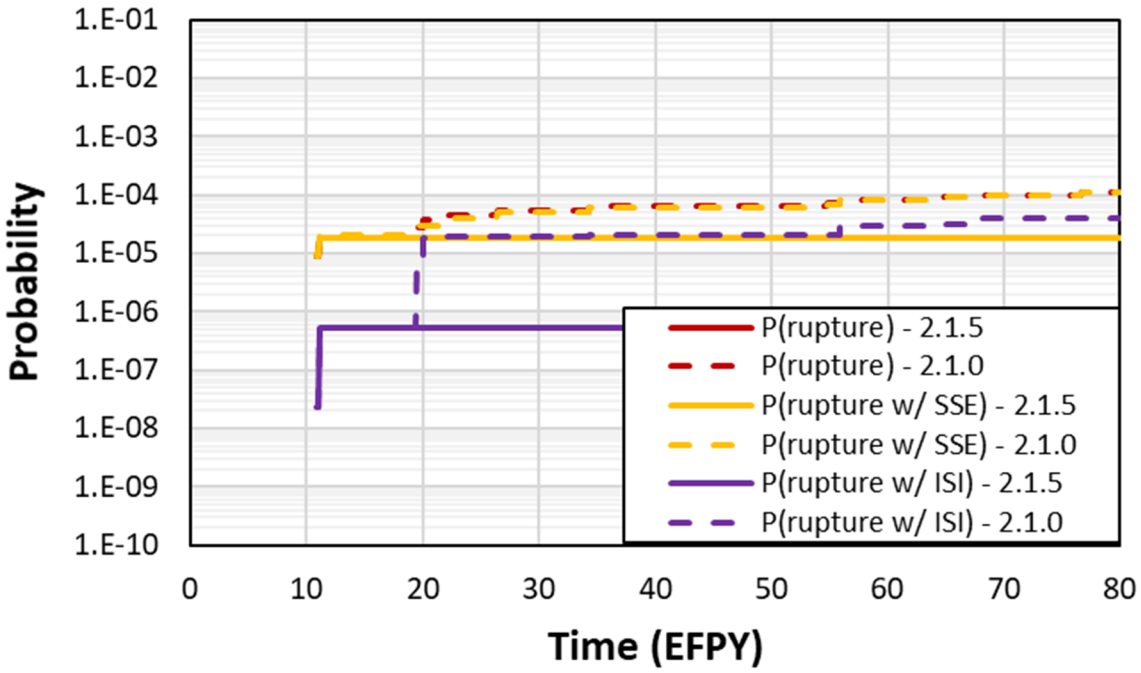

Figure 3-48 Case 2.1.5 time-dependent probabilities of rupture

3.4 Bin 3: CE and B&W RCP Nozzle DMWs

The following cases were used to analyze the RCP nozzle DMWs represented by Bin 3:

- Case 3.1.0: base case
- Case 3.1.1: initial flaws
- Case 3.1.2: more severe WRS

The cases and associated analyses are described in Sections 3.4.1 through 3.4.3, respectively.

3.4.1 Base Case

3.4.1.1 Case Description

The objective of Case 3.1.0 was to assess the base likelihood of failure caused by PWSCC initiation and growth without mechanical mitigation. The effects of leak detection, ISI, and SSE were also assessed. The analysis of this case used bounding values for the geometry and loading, both normal operating and SSE stresses, based on the licensing submittals referenced in Table 2-1 for the bin. The ISI parameters used were the same as those from the xLPR Inputs Group report [53]. Figure 3-49 shows the WRS profiles used to analyze the case. These profiles were based on the xLPR WRS Subgroup report [47]. More information on these WRS

profiles is in Section C3.1. Section B10 describes the specific inputs and other simulation details used to analyze the case.

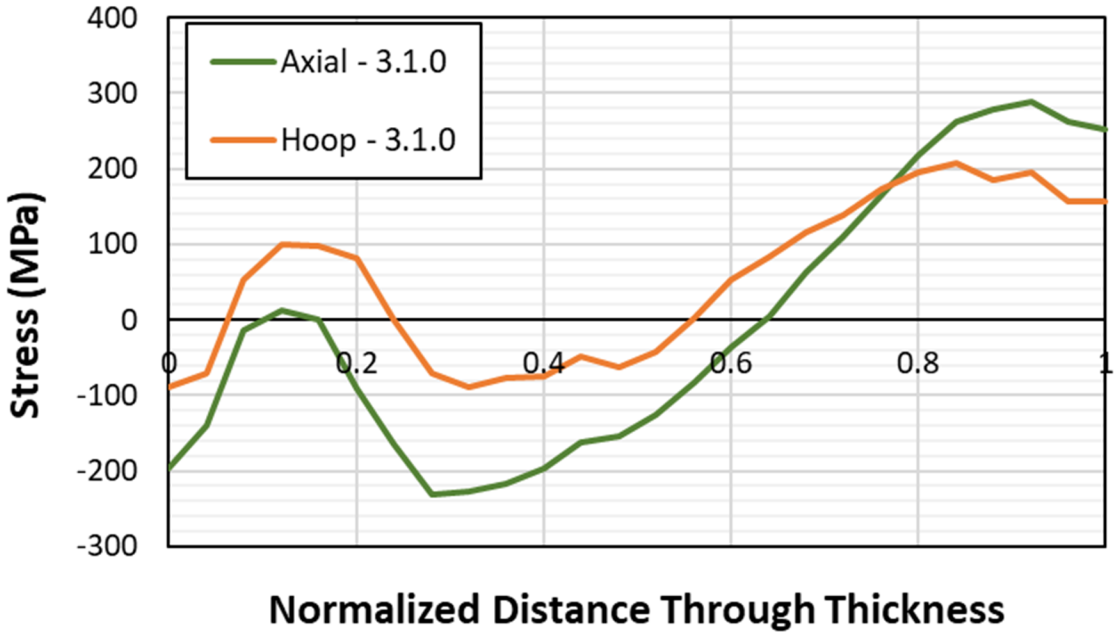

Figure 3-49 Case 3.1.0 WRS profiles

3.4.1.2 Results and Analysis

3.4.1.2.1 Probability of Rupture with Detection

There were no ruptures with a 1 gpm leak rate detection capability for this case.

3.4.1.2.2 Leak Rate Jump

There were no leak rate jump events for this case.

3.4.1.2.3 LBB Time Lapse

There were no circumferential crack leaks or ruptures for this case; therefore, this QoI cannot be reported.

3.4.1.2.4 LBB Ratio

There were no circumferential crack leaks or ruptures for this case; therefore, this QoI cannot be reported.

3.4.1.2.5 Standard Indicators

Figure 3-50 shows the probabilities of first crack for Case 3.1.0 as compared with Case 1.1.6a. Only axial cracks occur in Case 3.1.0, and the associated probability is around 3 x 10^{-4} at 80 EFPY. The probabilities of leakage and rupture were all zero with the sample size considered and are thus not plotted.

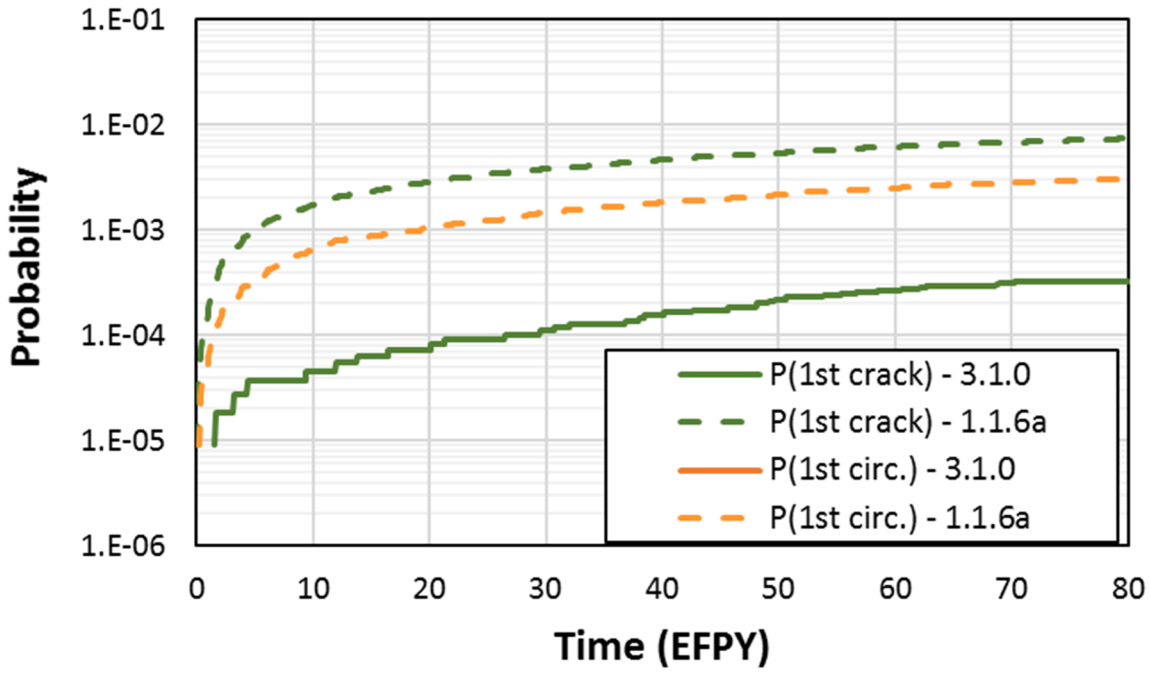

Figure 3-50 Case 3.1.0 time-dependent probabilities of first crack

3.4.2 Initial Flaws

3.4.2.1 Case Description

The objective of Case 3.1.1 was to assess the base likelihood of failure with pre-existing flaws and subsequent PWSCC growth of circumferential and axial cracks without mechanical mitigation. The effects of leak detection, ISI, and SSE were also assessed. This case used the same inputs as Case 3.1.0 except that, instead of Direct Model 1 for crack initiation, it used pre-existing axial and circumferential flaws. Section B11 describes the specific inputs and other simulation details used to analyze the case.

3.4.2.2 Results and Analysis

3.4.2.2.1 Probability of Rupture with Detection

There were no ruptures with a 1 gpm leak rate detection capability for this case.

3.4.2.2.2 Leak Rate Jump

There were no leak rate jump events for this case.

3.4.2.2.3 LBB Time Lapse

The mean LBB time lapses and standard errors with 1 and 10 gpm leak rate detection capabilities were respectively as follows:

- 78.1 ± 4.8 months (minimum observed: 25 months)
- 53.5 ± 3.3 month (minimum observed: 16 months)

Figure 3-51 shows the LBB time lapse CDF plots for Case 3.1.1. Since no ruptures occurred in Case 3.1.0, the results were compared with Case 1.1.6b. The LBB time lapses are noticeably longer for the RCP nozzle DMWs.

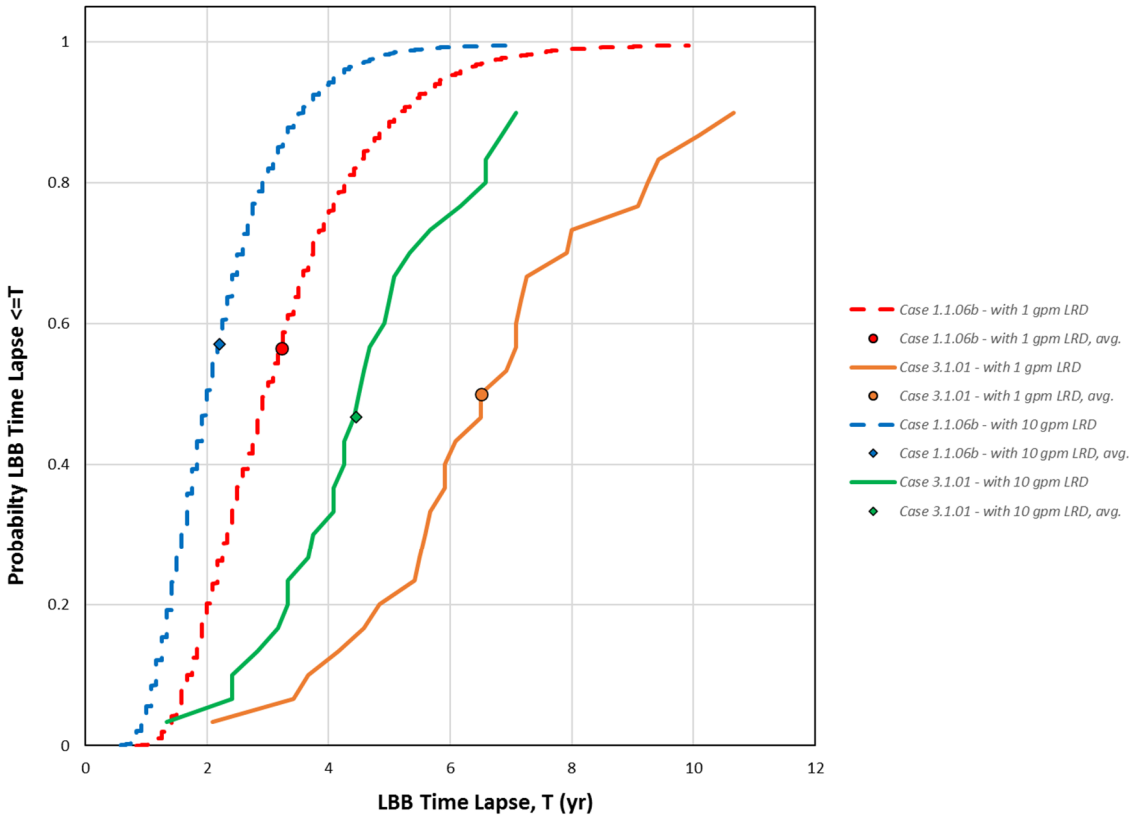

Figure 3-51 Case 3.1.1 LBB time lapse results

3.4.2.2.4 LBB Ratio

The mean LBB ratios and standard errors with 1 and 10 gpm leak rate detection capabilities were respectively as follows:

- 10.1 ± 0.12 (minimum observed: 8.64)
- 4.63 ± 0.04 (minimum observed: 4.17)

Figure 3-52 shows the LBB ratio CDF plots for Case 3.1.1 as compared with Case 1.1.6b. The results are similar, which is expected considering that the weld sizes in the two cases are similar.

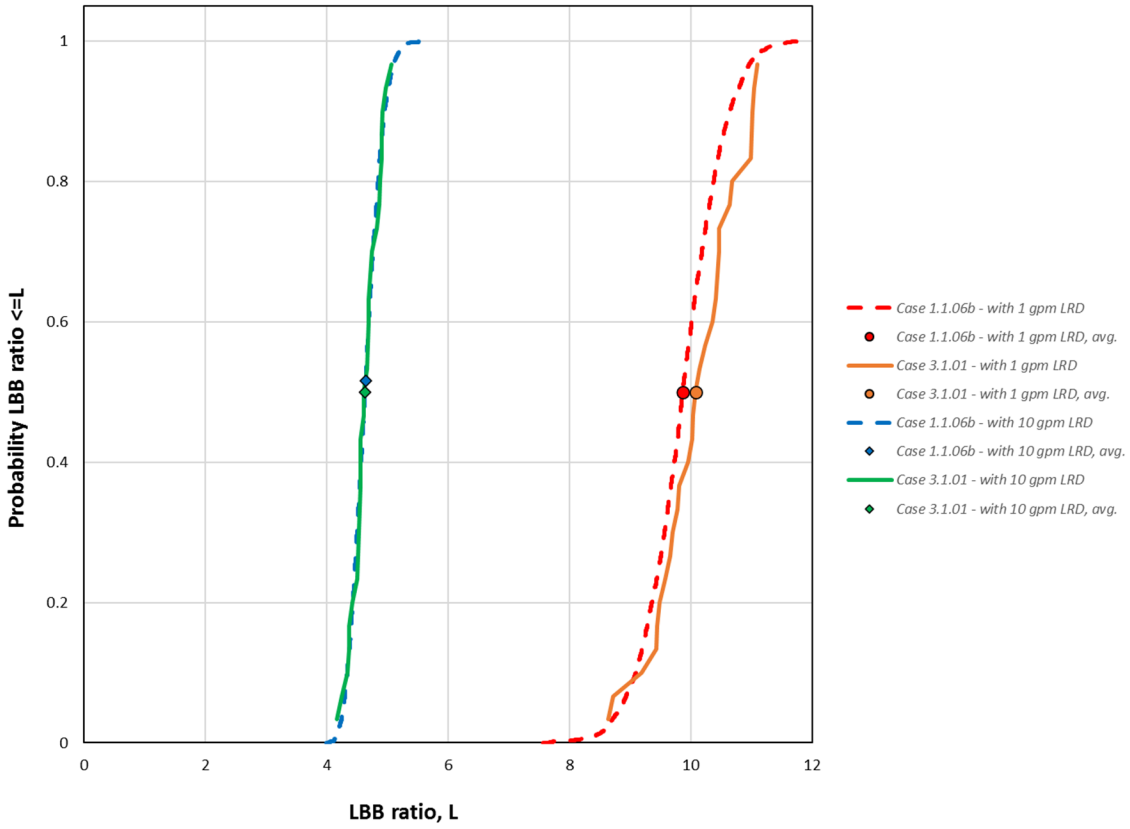

Figure 3-52 Case 3.1.1 LBB ratio results

3.4.2.2.5 Standard Indicators

Figure 3-53 shows the probabilities of first leak for Case 3.1.1. The probability of first leak is around 2.7×10^{-2} at 80 EFPY, and the probability of first circumferential crack leak is around 7.4×10^{-3}. The probability of first leak decreases to around 2.1×10^{-4} when a 10-year inspection frequency is considered.

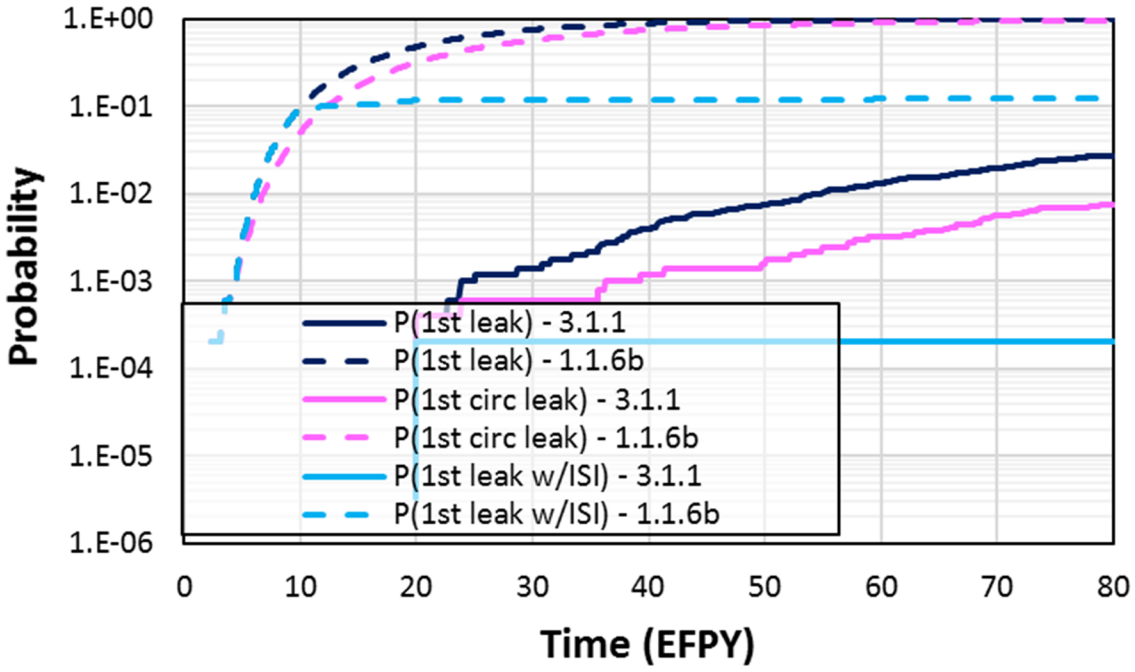

Figure 3-53 Case 3.1.1 time-dependent probabilities of first leak

Figure 3-54 shows the probabilities of rupture for Case 3.1.1. The probability of rupture is about 5.8×10^{-3} at 80 EFPY, which is slightly lower than the probability of first circumferential crack leak. The probability of rupture decreases to 2.8×10^{-7} with a 10-year inspection frequency.

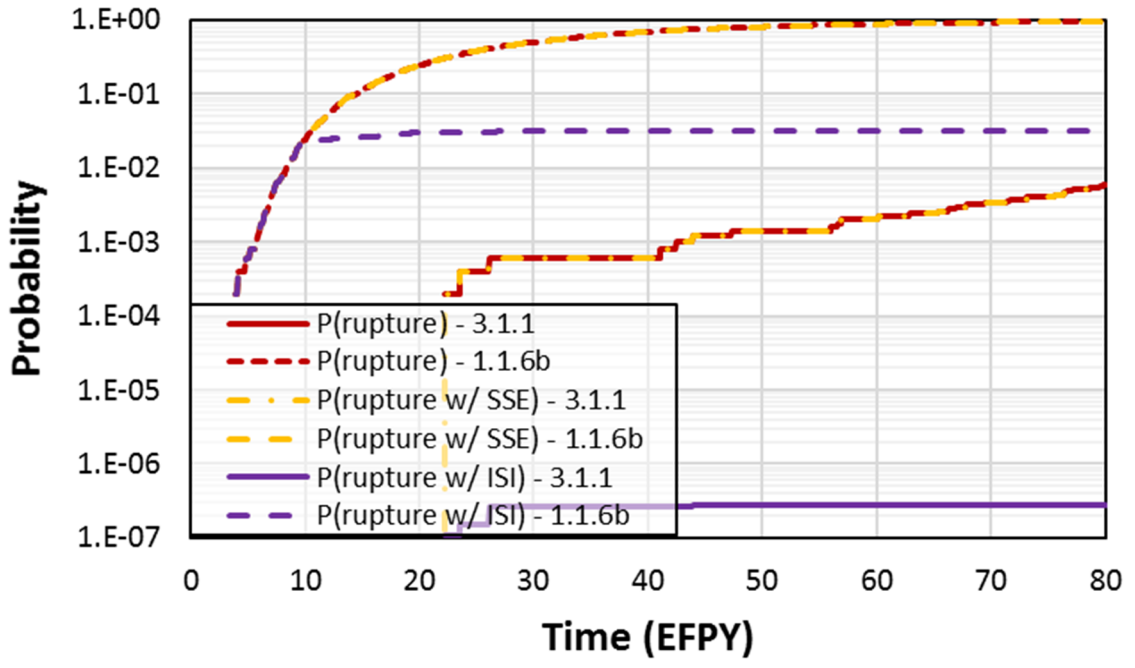

Figure 3-54 Case 3.1.1 time-dependent probabilities of rupture

3.4.3 More Severe WRS

3.4.3.1 Case Description

Case 3.1.2 was a sensitivity study of Case 3.1.0 considering a more severe WRS profile. This case used the same inputs as Case 3.1.0 but with a change to the mean hoop and axial WRS profiles. The standard deviations used to represent uncertainties in the WRS profiles were the same as in Case 3.1.0. Figure 3-55 shows the WRS profiles used to analyze the case. They were developed from FEA results corresponding with the greatest inside diameter stresses, which occur in the weld butter. Such a profile is considered more severe because the higher inside diameter stress favors PWSCC initiation, which has been shown through prior sensitivity analyses to have a large influence on the probability of rupture as documented in TLR-RES/DE/CIB-2021-11 [51]. Additional details on development of the WRS profiles are in Section C3.2. Section B12 describes the specific inputs and other simulation details used to analyze the case.

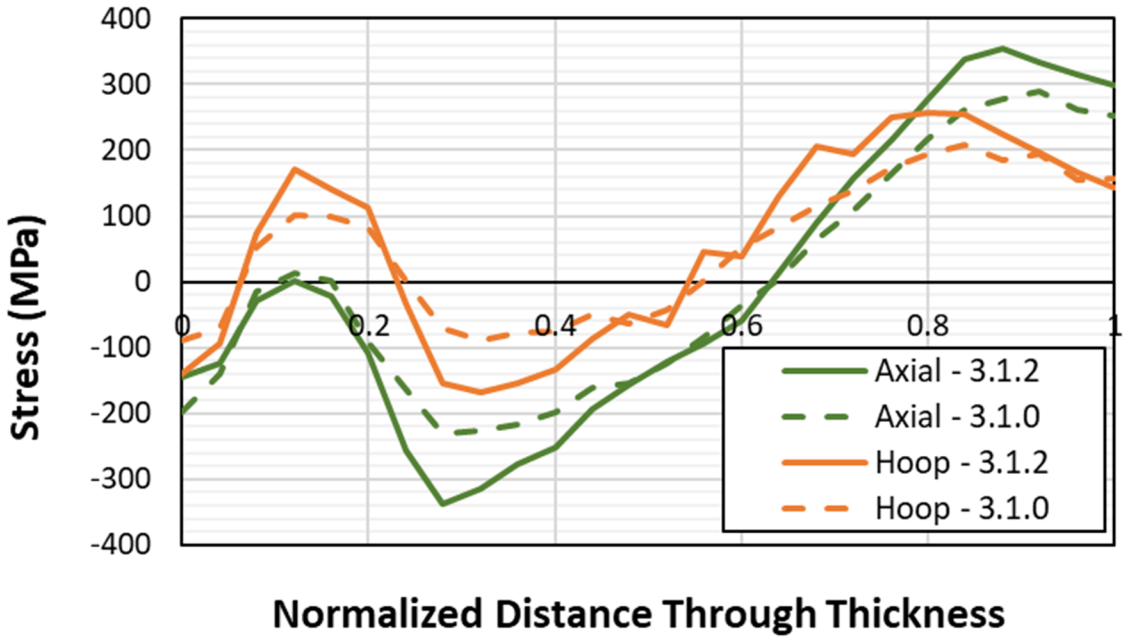

Figure 3-55 Case 3.1.2 WRS profiles

3.4.3.2 Results and Analysis

3.4.3.2.1 Probability of Rupture with Detection

There were no ruptures with a 1 gpm leak rate detection capability for this case.

3.4.3.2.2 Leak Rate Jump

There were no leak rate jump events for this case.

3.4.3.2.3 LBB Time Lapse

There were no circumferential crack leaks or ruptures for this case; therefore, this QoI cannot be reported.

3.4.3.2.4 LBB Ratio

There were no circumferential crack leaks or ruptures for this case; therefore, this QoI cannot be reported.

3.4.3.2.5 Standard Indicators

Figure 3-56 shows the probabilities of first crack for Case 3.1.2 as compared with Case 3.1.0. The more severe axial WRS profile was selected to increase the probability of circumferential crack initiation. However, the increased stress was not enough result in any circumferential cracks. Furthermore, the mean hoop WRS at the inside diameter was lower than in Case 3.1.0, which led to a decreased probability of axial crack occurrence.

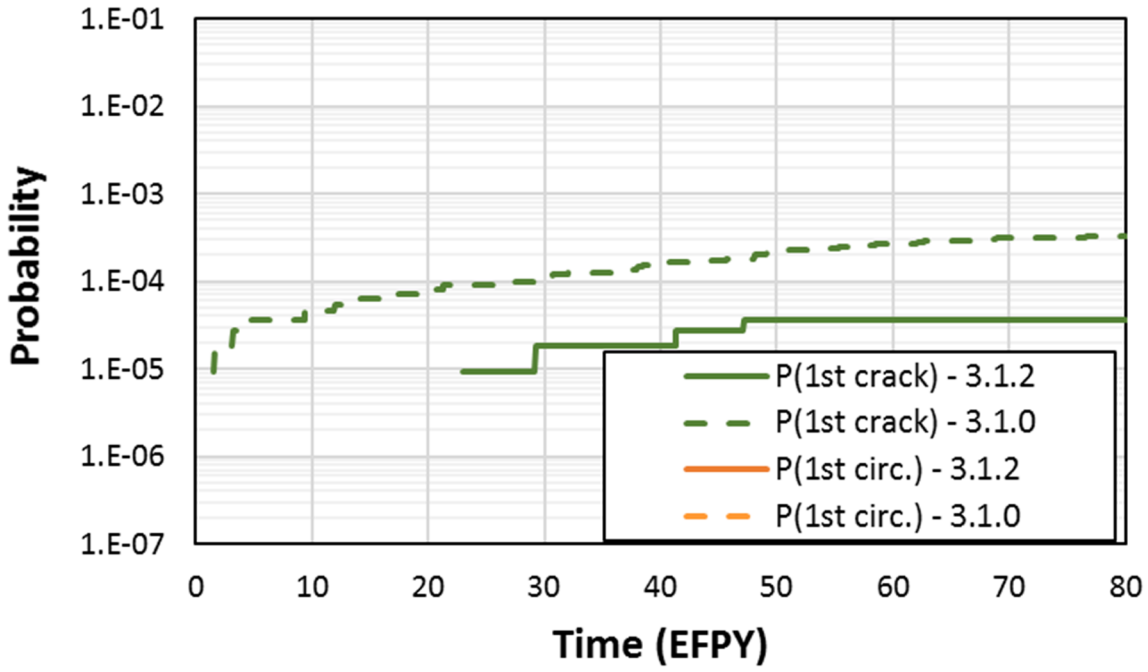

Figure 3-56 Case 3.1.2 time-dependent probabilities of first crack

3.5 Bin 4: Westinghouse Steam Generator Nozzle DMWs

The following cases were used to analyze the Westinghouse steam generator nozzle DMWs represented by Bin 4:

- Case 4.1.0: base case with inlay mitigation
- Case 4.1.1: initial flaws

- Case 4.1.2: more severe WRS
- Case 4.1.3: overlay mitigation
- Case 4.1.4: no mechanical mitigation

The cases and associated analyses are described in Sections 3.5.1 through 3.5.4.2.6, respectively.

3.5.1 Base Case

3.5.1.1 Case Description

The objective of Case 4.1.0 was to assess the base likelihood of failure caused by PWSCC initiation and growth with inlay mitigation. The effects of leak detection, ISI, and SSE were also assessed. Some steam generators have been replaced with a double-vee groove weld geometry with an Alloy 52 inlay. The steam generators at Point Beach Nuclear Plant, Unit 2; North Anna Power Station, Units 1 and 2; and Virgil C. Summer Nuclear Station, Unit 1 have this configuration. This case used bounding values for the geometry and loading, both normal operating and SSE, based on the licensing submittals referenced in Table 2-1 for the bin. The ISI parameters used were from the xLPR Inputs Group report [53]. The normal operating temperature was set to 328°C, which represents the conditions in the hot leg piping.

The DMW in this case has an inlay applied at 1 month to represent welds that were put in service with an inlay already applied. Since the xLPR code does not allow any mitigation to be applied as an initial condition, the application timing was set to 1 month, which is the first possible time step. The inlay material is Alloy 52, and the thickness is 3.3 millimeters (mm) based on the North Anna Power Station, Unit 2 geometry as reported in the April 22, 2013, letter from E. S. Grecheck, Vice President – Nuclear Engineering and Development, Virginia Electric and Power Company, to the NRC Document Control Desk [56]. Figure 3-57 shows the WRS profiles used to analyze the case. They were developed to represent the double-vee groove geometry with an Alloy 52 inlay applied. Additional details on the WRS profile development are in Section A1.1. Section B13 describes the specific inputs and other simulation details used to analyze the case.

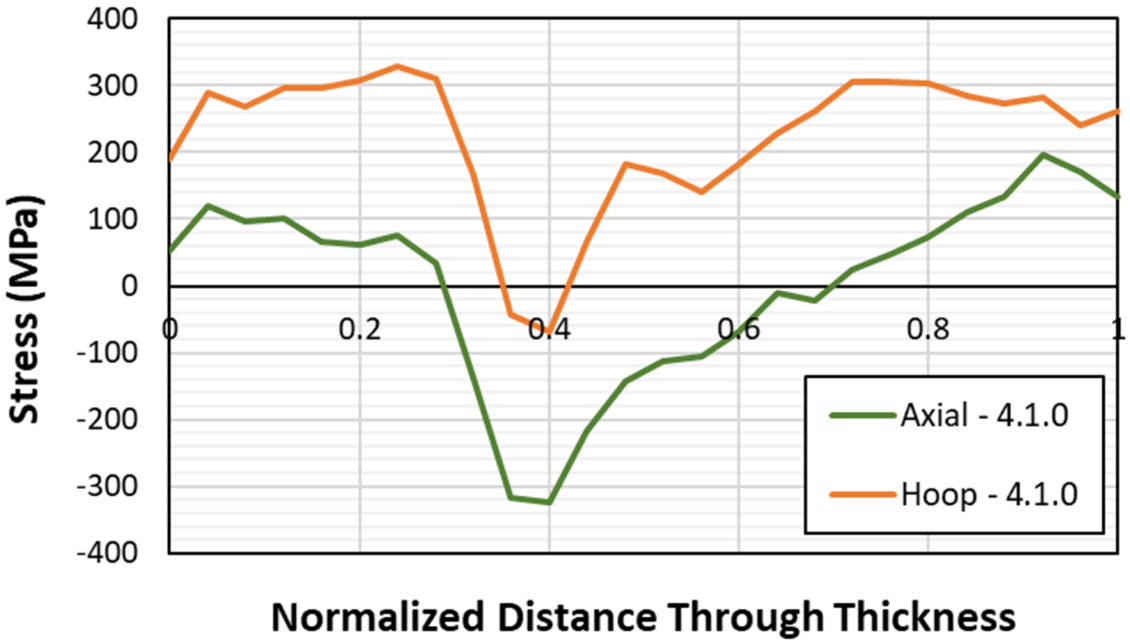

Figure 3-57 Case 4.1.0 WRS profiles

3.5.1.2 Results and Analysis

3.5.1.2.1 Probability of Rupture with Detection

There were no ruptures with a 1 gpm leak rate detection capability for this case.

3.5.1.2.2 Leak Rate Jump

There were no leak rate jump events for this case.

3.5.1.2.3 LBB Time Lapse

There were no circumferential crack leaks or ruptures for this case; therefore, this QoI cannot be reported.

3.5.1.2.4 LBB Ratio

There were no circumferential crack leaks or ruptures for this case; therefore, this QoI cannot be reported.

3.5.1.2.5 Standard Indicators

Figure 3-58 shows the probabilities of first crack for Case 4.1.0. The probabilities are higher as compared to Case 1.1.6a. This result is because of the FOI of 24 on crack initiation used for the Alloy 52 inlay, which did not offset the increased hoop and axial WRS at the inside diameter.

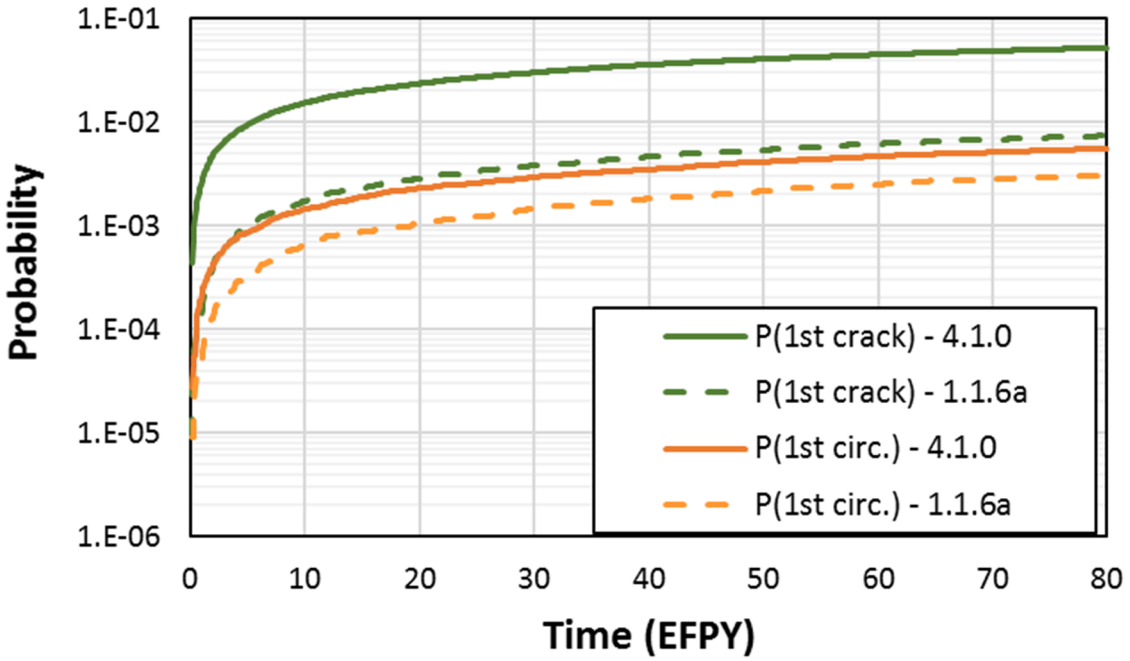

Figure 3-58 Case 4.1.0 time-dependent probabilities of first crack

Figure 3-59 shows the probabilities of first leak for Case 4.1.0. While the probability of first leak is slightly higher as compared to Case 1.1.6a, it is only because of the axial crack leaks. There were no circumferential crack leaks.

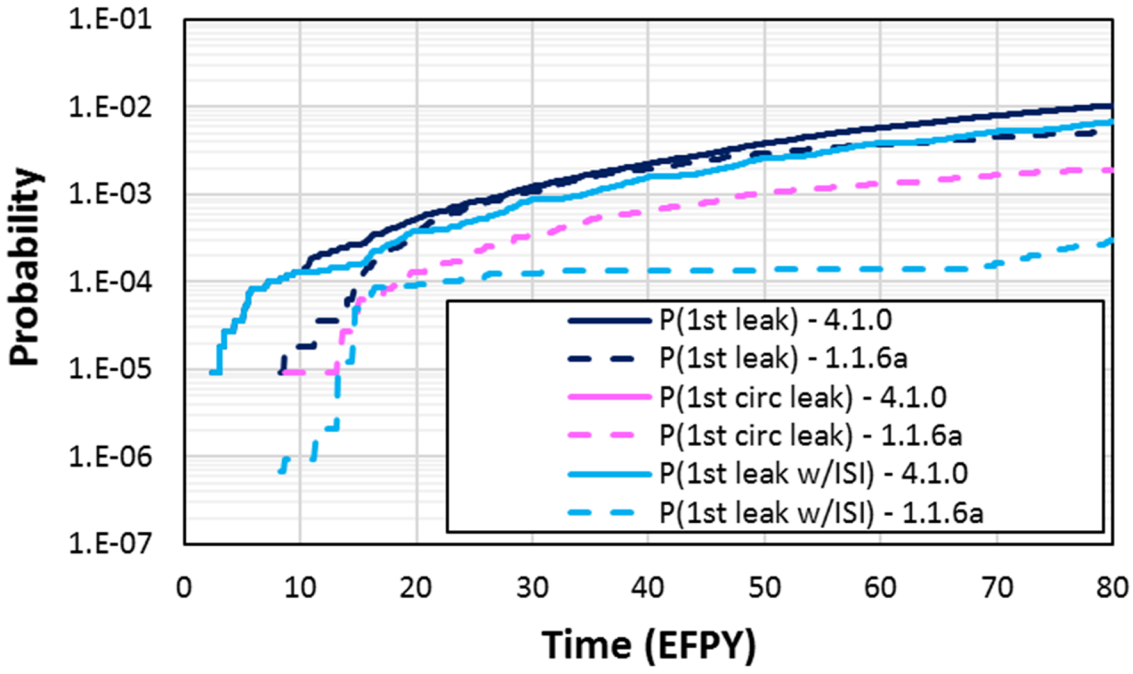

Figure 3-59 Case 4.1.0 time-dependent probabilities of first leak

3.5.2 Initial Flaws

3.5.2.1 Case Description

The objective of Case 4.1.1 was to assess the base likelihood of failure with pre-existing flaws and subsequent PWSCC growth of circumferential and axial cracks with inlay mitigation. The effects of leak detection, ISI, and SSE were also assessed. This case used the same inputs as Case 4.1.0 except that, instead of Direct Model 1 for crack initiation, it used pre-existing axial and circumferential flaws. The WRS profiles used were the same as in the Case 4.1.0 analysis. Section B14 describes the specific inputs and other simulation details used to analyze the case.

3.5.2.2 Results and Analysis

3.5.2.2.1 Probability of Rupture with Detection

Figure 3-60 shows the probability of rupture with a 1 gpm leak rate detection capability compared with the probability of leak rate jump. Case 4.1.1 generated a large probability of rupture with leak rate detection of 1.2×10^{-2} at 80 EFPY.

3.5.2.2.2 Leak Rate Jump

As shown in Figure 3-60, Case 4.1.1 generated leak rate jump events with a probability of 1.6×10^{-2} at 80 EFPY. A large portion of these realizations had ruptures with leak rate detection.

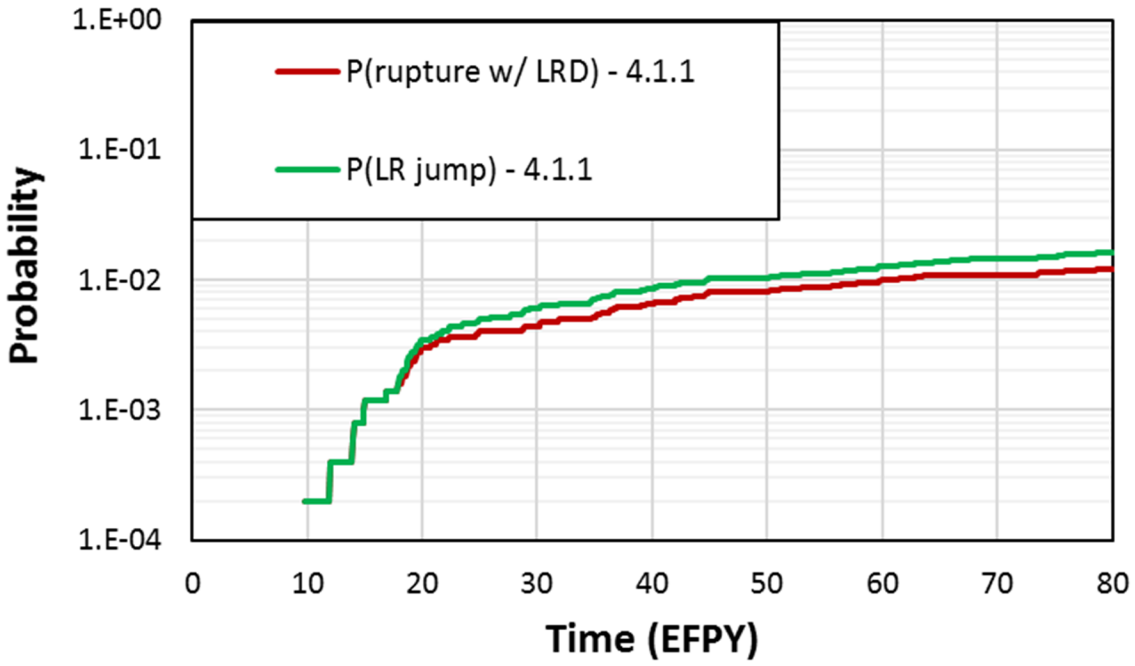

Figure 3-60 Case 4.1.1 probability of leak rate jump

3.5.2.2.3 LBB Time Lapse

The nature of the ruptures in Case 4.1.1 makes the LBB time lapse CDFs irrelevant.

3.5.2.2.4 LBB Ratio

The nature of the ruptures in Case 4.1.1 makes the LBB ratio CDFs irrelevant.

3.5.2.2.5 Standard Indicators

Figure 3-61 shows the probabilities of first leak for Case 4.1.1. The probability of first leak is lower as compared to Case 1.1.6b. Also, a comparison of the differences between the probabilities of first leak with the probabilities of first leak with ISI for each case show that a 10-year inspection frequency has less impact in Case 4.1.1. This result indicates that many of the cracks remain at shallow depths for long times before they grow through-wall and produce leakage. The probability of first leak is 2.5×10^{-1} at 80 EFPY. This probability is reduced by a factor of 2 (i.e., to 1.4×10^{-1}) when a 10-year inspection frequency is considered. This relatively low reduction is because of the inlay. Most of the cracks remain in the inlay, whose thickness is less than 10 percent of the weld thickness, and the ISI model parameters were set such that cracks with depths less than 10 percent of the weld thickness are not detected. For the few cracks that grew beyond the thickness of the inlay, they tended to then grow quickly to penetrate through-wall (e.g., leak in less than 10 EFPY), and only the ones close enough to the next inspection were detected. The probability of first circumferential crack leak is 1.88×10^{-2} at 80 EFPY.

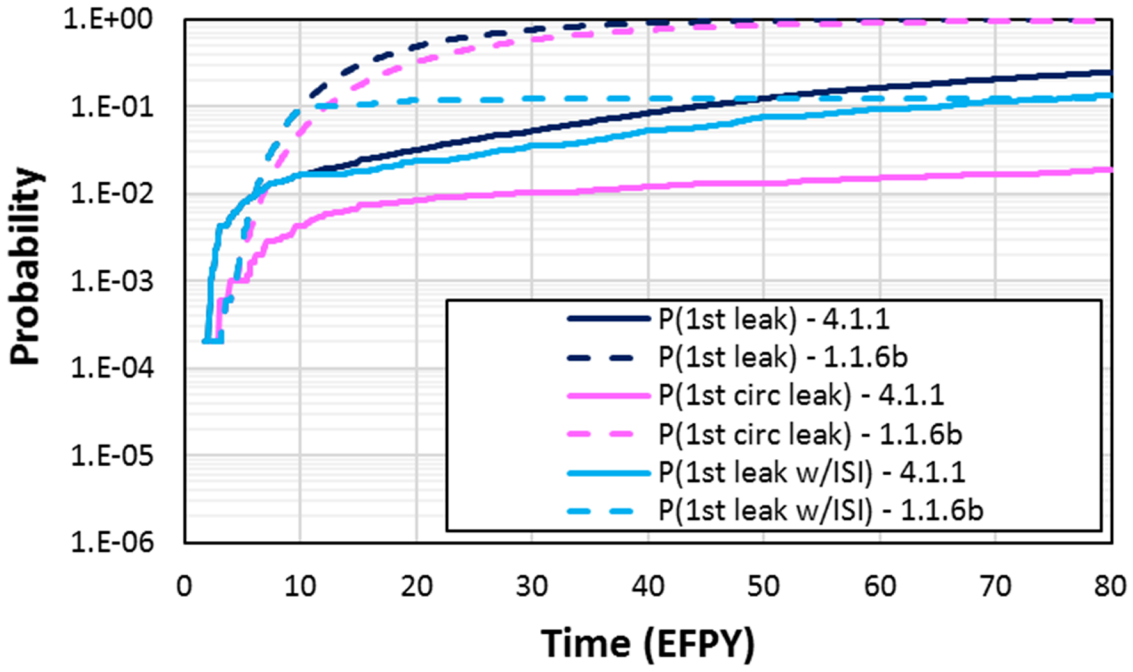

Figure 3-61 Case 4.1.1 time-dependent probabilities of first leak

Figure 3-62 shows the probabilities of rupture for the different simulations. The probability of rupture is close to the probability of first circumferential leak. It is equal to 1.6 x 10^{-2} at 80 EFPY, which is the same as the probability of leak rate jump.

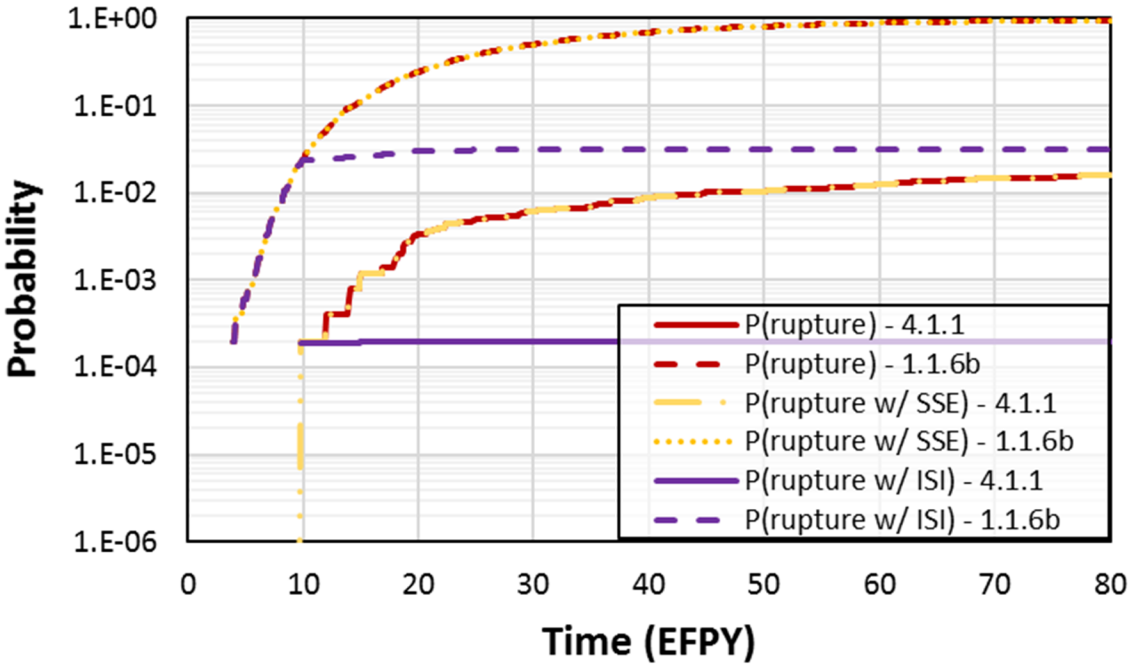

Figure 3-62 Case 4.1.1 time-dependent probabilities of rupture

3.5.2.3 Supplemental Analyses

While the results for Case 4.1.1 are conditional on having a circumferential crack, the high probability of rupture with leak rate detection (i.e., in the 1 x 10^{-2} range) was further investigated. The first area that was evaluated was the distribution used for the initial crack depth. It was a lognormal distribution with a geometric mean of 1.5 mm and a geometric standard deviation of 1.419. The probability of leak rate jump was equal to 1.6 x 10^{-2}, which roughly corresponds to the 98th percentile of the CDF. The same quantile on crack depth represents a depth of 3.2 mm, which is close to the inlay depth of 3.3 mm. Thus, about 1.6 percent of the realizations begin with a crack that is deeper or close to the depth of the inlay. In all these realizations, the cracks can grow faster in depth in the Alloy 82/182 weld material, while growth in length is reduced in the Alloy 52 inlay material. When these cracks grow through-wall, they have a trapezoidal shape with a smaller opening on the inside diameter and a larger opening on the outside diameter. Figure 3-63 illustrates one such crack.

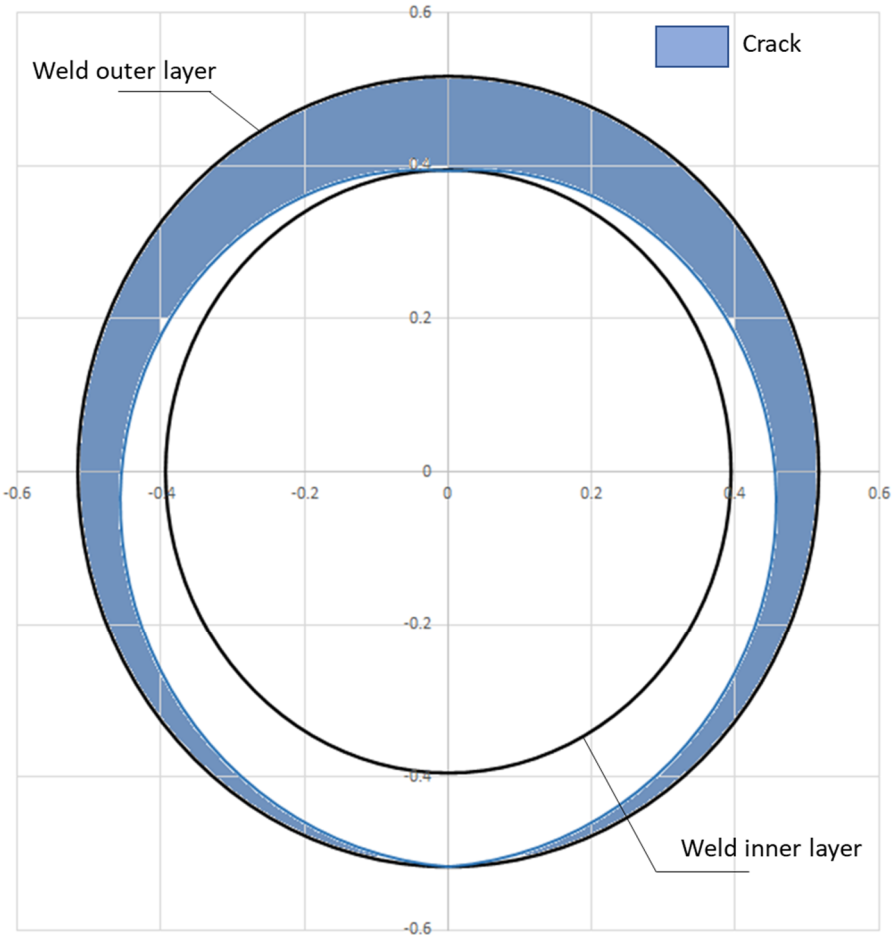

Figure 3-63 Case 4.1.1 through-wall crack representation for one realization

These cracks have low leak rates because of their small inside diameter crack opening areas. In flow Regime 1, the leak rate module only uses the inside diameter crack length to calculate the leak rate. Leak rates for the realizations that led to rupture ranged from 0.1 to 3.3 gpm, with 75 percent falling below the 1 gpm leak rate detection capability at the time of the rupture. Then, when the outside diameter crack length is equal to the circumference, the crack is unstable and leads to rupture.

The results generated by Case 4.1.1 are thus not the result of a problem in the xLPR code. However, the results are not necessarily valid because of some assumptions made in the models and inputs. Some of these assumptions are the following:

- The input distribution for the initial crack depth was assumed to be the same as the distribution used for Alloy 82/182 materials. This assumption may not be appropriate considering the PWSCC-resistant properties of the Alloy 52 inlay. It's possible that a more realistic initial crack depth would lead to the disappearance of, or strong reduction in, the rupture events.

- The trapezoidal shape of the TWCs penetrating the inlay does not match well with FEA models, which show bubble-shaped cracks resulting from such conditions. It is unknown how much the shape of the crack would affect the rupture results.
- The assumption of using only the inside diameter crack length to estimate the leak rate may not be appropriate in this case.

A series of deterministic analyses were performed by Rudland and others to evaluate the inlay process as a mitigation strategy for PWSCC as reported in [57] and [58]. WRS profiles were developed for inlays in several weld geometries and scenarios. PWSCC was then modeled using advanced FEA for several scenarios. Bubble-shaped crack growth was predicted in all cases where the crack penetrated the Alloy 52/152 inlay and entered the original Alloy 82/182 weld material, because the crack growth rate in the inlay was two orders of magnitude slower than in the original weld. As a simplification, the xLPR code uses a trapezoidal crack shape to approximate crack growth predicted with advanced FEA. Thus, while the xLPR code can reasonably approximate the general extent of such crack growth (e.g., length and depth), it cannot directly model the bubble shape.

Further investigation into these aspects is beyond the scope of this report. Nonetheless, the potential causes are outlined here, which may be pursued to enhance the current input recommendations and models to increase confidence in the results.

3.5.3 More Severe WRS

3.5.3.1 Case Description

Case 4.1.2 was a sensitivity study of Case 4.1.0 considering a more severe WRS profile. This case uses the same inputs as Case 4.1.0 but with a change to the mean hoop and axial WRS profiles. The standard deviations used to represent uncertainties in the WRS profiles were the same as in Case 4.1.0. Figure 3-64 shows the WRS profiles used to analyze the case. These profiles were developed using the same FEA as was used to develop the WRS profiles for Case 4.1.0; however, for Case 4.1.2, the WRS profiles were extracted from the location with the highest stresses on the inside diameter, rather than at the weld centerline. The WRS profile is considered more severe because the higher inside diameter stress favors PWSCC initiation, which has been shown through prior sensitivity analyses to have a large influence on the probability of rupture as documented in TLR-RES/DE/CIB-2021-11 [51]. Additional details on development of the WRS profiles are in Section C4.3. Section B15 describes the specific inputs and other simulation details used to analyze the case.

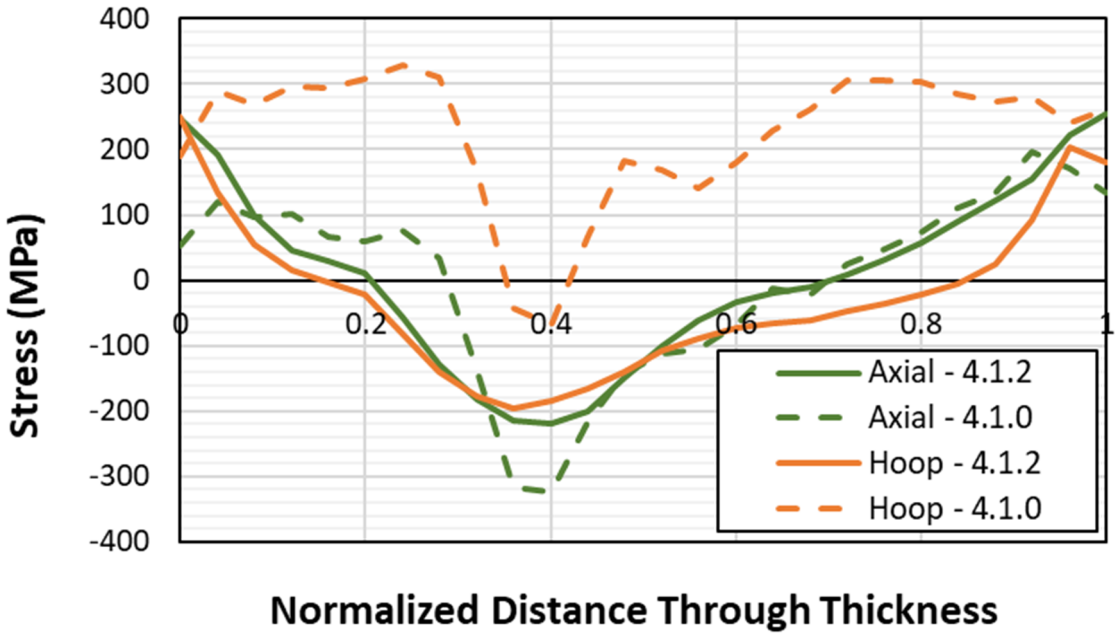

Figure 3-64 Case 4.1.2 WRS profiles

3.5.3.2 Results and Analysis

3.5.3.2.1 Probability of Rupture with Detection

Figure 3-65 shows the probability of rupture results with a 1 gpm leak rate detection capability. The results are like the probability of rupture without leak rate detection. When a 10-year inspection frequency is considered, the probability decreases to 2.4×10^{-6} at 80 EFPY, which leads to an annual frequency of 3×10^{-8}. The causes of these non-zero probabilities are like those presented for Case 4.1.1.

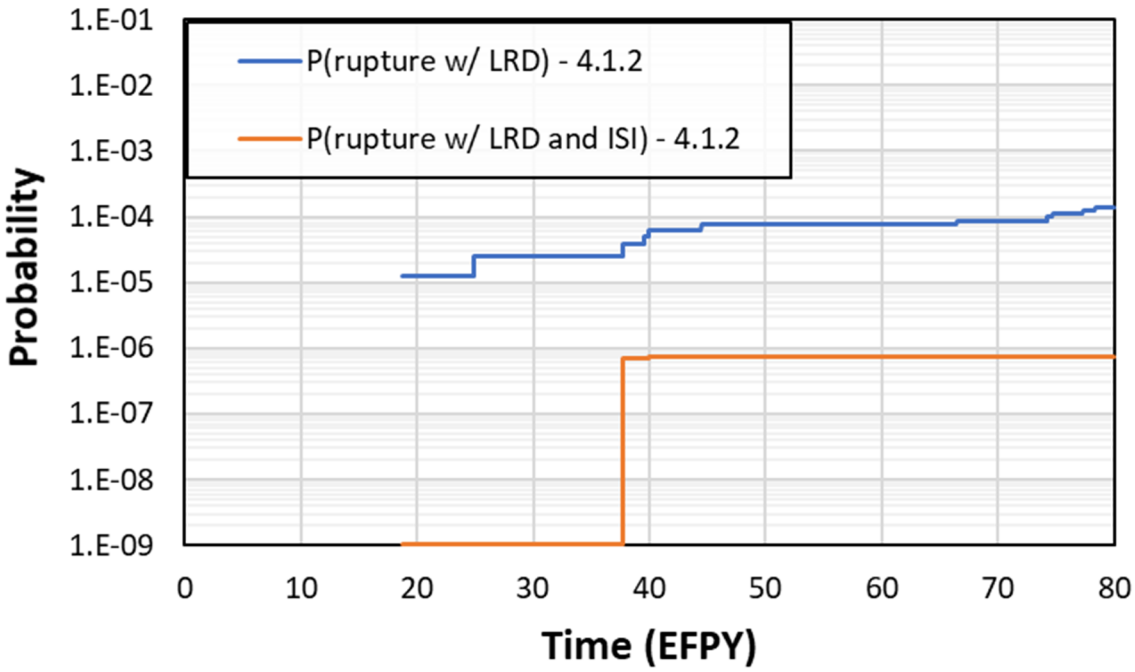

Figure 3-65 Case 4.1.2 time-dependent probabilities of rupture with leak rate detection

3.5.3.2.2 Leak Rate Jump

The probability of leak rate jump is equal to 2 x 10^{-4} at 80 EFPY, which represents an annual frequency of 2.5 x 10^{-6}. The causes for these non-zero probabilities are like those presented in the previous section for Case 4.1.1.

3.5.3.2.3 LBB Time Lapse

The nature of the ruptures in Case 4.1.2 makes the LBB time lapse CDFs irrelevant.

3.5.3.2.4 LBB Ratio

The nature of the ruptures in Case 4.1.2 makes the LBB time lapse CDFs irrelevant.

3.5.3.2.5 Standard Indicators

Figure 3-66 shows the probabilities of first crack for Case 4.1.2. Both the probabilities of first crack and first circumferential crack increase as compared to Case 4.1.0 due to the more severe WRS profile.

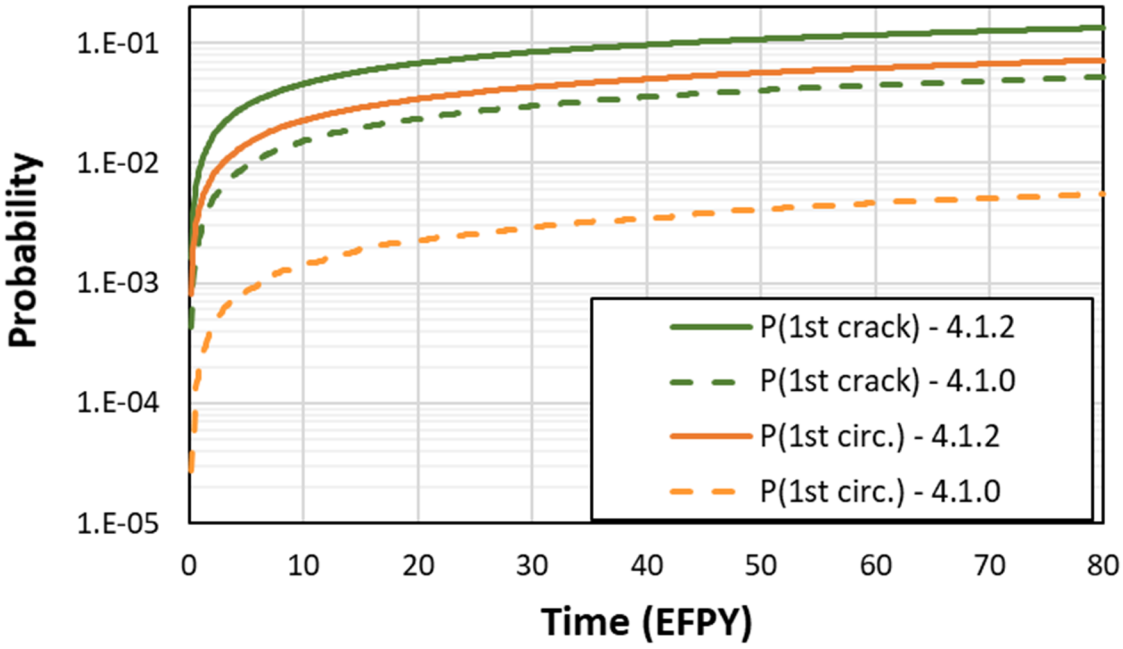

Figure 3-66 Case 4.1.2 time-dependent probabilities of first crack

Figure 3-67 shows the probabilities of first leak for Case 4.1.2. The new hoop WRS profile dips around 40 percent through the wall thickness, which leads to a reduction in the probability of first leak as compared to Case 4.1.0. All the leaks are from circumferential cracks because the probability of first circumferential crack leak lies on top of the probability of first leak. The probability of first leak with ISI is also reduced, because it applies only to the circumferential cracks.

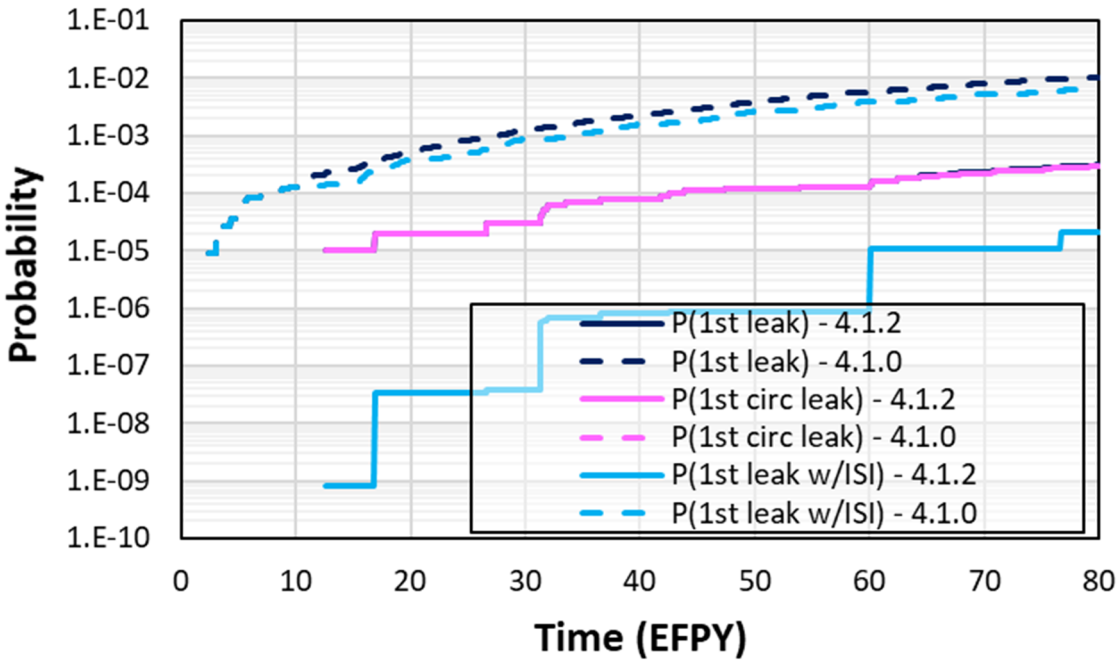

Figure 3-67 Case 4.1.2 time-dependent probabilities of first leak

Figure 3-68 shows the probabilities of rupture for Case 4.1.2. No ruptures were observed in Case 4.1.0, so no results from that case have been included for comparison. The probability of rupture is around 2 x 10^{-4} at 80 EFPY, and most of the ruptures lead to leak rate jumps. The probability of rupture when ISI is considered is around 5.8 x 10^{-7} at 80 EFPY, which leads to an annual frequency of 7.3 x 10^{-9}.

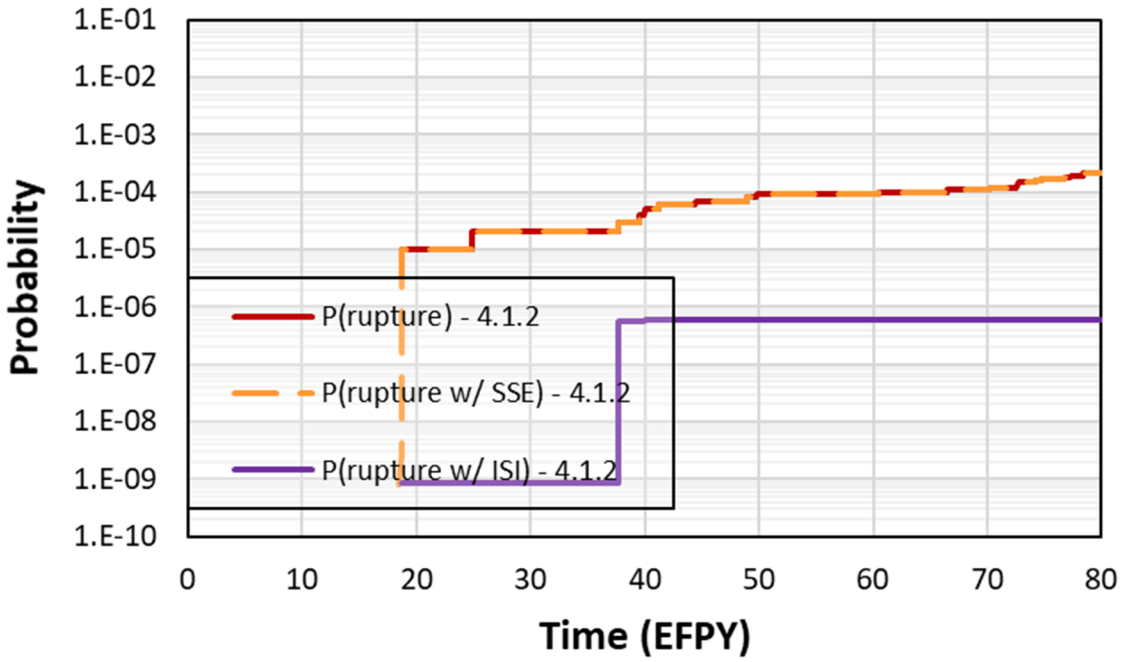

Figure 3-68 Case 4.1.2 time-dependent probabilities of rupture

3.5.4 Overlay Mitigation

3.5.4.1 Case description

Case 4.1.3 was a sensitivity study of Case 4.1.0 considering overlay instead of inlay mitigation. The steam generator welds represented by this sensitivity study case had overlays applied after 17 years of service, which was bounded in the analysis by applying the overlay at 20 EFPY. The WRS profiles from Case 4.1.0 were used to represent the unmitigated WRS profiles for Case 4.1.3. Although the Case 4.1.0 WRS profiles were generated for a double-vee groove weld with an Alloy 52/152 inlay, they are also applicable to the Case 4.1.3 Alloy 82/182 double-vee groove weld because the welding sequences are the same and the temperature-dependent stress strain curves are essentially identical between Alloy 52/152 and Alloy 82/182. The overlay WRS profiles for Case 4.1.3 were generated by using the same standard deviations as the unmitigated WRS profiles and applying the overlay rules in [47] to the mean values. The resulting mean overlay WRS profiles are plotted in Figure **3-69** along with the mean unmitigated WRS profiles for comparison. The overlay thickness was set to 0.04075 m, which is equal to one third of the original weld thickness. This represents the minimum overlay thickness for a full structural weld overlay as specified in EPRI Technical Report 1016602, “Materials Reliability Program: Technical Basis for Preemptive Weld Overlays for Alloy 82/182 Butt Welds in PWRs (MRP-169) Revision 1,” issued June 11, 2008 [59]. Section B16 describes the specific inputs and other simulation details used to analyze the case.

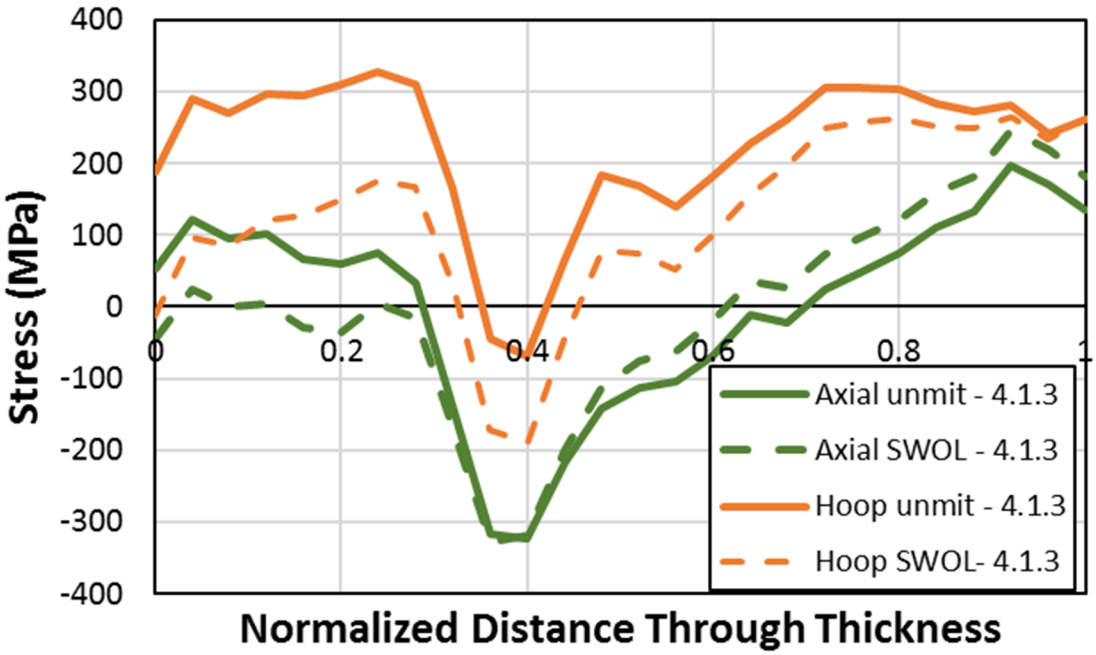

Figure 3-69 **Case 4.1.3 unmitigated and overlay mitigation WRS profiles**

3.5.4.2 Results and Analysis

3.5.4.2.1 Probability of Rupture with Detection

There were no ruptures with a 1 gpm leak rate detection capability for this case.

3.5.4.2.2 Leak Rate Jump

As shown in Figure 3-70, Case 4.1.3 generated leak rate jump events with a probability of 1.6×10^{-3} at 80 EFPY. Most of these events (i.e., 92 percent) occurred before the overlay was applied at 20 EFPY. The remaining events corresponded with realizations that had deep surface cracks when the overlay was applied. However, there were no ruptures with a 1 gpm leak rate detection capability as stated in Section 3.5.4.2.1. In this case, the highly tensile mean WRS value at the inside diameter and the highly compressive mean WRS value around 40 percent through the weld thickness led to larger inner crack lengths when the cracks penetrated through the weld thickness.

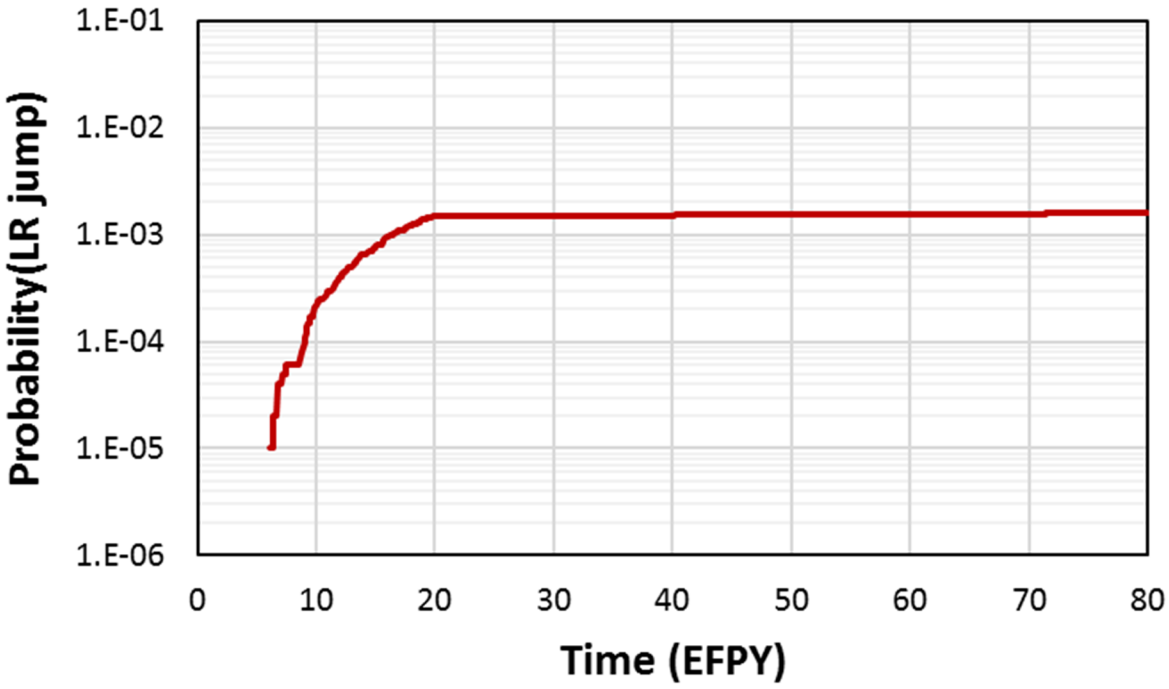

Figure 3-70 Case 4.1.3 time-dependent probability of leak rate jump

3.5.4.2.3 LBB Time Lapse

The mean LBB time lapses and standard errors with 1 and 10 gpm leak rate detection capabilities were respectively as follows:

- 5.31 ± 0.25 months (minimum observed: 0 months)
- 5.21 ± 0.24 months (minimum observed: 0 months)

Note that all results beyond 12 EFPY have been excluded for the reasons explained in Section 3.2.1.2.3. The minimum observations were estimated at 0 months. Some of the 0-month LBB time lapse estimates were because of the 1-month time step used for the simulation, and a smaller time step would have given a more accurate estimate in these realizations. One realization also had a break before detectable leak, which could have produced a negative LBB time lapse. However, the LBB time lapse in this instance was also estimated as 0 months because, when a pipe ruptures, it also leaks.

Figure 3-71 shows the LBB time lapse CDFs for Case 4.1.3 as compared with Case 1.1.6a. As this figure shows, the LBB time lapses in Case 4.1.3 are much lower than in Case 1.1.6a, which indicates shorter times from detectable leakage to rupture for steam generator nozzle DMWs. This result is partially influenced by the overlay application at 20 EFPY, as supported by the observation that no ruptures occurred thereafter. Thus, the CDF for Case 4.1.3 only reflects ruptures that occurred during the first 20 EFPY, and the overlay prevented cracks with slower growth rates from rupturing the pipe.

In some realizations, the LBB time lapses were 0 months, and these events all occurred before the overlay was applied. Because the LBB time lapse QoI was calculated based on the combined normal operating and non-probabilistically treated seismic loads as explained in Section 2.2.3, values less than or equal to zero mean that there is some seismic contribution to the failure frequency. This frequency is estimated in Section 3.5.4.2.6. Under the normal operating loads by themselves, these cracks did not rupture the pipe for an additional 2 to 15 months.

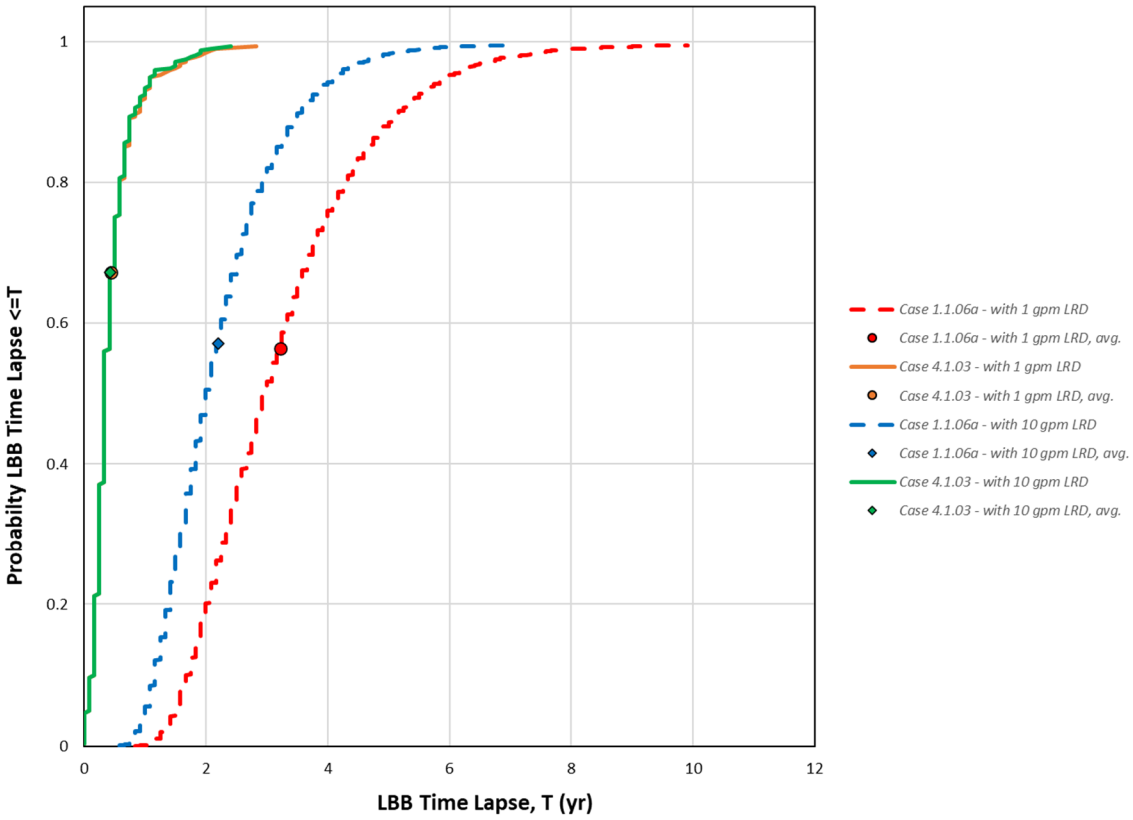

Figure 3-71 Case 4.1.3 LBB time lapse results

3.5.4.2.4 LBB Ratio

The mean LBB ratios and standard errors with 1 and 10 gpm leak rate detection capabilities were respectively as follows:

- 3.07 ± 0.05 (minimum observed: 0.85)
- 2.82 ± 0.04 (minimum observed: 0.85)

Like the LBB time lapse, the critical crack size calculations for the LBB ratio are based on the combined normal operating and non-probabilistically seismic loads as explained in Section 2.2.4. This explains why the minimum LBB ratios are lower than 1 despite there being no ruptures with leak rate detection. Figure 3-72 shows the LBB ratio CDF plots for Case 4.1.3 as compared with Case 1.1.6a.

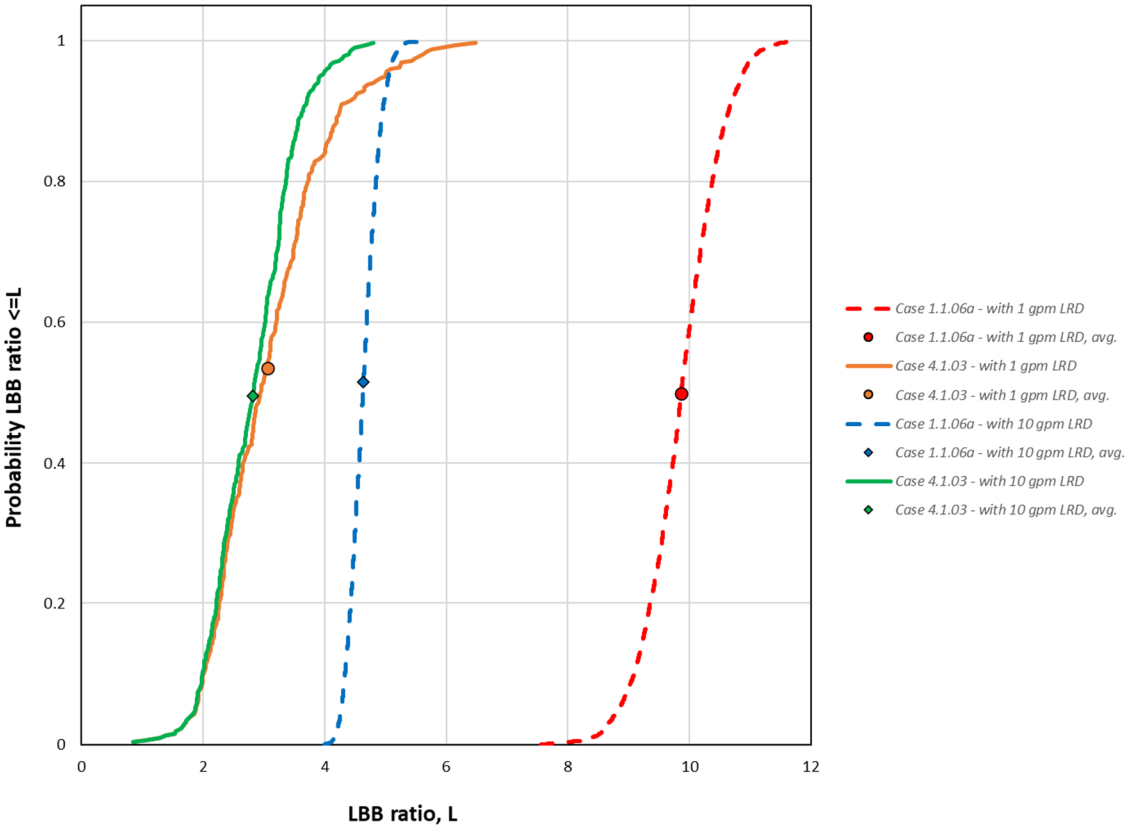

Figure 3-72 Case 4.1.3 LBB ratio results

3.5.4.2.5 Standard Indicators

Figure 3-73 shows the probabilities of first crack from Case 4.1.3 as compared to Case 4.1.0. Due to the relatively high mean hoop WRS value at the inside diameter, the likelihood of having a crack is high in both cases. However, in Case 4.1.3 the absence of the Alloy 52/152 inlay leads to an even higher probability of having a crack. Once the overlay is applied at 20 EFPY, the probabilities for Case 4.1.3 remain essentially flat.

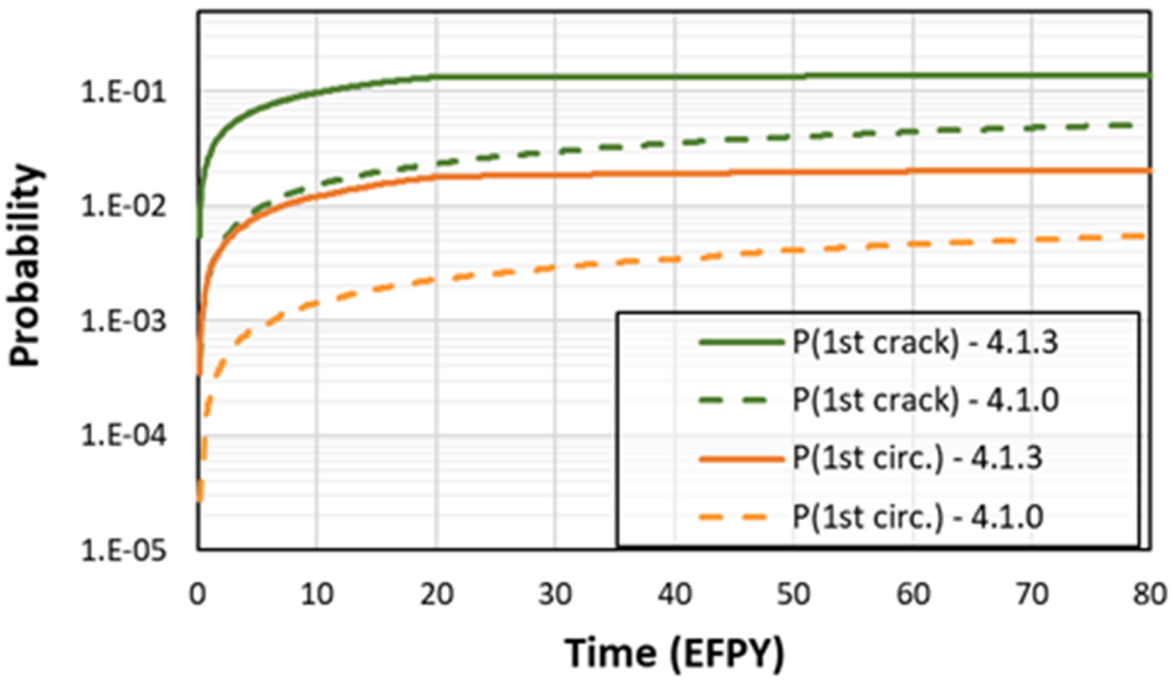

Figure 3-73 Case 4.1.3 time-dependent probabilities of first crack

Figure 3-74 shows the probabilities of first leak from Case 4.1.3 as compared to Case 4.1.0. The probabilities of first leak are higher in Case 4.1.3 for the first 20 EFPY because of the mean hoop WRS profile. When the overlay is applied, any TWCs become surface cracks that must then grow through the thickness of the overlay to become TWCs once again. The probability of such an event is very low (i.e., 4.4×10^{-3}) for the remaining 60 EFPY and halved (i.e., 1.99×10^{-3}) when a 10-year inspection frequency is considered. These results demonstrate a large improvement from using an overlay for PWSCC mitigation purposes.

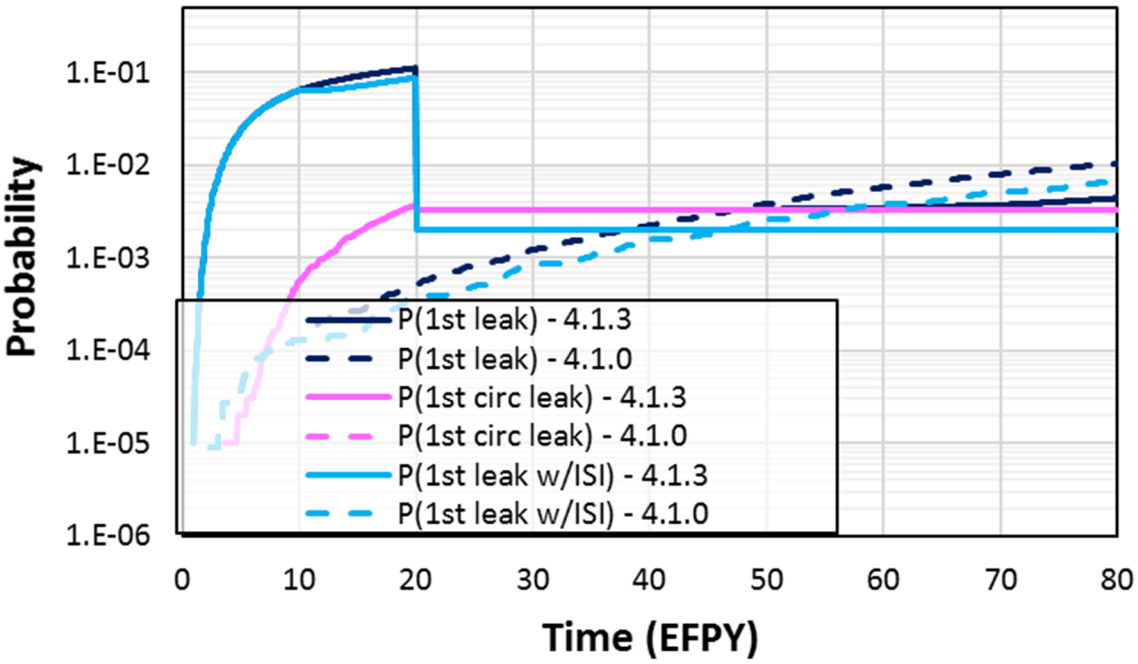

Figure 3-74 Case 4.1.3 time-dependent probabilities of first leak

Figure 3-75 shows the probabilities of rupture from Case 4.1.3 as compared to Case 4.1.0. In Case 4.1.0 there were no ruptures. In Case 4.1.3, the probability of rupture is very low (i.e., 3.3×10^{-3}) and reflects ruptures that only occurred during the first 20 EFPY before the overlay was applied. The probability of rupture is reduced by a factor of 5 (i.e., to 6.8×10^{-4}) when a 10-year inspection frequency is considered. Along with the results for first leak, these results demonstrate a large improvement from using an overlay for PWSCC mitigation purposes.

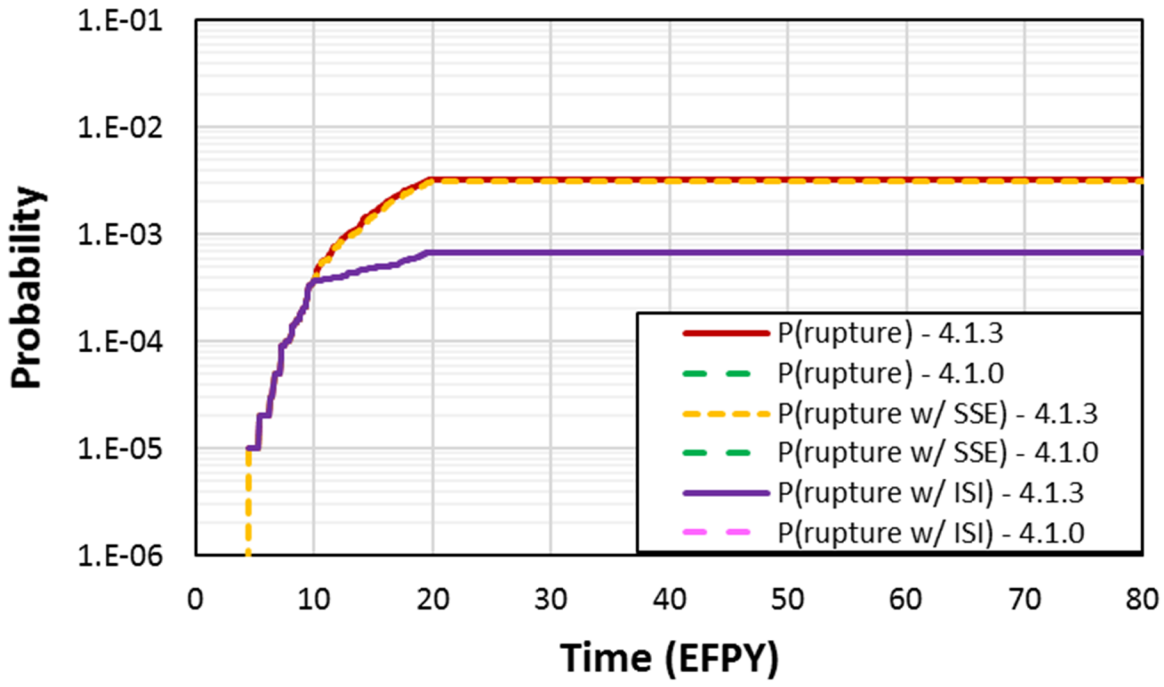

Figure 3-75 Case 4.1.3 time-dependent probability of rupture

3.5.4.2.6 Supplemental Analyses

In Case 4.1.3, 15 of the 100,000 realizations had potential ruptures under combined normal operating and non-probabilistically treated seismic loads before leak rate detection. Figure 3-76 shows an estimate of the probability of rupture with leak rate detection and probabilistically applied seismic loads. The results include a modification based on a 1×10^{-3} annual frequency of a seismic event leading to an applied bending stress of 161.9 MPa. The 1×10^{-3} annual frequency is the maximum from Section E.3.1 of [60]. This analysis considers probabilistically treated seismic events during the time between (a) the first potential rupture under combined normal operating and non-probabilistically treated seismic loads, and (b) the first rupture under the normal operating loads by themselves. Based on this analysis, the probability of rupture with leak rate detection when seismic events are probabilistically considered is around 6×10^{-8} at 20 EFPY, which gives an annual rupture frequency of around 3×10^{-9}. The probability is reported at 20 EFPY in this case because all 15 of the events occurred before the overlay mitigation was applied at 20 EFPY.

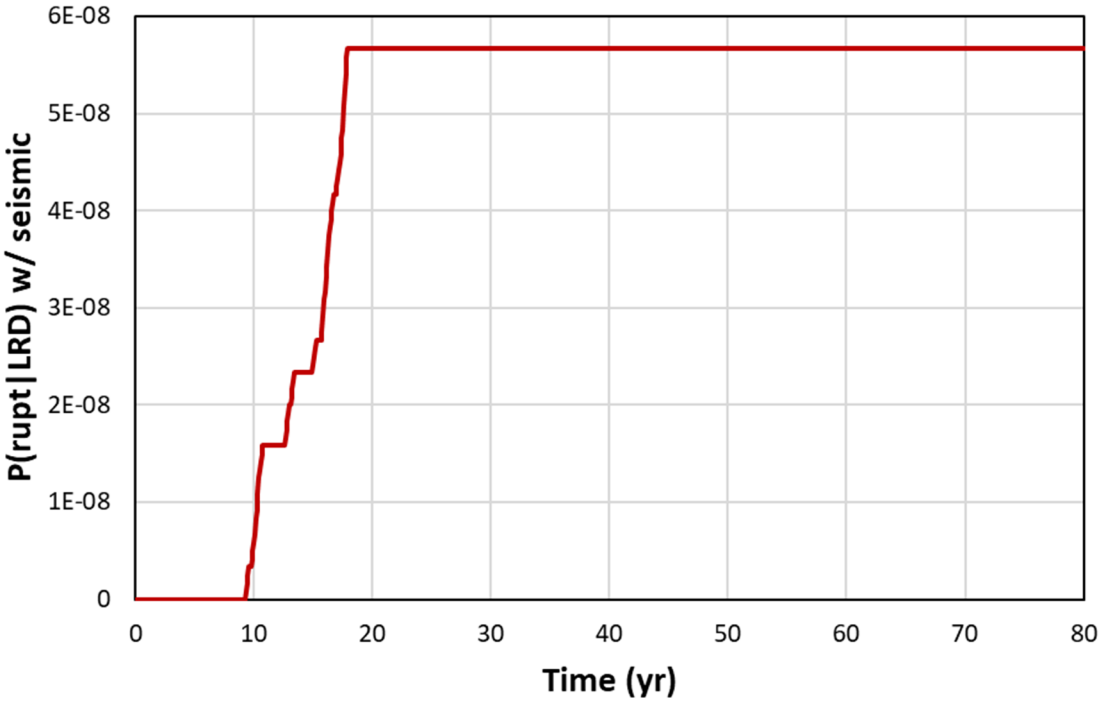

Figure 3-76 Case 4.1.3 time-dependent probability of rupture with leak rate detection under probabilistically treated seismic loads

3.5.5 No Mechanical Mitigation

3.5.5.1 Case description

Case 4.1.4 was a sensitivity study of Case 4.1.0 without mechanical mitigation. The WRS profiles from Case 4.1.0 were used to represent the WRS profiles for Case 4.1.4. Although the Case 4.1.0 WRS profiles were generated for a double-vee groove weld with an Alloy 52/152 inlay, they are also applicable to the Case 4.1.4 Alloy 82/182 double-vee groove weld because the welding sequences are the same and the temperature-dependent stress strain curves are essentially identical between Alloy 52/152 and Alloy 82/182. The normal operating temperature used to analyze this case reflects cold-leg operating conditions because those are the conditions for the limited number of inservice welds represented by this case. The WRS profiles are displayed in Figure 3-57. Section B17 describes the specific inputs and other simulation details used to analyze the case.

3.5.5.2 Results and Analysis

3.5.5.2.1 Probability of Rupture with Detection

There were no ruptures with a 1 gpm leak rate detection capability for this case.

3.5.5.2.2 Leak Rate Jump

As shown in Figure 3-77, Case 4.1.4 generated leak rate jump events with a probability of 3.2×10^{-4} at 80 EFPY, which corresponds to an annual frequency of 4.0×10^{-6}. However, there were no ruptures with a 1 gpm leak rate detection capability as stated in Section 3.5.5.2.1. The highly tensile mean axial WRS value at the insider diameter led to similar causes of leak rate jump as presented for Case 4.1.3 in Section 3.5.4.2.2.

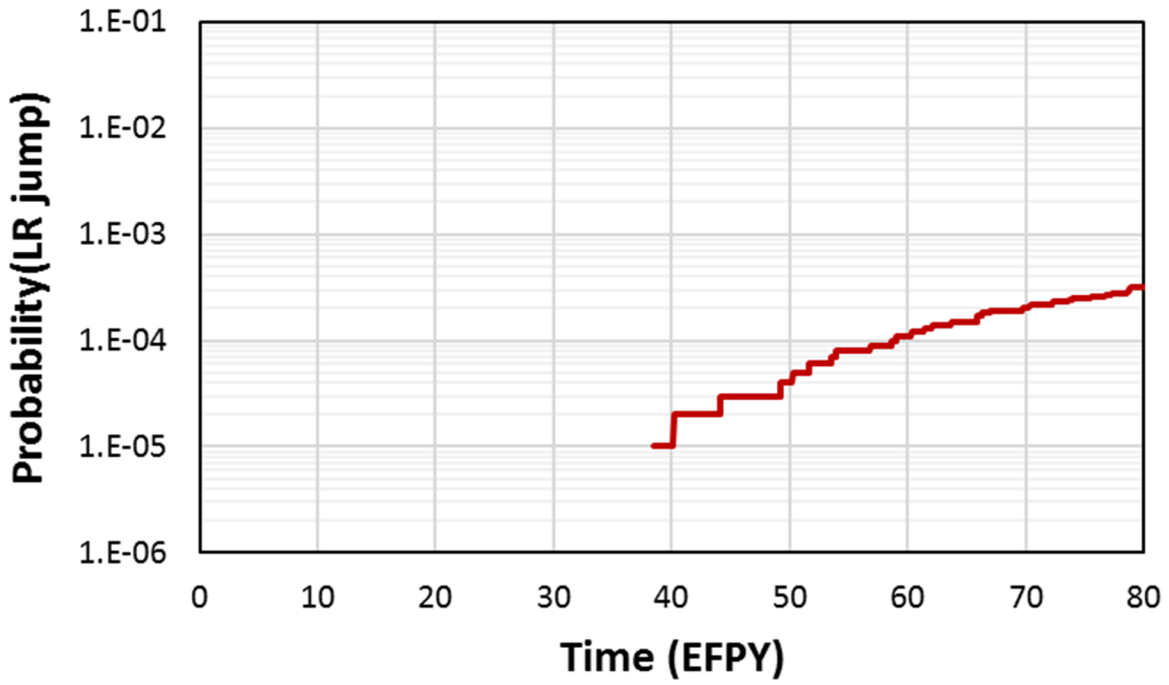

Figure 3-77 Case 4.1.4 time-dependent probability of leak rate jump

3.5.5.2.3 LBB Time Lapse

The mean LBB time lapses and standard errors with 1 and 10 gpm leak rate detection capabilities were respectively as follows:

- 23.8 ± 3.2 months (minimum observed: 0 months)
- 23.7 ± 3.2 months (minimum observed: 0 months)

Note that all results beyond 12 EFPY have been excluded for the reasons explained in Section 3.2.1.2.3. The minimum observations were estimated at 0 months because the time step used for the simulation was 1 month. A smaller time step would have yielded more accurate estimates of the LBB time lapses in these realizations.

Figure 3-78 shows the LBB time lapse CDFs for Case 4.1.4 as compared with Case 4.1.3. The LBB time lapses for Case 4.1.4 are higher as compared to Case 4.1.3, which indicates longer times from detectable leakage to rupture. This result is expected because the lower operating temperature used in the Case 4.1.4 analysis produced slower crack growth rates. Like

Case 4.1.3, in a few realizations, the LBB time lapses were zero in Case 4.1.4. Because the LBB time lapse QoI was calculated based on the combined normal operating and non-probabilistically treated seismic loads as explained in Section 2.2.3, values less than or equal to zero mean that there is some seismic contribution to the failure frequency. This frequency is estimated in Section 3.5.5.2.6. Under just the normal operating loads, these cracks did not rupture the pipe for an additional 16 to 24 months.

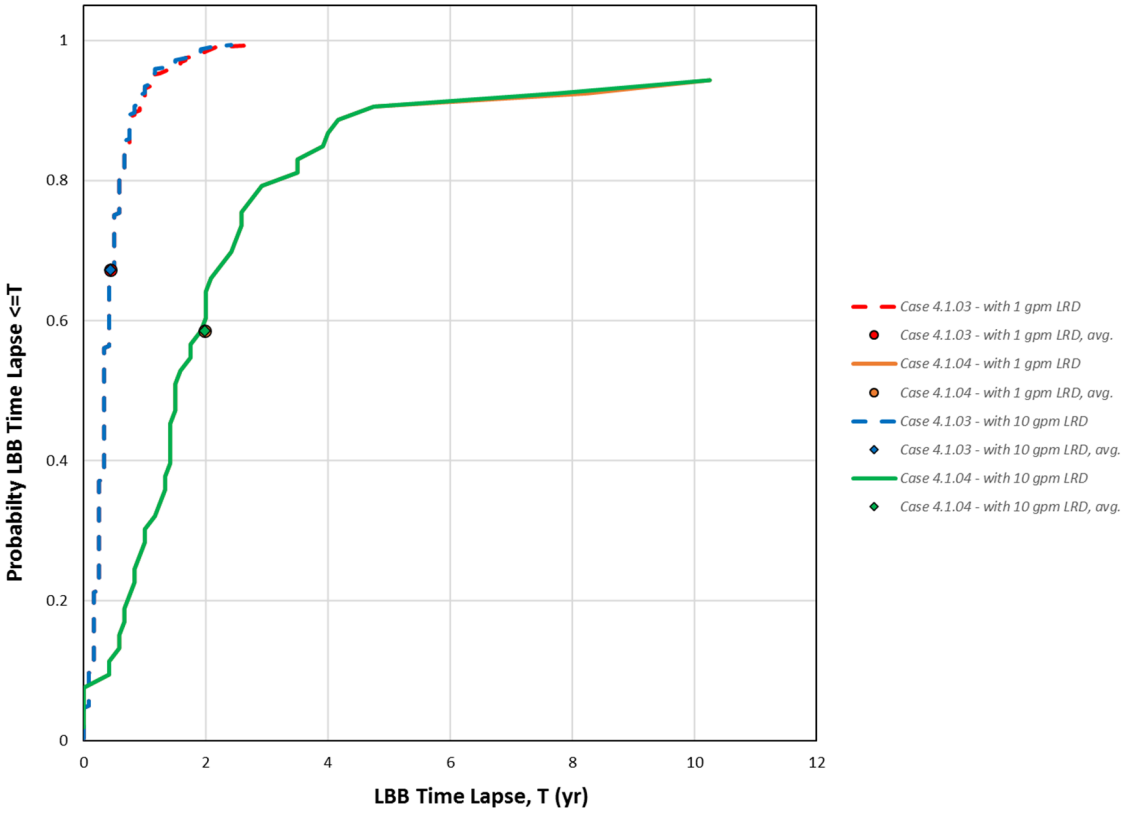

Figure 3-78 Case 4.1.4 LBB time lapse results

3.5.5.2.4 LBB Ratio

The mean LBB ratios and standard errors with 1 and 10 gpm leak rate detection capabilities were respectively as follows:

- 3.08 ± 0.12 (minimum observed: 1.45)
- 2.88 ± 0.09 (minimum observed: 1.45)

Like the LBB time lapse, the critical crack size calculations for the LBB ratio are based on the combined normal operating and non-probabilistically seismic loads as explained in Section 2.2.4. This explains the LBB ratio values lower than 2. Figure 3-79 shows the LBB ratio CDF plots for Case 4.1.4 as compared with Case 4.1.3. The overall distributions are similar, which is expected because the two cases use the same WRS profiles for the first 20 EFPY, and all the ruptures occur within the first 20 EFPY in Case 4.1.3.

In contrast with Case 4.1.3, the minimum LBB ratios observed were greater than 1 in Case 4.1.4. Despite the minimum LBB time lapses being estimated as 0 months, the minimum LBB ratios were greater than 1 because of the selected time step of 1 month. In addition, the reason for these discrepancies is that the crack sizes leading to either a 1 or 10 gpm leak rate as used in the LBB ratio calculations were estimated using a linear interpolation. The leakage crack sizes were still lower than the critical crack sizes. Thus, in each of these realizations, the detectable leak rate occurred in the beginning of the timestep when the crack was still stable, and the crack continued to grow and lead to rupture under the combined normal operating and non-probabilistically treated seismic loads at the end of the same timestep.

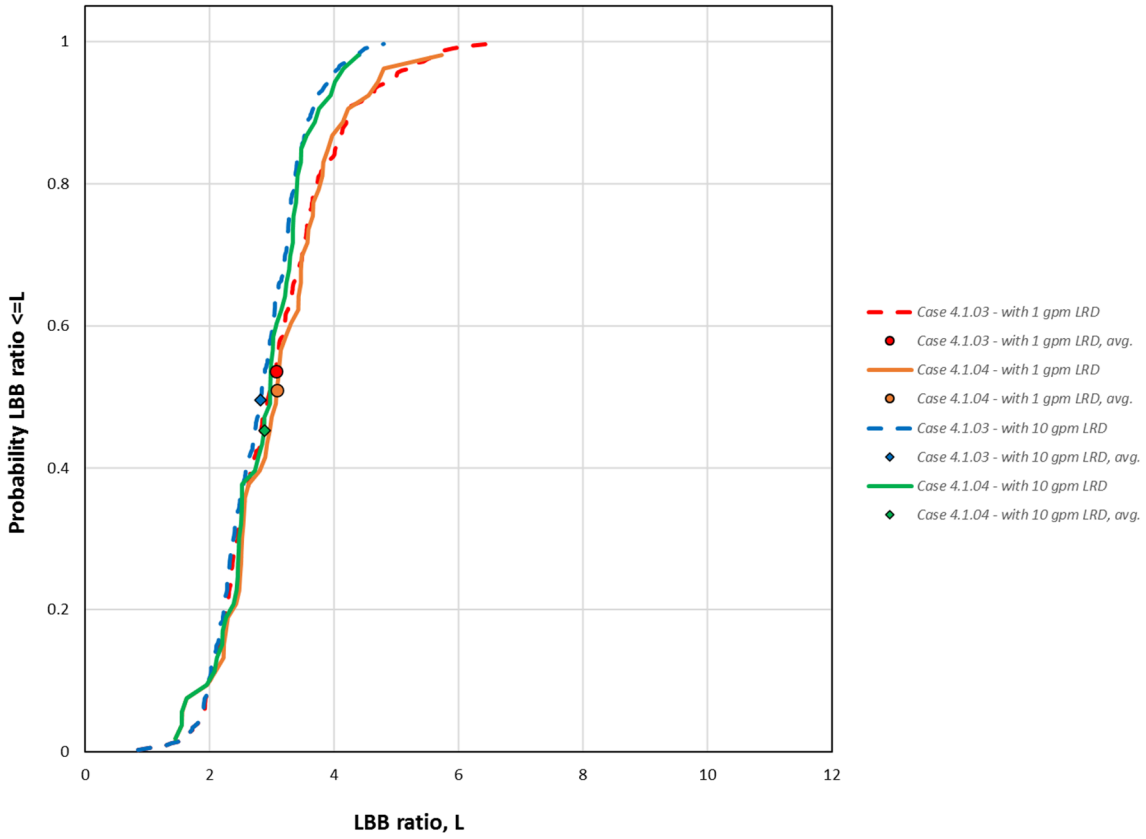

Figure 3-79 Case 4.1.4 LBB ratio results

3.5.5.2.5 Standard Indicators

Figure 3-80 shows the probabilities of first crack for Case 4.1.4 as compared with Case 4.1.0. Despite the lower operating temperature in Case 4.1.4, the likelihood of having a crack is higher than Case 4.1.0 because there is no Alloy 52/152 inlay.

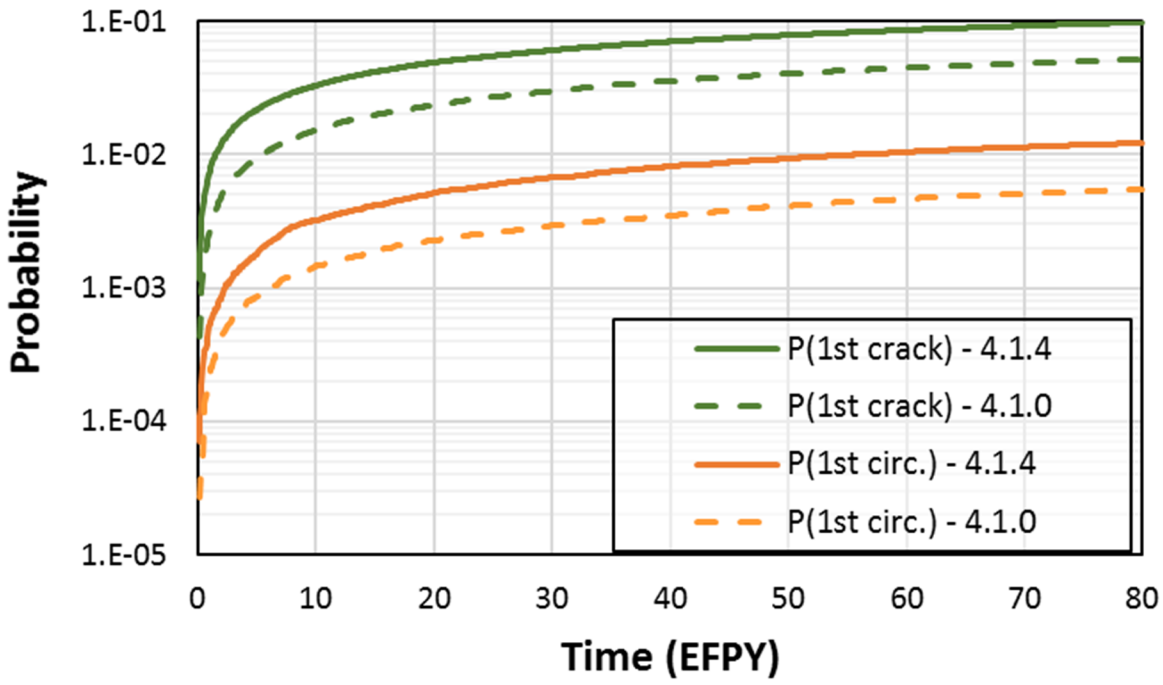

Figure 3-80 Case 4.1.4 time-dependent probabilities of first crack

Figure 3-81 shows the probabilities of first leak for Case 4.1.4 as compared to Case 4.1.0. As observed for Case 4.1.3, the probabilities of first leak in Case 4.1.4 are higher than in Case 4.1.0 because of the more tensile mean hoop WRS profile. However, due to the lower operating temperature, which reduces the crack growth rates, the influence of a 10-year inspection frequency is stronger for Case 4.1.4 and leads to a lower probability of first leak at 80 EFPY.

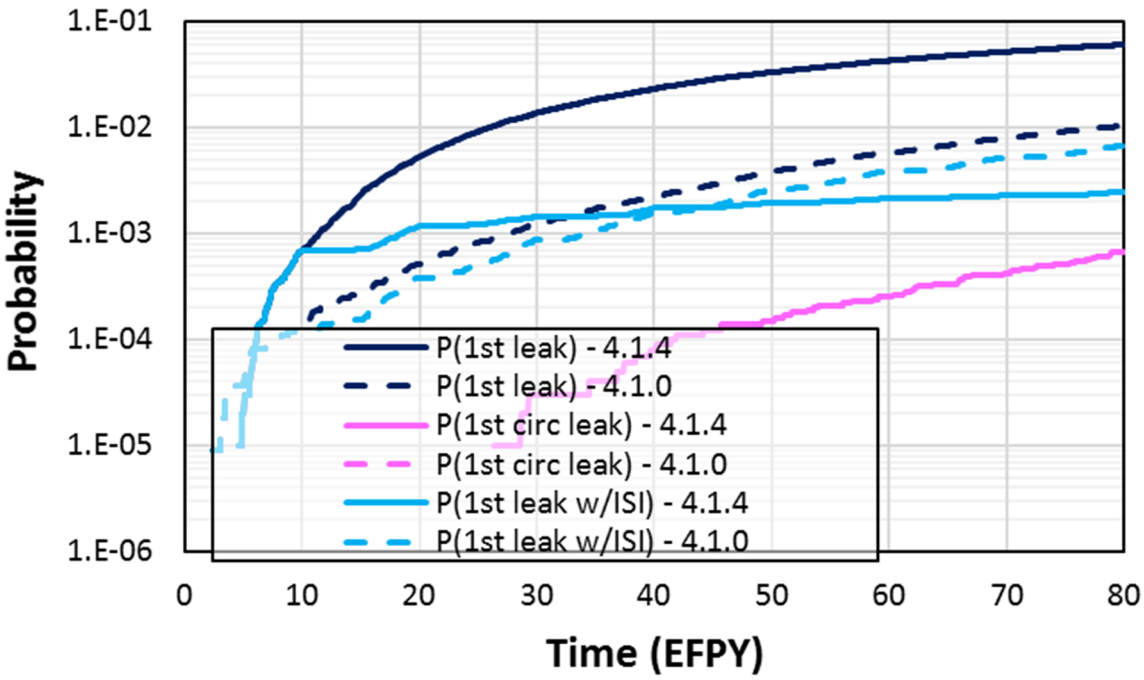

Figure 3-81 Case 4.1.4 time-dependent probabilities of first leak

Figure 3-82 shows the probabilities of rupture from Case 4.1.4 as compared to Case 4.1.0. In Case 4.1.0 there were no ruptures. In Case 4.1.4, the probability of rupture at 80 EFPY is low at 5.4×10^{-4}, which represents an annual rupture frequency of 6.75×10^{-6}. The probability becomes negligible (i.e., 6.5×10^{-10}) when a 10-year inspection frequency is considered.

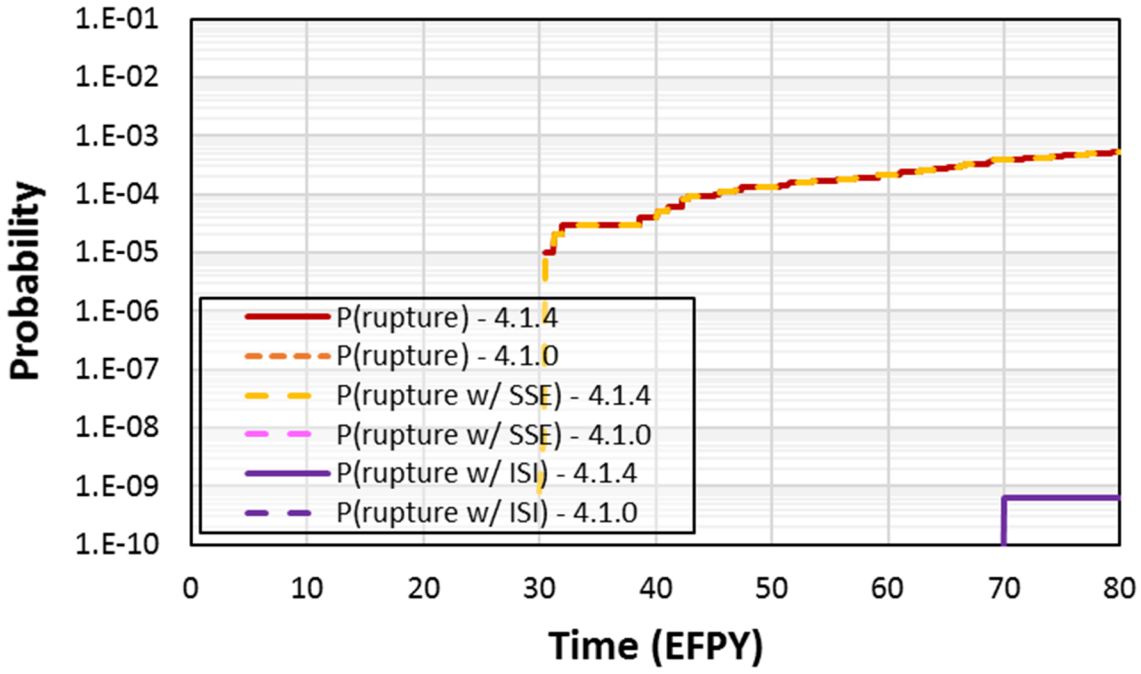

Figure 3-82 Case 4.1.4 time-dependent probabilities of rupture

3.5.5.2.6 Supplemental Analyses

In Case 4.1.4, 4 of the 100,000 realizations had potential ruptures before leak rate detection under combined normal operating and non-probabilistically treated seismic loads. Figure 3-83 shows an estimate of the probability of rupture with leak rate detection when seismic loads are considered probabilistically. Like for Case 4.1.3, the results include a modification based on a 1×10^{-3} annual frequency of a seismic event leading to an applied bending stress of 161.9 MPa. The 1×10^{-3} annual frequency is the maximum from Section E.3.1 of [60]. This analysis considers probabilistically treated seismic events during the time between (a) the first potential rupture under combined normal operating and non-probabilistically treated seismic loads, and (b) the first rupture under the normal operating loads by themselves. Based on this analysis, the probability of rupture with leak rate detection when seismic events are probabilistically considered is around 6.3×10^{-8} at 80 EPFY, which gives an annual rupture frequency of around 8×10^{-10}.

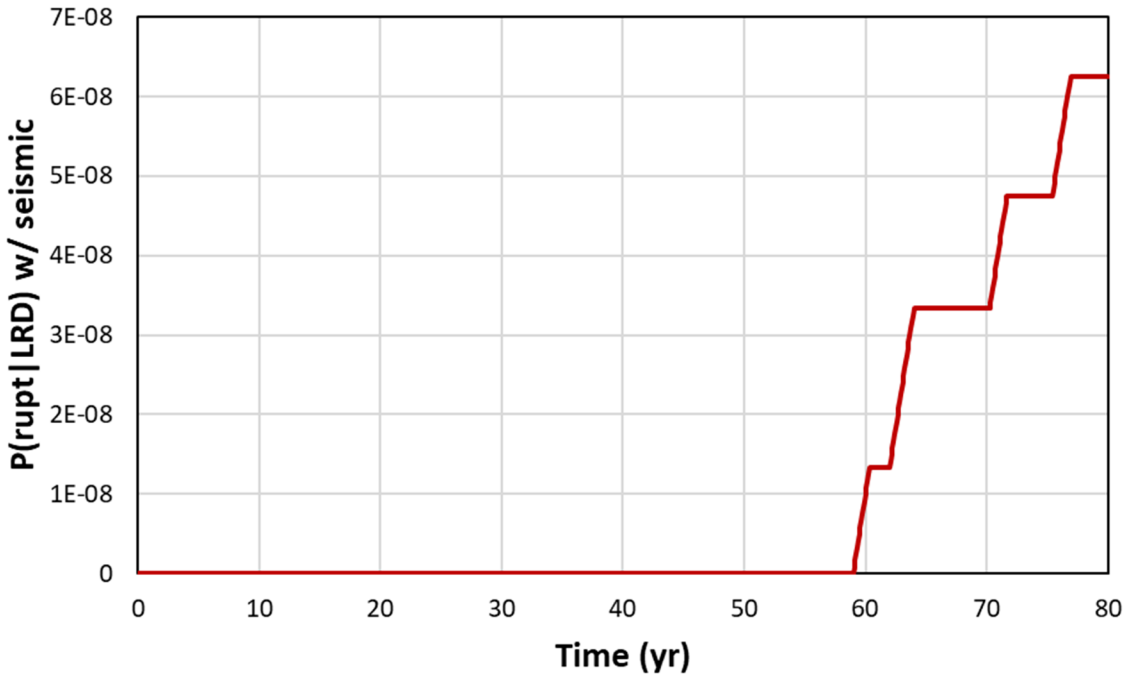

Figure 3-83 Case 4.1.4 time-dependent probability of rupture with leak rate detection under probabilistically treated seismic loads

3.6 Bin 5a: CE Hot Leg Branch Line Nozzle DMWs

The following cases were used to analyze the CE hot leg branch line nozzle DMWs represented by Bin 5a:

- Case 5.1.0: base case
- Case 5.1.1: initial flaws
- Case 5.1.2: more severe WRS

The cases and associated analyses are described in Sections 3.6.1 through 3.6.3, respectively.

3.6.1 Base Case

3.6.1.1 Case Description

The objective of Case 5.1.0 was to assess the base likelihood of failure caused by PWSCC initiation and growth without mechanical mitigation. The effects of leak detection, ISI, and SSE were also assessed. This case used bounding values for the geometry and loading, both normal operating and SSE, based on the licensing submittals referenced in Table 2-1 for the bin. This piping system contains aged cast austenitic stainless steels (SS), which may lead to lower fracture toughness. The ISI parameters used were the same as those used for the pressurizer surge line nozzle DMW analyses. The applicability of the pressurizer surge line nozzle ISI parameters to the CE hot leg branch line nozzle DMWs is documented in the

applicability assessment guidance for POD curves [61]. Figure 3-84 shows the WRS profiles used to analyze the case. They were generated from FEA results, and additional details on their development are in Section C5.2. Section B18 describes the specific inputs and other simulation details used to analyze the case.

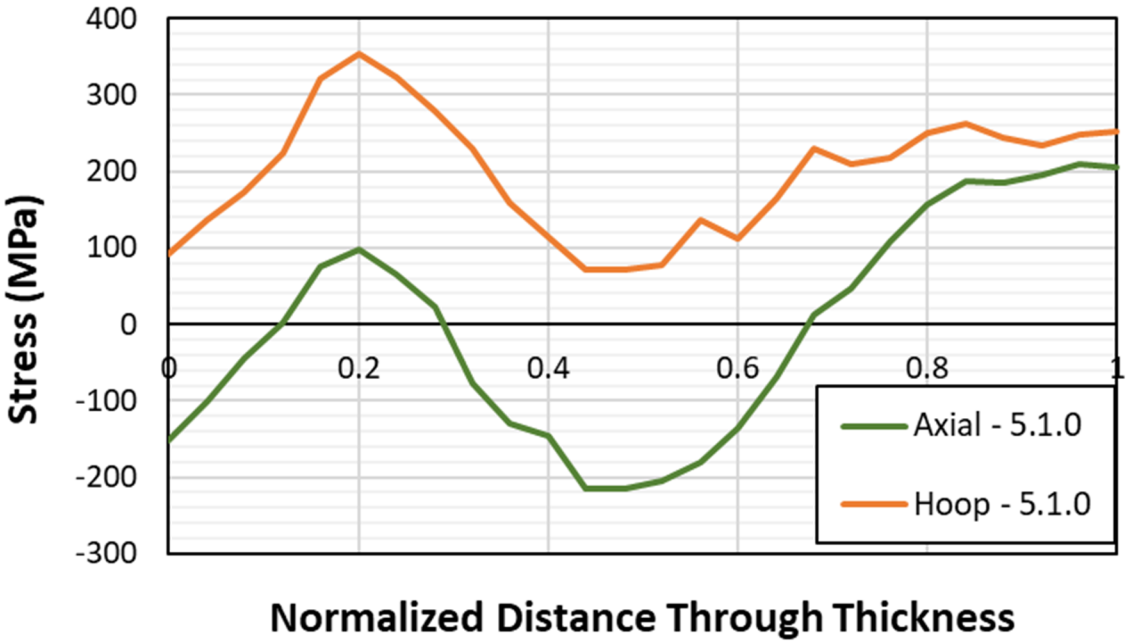

Figure 3-84 Case 5.1.0 WRS profiles

3.6.1.2 Results and Analysis

3.6.1.2.1 Probability of Rupture with Detection

There were no ruptures with a 1 gpm leak rate detection capability for this case

3.6.1.2.2 Leak Rate Jump

There were no leak rate jump events for this case.

3.6.1.2.3 LBB Time Lapse

There were no circumferential crack leaks or ruptures for this case; therefore, this QoI cannot be reported.

3.6.1.2.4 LBB Ratio

There were no circumferential crack leaks or ruptures for this case; therefore, this QoI cannot be reported.

3.6.1.2.5 Standard Indicators

Figure 3-85 shows the probabilities of first crack for Case 5.1.0 as compared with Case 1.1.6a. Due to the high mean hoop WRS value at the inside diameter, the likelihood of having an axial crack is higher in Case 5.1.0. However, there were no circumferential crack initiations because of the highly compressive mean axial WRS value at the inside diameter.

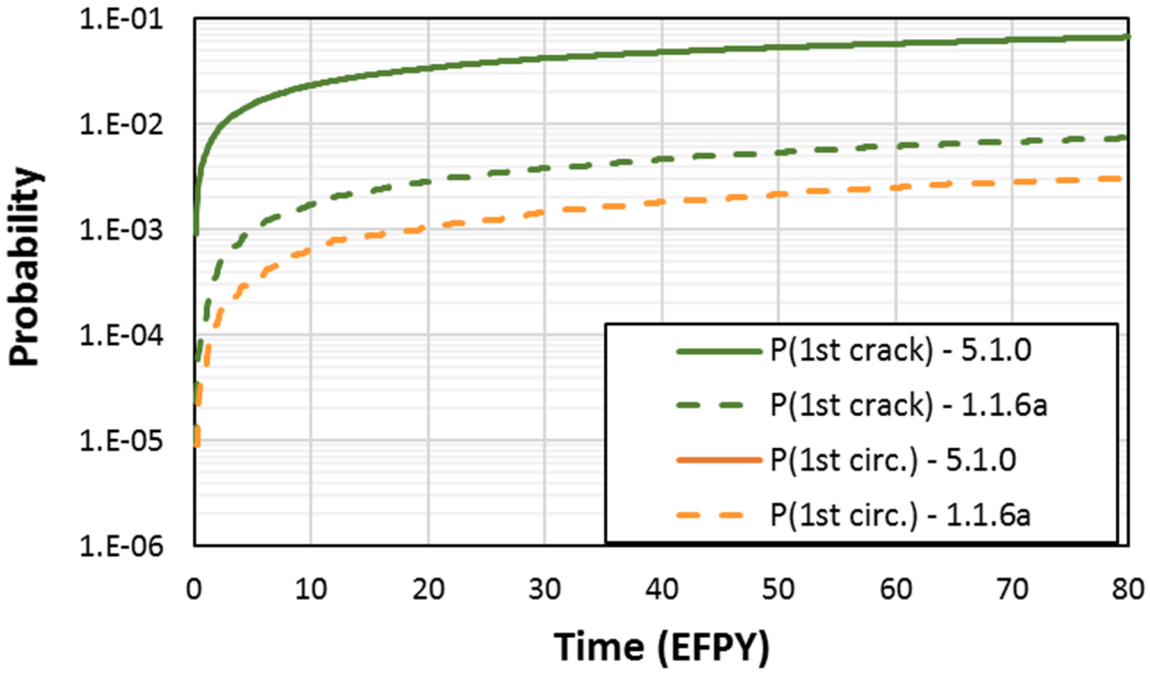

Figure 3-85 Case 5.1.0 time-dependent probabilities of first crack

Figure 3-86 shows the probabilities of first leak for Case 5.1.0 as compared with Case 1.1.6a. Like the probability of first crack, the probability of first leak results are higher in Case 5.1.0 because of the higher likelihood of axial cracks.

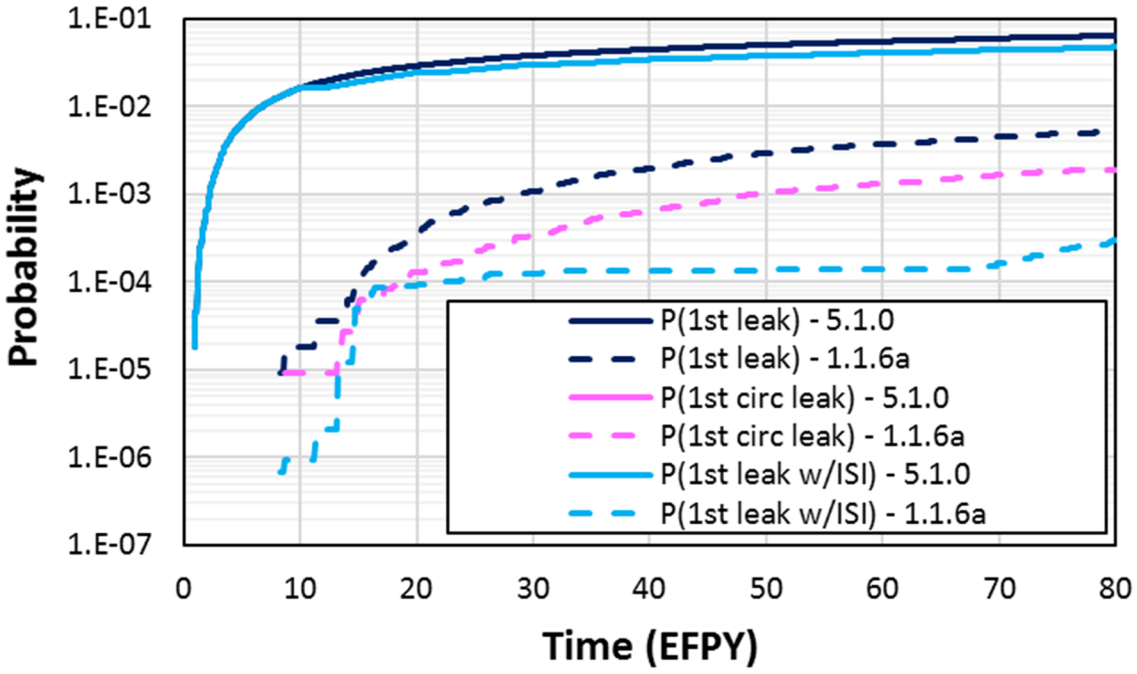

Figure 3-86 Case 5.1.0 time-dependent probabilities of first leak

3.6.2 Initial Flaws

3.6.2.1 Case Description

The objective of Case 5.1.1 was to assess the base likelihood of failure with pre-existing flaws and subsequent PWSCC growth of circumferential and axial cracks without mechanical mitigation. The effects of leak detection, ISI, and SSE were also assessed. This case used the same inputs as Case 5.1.0 except that, instead of Direct Model 1 for crack initiation, it used pre-existing axial and circumferential flaws. The WRS profiles used were the same as used in the Case 5.1.0 analysis. Section B19 describes the specific inputs and other simulation details used to analyze the case.

3.6.2.2 Results and Analysis

3.6.2.2.1 Probability of Rupture with Detection

There were no ruptures with a 1 gpm leak rate detection capability for this case.

3.6.2.2.2 Leak Rate Jump

There were no leak rate jump events for this case.

3.6.2.2.3 LBB Time Lapse

The mean LBB time lapses and standard errors with 1 and 10 gpm leak rate detection capabilities were respectively as follows:

- 54.3 ± 2.4 months (minimum observed: 23 months)
- 15.5 ± 0.6 months (minimum observed: 6 months)

Note that all results beyond 12 EFPY have been excluded for the reasons explained in Section 3.2.1.2.3.

Figure 3-87 shows the LBB time lapse CDF plots for Case 5.1.1 as compared with Case 1.1.6b. The lowest values are associated with the 10 gpm leak rate detection capability. Considering the smaller diameter pipe size in Case 5.1.1, a 10 gpm leak rate requires a larger crack angle and is thus closer to the critical crack size at rupture.

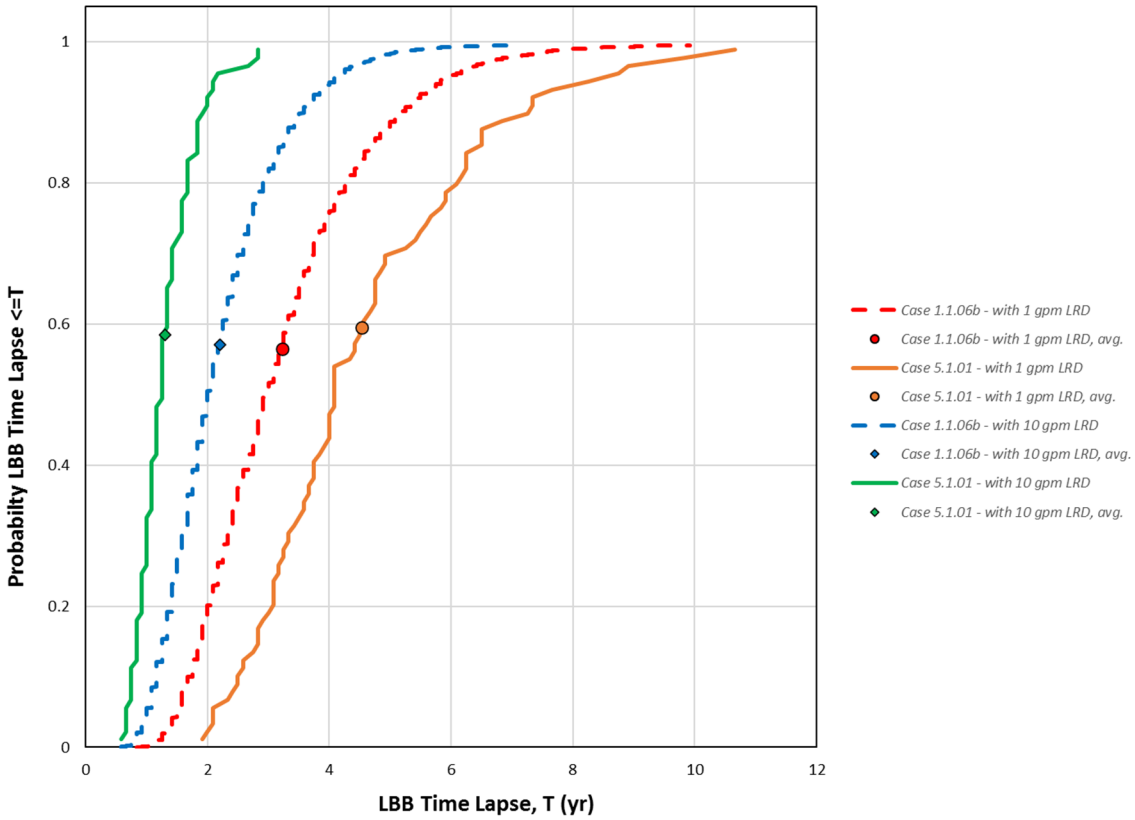

Figure 3-87 Case 5.1.1 LBB lapse time results

3.6.2.2.4 LBB Ratio

The mean LBB ratios and standard errors with 1 and 10 gpm leak rate detection capabilities were respectively as follows:

- 3.42 ± 0.02 (minimum observed: 2.93)
- 1.81 ± 0.01 (minimum observed: 1.66)

Figure 3-88 shows the LBB ratio CDF plots for Case 5.1.1. The results are lower as compared to Case 1.1.6b because of the smaller diameter of the piping. Figure 3-20 shows a similar comparison for the pressurizer surge line nozzle DMW, which also has a smaller diameter in comparison to the Westinghouse RVON and RVIN DMWs.

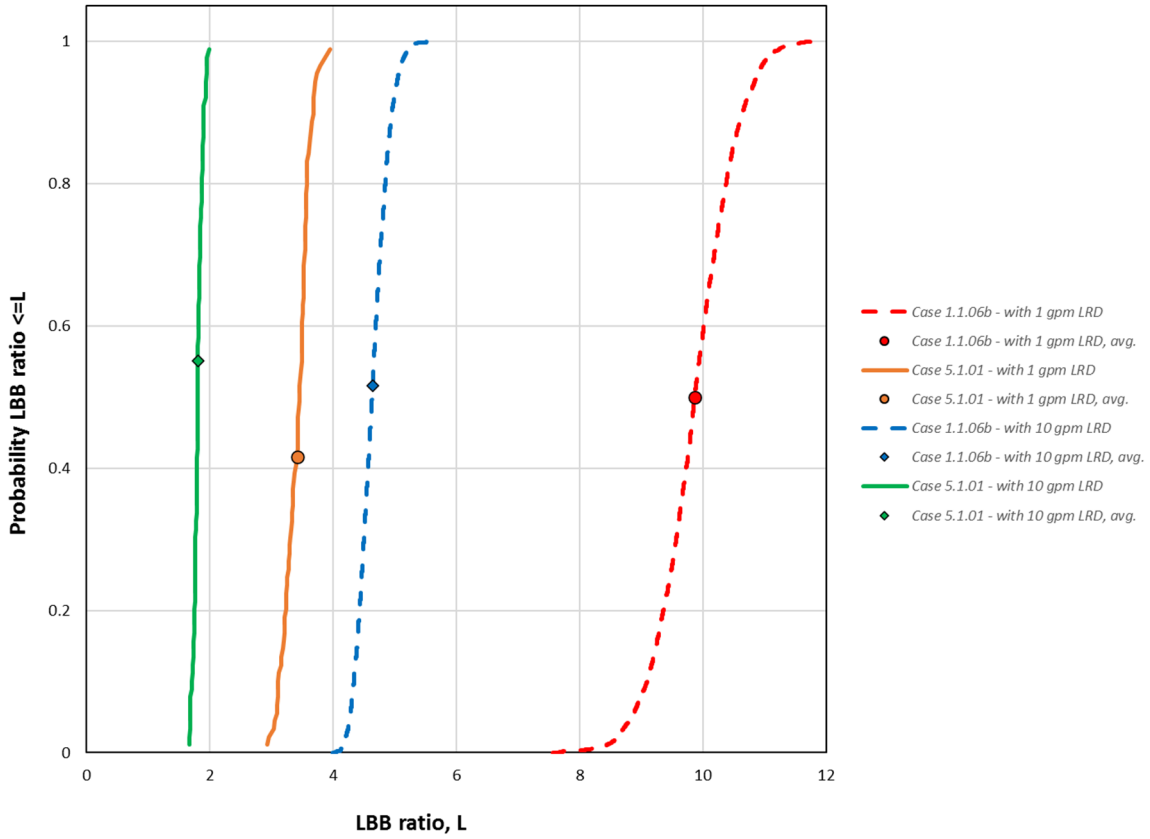

Figure 3-88 Case 5.1.1 LBB ratio results

3.6.2.2.5 Standard Indicators

Figure 3-89 shows the probabilities of first leak for Case 5.1.1. Compared to the Case 1.1.6b results, the probability of first leak is higher at 80 EFPY, and the impact of ISI is reduced because, at 10 EFPY, most of the realizations have already begun to leak. Of note, almost all the first leaks are caused by axial cracks. The probability of first circumferential crack leak is in the range of 2×10^{-2} at 80 EFPY.

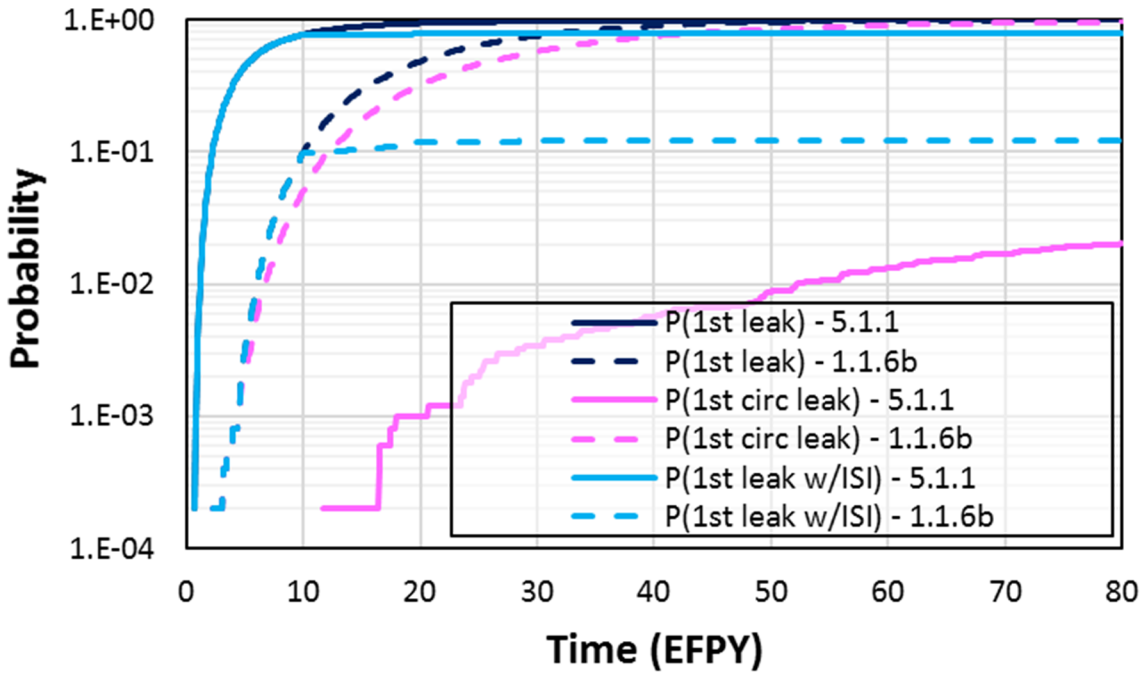

Figure 3-89 Case 5.1.1 time-dependent probabilities of first leak

Due to the low probability of first circumferential crack leak, the probability of rupture in Case 5.1.1 is also low and reaches about 1.76 x 10^{-2} at 80 EFPY as seen in Figure 3-90. When a 10-year inspection frequency is considered, the probability reduces to the 1 x 10^{-8} range.

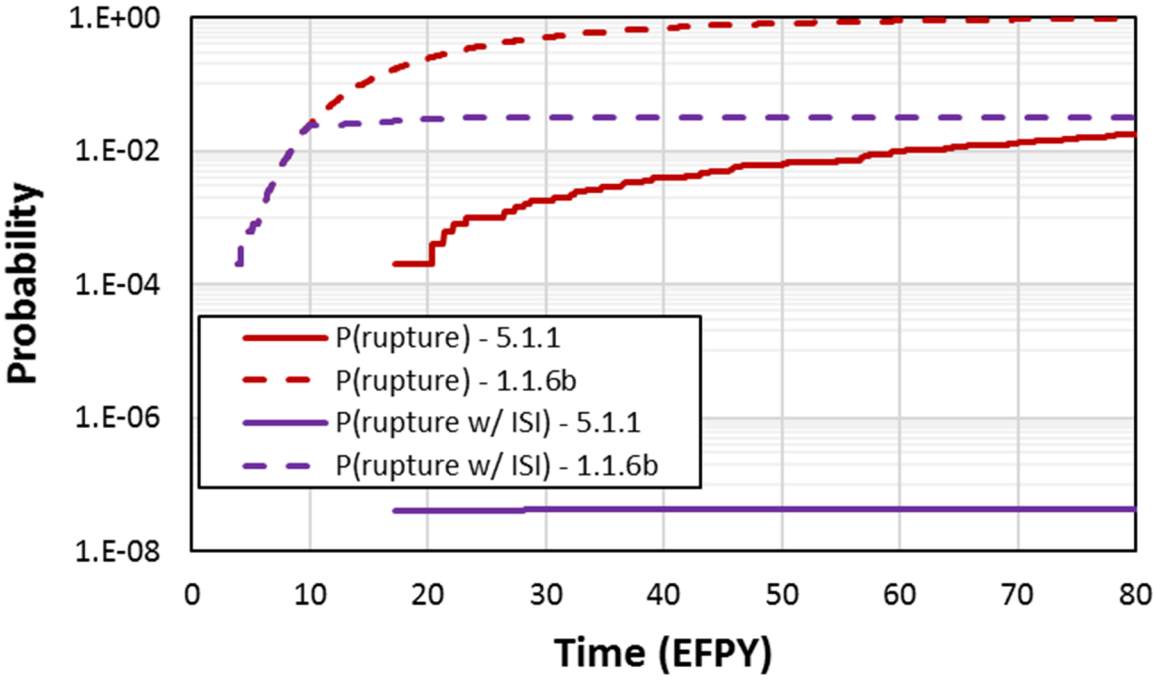

Figure 3-90 Case 5.1.1 time-dependent probabilities of rupture

3.6.3 More Severe WRS

3.6.3.1 Case Description

Case 5.1.2 was a sensitivity study of Case 5.1.0 considering a more severe WRS profile. This case used the same inputs as Case 5.1.0 but with a change to the mean hoop and axial WRS profiles. The standard deviations used to represent uncertainties in the WRS profiles were the same as in Case 5.1.0. Figure 3-91 shows the WRS profiles used to analyze the case. They were developed using FEA of a generic CE branch line geometry with the distance between the DMW and the SS weld changed to the maximum length of all welds represented by the bin. The WRS profile is considered more severe because, in general, a greater distance between the DMW and SS weld will result in more tensile stresses. Additional details on development of the WRS profiles are in Section C5.3. Section B20 describes the specific inputs and other simulation details used to analyze the case.

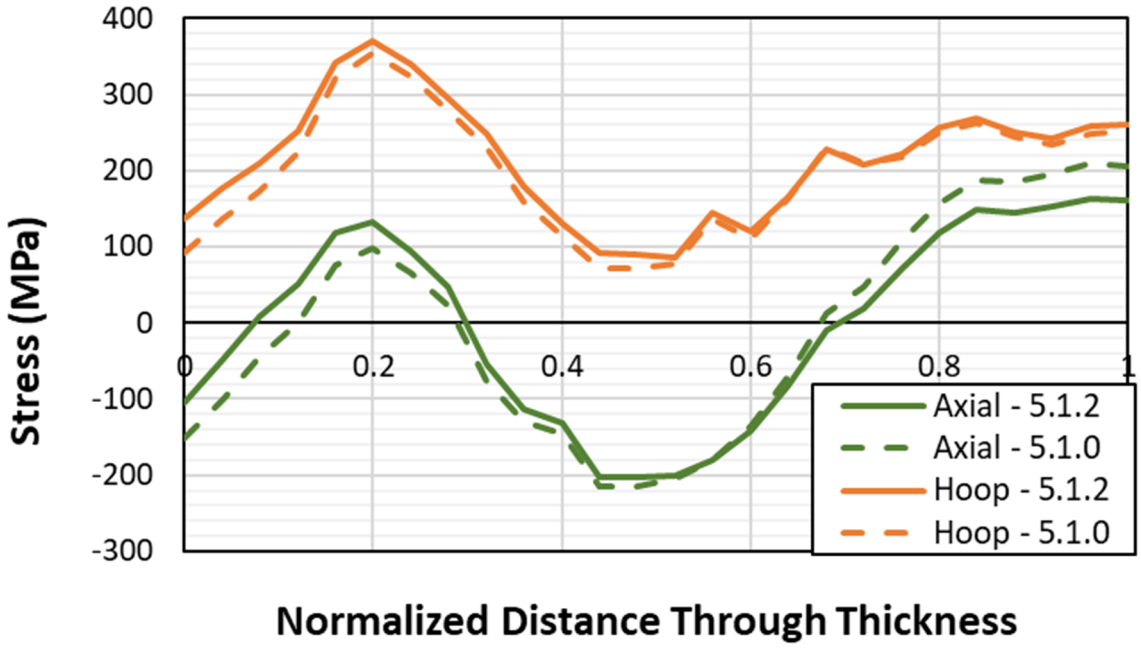

Figure 3-91 Case 5.1.2 WRS profiles

3.6.3.2 Results and Analysis

3.6.3.2.1 Probability of Rupture with Detection

There were no ruptures with a 1 gpm leak rate detection capability for this case.

3.6.3.2.2 Leak Rate Jump

There were no leak rate jump events for this case.

3.6.3.2.3 LBB Time Lapse

There were no circumferential crack leaks or ruptures for this case; therefore, this QoI cannot be reported.

3.6.3.2.4 LBB Ratio

There were no circumferential crack leaks or ruptures for this case; therefore, this QoI cannot be reported.

3.6.3.2.5 Standard Indicators

Figure 3-92 shows the probabilities of first crack for Case 5.1.2 as compared to Case 5.1.0. The use of a more severe WRS profile in Case 5.1.2 only slightly increased the probability of first crack. Although there were no circumferential crack initiations in Case 5.1.0, the probability of circumferential crack occurrence in Case 5.1.2 was 3.6 x 10^{-5} at 80 EFPY.

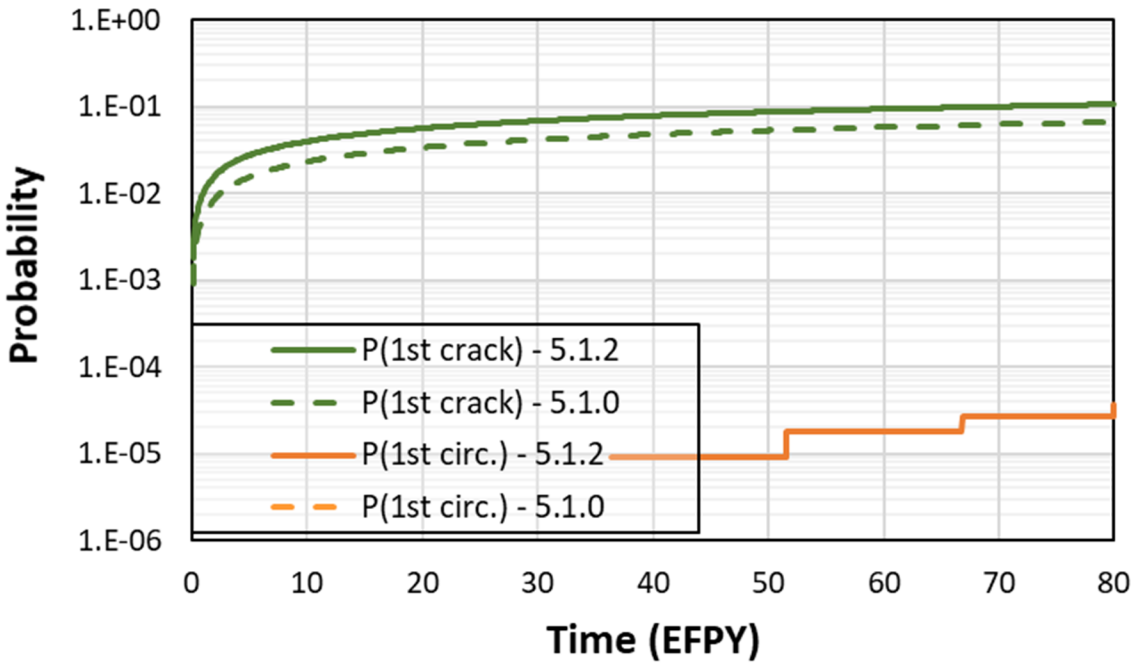

Figure 3-92 Case 5.1.2 time-dependent probabilities of first crack

Figure 3-93 shows the probability of first leak for Case 5.1.2. Like the probability of first crack, the more severe WRS profile led to an increase in the probability of first leak. However, the probability of first circumferential crack leak remained at zero. There were no occurrences of rupture over the 80-EFPY evaluation period.

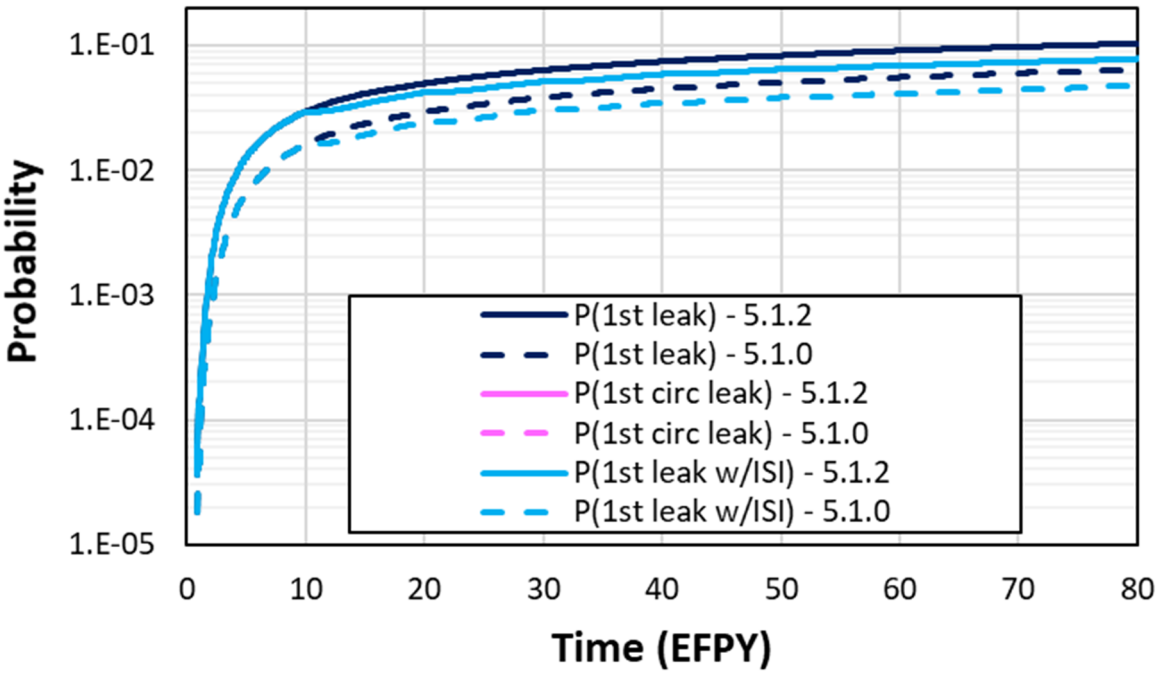

Figure 3-93 Case 5.1.2 time-dependent probabilities of first leak

3.7 Bin 5b: CE Cold Leg Branch Line Nozzle DMWs

The following cases were used to analyze the CE cold leg branch line nozzle DMWs represented by Bin 5b:

- Case 5.2.0: base case
- Case 5.2.1: initial flaws

The cases and associated analyses are described in Sections 3.7.1 and 3.7.2, respectively.

3.7.1 Base Case

3.7.1.1 Case Description

The objective of Case 5.2.0 was to assess the base likelihood of failure caused by PWSCC initiation and growth without mechanical mitigation. The effects of leak detection, ISI, and SSE were also assessed. The analysis of this case used bounding values for the geometry and loading, both normal operating and SSE stresses, based on the licensing submittals referenced in Table 2-1 for this bin. This piping system contains aged cast austenitic SS, which may lead to lower fracture toughness. The ISI parameters used were the same as those used for the pressurizer surge line nozzle DMW analyses. The applicability of the pressurizer surge line ISI parameters to the CE cold leg branch line nozzle DMWs is documented in the applicability assessment guidance for POD curves [61]. Figure 3-94 shows the WRS profiles used to analyze the case. They were developed using a general CE branch line geometry; therefore,

they are the same as the WRS profiles used in the analysis of Case 5.1.0. Section B21 describes the specific inputs and other simulation details used to analyze the case.

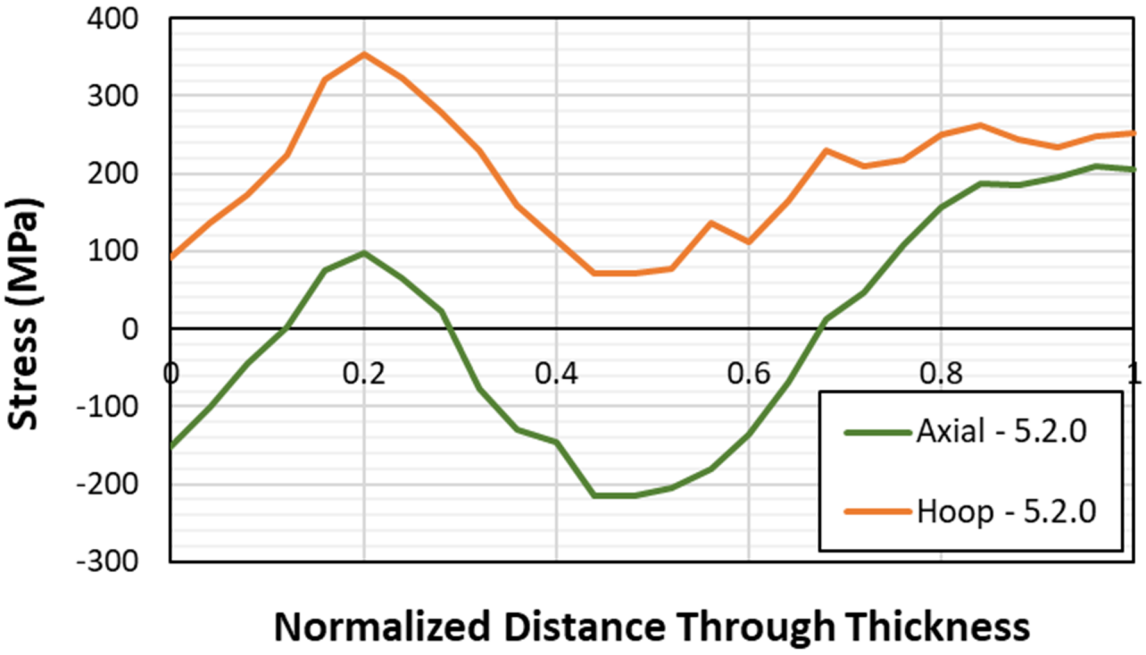

Figure 3-94 Case 5.2.0 WRS profiles

3.7.1.2 Results and Analysis

3.7.1.2.1 Probability of Rupture with Detection

There were no ruptures with a 1 gpm leak rate detection capability for this case.

3.7.1.2.2 Leak Rate Jump

There were no leak rate jump events for this case.

3.7.1.2.3 LBB Time Lapse

There were no circumferential crack leaks or ruptures for this case; therefore, this QoI cannot be reported.

3.7.1.2.4 LBB Ratio

There were no circumferential crack leaks or ruptures for this case; therefore, this QoI cannot be reported.

3.7.1.2.5 Standard Indicators

The Case 5.2.0 results were compared with Case 5.1.0 because the CE hot and cold leg branch line nozzle DMWs have similar geometries and the same WRS profiles. Figure 3-95 shows the

probabilities of first crack. The cold leg branch line results for Case 5.2.0 are lower than the hot leg branch line results from Case 5.1.0, and there were no occurrences of circumferential cracks.

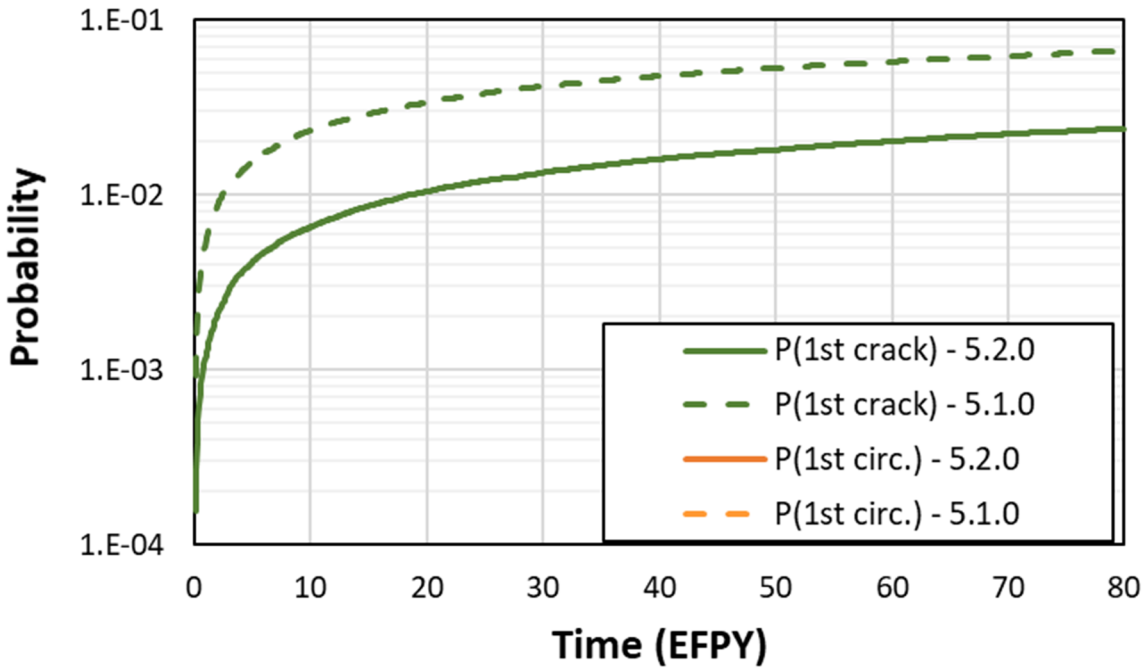

Figure 3-95 Case 5.2.0 time-dependent probabilities of first crack

Figure 3-96 shows the probabilities of first leak for Case 5.2.0 as compared with Case 5.1.0. Like the probability of first crack results, the results from Case 5.2.0 are lower than the results from Case 5.1.0.

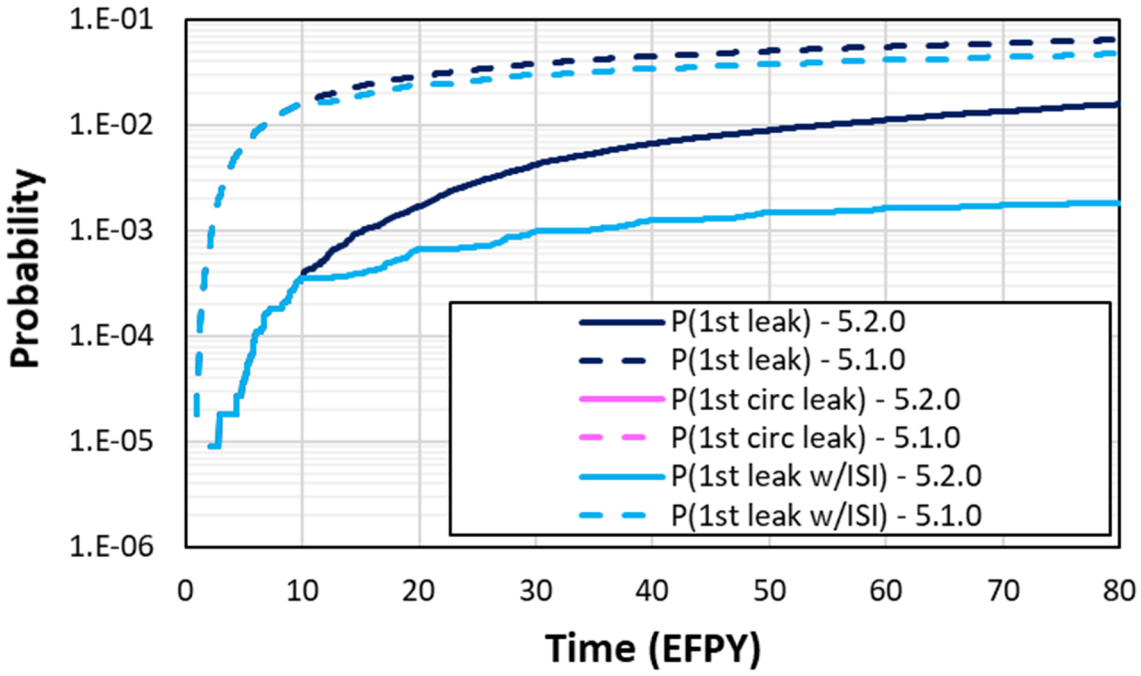

Figure 3-96 Case 5.2.0 time-dependent probabilities of first leak

3.7.2 Initial Flaws

3.7.2.1 Case Description

The objective of Case 5.2.1 was to assess the base likelihood of failure with pre-existing flaws and subsequent PWSCC growth of circumferential and axial cracks without mechanical mitigation. The effects of leak detection, ISI, and SSE were also assessed. This case used the same inputs as Case 5.2.0 except that, instead of Direct Model 1 for crack initiation, it used pre-existing axial and circumferential flaws. The WRS profiles were the same as used in the Case 5.2.0 analysis. Section B22 describes the specific inputs and other simulation details used to analyze the case.

3.7.2.2 Results and Analysis

3.7.2.2.1 Probability of Rupture with Detection

There were no ruptures with a 1 gpm leak rate detection capability for this case.

3.7.2.2.2 Leak Rate Jump

There were no leak rate jump events for this case.

3.7.2.2.3 LBB Time Lapse

The mean LBB time lapses and standard errors with 1 and 10 gpm leak rate detection capabilities were respectively as follows:

- 84.3 ± 5.2 months (minimum observed: 30 months)
- 31.8 ± 2.5 months (minimum observed: 11 months)

Note that all results beyond 12 EFPY have been excluded for the reasons explained in Section 3.2.1.2.3.

Figure 3-97 shows the LBB time lapse CDF plots for Case 5.2.1. When compared to Case 5.1.1, the LBB time lapses are longer for the cold leg branch line, which indicate that the hot leg branch line results can be considered as an upper bound for the welds represented by Bins 5a and 5b.

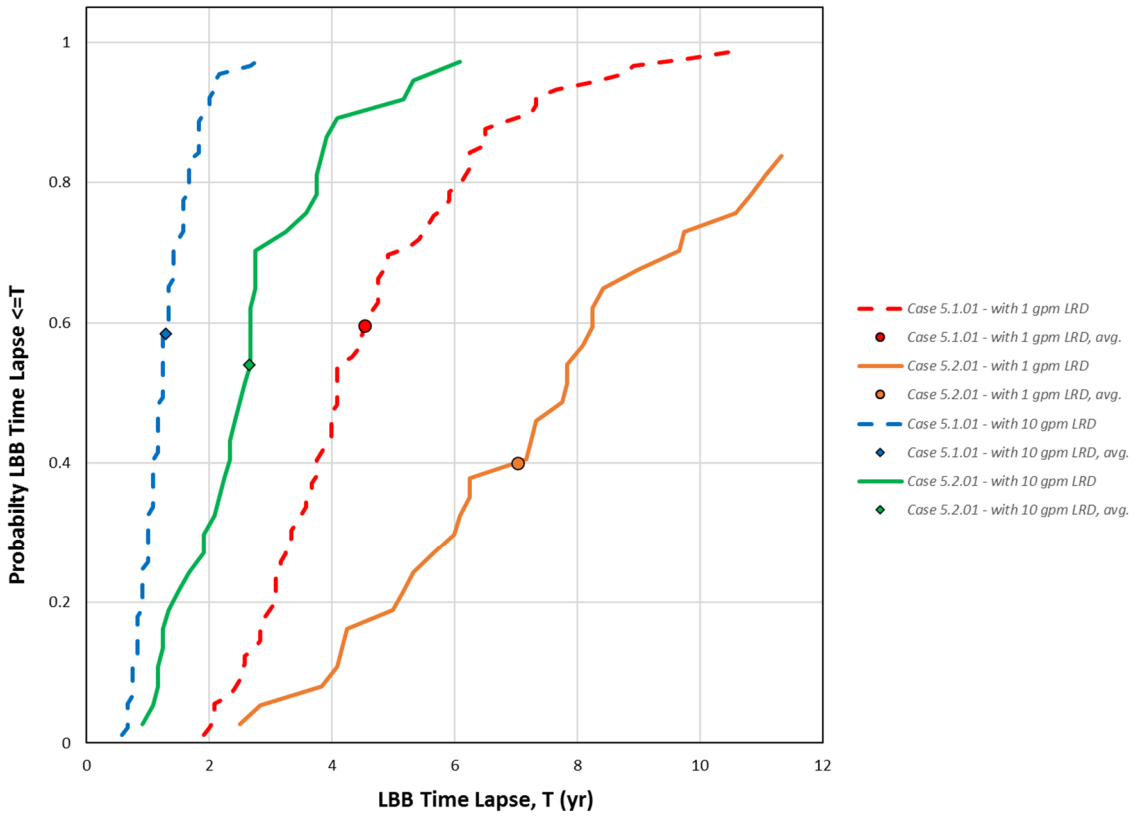

Figure 3-97 Case 5.2.1 LBB lapse time results

3.7.2.2.4 LBB Ratio

The mean LBB ratios and standard errors with 1 and 10 gpm leak rate detection capabilities were respectively as follows:

- 4.29 ± 0.03 (minimum observed: 3.88)
- 1.97 ± 0.01 (minimum observed: 1.85)

Figure 3-98 shows the LBB ratio CDF plots for Case 5.2.1 as compared with Case 5.1.1. Like the LBB time lapse results, the cold leg branch line LBB ratios are greater than the hot leg branch line ratios, which further indicate that the hot leg branch line results can be considered as an upper bound for Bins 5a and 5b.

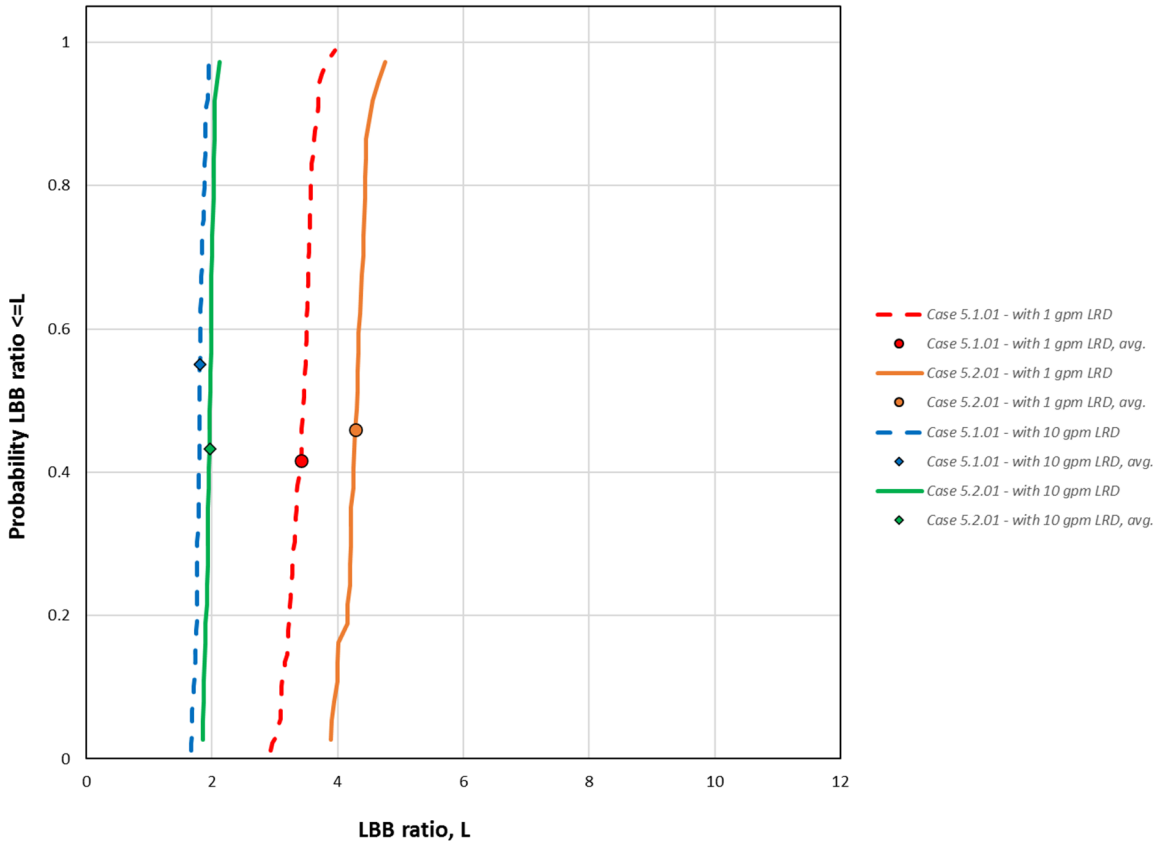

Figure 3-98 Case 5.2.1 LBB ratio results

3.7.2.2.5 Standard Indicators

Figure 3-99 shows the probabilities of first leak for Case 5.2.1. As compared to Case 5.1.1, the results are lower.

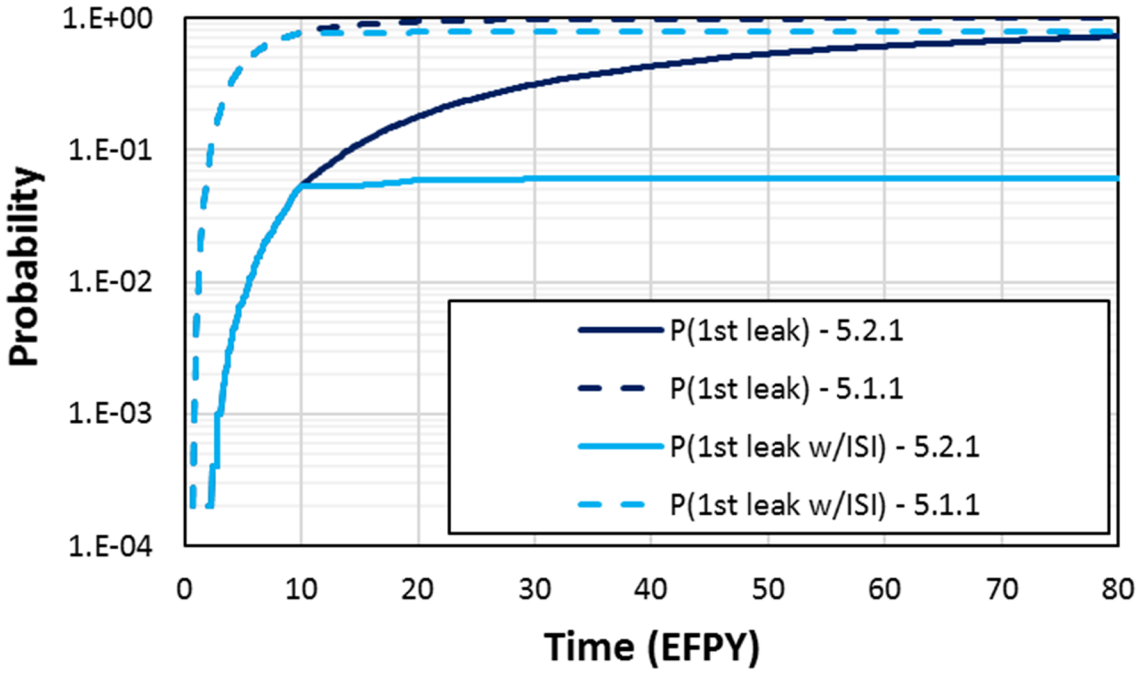

Figure 3-99 Case 5.2.1 time-dependent probabilities of first leak

Figure 3-100 shows the probabilities of rupture for Case 5.2.1. Like the probabilities of first leak, the cold leg branch line results are lower, which again indicates that the hot leg branch line results can be considered as an upper bound.

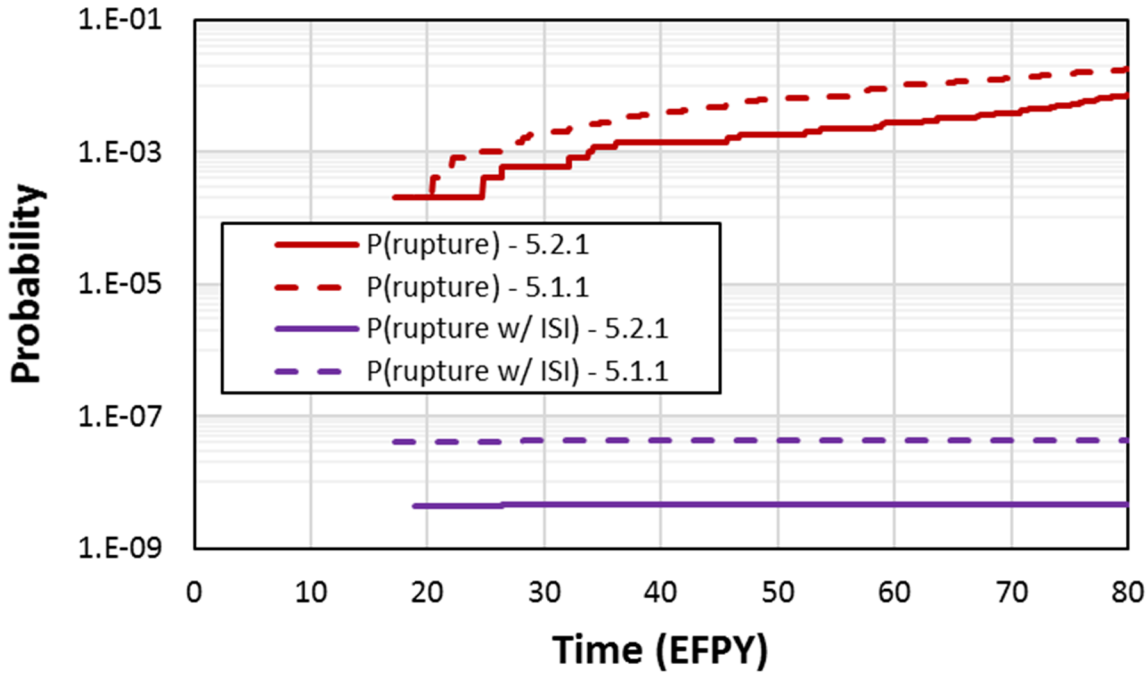

Figure 3-100 Case 5.2.1 time-dependent probabilities of rupture

3.8 Bin 6: Westinghouse Two- and Three-Loop RVON and RVIN DMWs

The following cases were used to analyze the Westinghouse two- and three-loop RVON DMWs represented by Bin 6:

- Case 1.3.0: base case
- Case 1.3.1: initial flaws

The cases and associated analyses are described in Sections 3.8.1 and 3.8.2, respectively.

3.8.1 Base Case

3.8.1.1 Case Description

The objective of Case 1.3.0 was to assess the base likelihood of failure caused by PWSCC initiation and growth without mechanical mitigation. The effects of leak detection, ISI, and SSE were also assessed. Since the present study is an extension of the prior study, this case was included in Bin 1, which was established in the prior study for Westinghouse four-loop RVON and RVIN DMWs. This case used bounding values for the geometry and loading, both normal operating and SSE, based on the licensing submittals referenced in Table 2-1 for the bin. The ISI parameters used were the same as in Case 1.1.0 from the prior study [2]. Figure 3-101 shows the WRS profiles used to analyze the case. They are the same as the WRS profiles used for Case 1.1.0 analysis. Additional information on this WRS profile can be found in Section C2.1. Section B23 describes the specific inputs and other simulation details used to analyze the case.

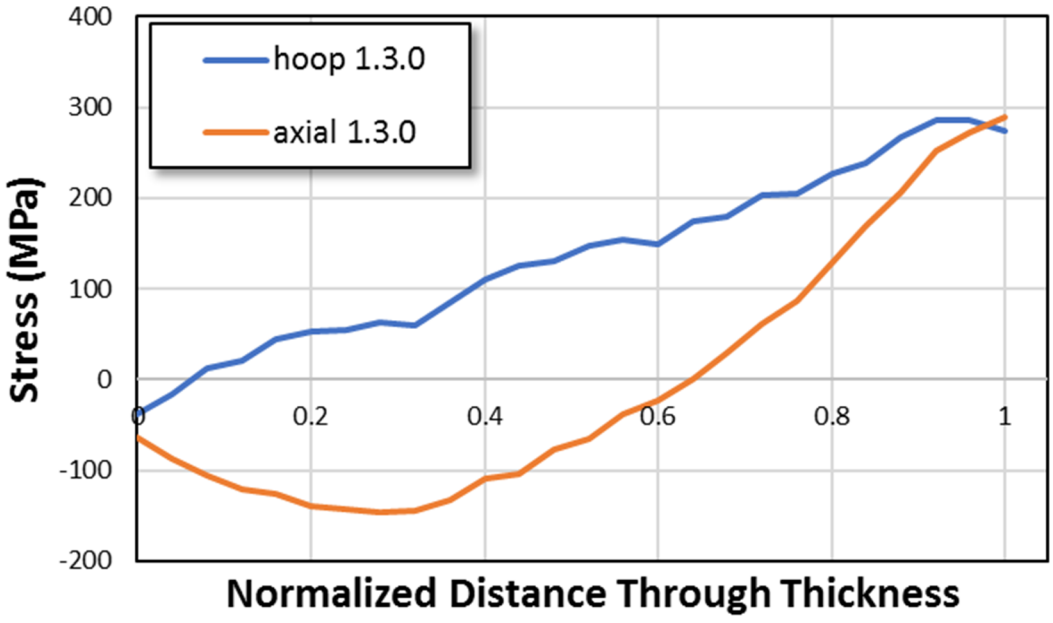

Figure 3-101 Case 1.3.0 WRS profiles

3.8.1.2 Results and Analysis

3.8.1.2.1 Probability of Rupture with Detection

There were no ruptures with a 1 gpm leak rate detection capability for this case.

3.8.1.2.2 Leak Rate Jump

There were no leak rate jump events for this case.

3.8.1.2.3 LBB Time Lapse

The mean LBB time lapses and standard errors with 1 and 10 gpm leak rate detection capabilities were respectively as follows:

- 34.0 ± 1.6 months (minimum observed: 13 months)
- 21.8 ± 1.2 months (minimum observed: 8 months)

Note that all results beyond 12 EFPY have been excluded for the reasons explained in Section 3.2.1.2.3.

Figure 3-102 shows the LBB time lapse CDF plots for Case 1.3.0. The results are equivalent to the Case 1.1.6a results. The small differences can be attributed to the statistical accuracy.

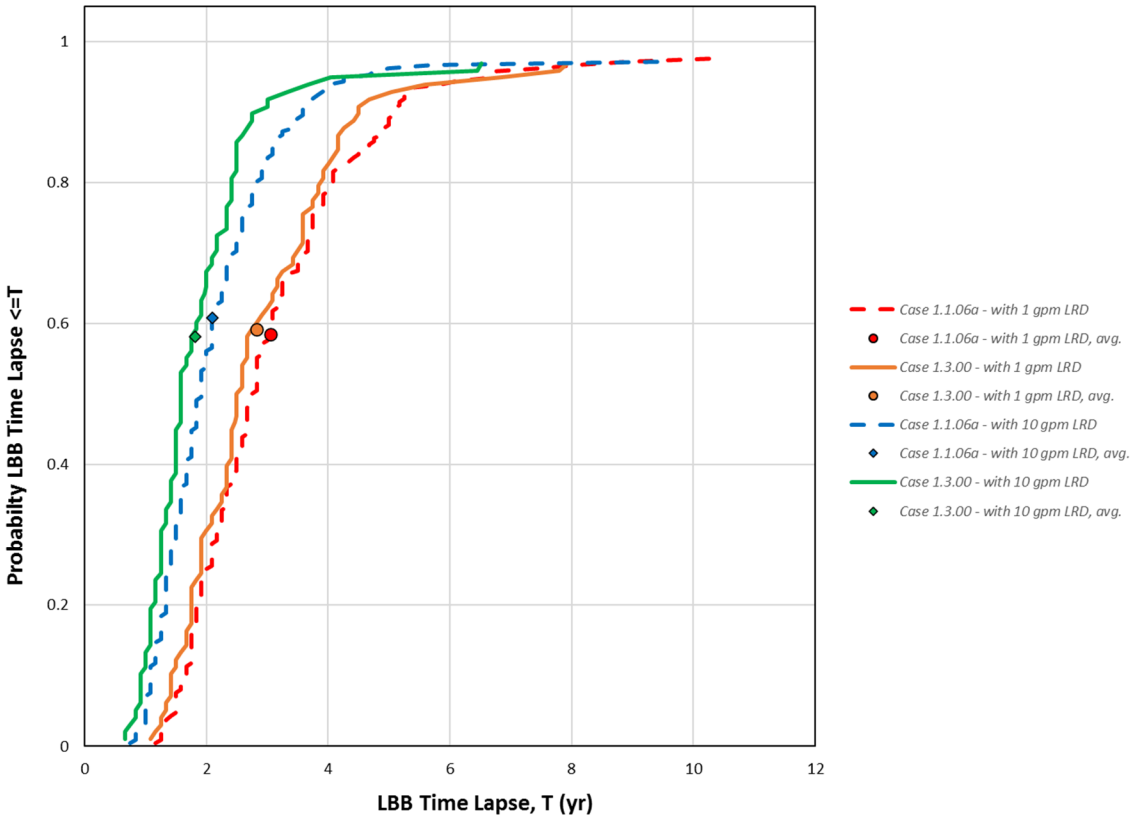

Figure 3-102 Case 1.3.0 LBB time lapse results

3.8.1.2.4 LBB Ratio

The mean LBB ratios and standard errors with 1 and 10 gpm leak rate detection capabilities were respectively as follows:

- 9.9 ± 0.1 (minimum observed: 7)
- 4.44 ± 0.04 (minimum observed: 3.51)

Figure 3-103 shows the LBB ratio CDF plots for Case 1.3.0. Like the LBB time lapses, the results are statistically equivalent to the Case 1.1.6a results.

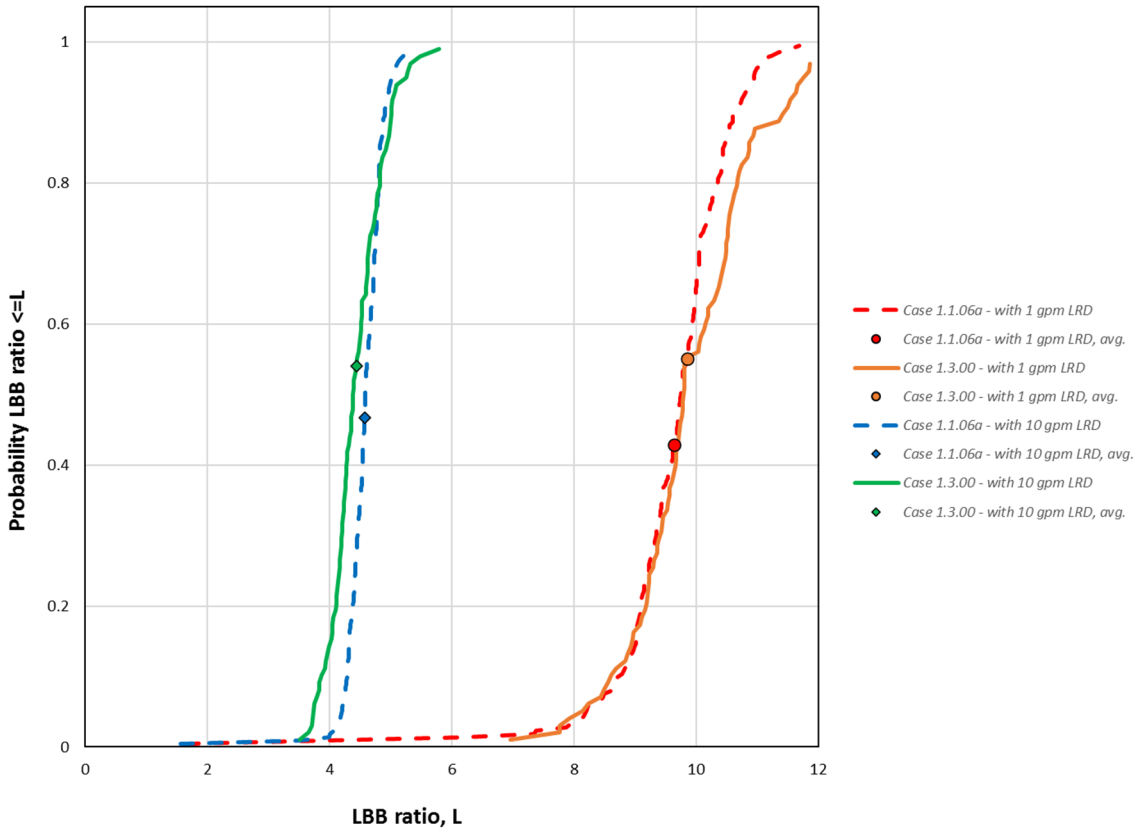

Figure 3-103 Case 1.3.0 LBB ratio results

3.8.1.2.5 Standard Indicators

Figure 3-104 shows the probabilities of first crack for Case 1.3.0. As compared to Case 1.1.6a, the probability of first crack is higher, while the probability of first circumferential crack is lower. Considering that circumferential crack ruptures are the primary concern, the Case 1.3.0 results are bounded by Case 1.1.6a.

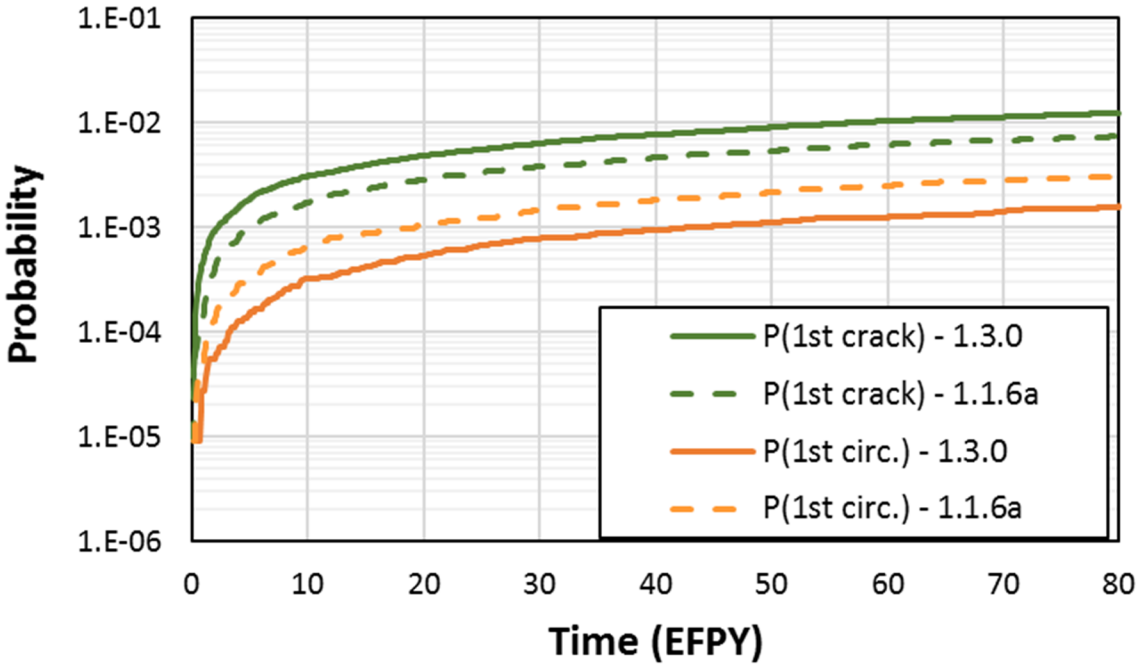

Figure 3-104 Case 1.3.0 time-dependent probabilities of first crack

Figure 3-105 shows the probabilities of first leak for Case 1.3.0. Like the probability of first crack, the Case 1.3.0 results are bounded by Case 1.1.6a because the probability of first circumferential leak in the former is lower.

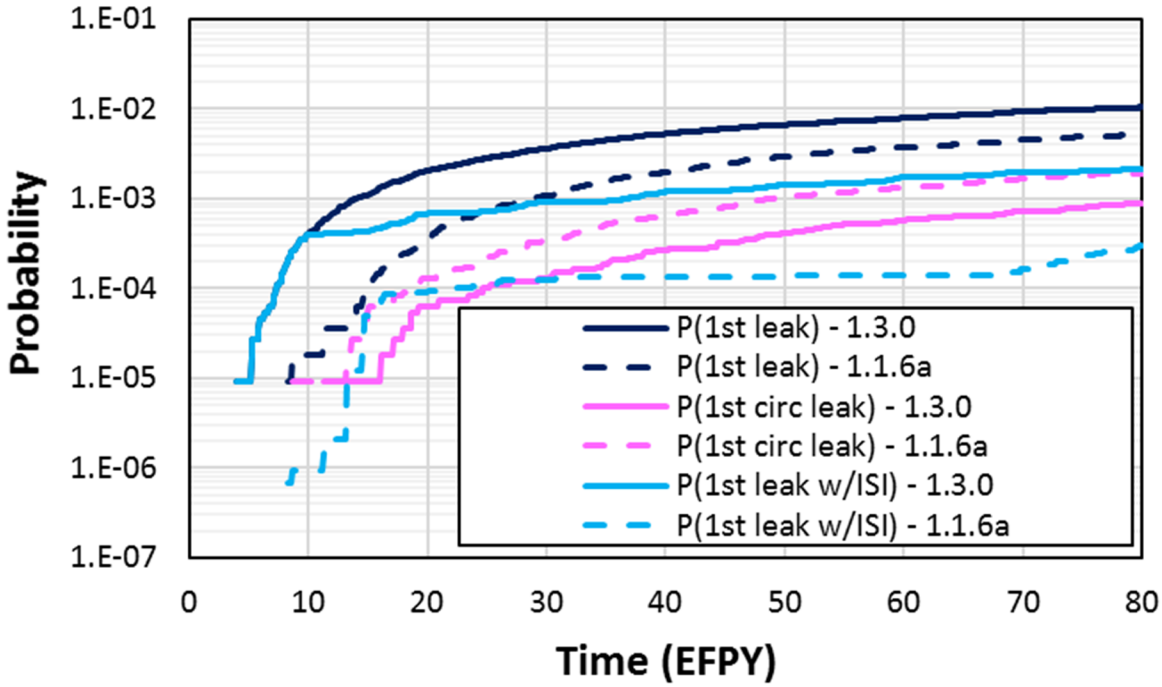

Figure 3-105 Case 1.3.0 time-dependent probabilities of first leak

Figure 3-106 shows the probabilities of rupture for Case 1.3.0 as compared to Case 1.1.6a. As expected from the first crack and first leak results, the Case 1.3.0 results are lower.

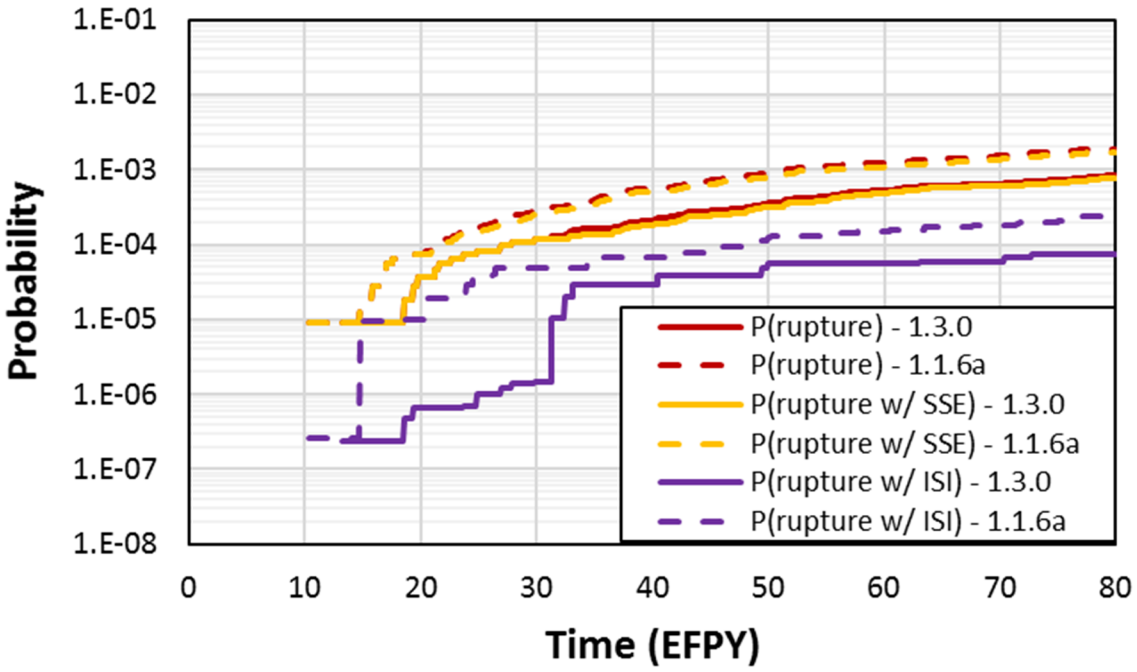

Figure 3-106 Case 1.3.0 time-dependent probabilities of rupture

3.8.2 Initial Flaws

3.8.2.1 Case Description

The objective of Case 1.3.1 was to assess the base likelihood of failure with pre-existing flaws and subsequent PWSCC growth of circumferential and axial cracks without mechanical mitigation. The effects of leak detection, ISI, and SSE were also assessed. This case used the same inputs as Case 1.3.0 except that, instead of Direct Model 1 for crack initiation, it used pre-existing axial and circumferential flaws. The WRS profiles were the same as used in the Case 1.3.0 analysis. Section B24 describes the specific inputs and other simulation details used to analyze the case.

3.8.2.2 Results and Analysis

3.8.2.2.1 Probability of Rupture with Detection

There were no ruptures with a 1 gpm leak rate detection capability for this case.

3.8.2.2.2 Leak Rate Jump

There were no leak rate jump events for this case.

3.8.2.2.3 LBB Time Lapse

The mean LBB time lapses and standard errors with 1 and 10 gpm leak rate detection capabilities were respectively as follows:

- 33.4 ± 0.2 months (minimum observed: 6 months)
- 20.9 ± 0.14 months (minimum observed: 6 months)

Note that all results beyond 12 EFPY have been excluded for the reasons explained in Section 3.2.1.2.3.

Figure 3-107 shows the LBB time lapse CDF plots for Case 1.3.1. The results are slightly lower as compared to Case 1.1.6b. However, the results are statistically close, and the difference is only a few months.

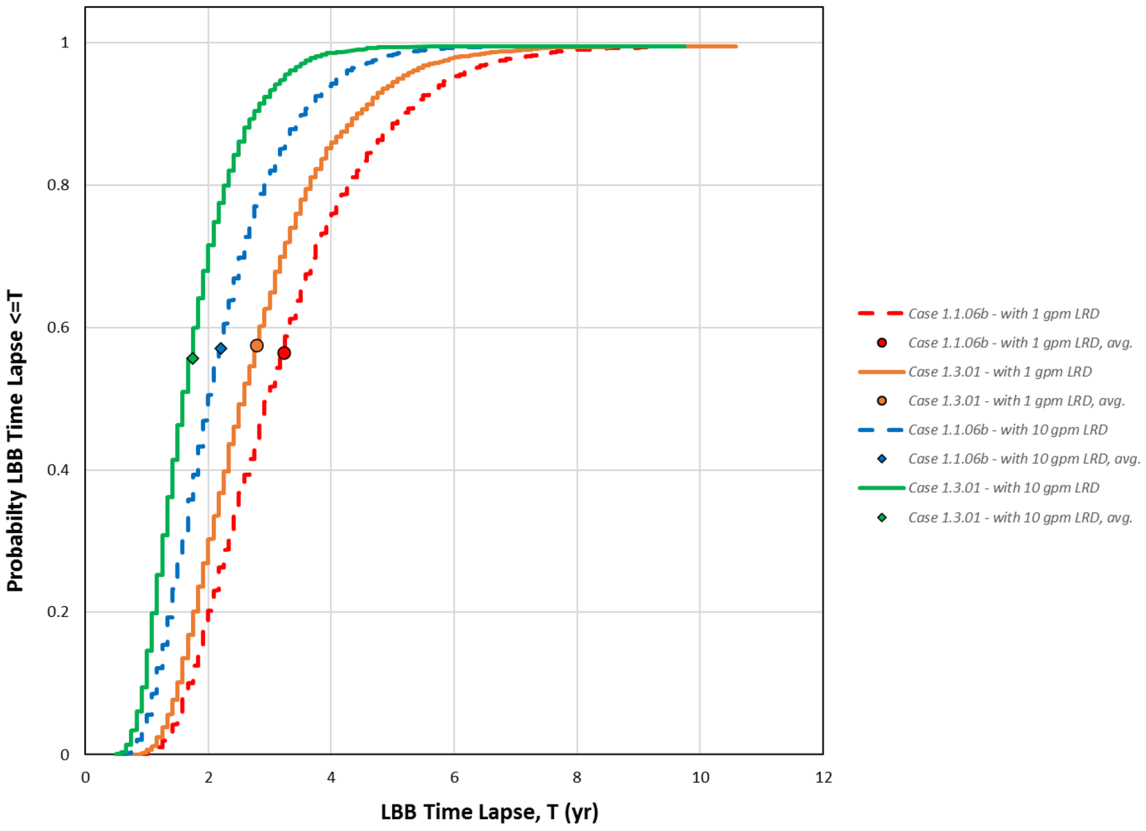

Figure 3-107 Case 1.3.1 LBB time lapse results

3.8.2.2.4 LBB Ratio

The mean LBB ratios and standard errors with 1 and 10 gpm leak rate detection capabilities were respectively as follows:

- 10.00 ± 0.01 (minimum observed: 6.33)
- 4.52 ± 0.01 (minimum observed: 3.42)

Figure 3-108 shows the LBB ratio CDF plots for Case 1.3.1. The results are statistically equivalent with Case 1.1.6b.

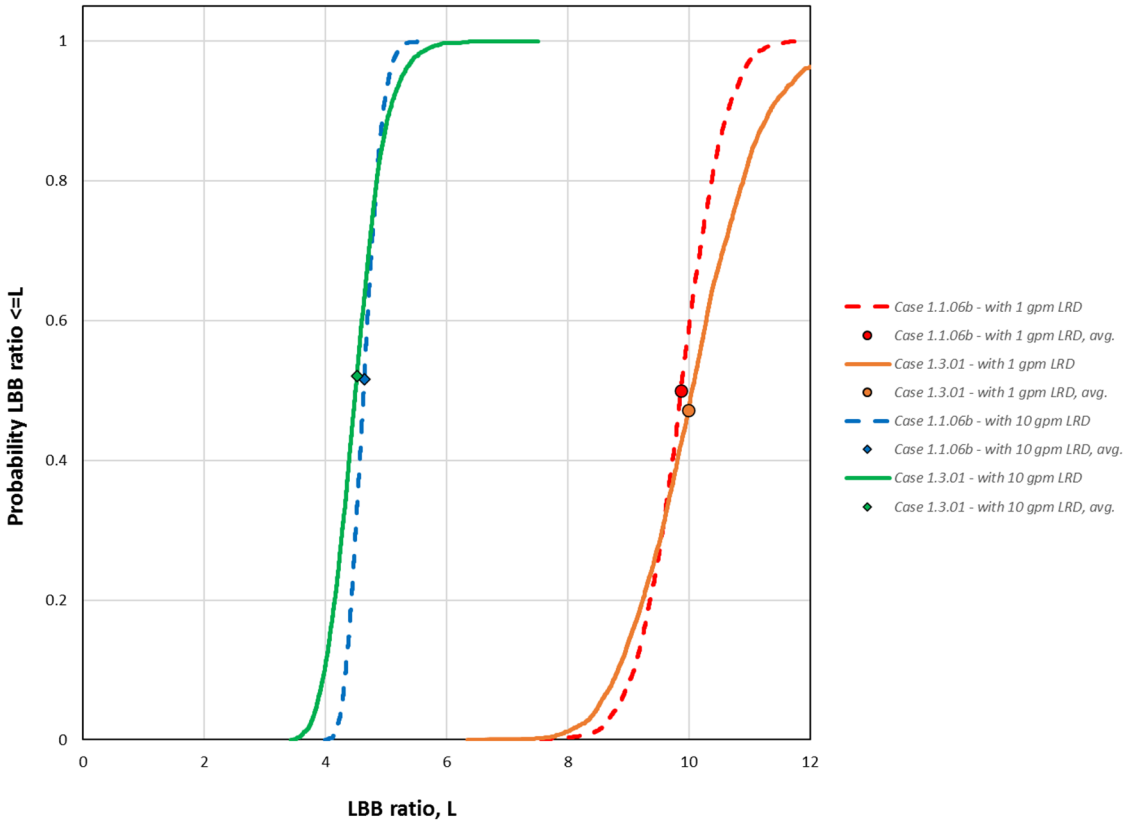

Figure 3-108 Case 1.3.1 LBB ratio results

3.8.2.2.5 Standard Indicators

Figure 3-109 shows the probabilities of first leak for Case 1.3.1. The probability of first leak is higher as compared to Case 1.1.6b. However, the increase is associated with axial cracks only, and the likelihood of circumferential crack leakage is slightly lower as highlighted by the probability of rupture shown in Figure 3-110.

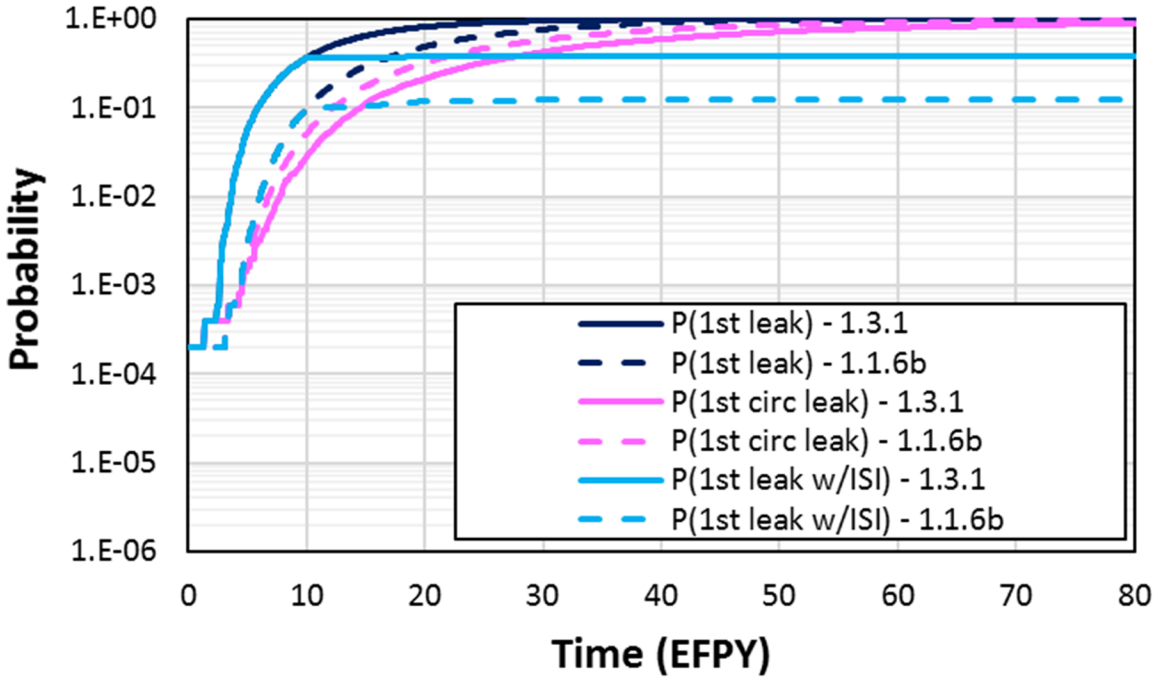

Figure 3-109 Case 1.3.1 time-dependent probabilities of first leak

Figure 3-110 shows the probabilities of rupture for Case 1.3.1. The probabilities of rupture with ISI are lower as compared to Case 1.1.6b.

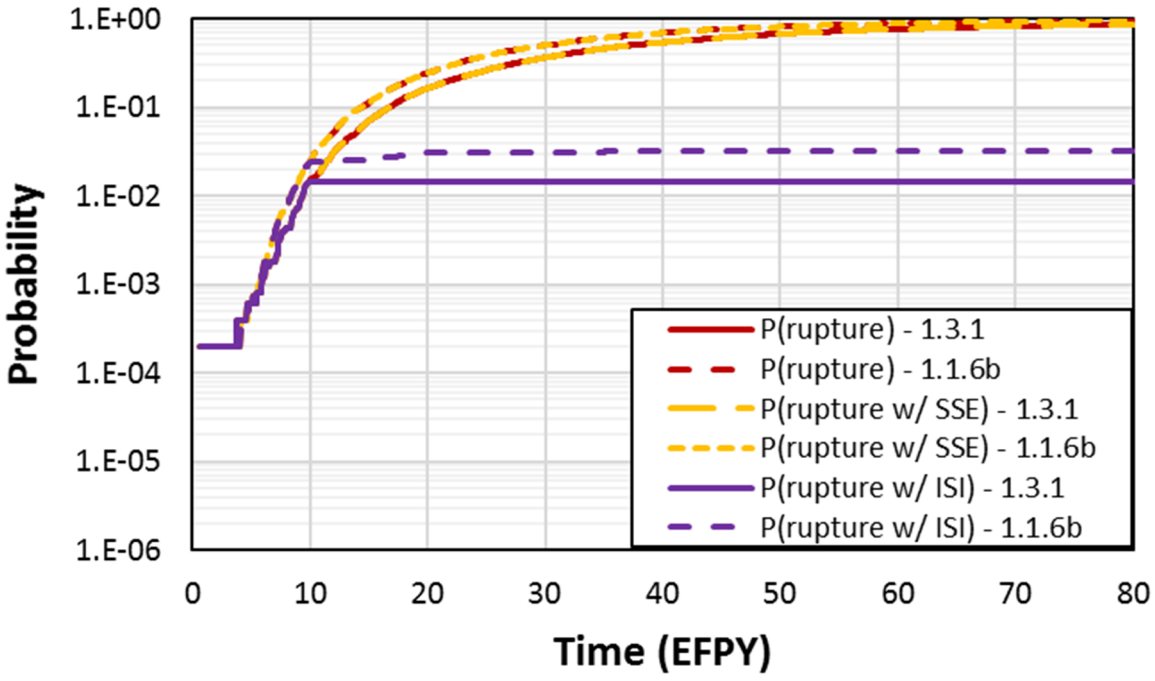

Figure 3-110 Case 1.3.1 time-dependent probabilities of rupture

4 PIPING SYSTEM FAILURE PROBABILITY

The xLPR code can only analyze one weld in a simulation. However, the piping systems of interest in this study contain multiple welds. Thus, a system-level analysis was necessary to combine the individual weld results and estimate a total probability of failure.

4.1 Methodology

In Section 4.2 of NUREG/CR-2189, "Probability of Pipe Fracture in the Primary Coolant Loop of a PWR Plant," Volume 5, "Probabilistic Fracture Mechanics Analysis, Load Combination Program, Project I Final Report," issued August 1981 [62], two methods are presented for combining the failure probabilities of multiple welds to estimate a single, system-level failure probability. The first method considers all welds to be independent. This method provides an upper bound on the probability of failure. The second method considers only a single weld associated with the worst-case conditions as the weld that will fail first. This method provides a lower bound on the probability of failure and considers the properties and conditions to be perfectly correlated among all the welds. In practice, the true probability should lie between these two bounds; however, depending on the analysis considered, one of the bounds may be more representative of the true value.

As discussed in Section 4 of the prior study [2], the first approach is based on independence among the results from each weld and is considered the most representative method for evaluating event probabilities for the following reasons:

- PWSCC is the dominant degradation mechanism for both crack initiation and crack growth. This mechanism does not affect all the piping system components similarly, nor at the same time during the simulated plant operating period. This contrasts with fatigue transients, which are modeled as occurring at the same time and with correlated intensities.
- The uncertain physical parameters that influence crack initiation and growth, such as the WRS, are not expected to be correlated among the welds included in these analyses.
- The operating conditions (e.g., temperature and pressure) could affect all the welds, but these parameters are constant in each realization. Therefore, by default, they are applied equally to each weld with respect to the expected value.

The probability of an event affecting multiple welds of the same type (e.g., multiple RVON welds within the same plant) is estimated using a classical statistical approach.

If a single weld has, at a given time, τ, a probability, p, of the event occurring, then the probability of having x welds experiencing the event out of a pool of N welds (with $0 \leq x \leq N$) is defined as follows:

$$P(event = x) = C_x^N p^x . (1-p)^{N-x} \quad \text{Equation 3}$$

where C_x^N is the notation for the combination of x elements from a pool of N elements.

This probability can be used to estimate the likelihood of each potential scenario, from no welds failing up to all N welds failing. If only the probability of at least one event occurring is of interest, then Equation 3 can be simplified as follows:

$$P(event \geq 1) = 1 - P(0\ event) = 1 - (1-p)^N \quad \text{Equation 4}$$

This concept can be extended to multiple weld types. For example, let $\{W_1, W_2, \dots, W_k\}$ be the k weld types considered, with the respective number of each type of weld being $\{N_1, N_2, \dots, N_k\}$, and the probabilities of having the event occurring at time τ be $\{p_1, p_2, \dots, p_k\}$. Then, the probability of having x_1 welds of type W_1, x_2 welds of type W_2, and so on up to x_n welds of type W_n, would be as follows:

$$P(events = \{x_1, x_2, \dots, x_n\}) = \prod_{i=1}^{k} C_{x_i}^{N_i} p_i^{x_i} . (1-p_i)^{N_i - x_i} \quad \text{Equation 5}$$

with the equivalent of Equation 4 becoming:

$$P(event \geq 1) = 1 - P(0\ event) = 1 - \prod_{i=1}^{k} (1-p_i)^{N_i} \quad \text{Equation 6}$$

As noted in the prior study, an underlying assumption of this method is that the event considered would have the same impact if it happens for any of the welds under consideration in the piping system. If for one loop or one weld, the event is of higher or lower consequence, then a quantitative impact factor needs to be included. In the present analysis, all the events considered have the same impact on the piping system regardless of the weld type.

4.2 Piping System Failure Frequency Results

4.2.1 Piping Systems Investigated

Two of the time-dependent QoIs (i.e., probability of leak rate jump and probability of rupture with a 1 gpm leak rate detection capability) were estimated to be essentially 0 in all the individual weld analyses performed as part of this study. Thus, any aggregation of these results at the system level would also be zero. In consequence, these QoIs cannot be used to illustrate the method for developing a system-level failure probability. Instead, the methodology was applied

to the probabilities of first crack, first leak, and rupture without leak rate detection both with and without a 10-year inspection frequency.

Three groupings were considered in the system analysis to provide an upper bound for the various piping system configurations in the PWR fleet. These combinations contain the maximum number of weld types for a given group of plants, but they do not necessarily represent actual piping system configurations. The three groupings are summarized in Table 4-1.

Table 4-1 Numbers of components bounding different plant designs

Grouping	RVON DMWs	Pressurizer Surge Line Nozzle DMWs	Steam Generator Inlet Nozzle DMWs	RCP Inlet Nozzle DMWs	Hot Leg Branch Line Nozzle DMWs	Cold Leg Branch Line Nozzle DMWs
Westinghouse 4-Loop PWRs	5 (Case 1.1.6a)	1 (Case 2.1.0)	Not Applicable	Not Applicable	Not Applicable	Not Applicable
Westinghouse 2-and 3-Loop PWRs	4 (Case 1.3.0)	Not Applicable	6 (Case 4.1.0)	Not Applicable	Not Applicable	Not Applicable
CE and B&W PWRs	Not Applicable	1 (Case 2.1.0)	Not Applicable	8 (Case 3.1.0)	2 (Case 5.1.0)	4 (Case 5.2.0)

The first grouping bounds all possible configurations in Westinghouse 4-loop PWRs. It consists of 9 welds:

- 4 RVON DMWs
- 4 RVIN DMWs
- 1 pressurizer surge line nozzle DMW

The RVIN DMWs were analyzed in the prior study [2], and the QoIs generated were at least one order of magnitude below those for the RVON DMW. Since no RVIN DMW cases were run in the present study, the 4 RVIN DMWs were conservatively represented by 1 RVON DMW. The plant-level aggregation used the individual weld results from Case 1.1.6a for the RVON DMWs and from Case 2.1.0 for the pressurizer surge line nozzle DMW. Section 4.2.2 presents the aggregated results for this grouping.

The second grouping bounds all possible configurations in Westinghouse two- and three-loop PWRs. It consists of 12 welds:

- 3 RVON DMWs
- 3 RVIN DMWs
- 3 steam generator inlet nozzle DMWs

- 3 steam generator outlet nozzle DMWs

As for the previous grouping, the 3 RVIN DMWs were conservatively represented by 1 RVON DMW. Only the steam generator inlet nozzle DMW was analyzed in this study. Because it is subject to higher operating temperatures, its results were also used to represent the steam generator outlet nozzle DMWs. The plant-level aggregation used the individual weld results from Case 1.3.0 for the RVON DMWs and from Case 4.1.0 for the steam generator inlet nozzle DMWs. Section 4.2.3 presents the aggregated results for this grouping.

The third grouping bounds all possible configurations in CE and B&W plants. It consists of 15 welds:

- 1 pressurizer surge line nozzle DMW
- 4 RCP inlet nozzle DMWs
- 4 RCP outlet nozzle DMWs
- 4 high-pressure injection nozzle DMWs
- 1 shutdown cooling nozzle DMW
- 1 pressurizer surge line to hot leg nozzle DMW

The high-pressure injection nozzle DMWs are connected to the cold leg, while the shutdown cooling and pressurizer surge line to hot leg nozzle DMWs are both connected to the hot leg. Because the RCP inlet nozzle DMWs are subject to higher operating temperatures, they were also used to represent the RCP outlet nozzle DMWs. The plant-level aggregation used the individual weld results from Case 2.1.0 for the pressurizer surge line nozzle DMW, Case 3.1.0 for the RCP nozzle DMWs, Case 5.1.0 for the hot leg branch line nozzle DMWs, and Case 5.2.0 for the cold leg branch line nozzle DMWs. Section 4.2.4 presents the aggregated results for this grouping.

4.2.2 Westinghouse Four-Loop PWRs

Figure 4-1 shows the time-dependent probability plots estimated using Equation 6 to bound Westinghouse four-loop PWRs. At 80 EFPY, the plant-level results are as follows:

- 6.9×10^{-2} probability of first crack
- 1.6×10^{-2} probability of first circumferential crack
- 5.6×10^{-2} probability of first leak
- 9.7×10^{-3} probability of first circumferential leak
- 2.2×10^{-2} probability of first leak with a 10-year inspection frequency
- 9.4×10^{-3} probability of rupture without ISI or leak rate detection
- 1.3×10^{-3} probability of rupture with a 10-year inspection frequency

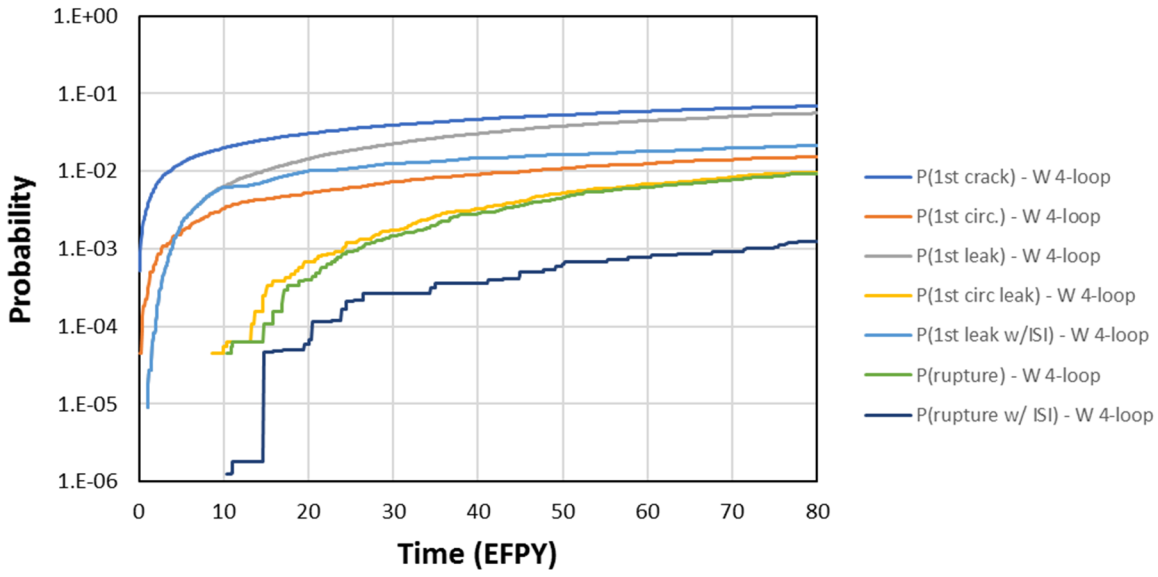

Figure 4-1 Bounding Westinghouse four-loop time-dependent probabilities

Each of these probabilities can be split into the contributions from each group of components. This approach approximates the contributions, which is more accurate for low probabilities. Figure 4-2 presents such a decomposition for the probability of first crack. As can be seen in this figure, the pressurizer surge line nozzle DMW and the 5 RVON DMWs have about the same contribution at 80 EFPY for this QoI.

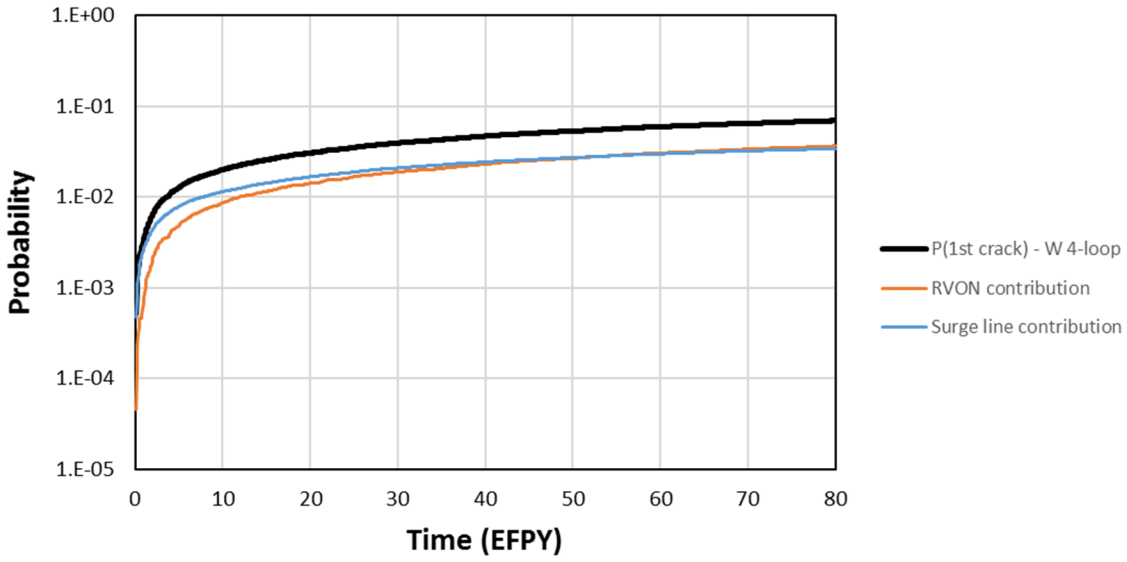

Figure 4-2 Westinghouse four-loop system probability of first crack and component contributions

Figure 4-3 presents a similar figure for the probability of first circumferential crack. It shows that the contribution from the RVON DMWs is dominant, and the contribution from the pressurizer surge line nozzle DMW has been reduced by more than 2 orders of magnitude.

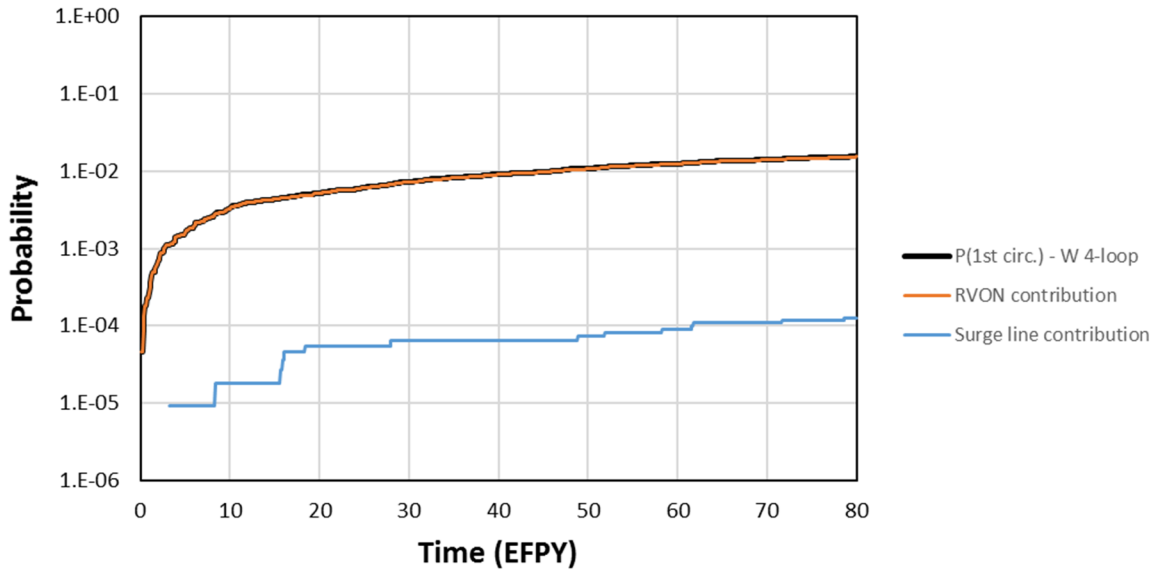

Figure 4-3 Westinghouse four-loop system probability of first circumferential crack and component contributions

Figure 4-4 shows the contributions to the time-dependent probability of first leak. Because of the smaller diameter of the piping, the pressurizer surge line nozzle DMW quickly leads to leakage as compared to the other welds considered, and thus it is the major contributor in the early years of plant operation. At 80 EFPY, the contribution of the 5 RVON DMWs are similar to the contribution from the 1 pressurizer surge line nozzle DMW.

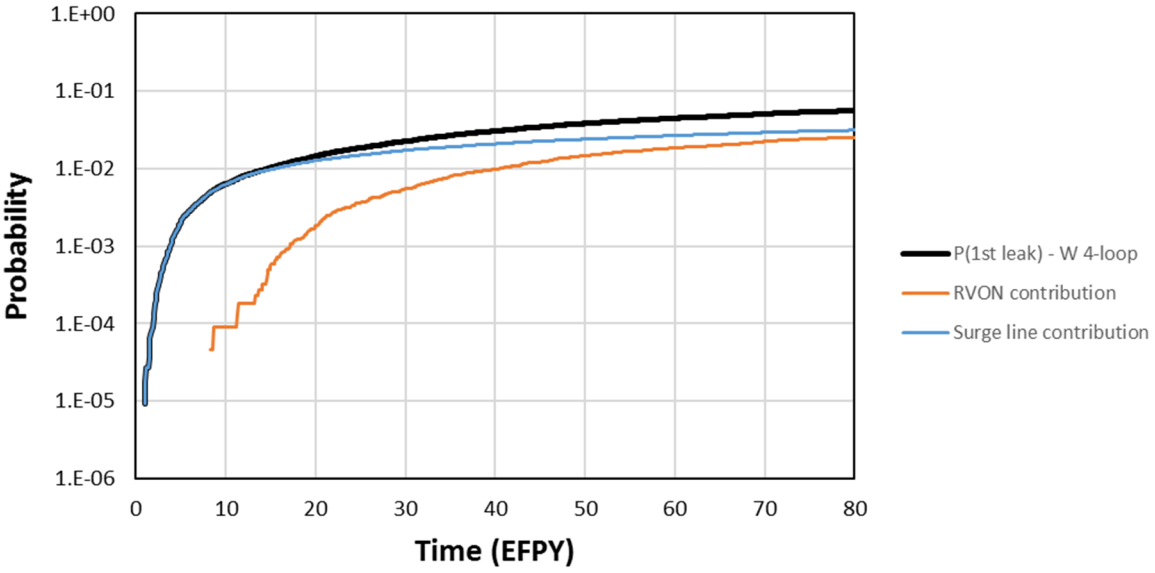

Figure 4-4 Westinghouse four-loop system probability of first leak and component contributions

As shown in Figure 4-5, the contribution from the pressurizer surge line nozzle DMW drives the probability of first leak with a 10-year inspection frequency. Figure 4-6 shows a similar trend for

the probability of first circumferential leak. Because there were fewer occurrences of circumferential cracks for the pressurizer surge line nozzle DMW, this probability is equivalent to the probability of the five RVON DMWs combined. These results illustrate that only one set of components could be considered to estimate the probability at the system level.

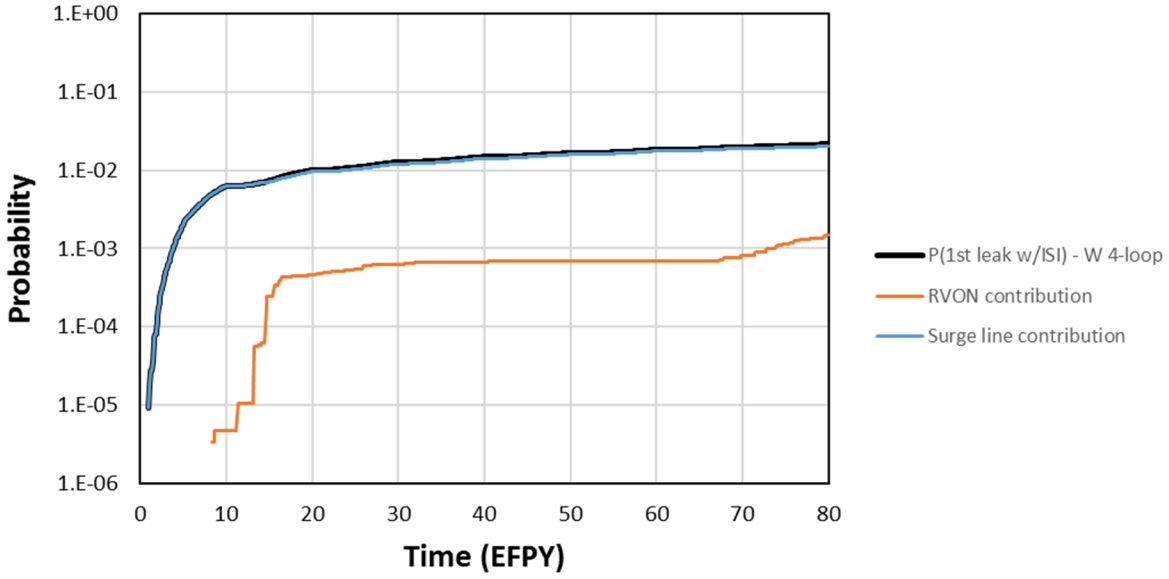

Figure 4-5 Westinghouse four-loop system probability of first leak with a 10-year inspection frequency and component contributions

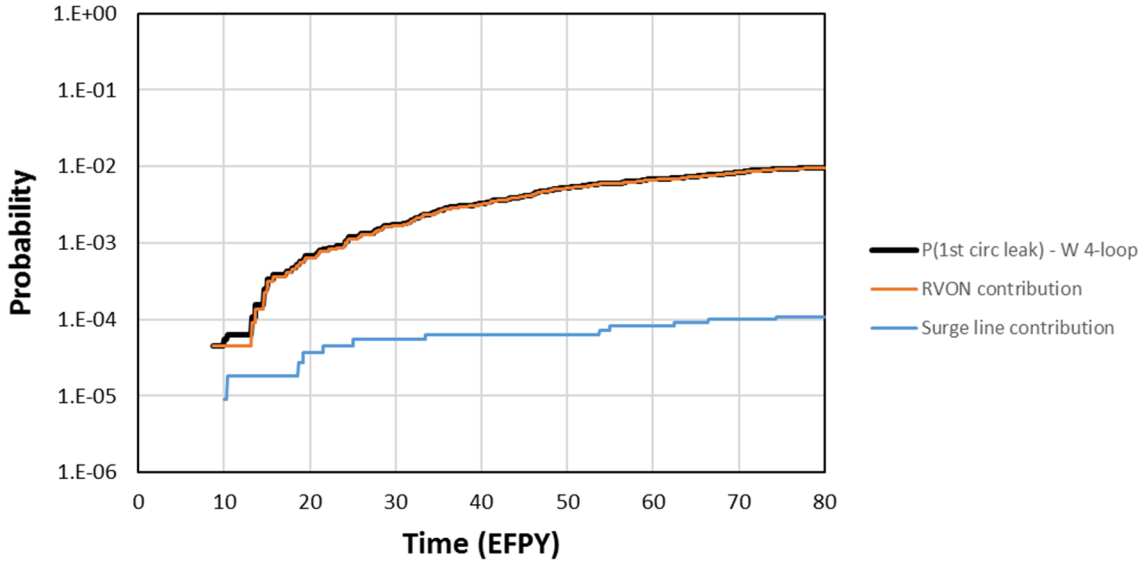

Figure 4-6 Westinghouse four-loop system probability of first circumferential leak and component contributions

Figure 4-7 and Figure 4-8 show the probabilities of rupture and rupture with a 10-year inspection frequency, respectively. Since only circumferential cracks lead to ruptures, these figures are

consistent with the probability of first circumferential leak where the system-level probability is driven by the five RVON DMWs.

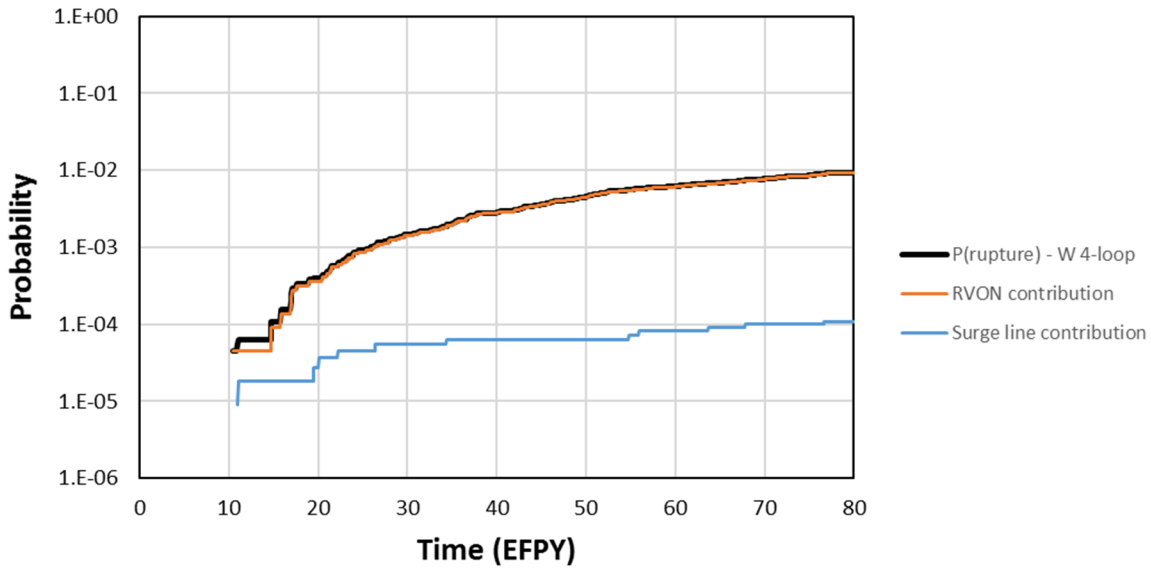

Figure 4-7 Westinghouse four-loop system probability of rupture and component contributions

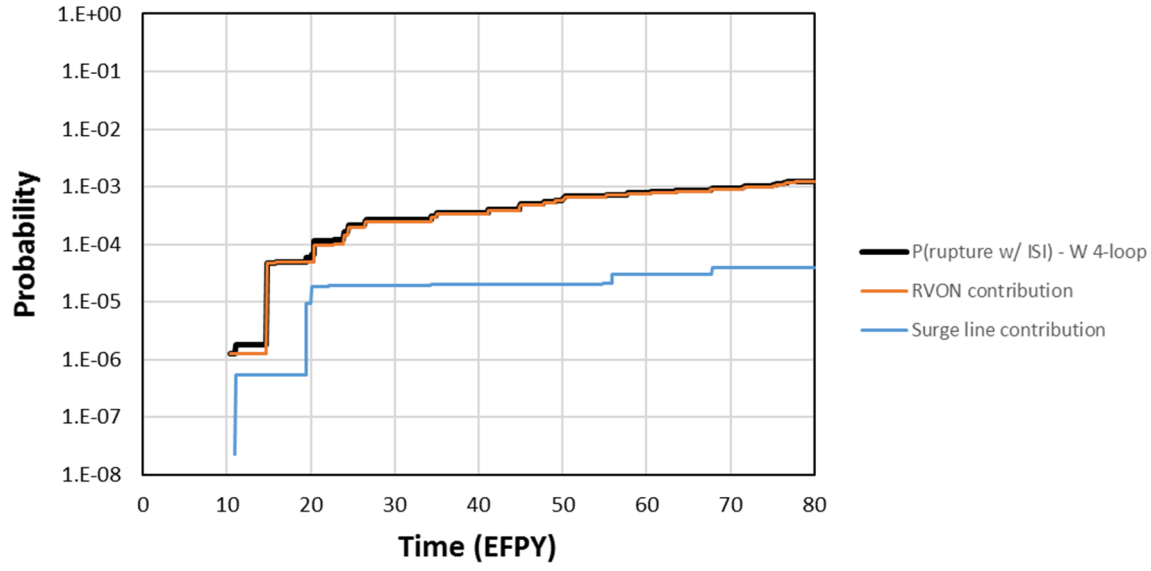

Figure 4-8 Westinghouse four-loop system probability of rupture with 10-year inspection frequency and component contributions

4.2.3 Westinghouse Two-loop and Three-Loop PWRs

Figure 4-9 shows the time-dependent probability plots estimated using Equation 6 to bound Westinghouse two- and three-loop PWRs. At 80 EFPY, the system-level results are as follows:

- 3.1×10^{-1} probability of first crack
- 3.9×10^{-2} probability of first circumferential crack
- 9.9×10^{-2} probability of first leak
- 3.5×10^{-3} probability of first circumferential leak
- 4.8×10^{-2} probability of first leak with a 10-year inspection frequency
- 3.3×10^{-3} probability of rupture without ISI or leak rate detection
- 3.2×10^{-4} probability of rupture with a 10-year inspection frequency

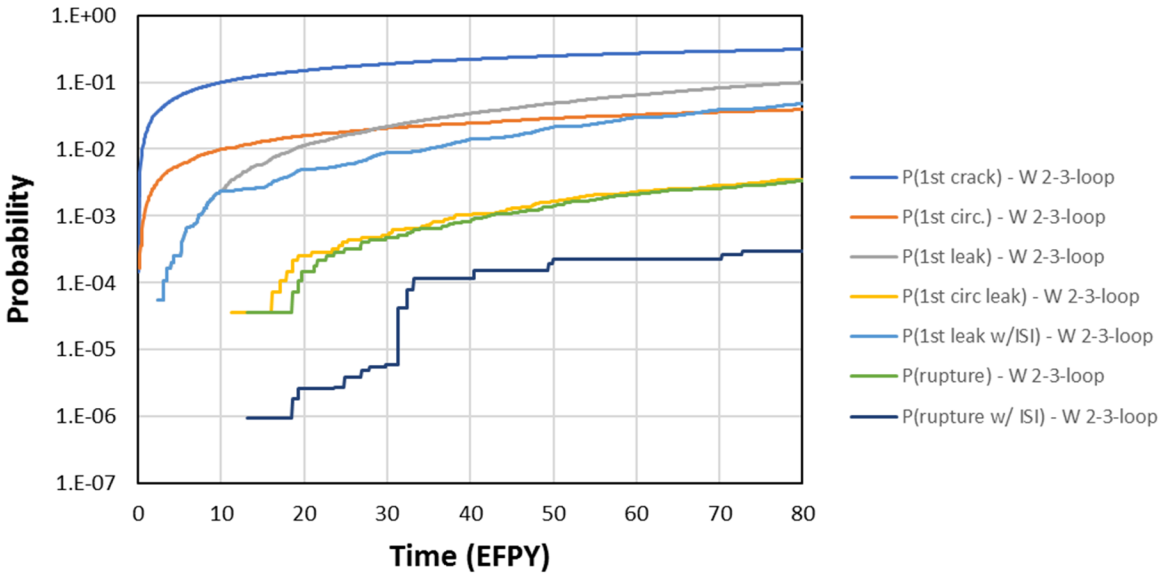

Figure 4-9 Westinghouse two- and three-loop time-dependent probabilities

Figure 4-10 presents the contributions of each weld type to the probability of first crack. As can be seen in this figure, the steam generator nozzle DMWs drive the probability. Figure 4-11 presents a similar figure for the probability of first circumferential crack. The contribution from the steam generator nozzle DMWs remains dominant.

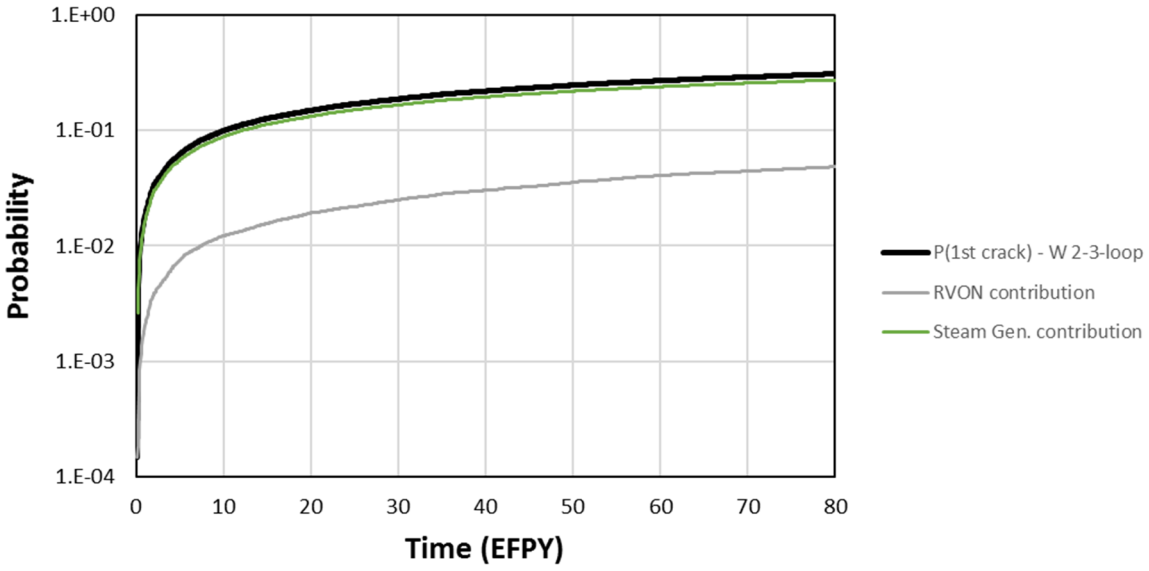

Figure 4-10 Westinghouse two- and three-loop system probability of first crack and component contributions

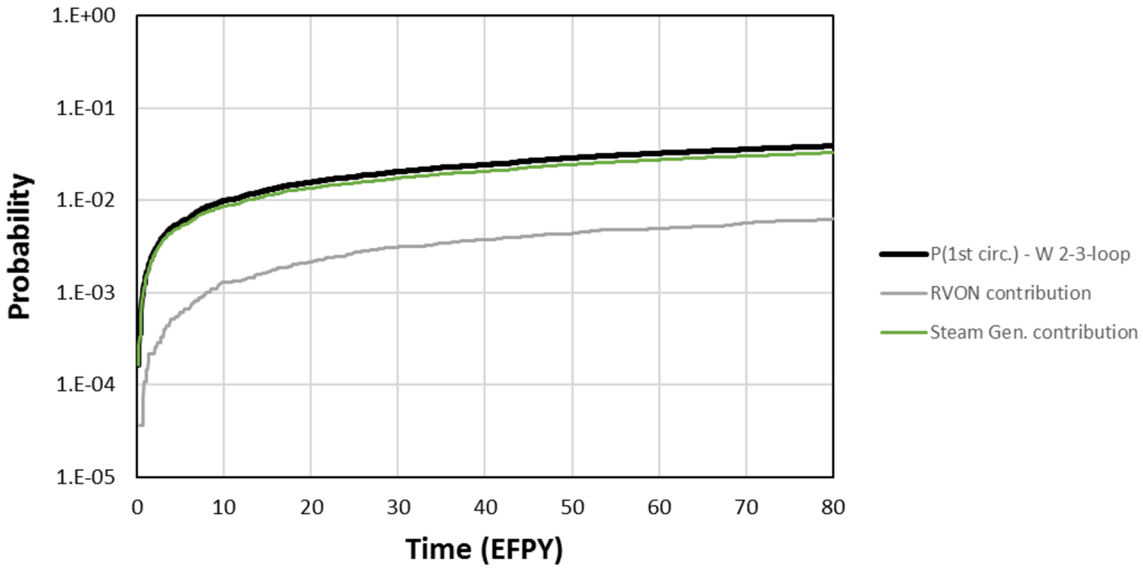

Figure 4-11 Westinghouse two- and three-loop system probability of first circumferential crack and component contributions

Figure 4-12 shows the contributions to the time-dependent probability of first leak. It shows that the steam generator nozzle DMWs and RVON DMWs have similar contributions that switch in importance over time. The steam generator nozzle DMWs become the biggest contributor over time when a 10-year inspection frequency is considered for the probability of first leak, as displayed in Figure 4-13.

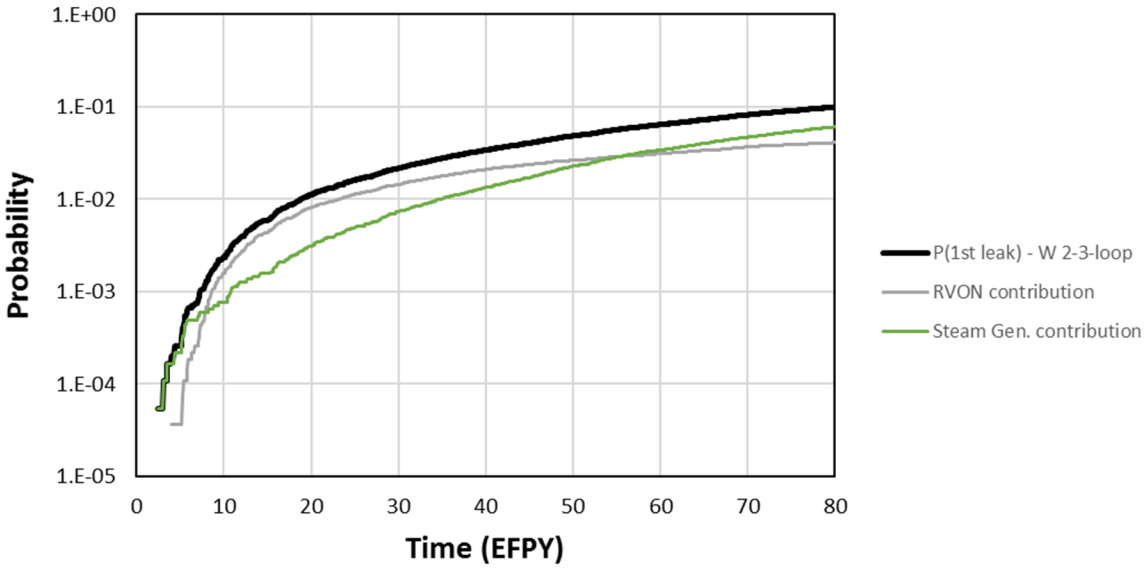

Figure 4-12 Westinghouse two- and three-loop system probability of first leak and component contributions

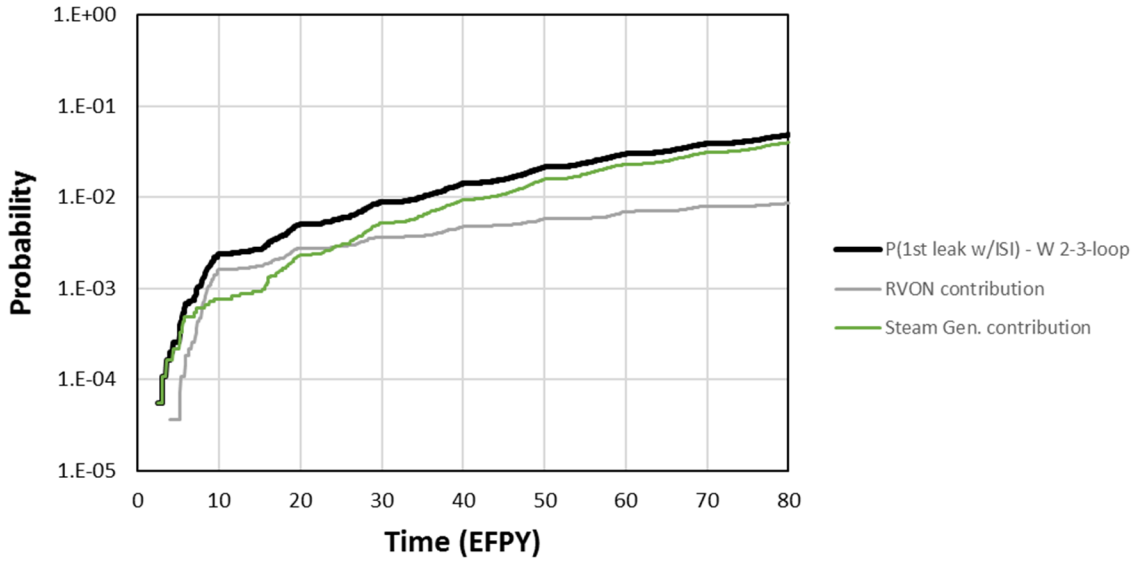

Figure 4-13 Westinghouse two- and three-loop system probability of first leak with a 10-year inspection frequency and component contributions

Figure 4-14 shows the probability of first leak for circumferential cracks only. Because of the slow circumferential crack growth in the steam generators nozzle DMWs, this probability is equivalent to the probability from the four RVON DMWs.

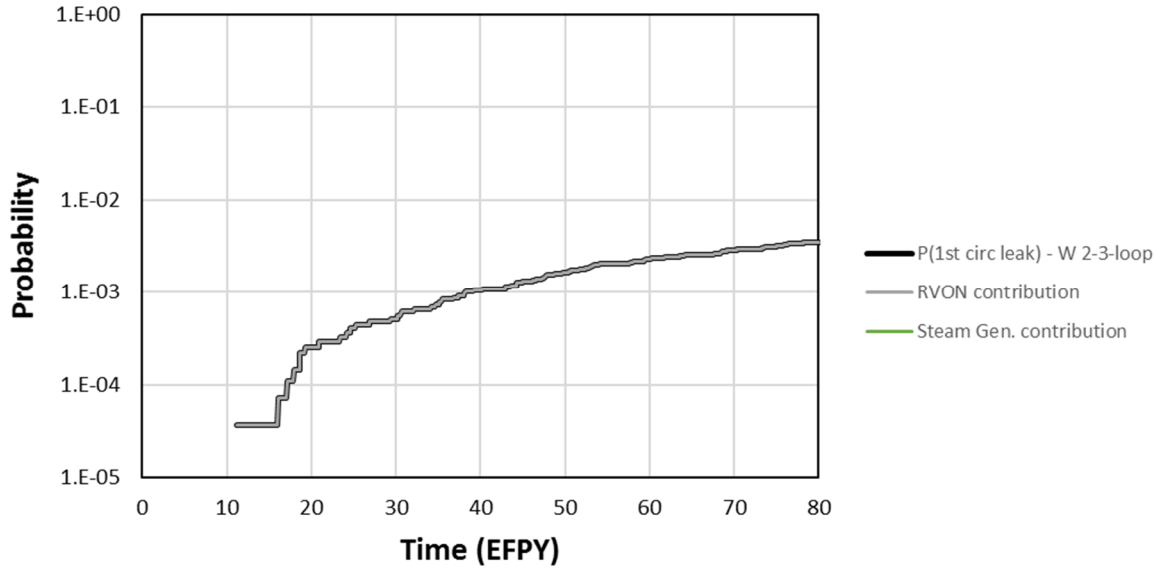

Figure 4-14 Westinghouse two- and three-loop system probability of first circumferential leak and component contributions

Figure 4-15 and Figure 4-16 show the probabilities of rupture and rupture with a 10-year inspection frequency, respectively. Since only circumferential cracks led to rupture, these figures are consistent with the probabilities of first circumferential crack leak with the system-level probability being driven by the four RVON DMWs.

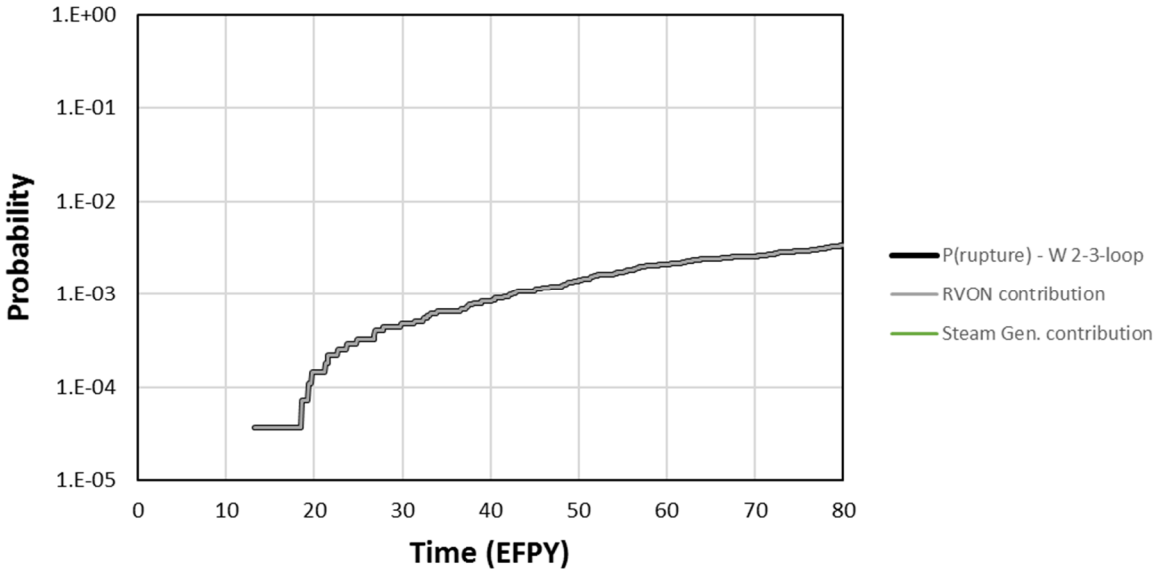

Figure 4-15 Westinghouse two- and three-loop system probability of rupture and component contributions

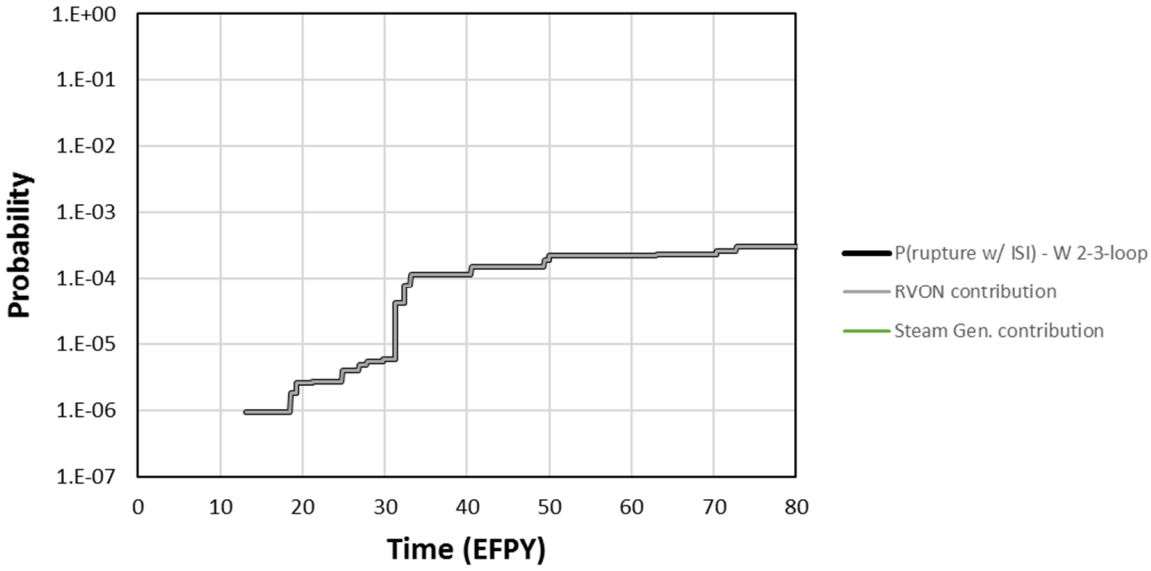

Figure 4-16 Westinghouse two- and three-loop system probability of rupture with a 10-year inspection frequency and component contributions

4.2.4 CE and B&W PWRs

Figure 4-17 shows the time-dependent probability plots estimated using Equation 6 to bound the CE and B&W PWRs. At 80 EFPY, the system-level results are as follows:

- 2.4×10^{-1} probability of first crack
- 1.3×10^{-4} probability of first circumferential crack
- 2.0×10^{-1} probability of first leak
- 1.1×10^{-4} probability of first circumferential leak
- 1.2×10^{-1} probability of first leak with a 10-year inspection frequency
- 1.1×10^{-4} probability of rupture without ISI or leak rate detection
- 4.0×10^{-5} probability of rupture with a 10-year inspection frequency

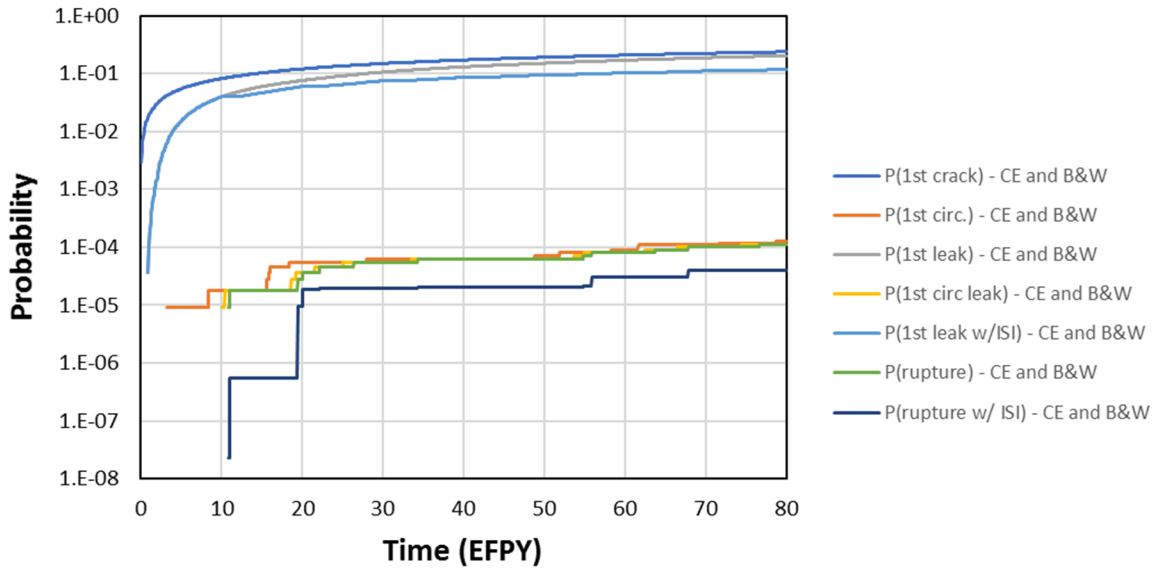

Figure 4-17 CE and B&W time-dependent probabilities

Figure 4-18 presents the decomposition for the probability of first crack. As can be seen in this figure, the hot leg branch line with 2 DMWs and the cold leg branch line with 4 DMWs are the biggest contributors, followed by the pressurizer surge line nozzle DMW and the RCP nozzle DMWs. Figure 4-19 presents a similar figure for the probability of first circumferential crack. Here the only contributor is the pressurizer surge line nozzle DMW because the other welds did not have any circumferential cracks over 80 EFPY for the sample sizes considered. As a result, the probabilities of first circumferential leak and rupture will also be dependent only on the pressurizer surge line nozzle DMW contribution.

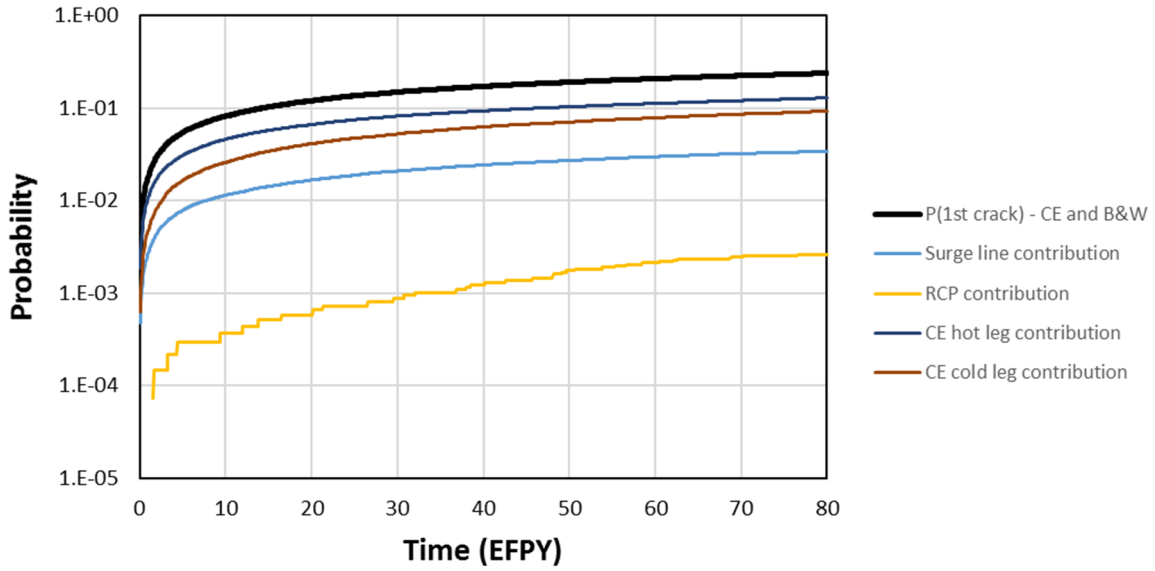

Figure 4-18 CE and B&W system probability of first crack and component contributions

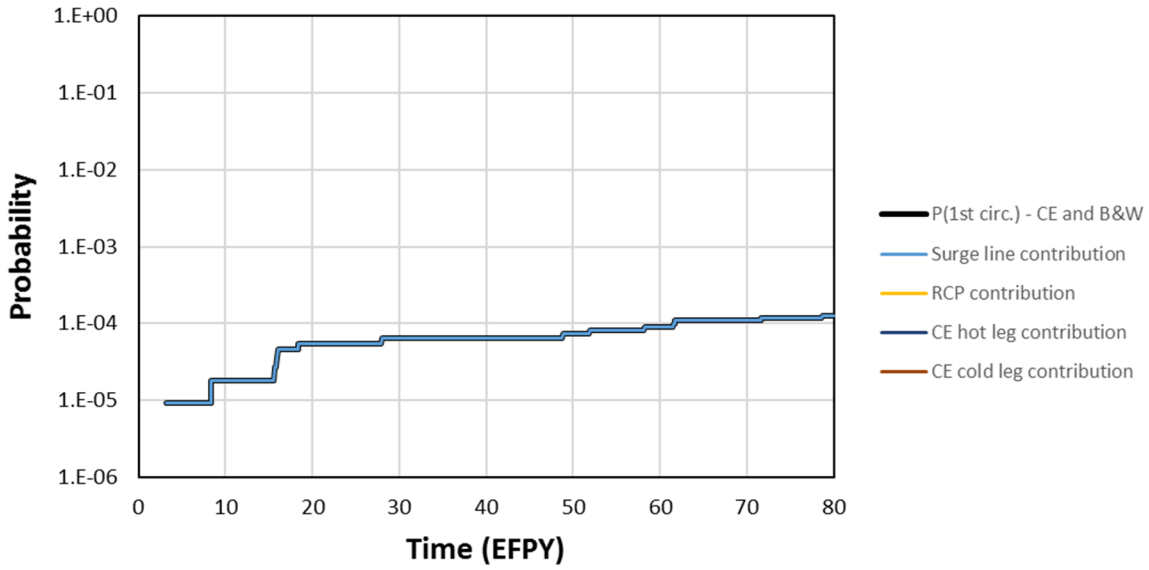

Figure 4-19 CE and B&W system probability of first circumferential crack and component contributions

Figure 4-20 shows the contribution to the time-dependent probability of first leak. The hot leg and cold leg branch line nozzle DMWs are the biggest contributors to the probability of first crack followed by the pressurizer surge line nozzle DMW. The RCP nozzle DMWs did not generate any leakage, so they are not a contributor. The hot leg branch line nozzle DMW becomes the dominant contributor when a 10-year inspection frequency is considered for the probability of first leak, as shown in Figure 4-21. Figure 4-22 shows the probability of first leak for circumferential cracks only. As expected, it is equivalent to the probability of first leak for the pressurizer surge line nozzle DMW.

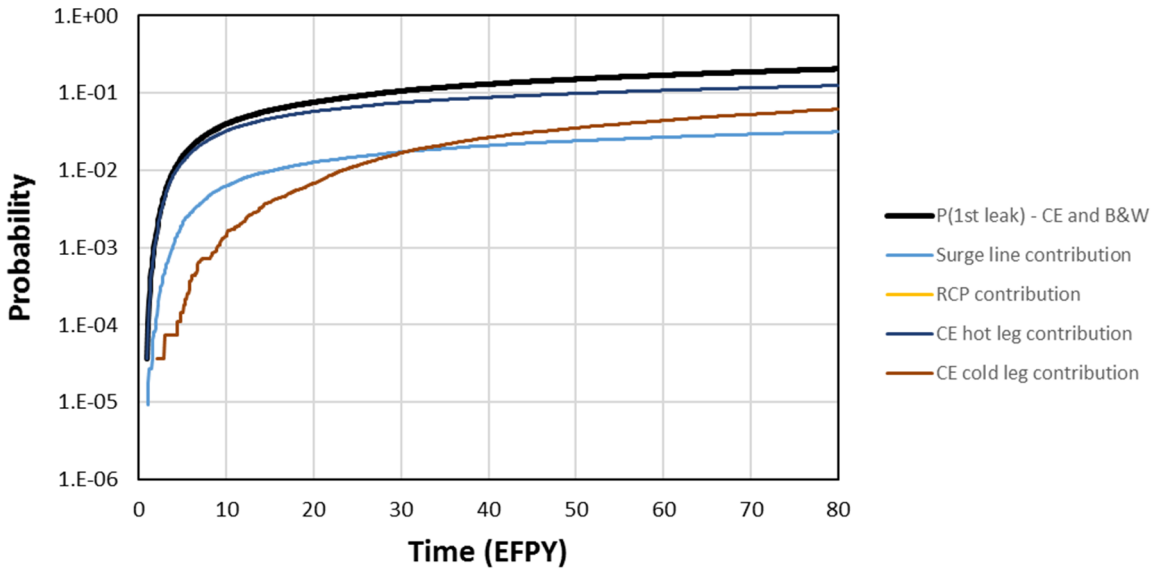

Figure 4-20 CE and B&W system probability of first leak and component contributions

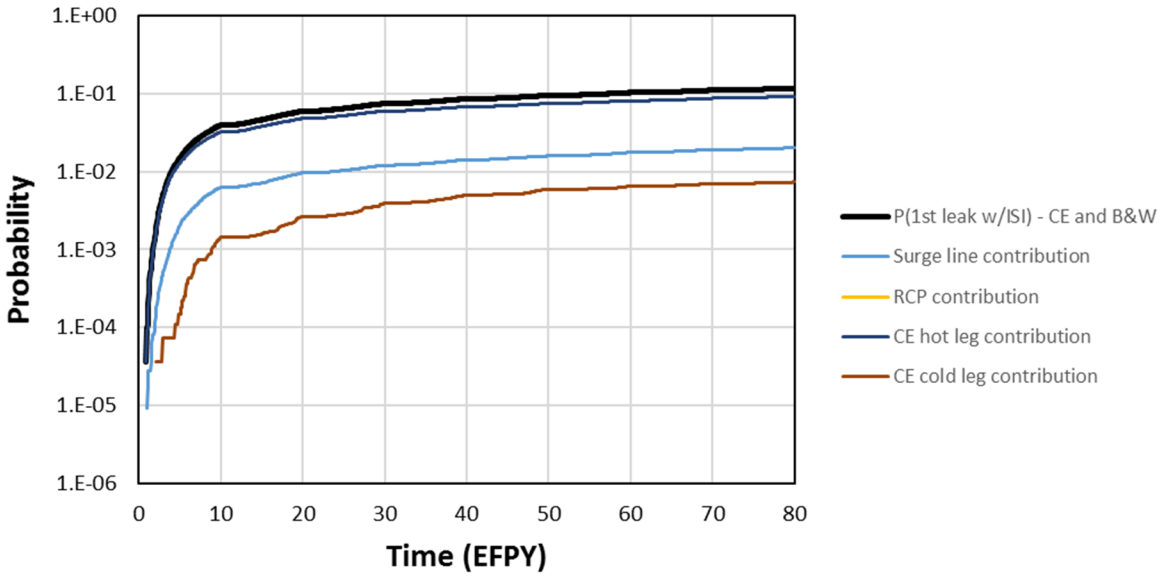

Figure 4-21 CE and B&W system probability of first leak with a 10-year inspection frequency and component contributions

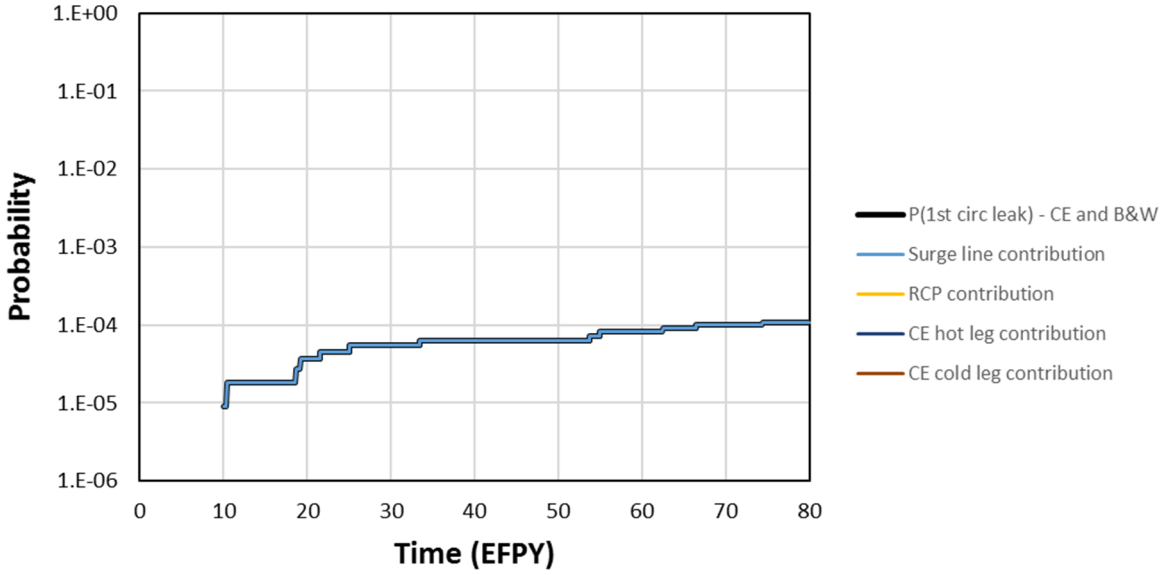

Figure 4-22 CE and B&W system probability of first circumferential leak and component contributions

Figure 4-23 and Figure 4-24 show probabilities of rupture and rupture with a 10-year inspection frequency, respectively. Since only circumferential cracks led to rupture, these figures are consistent with the probability of first circumferential leak, and the system-level probabilities are equivalent to their pressurizer surge line nozzle DMW equivalents.

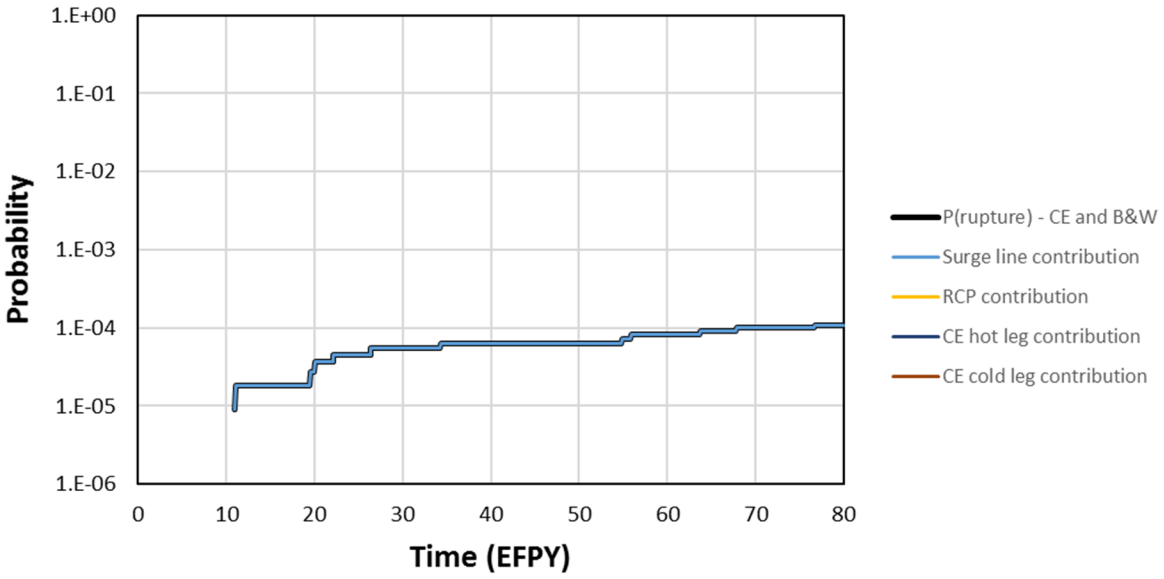

Figure 4-23 CE and B&W system probability of rupture and component contributions

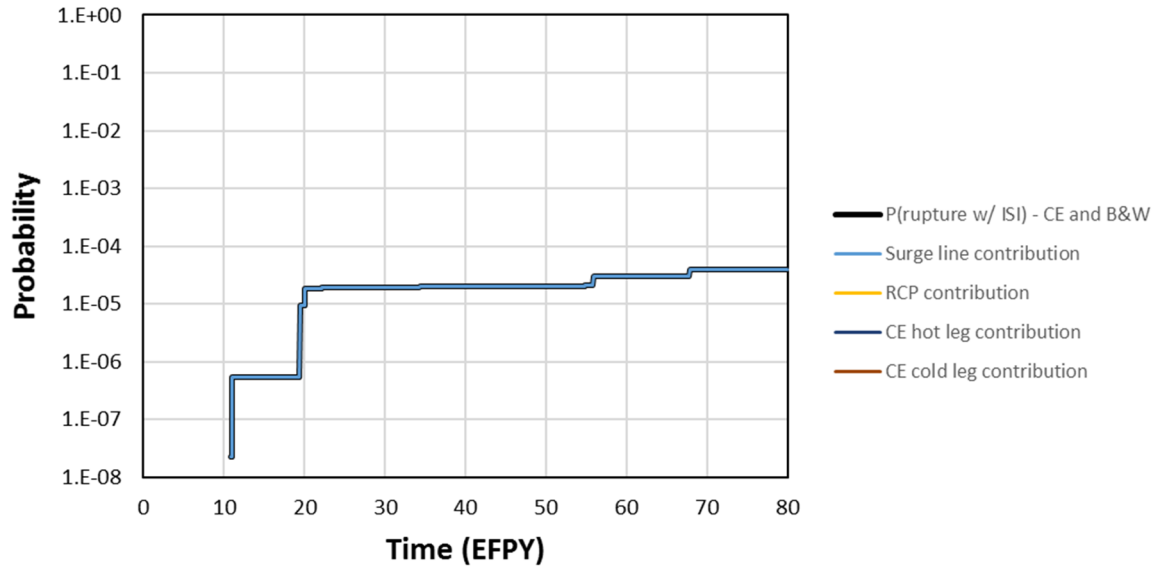

Figure 4-24 CE and B&W system probability of rupture with a 10-year inspection frequency and component contributions

5 ANALYSIS ASSUMPTIONS

5.1 Conservatisms

Biases in the overall analysis approach used for the present study make the results upper bound estimates. The models retain the biases presented in the report on sources and treatment of uncertainties in the xLPR code [63]. The following input assumptions contribute additional bias:

- The highest normal operating loads, pressures, and temperatures were used to represent the welds in each bin. The normal operating loads also reflect design-basis values.
- The smallest thicknesses and largest outside diameters were used to represent the welds in each bin. This approach leads to quicker times to through-wall cracks and higher applied stresses.
- A lower-bound hydrogen concertation was used in all cases. This approach leads to faster crack growth rates.
- For uniformity, a 10-year inspection frequency was used in all cases; however, many of the DMWs are currently required by 10 CFR 50.55a(g)(6)(ii)(F) to be inspected more frequently.
- An SSE frequency of occurrence of 1×10^{-3} events per year was assumed in conjunction with design-basis SSE stresses.

In addition, as described in Section 4, when combining the individual weld results into a system level analysis, assuming that the welds are independent provides an upper bound on the system-level probabilities.

5.2 Unknowns

The distance between the DMWs and the safe-end-to-pipe, or SS closure, welds represents an unknown. This distance influences the WRS profile, and a typical value was used for the analyses in this study. Sufficient information was not available to generate a distribution of these values for each bin.

6 ASSESSMENT OF NRC REGULATORY FRAMEWORK FOR LEAK-BEFORE-BREAK

This section evaluates NRC's current regulatory framework for LBB considering the results from this study. The evaluation focuses on the following elements:

- requirements in GDC 4
- guidance in SRP Section 3.6.3

Section 6.1 provides historical background on LBB in nuclear power plant piping systems. Potential changes to the above elements of NRC's regulatory framework are discussed in Sections 6.2 and 6.3, respectively.

6.1 Background on LBB for Nuclear Piping

In 1971 [64], the Atomic Energy Commission, the predecessor agency to the NRC, promulgated 10 CFR Part 50, Appendix A, "General Design Criteria for Nuclear Power Plants." GDC 4 of this appendix required that structures, systems, and components important to safety be protected against the dynamic effects of postulated large piping ruptures. GDC 4 was then conservatively applied to require all nuclear power reactors to employ massive pipe whip restraints and jet impingement shields to mitigate the dynamic effects of a postulated guillotine rupture in the largest piping in the reactor coolant system.

In 1975, the NRC staff was informed of newly defined asymmetric blowdown loads that result by postulating rapid-opening, double-ended ruptures at the most adverse location in the PWR primary piping system. The topic was designated as Unresolved Safety Issue A-2. In response to a conclusion based on analyses in 1980 that some plants might require extensive modifications to address this safety issue, Westinghouse Electric Corporation undertook a deterministic fracture mechanics evaluation to demonstrate that the assumed double-ended rupture is not a credible design-basis event for PWR piping base and weld metals. Westinghouse Electric Corporation reports WCAP-9570, "Mechanistic Fracture Evaluation of Reactor Coolant Pipe Containing a Postulated Circumferential Through-Wall Crack," Revision 2, issued June 1981 [65], and WCAP-9788, "Tensile and Toughness Properties of Primary Piping Weld Metal for Use in Mechanistic Fracture Evaluation," issued June 1981 [66], document the evaluations for piping base and weld metals, respectively.

Around the same time, the NRC staff published the results of a probabilistic PWR piping fracture study in NUREG/CR-2189, Volume 5 [62]. The Westinghouse Electric Corporation and NRC staff-sponsored studies used different methodologies; however, both studies supported the conclusion that double-ended ruptures in PWR primary system piping are extremely low probability events. The results of these studies were submitted to the NRC's Advisory Committee on Reactor Safeguards. In a June 14, 1983, letter to the NRC's Executive Director for Operations, the Advisory Committee on Reactor Safeguards stated that:

> Fracture mechanics analysis clearly indicates that in PWR primary piping a substantial range of stable crack sizes exists between those which give detectable leaks and the much larger size that results in sudden failure… However any relaxation of requirements to cope with double-ended guillotine break should be preceded by rigorous reexamination of the integrity of heavy component supports under all design conditions.

As a result of these developments, the NRC proposed to modify the requirements of GDC 4 in 1985 [67] and 1986 [68]. The resulting amendments to GDC 4 in 1986 [69] and 1987 [70] allow for analyses to serve as the basis for excluding the consideration of dynamic effects associated with certain piping system ruptures. These analyses constitute what is commonly referred to as the LBB concept. The deterministic and probabilistic analyses showed that, for the primary loop piping in PWRs, double-ended guillotine or longitudinal ruptures are extremely unlikely. The analyses depend on advanced fracture mechanics techniques and include investigations of potential indirect failure mechanisms which could lead to piping rupture. The objective of the LBB approach is to demonstrate by analysis that the detection of small flaws, either by ISI or by leakage monitoring systems, is assured long before the flaws could grow to critical or unstable sizes and lead to large breaks, such as the double-ended guillotine pipe rupture. Acceptable analytical procedures are outlined in NUREG-1061, "Report of the U.S. Nuclear Regulatory Commission Piping Review Committee," Volume 3, "Evaluation of Potential Pipe Breaks," issued November 1984 [71].

The general design criteria in 10 CFR Part 50, Appendix A [3], require that the emergency core cooling systems of nuclear power plants be capable of tolerating a double-ended guillotine break. Specifically, GDC 4 states that:

> Structures, systems, and components important to safety shall be designed to accommodate the effects of and to be compatible with the environmental conditions associated with normal operation, maintenance, testing, and postulated accidents, including loss-of-coolant accidents. These structures, systems, and components shall be appropriately protected against dynamic effects, including the effects of missiles, pipe whipping, and discharging fluids, that may result from equipment failures and from events and conditions outside the nuclear power unit. However, dynamic effects associated with postulated pipe ruptures in nuclear power units may be excluded from the design basis when analyses reviewed and approved by the Commission demonstrate that

> the probability of fluid system piping rupture is extremely low under conditions consistent with the design basis for the piping.

With loss of coolant accidents defined as:

> … those postulated accidents that result from the loss of reactor coolant at a rate in excess of the capability of the reactor coolant makeup system from breaks in the reactor coolant pressure boundary, up to and including a break equivalent in size to the double-ended rupture of the largest pipe of the reactor coolant system.

LBB technology was applied to commercial nuclear power plant piping beginning in the 1980's in the U.S. GDC 4 requires mitigation against the potential dynamic events from a postulated dynamic piping break (i.e., use of pipe whip restraints and jet impingement shields), unless it can be shown there is an extremely low probability of rupture. The NRC staff developed a deterministic LBB procedure documented in NUREG-1061, Volume 3 [71], which is based on a stringent set of screening criteria and a deterministic fracture mechanics flaw tolerance evaluation. In 1987, the NRC solicited public comments on SRP Section 3.6.3 [72], which incorporated the screening criteria and deterministic fracture mechanics review procedures. Per this guidance, for a piping system to be eligible for LBB analysis, it should, among other factors, have the following:

- no active degradation mechanisms that can be potential sources of pipe rupture (e.g. erosion, corrosion, and fatigue)
- no materials that are susceptible to brittle cleavage-type failure (i.e., fracture)
- remote causes of rupture from water hammer and other potential indirect sources

The failure mode of concern for PWR primary loop reactor coolant system piping is circumferential cracking in butt-welds. Axial cracking has not been an issue in seamless or seam-welded piping that is stress-relieved or solution-annealed.

Following the procedures in SRP Section 3.6.3, a crack size in the reactor coolant system piping is calculated for a leak rate equal to the plant leakage detection system threshold (e.g., 1 gpm) multiplied by a safety factor of 10 to account for uncertainties. Once the leakage crack size is determined at normal operating conditions, the critical crack size at normal plus SSE loading conditions is determined by limit load analysis with Z-factors or elastic-plastic fracture mechanics analysis, if the material toughness is low enough to require it. This includes a margin of 2 on the crack length or 1.4 on the stresses. Therefore, an extremely low probability of rupture is demonstrated deterministically by having a piping system with no active degradation mechanisms that can be potential sources of pipe rupture and an analytical flaw tolerance evaluation.

Around 2000, a new degradation mechanism was identified in PWR piping systems that were previously approved for LBB. The new mechanism was termed PWSCC. It is characterized by a long crack initiation time and a relatively fast crack growth rate. It occurs in the DMWs (i.e.,

Alloy 82/182 filler weld metals) between stainless and ferritic steel piping components. The susceptible welds were not stress-relieved, and the normal operating stresses were low, so subcritical crack growth was primarily driven by the WRS. A revision to SRP Section 3.6.3 issued in 2007 [5] clarified that the NRC staff considers PWSCC to be an active degradation mechanism in Alloy 600/82/182 materials in PWRs. After the occurrence of additional PWSCC events, more detailed deterministic and probabilistic analyses were conducted, such as reported in EPRI Technical Report 1020752, "Materials Reliability Program: Primary Water Stress Corrosion Cracking of Alloy 600—Proceedings of the 2007 International Conference and Exhibition (MRP-221)," issued in 2010 [73], and EPRI Technical Report 1011808 "Materials Reliability Program: Leak-Before-Break Evaluation for PWR Alloy 82/182 Welds (MRP-140)," issued 2005 [74].

From a deterministic viewpoint, there are two primary scenarios: (1) when the combined WRS and normal operating stresses produce a crack that grows quickly through the pipe wall thickness, and (2) when a surface crack grows a long distance around the inside circumference before becoming a TWC. The first scenario represents LBB behavior; however, the second has the opposite effect (i.e., represents undesirable break-before-leak behavior) unless more complicated analytical evaluations are performed which consider the effects of ISI.

6.2 General Design Criterion 4

The xLPR code was developed, in part, to calculate whether DMWs in PWR piping systems exhibit an extremely low probability of rupture consistent with the requirements of GDC 4 when subject to the effects of PWSCC. The Office of Nuclear Regulatory Research conducted the present study at the request of the Office of Nuclear Reactor Regulation because many PWR licensees eliminated the use of certain equipment that protected against the failure of these piping systems. The approvals for these systems were based on the NRC staff's approval of the licensees' deterministic LBB analyses. Since PWSCC had not been addressed in the original licensee analyses, a regulatory question remained as to whether the piping systems with PWSCC in PWRs continue to demonstrate an extremely low probability of rupture consistent with the requirements of GDC 4.

Indeed, PFM analyses were used to support the GDC 4 rulemakings that allow LBB analyses, and the Commission has always envisioned the use of PFM analyses to make the demonstrations required by this regulation. A deterministic approach, however, was favored historically. Successful application of the xLPR code in this study demonstrates that the probabilities of PWR piping system ruptures remain extremely low when subject to PWSCC, which serves to reinforce the role of PFM in making the demonstrations required by GDC 4. Accordingly, the Office of Nuclear Regulatory Research recommends no changes to the GDC 4 regulations.

6.3 Standard Review Plan Section 3.6.3

SRP Section 3.6.3 allows for an NRC staff-approved LBB analysis to permit a licensee to remove protective hardware such as pipe whip restraints and jet impingement barriers; redesign

pipe-connected components, their supports, and their internals; and make other related changes. Compliance with GDC 4 requires that components important to safety be designed to accommodate the effects of, and be compatible with, environmental conditions associated with normal operation, maintenance, testing, and postulated accidents, including loss of coolant accidents. LBB analyses should demonstrate that the probability of pipe rupture is extremely low under conditions consistent with the design basis for the piping to be consistent with GDC 4. Previously a deterministic evaluation, as described in Section 6.1, of the piping system that demonstrates sufficient margins against failure, including verified design and fabrication and an adequate ISI program, was assumed to satisfy the extremely low probability criterion.

The current SRP Section 3.6.3 review procedures state that the NRC staff should verify the applicant's or licensee's LBB analysis with consideration of the following factors:

1. The reviewer should verify that the licensee's or applicant's LBB evaluation uses design basis loads and is based on the as-built piping configuration, as opposed to the design configuration.

2. The reviewer should evaluate the potential for degradation by erosion, erosion-corrosion, and erosion-cavitation due to unfavorable flow conditions and water chemistry.

3. The review should evaluate the material susceptibility to corrosion, the potential for high residual stresses, and environmental conditions that could lead to degradation by stress-corrosion cracking.

4. The reviewer should evaluate the adequacy of the leakage detection systems associated with the reactor coolant system. Determination of leakage from a piping system under pressure involves uncertainties and, therefore, margins are needed.

5. The reviewer should verify that the potential for water hammer in the candidate piping systems is very low.

6. The reviewer should verify that the candidate piping is not susceptible to creep and creep-fatigue.

7. The reviewer should evaluate the corrosion resistance of piping, which can be demonstrated by the frequency and degree of corrosion in the specific piping systems.

8. The reviewer should assess the potential for indirect sources of pipe ruptures to ensure that indirect failure mechanisms defined in the plant safety analysis report are negligible causes of pipe rupture.

9. The reviewer should determine that the piping material will not become susceptible to brittle, cleavage-type failures over the full range of system operating temperatures.

10. The reviewer should determine that the candidate piping does not have a history of fatigue cracking or failure.

11. The reviewer should review the acceptability of the deterministic LBB evaluation procedure.

12. The reviewer should review the considerations for review of design certification and combined license applications.

The analyses in this and prior studies have demonstrated that previously approved LBB piping systems continue to demonstrate an extremely low probability of rupture consistent with the requirements of GDC 4 with the presence of active degradation mechanisms. As guidance, SRP Section 3.6.3 does not preclude licensees from other such probabilistic LBB demonstrations, which the NRC staff can review directly against the GDC 4 requirements on a case-by-case basis. Accordingly, in the absence of a strong industry interest in future LBB applications, the Office of Nuclear Regulatory Research recommends no immediate changes to SRP Section 3.6.3 to support probabilistic LBB applications. SRP Section 3.6.3 may be retained as-is to support the NRC staff's review of deterministic LBB analyses as needed.

Should a strong demand for probabilistic LBB guidance arise in the future, based on the results of this and the prior study, the Office of Nuclear Regulatory Research recommends a broad expansion of the deterministic review procedures as follows:

- Review procedure item 1 addresses the use of design-basis loads. For probabilistic LBB analyses, it is recommended that the reviewer instead verify that the input distributions represent the loads or stresses as applicable to the analysis.
- Review procedure items 2, 3, 5, 6, 7, and 10 address the potential for various damage and degradation mechanisms. For probabilistic LBB analyses, it is recommended that the reviewer should instead verify that the applicable mechanisms are explicitly modeled in the analysis with verified and validated models and inputs. The non-applicability or low potential of damage or degradation mechanisms not explicitly modeled in the analysis may be demonstrated following the existing deterministic review procedures.
- Review procedure item 4 addresses margins on the leakage detection system. For probabilistic LBB analyses, it is recommended that such margins are not necessary, provided uncertainties in the leak rate calculations have been explicitly modeled in the analysis.
- Review procedure item 8 addresses indirect sources of pipe ruptures to ensure that indirect failure mechanisms defined in the plant safety analysis report are negligible causes of pipe rupture. For probabilistic LBB analyses, it is recommended that the reviewer instead verify that the applicable indirect failure mechanisms are explicitly modeled in the analysis with verified and validated models and inputs. The non-applicability or low potential of indirect failure mechanisms not explicitly modeled in the analysis may be demonstrated following the existing deterministic review procedures.
- Review procedure item 9 addresses material susceptibility to brittle cleavage-type failures over the full range of system operating temperatures. For probabilistic LBB analyses, it is recommended that the reviewer should instead verify that the fracture

behavior of the materials is explicitly modeled in the analysis with verified and validated models and inputs.

- Review procedure item 11 addresses steps for an acceptable deterministic LBB evaluation procedure. For probabilistic LBB analyses, it is recommended that the reviewer verify the applicable inputs, models, computational sequences, and outputs. The pertinent QoI for the analysis is the probability of rupture, which should be extremely low consistent the requirements of GDC 4. The probability of rupture results may reflect any explicitly modeled detection capabilities as necessary (e.g., leak rate detection, ISI, or both as may be necessary).
- Review procedure item 12 addresses considerations for the review of design certification and combined license applications. For probabilistic LBB analyses, it is recommended that this item continue to apply.
- Not addressed in the current deterministic review procedures are review procedures for PFM analyses. For probabilistic LBB analyses, it is recommended that the reviewer verify that the analysis follows applicable guidance for preparing PFM submittals. The Office of Nuclear Regulatory Research is currently in the process of preparing such guidance.

7 SUMMARY AND CONCLUSIONS

Following the analyses performed for the prior study, the present generalization study extended the welds under consideration beyond primary piping systems in Westinghouse four-loop PWRs. All piping systems which have received prior LBB approvals from the NRC staff and which contain Alloy 82/182 DMWs that are susceptible to PWSCC were binned for this study as follows:

- Bin 1: Westinghouse four-loop RVON and RVIN DMWs
- Bin 2: Westinghouse pressurizer surge line nozzle DMWs
- Bin 3: CE and B&W RCP nozzle DMWs
- Bin 4: Westinghouse steam generator nozzle DMWs
- Bin 5a: CE hot leg branch line nozzle DMWs
- Bin 5b: CE cold leg branch line nozzle DMWs
- Bin 6: Westinghouse two- and three-loop RVON and RVIN DMWs

For each bin, a representative weld was analyzed using actual plant data when available and engineering judgement when not. Probability distributions were used to represent the material variability and inherent uncertainties associated with the WRS profiles, among other uncertainties. Otherwise, deterministic inputs for the analysis of each bin were selected such that they would bias the results towards higher probabilities of rupture, thereby bounding all welds represented by the bin. Based on experience, the highest normal operating loads, temperatures, and pressures were selected along with the highest outside diameters and thinnest wall thicknesses. The objective was to define a bounding, although realistic, weld for each bin. In some instances, this basic approach was revised to keep the representative weld within reasonable conditions (e.g., the highest load was not selected for one bin because it was associated with the only weld with MSIP® mitigation, and such mitigation was not considered for the base case).

A base case was analyzed for each bin. The base case included the effects of PWSCC initiation and growth for both circumferential and axial cracks with leak rate detection, ISI, and SSE events. These cases were used to estimate the base probability of rupture with a 1 gpm leak rate detection capability. Since these values were zero for all the base cases, even with a large sample size, other QoIs such as the time-dependent probabilities of first crack, first leak, and rupture both with and without ISI were also estimated. The base case was supplemented with a sensitivity study where each realization begins with one axial and one circumferential crack at the top dead center of the weld. As outlined in the prior study, two of the QoIs (i.e., the LBB ratio and LBB time lapse) are not impacted by crack initiation, and thus they can be more accurately estimated with this approach. Prior studies have outlined the importance of WRS and its associated uncertainties. Thus, an additional sensitivity study case considering a more severe WRS profile was also included for each bin. Other sensitivity studies were included to analyze the impacts of fatigue and mechanical mitigation, as appropriate.

Bin 1 covered Westinghouse four-loop RVON and RVIN DMWs. Although these welds were the focus of the prior study, they were reanalyzed as part of the present study to provide a consistent basis for comparison for all the cases. As in the prior study, the probability of rupture with a 1 gpm leak rate detection capability was estimated to be zero in all cases.

Bin 2 covered Westinghouse pressurizer surge line nozzle DMWs. The probability of rupture with a 1 gpm leak rate detection capability was estimated to be zero in all cases, except in the sensitivity study case that included a weld overlay for mitigation purposes. Although counterintuitive, because of the overlay, some circumferential cracks grew slowly in depth through the more PWSCC-resistant Alloy 52/152 overlay while growing more quickly in length in the more PWSCC-susceptible Alloy 82/182 original weld metal. However, the occurrence of such events was below 1×10^{-6} ruptures per year. When the effects of a 10-year inspection frequency are also considered, the frequency drops to 1×10^{-9} ruptures per year. It should be noted that this inspection frequency was selected for consistency across all the bins to enable comparisons of the results; however, the surge line is currently required by 10 CFR 50.55a(g)(6)(ii)(F) to be inspected more frequently (i.e., every other refueling outage, which is approximately every 3 to 4 years). Modeling such a frequency would only further reduce the annual frequency of rupture. Due to their smaller diameters and different leak rates, the pressurizer surge line nozzle DMWs required larger relative crack sizes to generate 1 or 10 gpm leak rates. These relatively larger crack sizes resulted in lower LBB ratios and LBB time lapses as compared to the Bin 1 results.

Bin 3 covered CE and B&W RCP nozzle DMWs. The probability of rupture with a 1 gpm leak rate detection capability was estimated to be zero in all cases. None of the cases generated a rupture. As a result, the LBB ratio and LBB time lapse QoIs could not be estimated. Based on the prior study, these results were expected given the lower operating temperature of the cold leg where these welds are located. Of note, the base case had a higher probability of first crack as compared to the sensitivity study case with a more severe WRS profile. All the cracks in the base case were axial. The more severe WRS profile was selected to increase the likelihood of circumferential crack initiation; however, it was not enough to initiate any circumferential cracks, and the companion hoop WRS profile was also lower leading to a lower probability of axial cracks.

Bin 4 covered Westinghouse steam generator nozzle DMWs. The base case was defined differently from the other base cases because the inlay was modeled from the beginning of the simulation on account it being applied before the components were placed in service. The probability of rupture with a 1 gpm leak rate detection capability was estimated to be zero in all cases except Case 4.1.2, which was a sensitivity study considering a more severe WRS profile. This case resulted in a probability of rupture with a 1 gpm leak rate detection capability of 1×10^{-4}, which equates to 1.4×10^{-6} ruptures per year. However, the frequency was reduced by 2 orders of magnitude to 7.3×10^{-9} ruptures per year when a 10-year inspection frequency is considered.

Bins 5a and 5b covered CE hot and cold leg branch line nozzle DMWs, respectively. The probability of rupture with a 1 gpm leak rate detection capability was zero in all cases. The cold

leg branch line nozzle DMW probabilities of first crack and first leak at 80 EFPY were lower than their hot leg equivalents by roughly a factor of 3. As compared to the Bin 1 results, the smaller diameter piping in Bins 5a and 5b resulted in lower LBB ratios. The LBB time lapses, however, were on average in the same range or higher due to the slower crack growth.

Bin 6 covered Westinghouse two- and three-loop RVON and RVIN DMWs. The probability of rupture with a 1 gpm leak rate detection capability was zero in all cases. The results demonstrate that the Westinghouse four-loop RVON and RVIN DMW analysis results also bound the two- and three-loop designs.

The xLPR code analyzes the risks associated with a single weld; however, GDC 4 requires an aggregation of the results at the system-level. Thus, a piping system-level analysis was necessary to combine the individual bin results and estimate the total probability of rupture for the various PWR piping systems of interest in this study. The probability of rupture with a 1 gpm leak rate detection capability and ISI, as necessary, served as the QoI used to assess whether such piping systems demonstrate an extremely low probability of rupture consistent with the requirements of GDC 4. Since these estimated probabilities were zero in all the base cases, aggregation of the results at the system-level was also zero. Some of the estimates for the sensitivity study cases were non-zero, and these cases were studied and explained. The system-level results for the probability of rupture with detection are thus below the acceptance criterion of 1×10^{-6} ruptures per reactor-year and, therefore, the piping systems continue to meet the requirements of GDC 4.

To illustrate the contributions of the various welds at the system-level, the probabilities of first crack, first leak, and rupture with and without a 10-year inspection frequency were estimated for three groupings of components that bound the various configurations in operating PWRs. The groupings were for Westinghouse four-loop PWR piping systems, Westinghouse two- and three-loop PWR piping systems, and CE and B&W PWR piping systems with prior LBB approvals. The aggregation method considered all the welds to be independent consistent with the prior study. The largest contributing welds types were shown to vary depending on the QoI under consideration.

Successful application of the xLPR code in this study to demonstrate that the probabilities of PWR piping system ruptures remain extremely low when subject to PWSCC serves to reinforce the role of PFM for making the demonstrations required by GDC 4. Accordingly, the Office of Nuclear Regulatory Research recommends no changes to the GDC 4 regulations as result. Additionally, in the absence of a strong industry interest in future LBB applications, the Office of Nuclear Regulatory Research recommends no changes to SRP Section 3.6.3 to support probabilistic LBB applications. Should a strong demand for probabilistic LBB guidance arise in the future, a broad expansion of the deterministic review procedures may be considered based on the results of this study.

8 REFERENCES

[1] NRC, NUREG-2247, “Extremely Low Probability of Rupture Version 2 Probabilistic Fracture Mechanics Code,” August 2021, ADAMS Accession Number ML21225A736.

[2] NRC, TLR-RES/DE/REB-2021-09, “Probabilistic Leak-Before-Break Evaluation of Westinghouse Four-Loop Pressurized-Water Reactor Primary Coolant Loop Piping using the Extremely Low Probability of Rupture Code,” August 13, 2021, ADAMS Accession Number ML21217A08.

[3] *U.S. Code of Federal Regulations*, “Domestic Licensing of production and utilization facilities,” Part 50, Chapter I, Title 10, “Energy.”

[4] R. Hardies, “xLPR Version 2.0 Technical Basis Document—Acceptance Criteria,” October 28, 2016, ADAMS Accession Number ML16271A436.

[5] NRC, NUREG-0800, “Standard Review Plan for the Review of Safety Analysis Reports for Nuclear Power Plants: LWR Edition,” Section 3.6.3, “Leak-Before-Break Evaluation Procedures,” Revision 1, March 2007, ADAMS Accession Number ML063600396.

[6] Babcock and Wilcox, BAW-1847, Revision 1, “Leak-Before-Break Evaluations of Margins Against Full Break for RCS Primary Piping of B&W Designed NSS,” Lynchburg, Virginia, September 1985, ADAMS Accession Number ML20138R230.

[7] Combustion Engineering, Inc., CEN-367, “Leak-Before-Break Evaluation of Primary Coolant Loop Piping in Combustion Engineering Designed Nuclear Steam Supply Systems,” Windsor, Connecticut, November 1987, ADAMS Accession Number ML20236U854.

[8] Westinghouse Electric Corporation, WCAP 10565, “Technical Bases for Eliminating Large Primary Loop Pipe Rupture as the Structural Design Basis for Beaver Valley Unit 2,” Pittsburgh, PA, May 1984, ADAMS Accession Number ML19273A299.

[9] Westinghouse Electric Corporation, WCAP-12093, “Evaluation of Thermal Stratification for the Beaver Valley Unit 2 Pressurizer Surge Line,” Pittsburgh, PA, December 1988, ADAMS Accession Number ML19297H298.

[10] Westinghouse Electric Corporation, WCAP-10553, “Technical Bases for Eleminating Large Primary Loop Pipe Rupture as the Structural Design Basis for Byron Units 1 and 2 and Braidwood Units 1 and 2,” Pittsburgh, PA, May 1984, ADAMS Accession Number ML19269A541.

[11] Westinghouse Electric Corporation, WCAP 10691, “Technical Bases for Eliminating Large Primary Loop Pipe Rupture as a Structural Design Basis for Callaway and Wolf Creek Plants,” Pittsburgh, PA, October 1984, ADAMS Accession Number ML19269A700.

[12] Westinghouse Electric Corporation, WCAP 10546, “Technical Bases for Eliminating Large Primary Loop Pipe Rupture as the Structural Design Basis for Catawba Units 1 & 2,” Pittsburgh, PA, April 1984, ADAMS Accession Number ML19269A109.

[13] Westinghouse Electric Corporation, “WCAP-10527, Technical Bases for Eliminating Large Primary Loop Pipe Rupture as the Structural Design Basis for Comanche Peak Units 1 and 2,” Pittsburgh, PA, April 1984, ADAMS Accession Number ML19268E842.

[14] Westinghouse Electric Corporation, WCAP-12248, “Evaluation of Thermal Stratification for the Comanche Peak Unit 1 Pressurizer Surge Line,” Pittsburgh, PA, April 1989, ADAMS Accession Number ML19297H610.

[15] Westinghouse Electric Corporation, WCAP-13100, “Technical Justification for Eliminating Pressurizer Surge Line Rupture from the Structural Design Basis for Comanche Peak Unit 2,” Pittsburgh, PA, December 1991, ADAMS Accession Number ML20034D232.

[16] Westinghouse Electric Company, WCAP-15131, Revision 1, “Technical Justification for Eliminating Large Primary Loop Pipe Rupture as the Structural Design Basis for the D. C. Cook Units 1 and 2 Nuclear Power Plants,” Pittsburgh, PA, October 1999, ADAMS Accession Number ML993230342.

[17] Westinghouse Electric Company, WCAP-15434, Revision 1, “Technical Justification for Eliminating Pressurizer Surge Line Rupture as the Structural Design Basis for D. C. Cook Units 1 and 2 Nuclear Power Plants,” Pittsburgh, PA, August 2000, ADAMS Accession Number ML003744815.

[18] Westinghouse Electric Corporation, WCAP-12825 “Technical Justification for Eliminating, Large Primary Loop Pipe Rupture as the Structural Design Basis for the Joseph M. Farley Units 1 and 2 Nuclear Power Plants,” Pittsburgh, PA, January 1991, ADAMS Accession Number ML19310D161.

[19] Westinghouse Electric Corporation, WCAP-12835, “Technical Justification for Eliminating Pressurizer Surge Line Rupture from the Structural Design Basis for Farley Units 1 and 2,” Pittsburgh, PA, April 1991, ADAMS Accession Number ML19312B430.

[20] Westinghouse Electric Corporation, WCAP-10585, “Technical Bases for Eliminating Large Primary Loop Pipe Rupture as the Structural Design Basis for McGuire Units 1 and 2,” Pittsburgh, PA, June 1984, ADAMS Accession Number ML19273A509.

[21] Structural Integrity Associates, Inc, SIR-98-096, “Pressurizer Surge Line Leak-Before-Break Evaluation Millstone Nuclear Power Station, Unit 2," San Jose, CA, October 1998, ADAMS Accession Number ML20195C773.

[22] Structural Integrity Associates, Inc, SIR-98-070, “Leak-Before-Break Evaluation High Energy Shutdown Cooling Piping Millstone Nuclear Power Station, Unit 2,” San Jose, CA, July 1998, ADAMS Accession Number ML20236U636.

[23] Structural Integrity Associates, Inc, SIR-98-048, “Leak-Before-Break Evaluation High Energy Safety Injection Piping Millstone Nuclear Power Station, Unit 2,” San Jose, CA, July 1998, ADAMS Accession Number ML20236U636.

[24] Westinghouse Electric Corporation, WCAP-10587, “Technical Bases for Eliminating Large Primary Loop Pipe Rupture as a Structural Design Basis Millstone Unit 3,” Pittsburgh, PA, June 1984, ADAMS Accession Number ML19269A552.

[25] Westinghouse Electric Corporation, WCAP-11163, “Technical Bases for Eliminating Large Primary Loop Pipe Rupture as a Structural Design Basis for North Anna Units 1 & 2,” Pittsburgh, PA, August 1986, ADAMS Accession Number ML19292G229.

[26] Westinghouse Electric Company, WCAP-14439-NP, Revision 0, “Technical Justification for Eliminating Large Primary Loop Pipe Rupture as the Structural Design Basis for the Point Beach Nuclear Plant, Units 1 and 2 for the Power Uprate and License Renewal Program,” Pittsburgh, PA, September 2003, ADAMS Accession Number ML033210554.

[27] Westinghouse Electric Company, WCAP-15065, “Technical Justification for Eliminating Pressurizer Surge Line Rupture as the Structural Design Basis for the Point Beach Units 1 and 2 Nuclear Plants,” Pittsburgh, PA, August 1998, ADAMS Accession Number ML993420097.

[28] Westinghouse Electric Corporation, WCAP-10929, Revision 1, “Technical Bases for Eliminating Large Primary Loop Pipe Rupture as the Structural Design Basis for Prairie Island Unit 2,” Pittsburgh, PA, July 1986, ADAMS Accession Number ML19292F919.

[29] Westinghouse Electric Corporation, WCAP-12876, “Technical Justification for Eliminating Pressurizer Surge Line Rupture as the Structural Design Basis for Prairie Island Unit 1,” Pittsburgh, PA, March 1991, ADAMS Accession Number ML20081K353.

[30] NRC, NUREG-1785, “Safety Evaluation Report Related to the License Renewal of H.B. Robinson Steam Electric Plant, Unit 2,” March 2004, ADAMS Accession Number ML040990702.

[31] Westinghouse Electric Corporation, WCAP-13659, “Technical Justification for Eliminating Large Primary Loop Pipe Rupture as the Structural Design Basis for the Salem Generating

Station Units 1 and 2," Pittsburgh, PA, May 1993, ADAMS Accession Number ML18100A467.

[32] Westinghouse Electric Corporation, WCAP-10567, "Technical Bases for Eliminating Large Primary Loop Pipe Rupture as the Structural Design Basis for Seabrook Units 1 & 2," Pittsburgh, PA, June 1984, ADAMS Accession Number ML19277H797.

[33] Westinghouse Electric Corporation, WCAP-12011, "Technical Justification for Eliminating Large Primary Loop Pipe Rupture as the Structural Design Basis for Sequoyah Units 1 & 2," Pittsburgh, PA, October 1988, ADAMS Accession Number ML19261A197.

[34] Westinghouse Electric Corporation, WCAP-12775, "Technical Justificaiton for Eliminating Pressurizer Surge Line Rupture as the Structural Design Basis for Sequoyah Units 1 and 2," Pittsburgh, PA, December 1990, ADAMS Accession Number ML19310E553.

[35] Westinghouse Electric Corporation, WCAP-10699, "Technical Bases for Eliminating Large Primary Loop Pipe Rupture as a Structural Design Basis for Shearon Harris Unit 1," Pittsburgh, PA, September 1984, ADAMS Accession Number ML19269A914.

[36] Westinghouse Electric Corporation, WCAP-10559, "Technical Bases for Eliminating Large Primary Loop Pipe Rupture as the Structural Design Basis for South Texas Project Units 1 and 2," Pittsburgh, PA, May 1984, ADAMS Accession Number ML19273A409.

[37] Westinghouse Electric Corporation, WCAP 10489, "Technical Bases for Eliminating Pressurizer Surge Line Ruptures as the Structural Design Basis for South Texas Project," Pittsburgh, PA, February 1984, ADAMS Accession Number ML19276D352.

[38] Westinghouse Electric Corporation, WCAP-11256, "Additional Information in Support of the Elimination of Postulated Pipe Ruptures in the Pressurizer Surge Lines of South Texas Units 1 and 2," Pittsburgh, PA, September 1986, ADAMS Accession Number ML19292F907.

[39] Westinghouse Electric Corporation, WCAP-13206, "Technical Justification for Eliminating Large Primary Loop Pipe Rupture as the Structural Design Basis for the Virgil C. Summer Nuclear Power Plant," Pittsburgh, PA, April 1992, ADAMS Accession Number ML19311A870.

[40] Westinghouse Electric Corporation, WCAP-13605, "Primary Loop Leak-Before-Break Reconciliation to Account for the Effects of Steam Generator Replacement/Uprating," Pittsburgh, PA, March 1993, ADAMS Accession Number ML19311A986.

[41] Westinghouse Electric Corporation, WCAP 10551, “Technical Bases for Eliminating Large Primary Loop Pipe Rupture as the Structural Design Basis for Alvin W. Vogtle Units 1 and 2,” Pittsburgh, PA, May 1984, ADAMS Accession Number ML19269A160.

[42] Westinghouse Electric Corporation, WCAP-12218, “Evaluation of Thermal Stratification for the Vogtle Unit 2 Pressurizer Surge Line,” Pittsburgh, PA, March 1989, ADAMS Accession Number ML19302D775.

[43] Westinghouse Electric Company, WCAP-17187-NP, “Technical Justification for Eliminating Pressurizer Surge Line Rupture as the Structural Design Basis for Waterford Steam Electric Station, Unit 3 Using Leak-Before-Break Methodology,” Pittsburgh, PA, February 2010, ADAMS Accession Number ML100550607.

[44] Westinghouse Electric Corporation, WCAP-11985, “Technical Justification for Eliminating Large Primary Loop Pipe Rupture as the Structural Design Basis for Watts Bar Units 1 and 2,” Pittsburgh, PA, November 1988, ADAMS Accession Numbers ML082630351 and ML082700693.

[45] Westinghouse Electric Corporation, WCAP-12773, “Technical Justification for Eliminating Pressurizer Surge Line Rupture as the Structural Design Basis for Watts Bar Units 1 and 2,” Pittsburgh, PA, December 1990, ADAMS Accession Number ML073601054.

[46] NRC and EPRI, “Memorandum of Understanding between U.S. Nuclear Regulatory Commission and Electric Power Research Institute, Inc. on Cooperative Nuclear Safety Research, xLPR Version 2 Code Documentation and Leak-Before-Break Applications,” May 16, 2017, ADAMS Accession Number ML17040A146.

[47] F. Brust, “xLPR Models Subgroup Report—Welding Residual Stresses,” Version 1.0, October 5, 2016, ADAMS Accession Number ML16341B049.

[48] EPRI, Technical Report 1022852, “Materials Reliability Program: Probabilistic Assessment of Chemical Mitigation of Primary Water Stress Corrosion Cracking in Nickel-Base Alloys (MRP-307),” Palo Alto, CA, June 29, 2011.

[49] ASME, Boiler and Pressure Vessl Code Case N-770-5, “Alternative Examination Requirements and Acceptance Standards for Class 1 PWR Piping and Vessel Nozzle Butt Welds Fabricated With UNS N06082 or UNS W86182 Weld Filler Material With or Without Application of Listed Mitigation Activities,” New York, NY, Approval Date: November 7, 2016.

[50] T. Seuaciuc-Osorio, xLPR-MVR-ISI, Version 1.0, “xLPR Module Validation Report for ISI Module,” June 13, 2016.

[51] NRC, TLR-RES/DE/CIB-2021-11, “Sensitivity Studies and Analyses Involving the Extremely Low Probability of Rupture Code,” May 14, 2021, ADAMS Accession Number ML21133A485.

[52] EPRI, Technical Report 3002010756, “Materials Reliability Program: Recommended Factors of Improvement for Evaluating Primary Water Stress Corrosion Cracking (PWSCC) Growth Rates of Thick-Wall Alloy 690 Materials and Alloy 52, 152, and Variants Welds (MRP 386),” Palo Alto, CA, December 22, 2017.

[53] M. Homiack, “xLPR Group Report—Inputs Group,” Version 1.0, December 19, 2017, ADAMS Accession Number ML19337B876.

[54] Structural Integrity Associates, Inc., Report Number 1301103.401, “Flaw Tolerance Evaluation of St. Lucie Surge Line Welds Using ASME Code Section XI, Appendix L,” San Jose, CA, May 2015, ADAMS Accession Number ML15314A162.

[55] Structural Integrity Associates, Inc., Report Number 1100756.401, Revision 1, “Flaw Tolerance Evaluation of Turkey Point Surge Line Welds Using ASME Code Section XI, Appendix L,” San Jose, CA, May 2012, ADAMS Accession Number ML12361A261.

[56] E. S. Grecheck, Vice President–Nuclear Engineering and Development, Virginia Electric and Power Company, letter to NRC Document Control Desk, “Virginia Electric and Power Company (Dominion) North Anna Power Station Unit 2 ASME Inservice Inspection Program Examination Results and Revised Request for Alternative to ASME Code Steam Generator Nozzle-to-Vessel Weld Examination Requirements Alternative Request N2-I4-LMT-001-R1,” April 22, 2013, ADAMS Accession Number ML13114A253.

[57] D. Rudland and others, “Evaluation of the Inlay Process as a Mitigation Strategy for Primary Water Stress Corrosion Cracking in Pressurized Water Reactors,” April 2010, ADAMS Accession Number ML101260554.

[58] D. Rudland and others, “PWSCC Crack Growth Mitigation With Inlay,” PVP2011-57954, in *Proceedings of the ASME 2011 Pressure Vessels & Piping Division Conference*, Baltimore, MD, 2011.

[59] EPRI, Technical Report 1016602, “Materials Reliability Program: Technical Basis for Preemptive Weld Overlays for Alloy 82/182 Butt Welds in PWRs (MRP-169) Revision 1,” Palo Alto, CA, June 11, 2008.

[60] EPRI, Technical Report 1015400, “Materials Reliability Program: Advanced FEA Evaluation of Growth of Postulated Circumferential PWSCC Flaws in Pressurizer Nozzle Dissimilar Metal Weld (MRP-216, Rev. 1),” Palo Alto, CA, August 10, 2007.

[61] C. Harrington, MRP Project Manager, EPRI, letter to NRC Document Control Desk, MRP 2021-015, “Transmittal of Applicability Assessment Guidance for Probability of Detection Curves,” September 28, 2021, ADAMS Accession Number ML21271A585.

[62] NRC, NUREG/CR-2189, “Probability of Pipe Fracture in the Primary Coolant Loop of a PWR Plant,” Volume 5, “Probabilistic Fracture Mechanics Analysis, Load Combination Program, Project I Final Report,” August 1981, ADAMS Accession Number ML15300A304.

[63] M. Erickson, “xLPR Technical Report—Sources and Treatment of Uncertainties,” Version 2.0, November 16, 2020, ADAMS Accession Number ML19337C165.

[64] Atomic Energy Commission, “General Design Criteria for Nuclear Power Plants,” *Federal Register*, pp. 3255–3260, February 20, 1971.

[65] Westinghouse Electric Corporation, WCAP-9570, Revision 2, “Mechanistic Fracture Evaluation of Reactor Coolant Pipe Containing a Postulated Circumferential Through-wall Crack,” Pittsburgh, PA, June 1981, ADAMS Accession Number ML19352B279.

[66] Westinghouse Electric Corporation, WCAP 9788, “Tensile and Toughness Properties of Primary Piping Weld Metal for Use in Mechanistic Fracture Evaluation,” Pittsburgh, PA, June 1981, ADAMS Accession Number ML19352B277.

[67] NRC, “Modification of General Design Criterion 4 Requirements for Protection Against Dynamic Effects of Postulated Pipe Ruptures,” *Federal Register*, pp. 27,006–27,009, July 1, 1985.

[68] NRC, “Modification of General Design Criterion 4 Requirements for Protection Against Dynamic Effects of Postulated Pipe Ruptures,” *Federal Register*, pp. 26,393–26,399, July 23, 1986.

[69] NRC, “Modification of General Design Criterion 4 Requirements for Protection Against Dynamic Effects of Postulated Pipe Ruptures,” *Federal Register*, pp. 12,502–12,505, April 11, 1986.

[70] NRC, “Modification of General Design Criterion 4 Requirements for Protection Against Dynamic Effects of Postulated Pipe Ruptures,” *Federal Register*, pp. 41,288–41,295, October 27, 1987.

[71] NRC, NUREG-1061, “Report of the U.S. Nuclear Regulatory Commission Piping Review Committee,” Volume 3, “Evaluation of Potential Pipe Breaks,” November 1984, ADAMS Accession Number ML15300A304.

[72] NRC, “Standard Review Plan; Public Comment Solicited,” *Federal Register*, pp. 32,626–32,633, August 28, 1987.

[73] EPRI, Technical Report 1020752, “Materials Reliability Program: Primary Water Stress Corrosion Cracking of Alloy 600–Proceedings of the 2007 International Conference and Exhibition (MRP-221),” Palo Alto, CA, February 25, 2010.

[74] EPRI, Technical Report 1011808, “Materials Reliability Program: Leak-Before-Break Evaluation for PWR Alloy 82/182 Welds (MRP-140),” Palo Alto, CA, November 3, 2005.

[75] M. Benson, “Phase 2b Finite Element Round Robin Results Technical Letter Report,” December 2015, ADAMS Accession Number ML16020A034.

[76] EPRI, Technical Report 1009549, “Materials Reliability Program: Alloy 82/182 Pipe Butt Weld Safety Assessment for U.S. PWR Plant Designs (MRP-113),” Palo Alto, CA, January 31, 2006.

[77] R. J. Murillo, Licensing Manager, Waterford 3, Entergy Nuclear South, Entergy Operations, Inc., letter to NRC Document Control Desk, “Summary of Design and Analyses of Weld Overlays for Pressurizer and Hot Leg Nozzle Dissimilar Metal Welds for Alloy 600 Mitigation, Waterford Steam Electric Station, Unit 3 (Waterford 3),” May 10, 2008, ADAMS Accession Number ML081350064.

[78] EPRI, Technical Update 1009801, “Materials Reliability Program: Resistance to Primary Water Stress Corrosion Cracking of Alloys 690, 52, and 152 in Pressurized Water Reactors (MRP-111),” Palo Alto, CA, March 29, 2004.

[79] Westinghouse Electric Company, WCAP-17128-NP, Revision 1, “Flaw Evaluation of CE Design RCP Suction and Discharge Nozzle Dissimilar Metal Welds, Phase III Study,” Pittsburgh, PA, May 2010, ADAMS Accession Number ML12306A291.

[80] Westinghouse Electric Company, WCAP-11164-NP, Revision 2, “Technical Justification for Eliminating Large Primary Loop Pipe Rupture as the Structural Design Basis for North Anna Units 1 and 2 Nuclear Power Plants for the Subsequent License Renewal Program (80 Years) Leak-Before-Break Evaluation,” Pittsburgh, PA, January 2020, ADAMS Accession Number ML20246G707.

[81] NRC, NUREG/CR-6142, “Tensile-Property Characterization of Thermally Aged Cast Stainless Steels,” February 1994, ADAMS Accession Number ML052580136.

[82] M. Uddin and others, “Flaw Evaluation Procedure for Cast Austenitic Stainless Steel Materials Using A Newly Developed Statistical Thermal Aging Model,” PVP2019-93711, in

Proceedings of the ASME 2019 Pressure Vessels & Piping Conference, San Antonion, TX, 2019.

[83] F. W. Brust and others, “Part Repair and Start/Stop Effects and Three Dimensional Residual Stress in Dissimilar Metal Welds,” PVP2015-45785, in *Proceedings of the ASME 2015 Pressure Vessels and Piping Conference*, Boston, MA, 2015.

[84] F. W. Brust and others, Chapter 7, “Residual Stress and Distortion,” in *Welding Handbook*, 10th Edition, Volume 1, Miami, FL, American Welding Society, 2019.

[85] C. Harrington, MRP Project Manager, EPRI, letter to NRC Document Control Desk, MRP 2021-014, “Transmittal of xLPR Welding Residual Stress Essential Parameters and Profile Selection,” September 28, 2021, ADAMS Accession Number ML21271A591.

[86] NRC, NUREG-2162, “Weld Residual Stress Finite Element Analysis Validation: Part 1 – Data Development Effort,” March 2014, ADAMS Accession Number ML14087A118.

[87] NRC, "NUREG-2228, Weld Residual Stress Finite Element Analysis Validation, Part II – Proposed Validation Procedure, Final Report,” July 2020, ADAMS Accession Number ML20212L592.

[88] H. J. Rathburn and others, “NRC Welding Residual Stress Validation Program International Round Robin Program and Findings,” PVP2011-57642, in *Proceedings of the ASME 2011 Pressure Vessels & Piping Division Conference*, Baltimore, MD, 2011.

[89] F. W. Brust and others, “Weld Residual Stress Analysis and Axial PWSCC Predictions in a Double Vee Groove Large Diameter Nozzle,” PVP2013-98065, in *Proceedings of the ASME 2013 Pressure Vessels and Piping Conference*, Paris, France, 2013.

[90] F. W. Brust and others, “Natural PWSCC Crack Growth in Dissimilar Metal Welds with Inlay,” PVP2010-26108, in *Proceedings of ASME 2010 Pressure Vessels and Piping Division/K-PVP Conference*, Bellevue, WA, 2010.

APPENDIX A
SUMMARY OF RESULTS

The following table summarizes the results of the probabilistic LBB evaluation of representative PWR piping welds using the xLPR code. The numerical results are presented as mean estimates for each case with the standard error to provide an indication of the level of uncertainty in the estimates. The results for the probability of rupture with a 1 gpm leak rate detection capability were zero for all the bases cases and are thus not reported in the table.

Case No.	xLPR Beta Version	Sample Size	Mean Occurrence of Leak Rate Jump at 80 EFPY	Mean LBB Time Lapse [1]		Mean LBB Ratio		Probability of 1st Crack at 80 EFPY	Probability of 1st Leak at 80 EFPY	Probability of Rupture at 80 EFPY [2]
				1 gpm Leak Rate Detection Capability (Months)	10 gpm Leak Rate Detection Capability (Months)	1 gpm Leak Rate Detection Capability	10 gpm Leak Rate Detection Capability			
1.1.6a	xLPR v2.0d	100,000	0	36.5 ± 1.2	25.1 ± 0.90	9.6 ± 0.07	4.6 ± 0.02	$7.4 \times 10^{-3} \pm 2.7 \times 10^{-4}$	$5.14 \times 10^{-3} \pm 2.3 \times 10^{-4}$	$1.85 \times 10^{-3} \pm 1.4 \times 10^{-4}$
1.1.6b	xLPR v2.0d	5,000	0	38.7 ± 0.3	26.4 ± 0.2	9.9 ± 0.01	4.6 ± 0.00	1 ± 0	$9.9 \times 10^{-1} \pm 1.1 \times 10^{-3}$	$9.6 \times 10^{-1} \pm 3.0 \times 10^{-3}$
1.1.6c	xLPR v2.0d	100,000	0	36.5 ± 1.2	25.1 ± 0.90	9.6 ± 0.07	4.6 ± 0.02	$7.4 \times 10^{-3} \pm 2.7 \times 10^{-4}$	$5.14 \times 10^{-3} \pm 2.3 \times 10^{-4}$	$1.85 \times 10^{-3} \pm 1.4 \times 10^{-4}$
1.3.0	xLPR v2.0d	100,000	0	33.9 ± 1.6	21.8 ± 1.8	9.9 ± 0.1	4.4 ± 0.04	$1.24 \times 10^{-2} \pm 3.5 \times 10^{-4}$	$1.04 \times 10^{-2} \pm 3.2 \times 10^{-4}$	$8.36 \times 10^{-4} \pm 9.1 \times 10^{-5}$
1.3.1	xLPR v2.0d	5,000	0	33.4 ± 0.2	20.9 ± 0.1	10 ± 0.02	4.5 ± 0.01	1 ± 0	$9.73 \times 10^{-1} \pm 2.3 \times 10^{-3}$	$7.5 \times 10^{-1} \pm 6.1 \times 10^{-3}$
2.1.0	xLPR v2.0d	100,000	0	6.5 ± 0.7	1.1 ± 0.1	4.4 ± 0.1	2.0 ± 0.07	$3.40 \times 10^{-2} \pm 5.7 \times 10^{-4}$	$3.12 \times 10^{-2} \pm 5.5 \times 10^{-4}$	$1.09 \times 10^{-4} \pm 3.3 \times 10^{-5}$

Case No.	xLPR Beta Version	Sample Size	Mean Occurrence of Leak Rate Jump at 80 EFPY	Mean LBB Time Lapse [1]		Mean LBB Ratio		Probability of 1st Crack at 80 EFPY	Probability of 1st Leak at 80 EFPY	Probability of Rupture at 80 EFPY [2]
				1 gpm Leak Rate Detection Capability (Months)	10 gpm Leak Rate Detection Capability (Months)	1 gpm Leak Rate Detection Capability	10 gpm Leak Rate Detection Capability			
2.1.1	xLPR v2.0d	5,000	0	6.6 ± 0.1	1.28 ± 0.02	4.5 ± 0.02	2.0 ± 0.01	1 ± 0	1.00×10^{-0} [3] ± 2. x 10^{-4}	8.69×10^{-1} ± 4.8×10^{-3}
2.1.2	xLPR v2.0d	100,000	0	4.6 ± 0.2	1.3 ± 0.08	3.7 ± 0.07	2.0 ± 0.03	3.58×10^{-1} ± 1.5×10^{-3}	3.57×10^{-1} ± 1.5×10^{-3}	1.03×10^{-3} ± 1.0×10^{-4}
2.1.3	xLPR v2.0d	100,000	2×10^{-5} ± 1.4×10^{-5}	11.7 ± 5.6	10.8 ± 5.7	2.1 ± 0.4	1.4 ± 0.1	1.90×10^{-2} ± 4.3×10^{-4}	6.4×10^{-5} ± 2.5×10^{-5}	8.2×10^{-5} ± 2.9×10^{-5} [4]
2.1.4	xLPR v2.0d	100,000	0	2.5 ± 0.3	0.73 ± 0.14	4.8 ± 0.7	2.5 ± 0.5	3.40×10^{-2} ± 5.7×10^{-4}	3.12×10^{-2} ± 5.5×10^{-4}	1. x 10^{-4} ± 3.2×10^{-5}
2.1.5	xLPR v2.0d	100,000	0	4.5 ± 0.5	1 ± 0.00	4.5 ± 0.2	2.1 ± 0.2	1.20×10^{-2} ± 3.5×10^{-4}	8.4×10^{-3} ± 2.9×10^{-4}	1.8×10^{-5} ± 1.4×10^{-5}
3.1.0	xLPR v2.0d	100,000	0	NA[5]	NA[5]	NA[5]	NA[5]	3.3×10^{-4} ± 5.7×10^{-5}	0 ± 0	0 ± 0
3.1.1	xLPR v2.0d	5,000	0	78 ± 7	53 ± 4	10.1 ± 0.1	4.63 ± 0.04	1 ± 0	2.7×10^{-2} ± 2.3×10^{-3}	5.8×10^{-3} ± 1.1×10^{-3}
3.1.2	xLPR v2.0d	100,000	0	NA[5]	NA[5]	NA[5]	NA[5]	3.6×10^{-5} ± 1.9×10^{-5}	0 ± 0	0 ± 0
4.1.0	xLPR v2.0d	100,000	0	NA[5]	NA[5]	NA[5]	NA[5]	5.21×10^{-2} ± 7.0×10^{-4}	1.04×10^{-2} ± 3.2×10^{-4}	0 ± 0
4.1.1	xLPR v2.0d	5,000	1.6×10^{-2} ± 4.0×10^{-4}	NA[5]	NA[5]	NA[5]	NA[5]	1 ± 0	2.5×10^{-1} ± 6.1×10^{-3}	1.6×10^{-2} ± 1.8×10^{-3}

Case No.	xLPR Beta Version	Sample Size	Mean Occurrence of Leak Rate Jump at 80 EFPY	Mean LBB Time Lapse [1]		Mean LBB Ratio		Probability of 1st Crack at 80 EFPY	Probability of 1st Leak at 80 EFPY	Probability of Rupture at 80 EFPY [2]
				1 gpm Leak Rate Detection Capability (Months)	10 gpm Leak Rate Detection Capability (Months)	1 gpm Leak Rate Detection Capability	10 gpm Leak Rate Detection Capability			
4.1.2	xLPR v2.0d	100,000	$2.5 \times 10^{-4} \pm 5.0 \times 10^{-5}$	NA[5]	NA[5]	NA[5]	NA[5]	$1.3 \times 10^{-1} \pm 1.1 \times 10^{-3}$	$3.1 \times 10^{-3} \pm 5.6 \times 10^{-5}$	$2.1 \times 10^{-4} \pm 4.6 \times 10^{-5}$
4.1.3	xLPR v2.0d	100,000	$1.6 \times 10^{-3} \pm 1.3 \times 10^{-4}$	5.31 ± 0.25	5.21 ± 0.24	3.07 ± 0.05	2.82 ± 0.04	$1.38 \times 10^{-1} \pm 1.1 \times 10^{-3}$	$4.4 \times 10^{-3} \pm 2.1 \times 10^{-4}$	$3.3 \times 10^{-3} \pm 1.8 \times 10^{-4}$
4.1.4	xLPR v2.0d	100,000	$1.6 \times 10^{-3} \pm 1.3 \times 10^{-4}$	23.8 ± 3.2	23.7 ± 3.2	3.08 ± 0.12	288 ± 0.09	$9.8 \times 10^{-2} \pm 9.4 \times 10^{-4}$	$6.0 \times 10^{-2} \pm 7.5 \times 10^{-4}$	$5.4 \times 10^{-4} \pm 7.5 \times 10^{-5}$
5.1.0	xLPR v2.0d	100,000	$3.2 \times 10^{-4} \pm 5.7 \times 10^{-5}$	NA[5]	NA[5]	NA[5]	NA[5]	$6.62 \times 10^{-2} \pm 7.9 \times 10^{-4}$	$6.42 \times 10^{-2} \pm 7.8 \times 10^{-4}$	0 ± 0
5.1.1	xLPR v2.0d	5,000	0	54.3 ± 2.4	15.6 ± 0.6	3.4 ± 0.02	1.8 ± 0.01	1 ± 0	$9.95 \times 10^{-1} \pm 1.0 \times 10^{-3}$	$1.8 \times 10^{-2} \pm 2.0 \times 10^{-3}$
5.1.2	xLPR v2.0d	100,000	0	NA[5]	NA[5]	NA[5]	NA[5]	$1.06 \times 10^{-1} \pm 9.7 \times 10^{-4}$	$1.03 \times 10^{-1} \pm 9.6 \times 10^{-4}$	0 ± 0
5.2.0	xLPR v2.0d	100,000	0	NA[5]	NA[5]	NA[5]	NA[5]	$2.38 \times 10^{-2} \pm 4.8 \times 10^{-4}$	$1.57 \times 10^{-2} \pm 3.9 \times 10^{-4}$	0 ± 0
5.2.1	xLPR v2.0d	5,000	0	84 ± 5	32 ± 2.5	4.29 ± 0.03	1.97 ± 0.01	1 ± 0	$3.4 \times 10^{-1} \pm 6.7 \times 10^{-3}$	$1.00 \times 10^{-3} \pm 4.5 \times 10^{-4}$

Notes:

(1) All results beyond 12 EFPY excluded as they strongly influence the mean for the reasons explained in Section 3.2.1.2.3.
(2) Excludes the effects of leak rate detection and ISI.
(3) The probability is 0.9998, which was rounded up to 1.00×10^{-0} at two significant digits
(4) The probability of rupture is higher than the probability of first leak in Case 2.1.3 due to surface crack rupture.
(5) Indicates that the QoI could not be calculated (i.e., there were no ruptures in the simulation).

APPENDIX B
ANALYSIS INPUTS

B1 Case 1.1.6a

The objective of Case 1.1.6a was to assess the base likelihood of failure caused by PWSCC initiation and growth with without mechanical mitigation for Westinghouse 4-loop RVON and RVIN DMWs.

The random seeds used for the Case 1.1.6a analyses were as follow:

Simulation Description	Replicate Simulation No.	Epistemic Random Seed	Aleatory Random Seed
100,000-realization composite simulation using the epistemic (outer) loop	1	1515	13118
	2	1974	713705
	3	2002	1503
	4	2004	909
	5	2010	907
	6	3131	131521
	7	4512	1685
	8	5121	919
	9	41520	2025
	10	1415	23118

The other inputs were developed using the Case 1.1.6 input set from the prior study [2] as a template with the following modifications:

Global ID	Name	Value / Distribution Parameters	Units	Basis
N/A	Case Description	1.1.06a	-	Based on case description

Global ID	Name	Value / Distribution Parameters	Units	Basis
3002	Unmitigated H2 level	25 Constant	cc/kg	Bounds the operating experience of PWRs as reported in [48]

B2 Case 1.1.6b

The objective of Case 1.1.6b was to assess the base likelihood of failure with pre-existing flaws and subsequent PWSCC growth of circumferential and axial cracks without mechanical mitigation for Westinghouse 4-loop RVON and RVIN DMWs.

The random seeds used for the Case 1.1.6b analyses were as follow:

Simulation Description	Epistemic Random Seed	Aleatory Random Seed
5000-realization simulation using the epistemic (outer) loop	6128	369

The other inputs were developed using the Case 1.1.6a input set as a template with the following modifications:

Global ID	Name	Value / Distribution Parameters	Units	Basis
N/A	Case Description	1.1.06b	-	Based on case description
0501	Crack Initiation Type Choice	0	-	Based on case description
1209	Number of Flaws (Circ)	1 Constant	-	Considers the impact of one circumferential crack and one axial crack because the likelihood of multiple cracks is low enough to not affect the results as demonstrated in [2]
1210	Initial Flaw Full-Length (Circ) (*)	Lognormal (1, 4.3E-3, 2.226)	m	Based on PWSCC initial flaw sizes
1211	Multiplier Starting Full-Length (Circ)	1 Constant	-	Based on PWSCC initial flaw sizes
1212	Initial Flaw Depth (Circ) (*)	Lognormal (1, 1.5E-3, 1.419, min=5E-4, max=0.0663)	m	Based on PWSCC initial flaw sizes

Global ID	Name	Value / Distribution Parameters	Units	Basis
1213	Multiplier Starting Depth (Circ)	1 Constant	-	Based on PWSCC initial flaw sizes
1214	Number of Flaws (Axial)	1 Constant	-	Considers the impact of one circumferential crack and one axial crack because the likelihood of multiple cracks is low enough to not affect the results as demonstrated in [2]
1215	Initial Flaw Full-Length (Axial) (*)	Lognormal (1, 4.3E-3, 2.226)	m	Based on PWSCC initial flaw sizes
1216	Multiplier Starting Full-Length (Axial)	1 Constant	-	Based on PWSCC initial flaw sizes
1217	Initial Flaw Depth (Axial) (*)	Lognormal (1, 1.5E-3, 1.419, min=5E-4, max=0.0663)	m	Based on PWSCC initial flaw sizes
1218	Multiplier Starting Depth (Axial)	1 Constant	-	Based on PWSCC initial flaw sizes

B3 Case 1.1.6c

The objective of Case 1.1.6c was to assess the base likelihood of failure caused by PWSCC initiation and growth without mechanical mitigation for Westinghouse 4-loop RVON and RVIN DMWs when a 5-years in-service inspection schedule is considered.

The random seeds used for the Case 1.1.6c analyses were as follow:

Simulation Description	Replicate Simulation No.	Epistemic Random Seed	Aleatory Random Seed
100,000-realization composite simulation using the epistemic (outer) loop	1	1515	13118
	2	1974	713705
	3	2002	1503
	4	2004	909
	5	2010	907
	6	3131	131521
	7	4512	1685
	8	5121	919
	9	41520	2025
	10	1415	23118

The other inputs were developed using the Case 1.1.6 input set from the prior study [2] as a template with the following modifications:

Global ID	Name	Value / Distribution Parameters	Units	Basis
N/A	Case Description	1.1.06c	-	Based on case description
0811	Inspection Schedule Input Type	1		Inspection schedule set by frequency
0812	Pre-Mitigation Inspection Freq.	0.2	yr-1	Annual frequency set to one inspection every 5 years
0813	Post-Mitigation Inspection Freq.	0.2	yr-1	Not necessary, but set to the same value as Global ID 0812 for completeness

Global ID	Name	Value / Distribution Parameters	Units	Basis
3002	Unmitigated H2 level	25 Constant	cc/kg	Bounds the operating experience of PWRs as reported in [48]

B4 Case 2.1.0

The objective of Case 2.1.0 was to assess the base likelihood of failure caused by PWSCC initiation and growth without mechanical mitigation for Westinghouse pressurizer surge line nozzle DMWs. The effects of leak detection, ISI, and SSE were also assessed.

The random seeds used for the Case 2.1.0 analyses were as follow:

Simulation Description	Replicate Simulation No.	Epistemic Random Seed	Aleatory Random Seed
100,000-realization composite simulation using the epistemic (outer) loop	1	1515	13118
	2	1974	713705
	3	2002	1503
	4	2004	909
	5	2010	907
	6	3131	131521
	7	4512	1685
	8	5121	919
	9	41520	2025
	10	1415	23118

The other inputs were developed using the Case 3, Scenario 3, input set from the xLPR Inputs Group report [53] as a template with the following modifications:

Global ID	Name	Value / Distribution Parameters	Units	Basis
N/A	Case Description	2.1.00	-	Based on case description
0001	Plant Operation time	960	mon	Based on case description
0402	Period End Time (Op Period #1)	961	mon	Based on case description
0403	Input Type Choice (Op Period #1)	2	-	Based on case description

Global ID	Name	Value / Distribution Parameters	Units	Basis
0405	Period End Time (Op Period #2)	962	mon	Based on case description
0811	Inspection Schedule Input Type	1	-	Inspection schedule set by frequency
0812	Pre-Mitigation Inspection Freq	0.1	1/yr	Annual frequency set to one inspection every 10 years
0820	Number of cracks detected	1	-	Based on case description
0904	Max time between 2 check - single TWC - CC	1	mon	Based on case description
All uncertain variables, except Global ID 2528	Data Source	Epistemic	-	Outer loop preserves LHS structure
1001	Effective Full Power Years (EFPY)	80 Constant	yr	Based on case description
1101	Pipe Outer Diameter	0.3556 Constant	m	Typical value for Westinghouse four-loop pressurizer surge line
1102	Pipe Wall Thickness	0.028575 Constant	m	Minimum pipe wall thickness for Westinghouse four-loop pressurizer surge line

Global ID	Name	Value / Distribution Parameters	Units	Basis
1103	Weld Width	0.02648 Constant	m	Outside diameter weld width from Figure 1 of [75]
1104	Weld Material Thickness	0.028575 Constant	m	Set to same value as Global ID 1102
3002	Unmitigated H2 Level	25 Constant	cc/kg	Bounds the operating experience of PWRs as reported in [48]
3102	Operating Temperature	345 Constant	°C	Typical operating temperature for Westinghouse four-loop pressurizer surge line as reported in [76]
4001	Earthquake Probability	1E-3 Constant	1/yr	From Section E.3.1 of [60], the maximum earthquake probability is 1E-3
4002	Earthquake Δ Total Membrane	169.64 Constant	MPa	Maximum SSE load from Figure 2-6 of [60] is combined membrane and bending
4003	Earthquake Δ Inertial Bending	0 Constant	MPa	Maximum SSE load from Figure 2-6 of [60] is combined membrane and bending
4004	Earthquake Δ Anchor Bending	0 Constant	MPa	Maximum SSE load from Figure 2-6 of [60] is combined membrane and bending

Global ID	Name	Value / Distribution Parameters	Units	Basis
4005	Sigma_SSa	0 Constant	MPa	Based on case description
4006	Sigma_SSh	0 Constant	MPa	Based on case description
4101	Fx (Dead Weight)	0 Constant	kN	Set to 0 because all loads input as stresses instead of forces and moments
4102	Mx (Dead Weight)	0 Constant	kN-m	Set to 0 because all loads input as stresses instead of forces and moments
4103	My (Dead Weight)	0 Constant	kN-m	Set to 0 because all loads input as stresses instead of forces and moments
4104	Mz (Dead Weight)	0 Constant	kN-m	Set to 0 because all loads input as stresses instead of forces and moments
4105	Fx (Thermal Expansion)	0 Constant	kN	Set to 0 because all loads input as stresses instead of forces and moments
4106	Mx (Thermal Expansion)	0 Constant	kN-m	Set to 0 because all loads input as stresses instead of forces and moments
4107	My (Thermal Expansion)	0 Constant	kN-m	Set to 0 because all loads input as stresses instead of forces and moments

Global ID	Name	Value / Distribution Parameters	Units	Basis
4108	Mz (Thermal Expansion)	0 Constant	kN-m	Set to 0 because all loads input as stresses instead of forces and moments
4121	Membrane Stress (DW)	0 Constant	MPa	Stress from [60] is combined DW and thermal, so this input is set to 0, and Global ID 4123 contains the DW contribution
4122	Maximum Bending Stress (DW)	0 Constant	MPa	Stress from [60] is combined DW and thermal, so this input is set to 0, and Global ID 4124 contains the DW contribution
4123	Membrane Stress (Thermal)	5.06 Constant	MPa	Stress from [60] is combined DW and thermal; used the limiting thermal maximum across all plants represented in Figure 2-7, Plant C
4124	Bending Stress (Thermal)	100.32 Constant	MPa	Stress from [60] is combined DW and thermal; used the limiting thermal maximum across all plants represented in Figure 2-8, Plant I

Global ID	Name	Value / Distribution Parameters		Units	Basis
-	Hoop WRS Pre-Mitigation	Mean	Std. Dev.	MPa	Mean profile and standard deviation are based on 10 FEA results as reported in Figures 14 and 15 of [75]
		-32.21	76.7		
		16.12	76.7		
		51.74	76.7		
		61.55	76.7		
		76.59	76.7		
		90.81	76.7		
		110.18	76.7		
		87.32	76.7		
		78.81	76.7		
		68.77	76.7		
		44.21	76.7		
		-10.78	76.7		
		-61.59	76.7		
		-85.78	76.7		
		-91.10	76.7		
		-59.64	76.7		
		-14.89	76.7		
		30.41	76.7		
		79.04	76.7		
		112.83	76.7		
		147.84	76.7		
		172.87	76.7		
		192.41	76.7		
		171.25	76.7		
		145.10	76.7		
		128.88	76.7		

Global ID	Name	Value / Distribution Parameters	Units	Basis
-	Axial WRS Pre-Mitigation	Mean / Std. Dev. -176.05 / 57.9 -155.45 / 57.9 -135.68 / 57.9 -122.95 / 57.9 -108.40 / 57.9 -107.12 / 57.9 -102.24 / 57.9 -98.37 / 57.9 -105.16 / 57.9 -121.23 / 57.9 -152.48 / 57.9 -188.90 / 57.9 -208.65 / 57.9 -205.37 / 57.9 -173.00 / 57.9 -127.62 / 57.9 -61.80 / 57.9 13.09 / 57.9 87.12 / 57.9 160.00 / 57.9 228.12 / 57.9 296.98 / 57.9 352.88 / 57.9 351.06 / 57.9 339.51 / 57.9 335.30 / 57.9	MPa	Mean profile and standard deviation are based on 10 FEA results as reported in Figures 14 and 15 of [75]
5004	Lower bound POD, POD_0	0	-	Even though it is not used, the default 0.999 value would lead to 99.9 percent probability of detection for a crack of zero depth

Global ID	Name	Value / Distribution Parameters	Units	Basis
5101-5110	Pre-Mitigation Inspection Properties	beta_0 (circ): Normal (2.71, 0.21) beta_1 (circ): Normal (0.31, 0.45) beta_0 (axial): Normal (-0.8, 0.38) beta_1 (axial): Normal (8.3, 1.45) a (circ): Normal (0.034, 0.006) b (circ): Normal (0.955, 0.013) a (axial): Normal (0.041, 0.011) b (axial): Normal (0.88, 0.029) Sigma_depth (circ): 0.072 Sigma_depth (axial): 0.078	-	Based on [50]
Correlation 5101-5102	Intercept, B0 (circ) Intercept, B1 (circ)	-0.86	-	Based on [50]
Correlation 5103-5104	Intercept, B0 (axial) Intercept, B1 (axial)	-0.93	-	Based on [50]
Correlation 5105-5106	a (circ) b (circ)	-0.867	-	Based on [50]
Correlation 5107-5108	a (axial) b (axial)	-0.87	-	Based on [50]

B5 Case 2.1.1

The objective of Case 2.1.1 was to assess the base likelihood of failure with pre-existing flaws and subsequent PWSCC growth of circumferential and axial cracks without mechanical mitigation for Westinghouse pressurizer surge line nozzle DMWs. The effects of leak detection, ISI, and SSE were also assessed.

The random seeds used for the Case 2.1.1 analyses were as follow:

Simulation Description	Epistemic Random Seed	Aleatory Random Seed
5000-realization simulation using the epistemic (outer) loop	6128	369

The other inputs were developed using the Case 2.1.0 input set as a template with the following modifications:

Global ID	Name	Value / Distribution Parameters	Units	Basis
N/A	Case Description	2.1.01	-	Based on case description
0501	Crack Initiation Type Choice	0	-	Based on case description
1209	Number of Flaws (Circ)	1 Constant	-	Considers the impact of one circumferential crack and one axial crack because the likelihood of multiple cracks is low enough to not affect the results as demonstrated in [2]
1210	Initial Flaw Full-Length (Circ) (*)	Lognormal (1, 4.3E-3, 2.226)	m	Based on PWSCC initial flaw sizes
1211	Multiplier Starting Full-Length (Circ)	1 Constant	-	Based on PWSCC initial flaw sizes

Global ID	Name	Value / Distribution Parameters	Units	Basis
1212	Initial Flaw Depth (Circ) (*)	Lognormal (1, 1.5E-3, 1.419, min=5E-4, max=0.0663)	m	Based on PWSCC initial flaw sizes
1213	Multiplier Starting Depth (Circ)	1 Constant	-	Based on PWSCC initial flaw sizes
1214	Number of Flaws (Axial)	1 Constant	-	Considers the impact of one circumferential crack and one axial crack because the likelihood of multiple cracks is low enough to not affect the results as demonstrated in [2]
1215	Initial Flaw Full-Length (Axial) (*)	Lognormal (1, 4.3E-3, 2.226)	m	Based on PWSCC initial flaw sizes
1216	Multiplier Starting Full-Length (Axial)	1 Constant	-	Based on PWSCC initial flaw sizes
1217	Initial Flaw Depth (Axial) (*)	Lognormal (1, 1.5E-3, 1.419, min=5E-4, max=0.0663)	m	Based on PWSCC initial flaw sizes
1218	Multiplier Starting Depth (Axial)	1 Constant	-	Based on PWSCC initial flaw sizes

B6 Case 2.1.2

Case 2.1.2 was a sensitivity study of Case 2.1.0 considering a more severe WRS profile for Westinghouse pressurizer surge line nozzle DMWs.

The random seeds used for the Case 2.1.2 analyses were as follow:

Simulation Description	Replicate Simulation No.	Epistemic Random Seed	Aleatory Random Seed
100,000-realization composite simulation using the epistemic (outer) loop	1	1515	13118
	2	1974	713705
	3	2002	1503
	4	2004	909
	5	2010	907
	6	3131	131521
	7	4512	1685
	8	5121	919
	9	41520	2025
	10	1415	23118

The other inputs were developed using the Case 2.1.0 input set as a template with the following modifications:

Global ID	Name	Value / Distribution Parameters	Units	Basis
N/A	Case Description	2.1.02	-	Based on case description

Global ID	Name	Value / Distribution Parameters		Units	Basis
-	Hoop WRS Pre-Mitigation	Mean	Std. Dev.	MPa	More severe hoop WRS profile estimated from FEA results for the weld butter as discussed in Section C2.2
		208.41	76.7		
		292.19	76.7		
		338.16	76.7		
		358.36	76.7		
		330.63	76.7		
		369.53	76.7		
		394.38	76.7		
		377.63	76.7		
		306.73	76.7		
		138.90	76.7		
		11.55	76.7		
		-82.04	76.7		
		-96.97	76.7		
		-75.07	76.7		
		-37.10	76.7		
		3.23	76.7		
		72.29	76.7		
		140.58	76.7		
		214.52	76.7		
		308.49	76.7		
		346.74	76.7		
		428.52	76.7		
		417.46	76.7		
		446.92	76.7		
		409.06	76.7		
		382.11	76.7		

Global ID	Name	Value / Distribution Parameters		Units	Basis
N/A	Axial WRS Pre-Mitigation	Mean	Std. Dev.	MPa	More severe axial WRS profile estimated from FEA results for the weld butter as discussed in Section C2.2
		-118.00	57.9		
		-60.80	57.9		
		-25.21	57.9		
		-21.12	57.9		
		-20.85	57.9		
		-18.21	57.9		
		-17.66	57.9		
		-107.85	57.9		
		-226.94	57.9		
		-323.93	57.9		
		-369.72	57.9		
		-331.22	57.9		
		-247.03	57.9		
		-249.79	57.9		
		-217.62	57.9		
		-160.65	57.9		
		-66.23	57.9		
		-42.58	57.9		
		33.29	57.9		
		112.75	57.9		
		196.05	57.9		
		303.46	57.9		
		371.40	57.9		
		479.99	57.9		
		510.97	57.9		
		529.34	57.9		

B7 Case 2.1.3

Case 2.1.3 was a sensitivity study of Case 2.1.0 considering overlay mitigation for Westinghouse pressurizer surge line nozzle DMWs.

The random seeds used for the Case 2.1.3 analyses were as follow:

Simulation Description	Replicate Simulation No.	Epistemic Random Seed	Aleatory Random Seed
100,000-realization composite simulation using the epistemic (outer) loop	1	1515	13118
	2	1974	713705
	3	2002	1503
	4	2004	909
	5	2010	907
	6	3131	131521
	7	4512	1685
	8	5121	919
	9	41520	2025
	10	1415	23118

The other inputs were developed using Case 3, Scenario 9, from the xLPR Inputs Group report [53] as a template with the following modifications:

Global ID	Name	Value / Distribution Parameters	Units	Basis
N/A	Case Description	2.1.03	-	Based on case description
0301	Mitigation Type Choice	1	-	Based on case description
0305	Stress Mitigation Choice	2	-	Based on case description

Global ID	Name	Value / Distribution Parameters	Units	Basis
0306	Stress Mitigation Time	300	mon	Average overlay mitigation application for the set of pressurizer surge line nozzles represented by bin
0803	Post-Overlay Trunc Meas Error	1	-	Consistent with pre-mitigation approach
0804	Post-Overlay Eval Length Effects	0	-	Default value
0805	Full Structural WOL	0	-	Minimum overlay thickness selected is consistent with an optimized weld overlay
0813	Post-Mitigation Inspection Freq.	0.1	1/yr	Annual frequency set to one inspection every 10 years
0815	Post-Overlay Ligament Flag	0	-	Default value
1105	Weld Overlay Thickness	0.0125 Constant	m	Smallest overlay thickness for Waterford, Unit 3 from [77], which bounds the welds represented by bin

Global ID	Name	Value / Distribution Parameters	Units	Basis
2701	Yield Strength, Sigy	Lognormal (317, 54.99, min=209, max=466)	MPa	Alloy 52/152 material property from xLPR Inputs Group report [53]
2702	Ultimate Strength, Sigu	Lognormal (542, 26.81, min=483, max=608)	MPa	Alloy 52/152 material property from xLPR Inputs Group report [53]
2705	Elastic Modulus, E	Normal (196800, 29520, min=167280, max=226320)	MPa	Alloy 52/152 material property from xLPR Inputs Group report [53]
2706	Material Init J-Resistance, Jic	Normal (524.3, 182, min=225.1, max=947.4)	N/mm	Alloy 52/152 material property from xLPR Inputs Group report [53]
2707	Material Init J-Resist Coef, C	Normal (586, 76.2, min=460.9, max=763.6)	N/mm	Alloy 52/152 material property from xLPR Inputs Group report [53]
2708	Material Init J-Resist Exponent, m	Normal (0.661, 0.074, min=0.2, max=1)	-	Alloy 52/152 material property from xLPR Inputs Group report [53]

Global ID	Name	Value / Distribution Parameters	Units	Basis
2743	Multiplier proport. Const. A (DM1)	Lognormal (0.0417, 17.99)	-	Based on minimum FOI of 24 from Pacific Northwest National Laboratories test data on Alloy 52/152 crack initiation and using a similar method as in [78]. The Alloy 82/182 distribution median from the xLPR Inputs Group report [53] was divided by this FOI. Note that this input was is not used in the simulation because cracks initiate on the inside diameter, not on the outside diameter where the overlay is applied. It was included for completeness.

Global ID	Name	Value / Distribution Parameters	Units	Basis
2788	Power Law Constant, Alpha	2.01E-12 Constant	(m/s)(MPa-m1/2)^(-beta)	Set equal to the Alloy 82/182 power law constant since the FOI for Alloy 52/152 is applied in Global ID 2796
2789	Power Law Exponent, Beta	1.6 Constant	-	Alloy 52/152 material property from xLPR Inputs Group report [53]
2790	SIF Threshold, Kth	0 Constant	MPa-$m^{1/2}$	Alloy 52/152 material property from xLPR Inputs Group report [53]
2791	Activation Energy, Qg	Normal (130, 20)	kJ/mol	Alloy 52/152 material property from xLPR Inputs Group report [53]
2792	Comp-to-Comp Variab Factor, fcomp	Lognormal (1, 1.803, min=0.313, max=2.64)	-	Alloy 52/152 material property from xLPR Inputs Group report [53]
2793	Within-Comp Variab Factor, fflaw	Lognormal (1, 1.617, min=0.309, max=3.24)	-	Alloy 52/152 material property from xLPR Inputs Group report [53]

Global ID	Name	Value / Distribution Parameters	Units	Basis
2794	Peak-to-Valley ECP Ratio - 1, P-1	1 Constant	-	Alloy 52/152 material property from xLPR Inputs Group report [53]
2795	Charact Width of Peak vs ECP, c	1 Constant	mV	Alloy 52/152 material property from xLPR Inputs Group report [53]
2796	Factor of Improvement, IF	324 Constant	-	Represents 75th percentile FOI from [52]
2797	Reference Temperature	325 Constant	Cdeg	Alloy 52/152 material property from xLPR Inputs Group report [53]
Correlation 2701-2702	Yield Strength, Sigy Ultimate Strength, Sigu	0.709	-	Alloy 52/152 material property from xLPR Inputs Group report [53]
4351	Hoop WRS Post-Mitigation	Epistemic	-	Uncertainty applied to the post-mitigation WRS profile
4353	Axial WRS Post-Mitigation	Epistemic	-	Uncertainty applied to the post-mitigation WRS profile

Global ID	Name	Value / Distribution Parameters		Units	Basis
N/A	Hoop WRS Post-mitigation	Mean	Std. Dev.	MPa	Overlay mitigation rules from [47] applied to the unmitigated mean WRS profile. Standard deviation set equal to the unmitigated WRS profile standard deviation.
		-232.21	76.7		
		-175.88	76.7		
		-132.26	76.7		
		-114.45	76.7		
		-91.41	76.7		
		-69.19	76.7		
		-41.82	76.7		
		-56.68	76.7		
		-57.19	76.7		
		-59.23	76.7		
		-75.79	76.7		
		-122.78	76.7		
		-165.59	76.7		
		-181.78	76.7		
		-179.1	76.7		
		-139.64	76.7		
		-86.89	76.7		
		-33.59	76.7		
		23.04	76.7		
		64.83	76.7		
		107.84	76.7		
		140.867	76.7		
		168.41	76.7		
		155.25	76.7		
		137.1	76.7		
		128.88	76.7		

Global ID	Name	Value / Distribution Parameters	Units	Basis
N/A	Axial WRS Post-mitigation	Mean / Std. Dev. -71.85 / 57.9 -110.84 / 57.9 -152.67 / 57.9 -189.00 / 57.9 -238.47 / 57.9 -274.20 / 57.9 -207.02 / 57.9 -154.39 / 57.9 -122.41 / 57.9 -82.01 / 57.9 -15.66 / 57.9 24.11 / 57.9 32.11 / 57.9 22.69 / 57.9 69.42 / 57.9 143.87 / 57.9 202.51 / 57.9 203.98 / 57.9 215.93 / 57.9 213.70 / 57.9 164.56 / 57.9 119.35 / 57.9 78.72 / 57.9 32.64 / 57.9 -25.57 / 57.9 -64.50 / 57.9	MPa	Overlay mitigation rules from [47] applied to the unmitigated mean WRS profile. Standard deviation set equal to the unmitigated WRS profile standard deviation.
5201	Depth repair threshold x_TH (during)	0 Constant	-	Set to pre-mitigation value because no applicable values for overlays
5202	Depth repair threshold x_TH (post)	0 Constant	-	Set to pre-mitigation value because no applicable values for overlays

Global ID	Name	Value / Distribution Parameters	Units	Basis
5301-5312	Post-Overlay Inspection Properties	beta_0 (circ): Normal (2.71, 0.21) beta_1 (circ): Normal (0.31, 0.45) beta_0 (axial): Normal (-0.8, 0.38) beta_1 (axial): Normal (8.3, 1.45) a (circ): Normal (0.034, 0.006) b (circ): Normal (0.955, 0.013) a (axial): Normal (0.041, 0.011) b (axial): Normal (0.88, 0.029) Sigma_depth (circ): 0.072 Sigma_depth (axial): 0.078 x_small: 0.1 x_LB: 0	-	Set equal to the pre-mitigation inspection property values because no applicable values for overlays
Correlation 5301-5302	Intercept, B0 (circ) Slope, B1 (circ)	-0.86	-	Set equal to the pre-mitigation inspection property values because no applicable values for overlays
Correlation 5301-5302	Intercept, B0 (axial) Slope, B1 (axial)	-0.93	-	Set equal to the pre-mitigation inspection property values because no applicable values for overlays
Correlation 5301-5302	a (circ) b (circ)	-0.867	-	Set equal to the pre-mitigation inspection property values because no applicable values for overlays

Global ID	Name	Value / Distribution Parameters	Units	Basis
Correlation 5301-5302	a (axial) b (axial)	-0.87	-	Set equal to the pre-mitigation inspection property values because no applicable values for overlays

B8 Case 2.1.4

The objective of Case 2.1.4 was to assess the base likelihood of failure caused by fatigue initiation and growth without mechanical mitigation for Westinghouse pressurizer surge line nozzle DMWs.

The random seeds used for the Case 2.1.4 analyses were as follow:

Simulation Description	Replicate Simulation No.	Epistemic Random Seed	Aleatory Random Seed
100,000-realization composite simulation using the epistemic (outer) loop	1	1515	13118
	2	1974	713705
	3	2002	1503
	4	2004	909
	5	2010	907
	6	3131	131521
	7	4512	1685
	8	5121	919
	9	41520	2025
	10	1415	23118

The other inputs were developed using Case 2.1.0 input set as a template with the following modifications:

Global ID	Name	Value / Distribution Parameters	Units	Basis
-	Case Description	2.1.04		Based on case description
0411	Transient Type Selection (Load 1)	2	-	Option to consider thermal stratification with heatup transient
0411.2	Transient Type Selection (Load 2)	2	-	Option to consider thermal stratification with cooldown transient

Global ID	Name	Value / Distribution Parameters	Units	Basis
0411.3	Transient Type Selection (Load 3)	1	-	Option to consider plant loading transient without thermal stratification
0411.4	Transient Type Selection (Load 4)	1	-	Option to consider plant unloading transient without thermal stratification
0411.5	Transient Type Selection (Load 5)	1	-	Option to consider step load increase transient without thermal stratification
0411.6	Transient Type Selection (Load 6)	1	-	Option to consider step load decrease transient without thermal stratification
0411.7	Transient Type Selection (Load 7)	1	-	Option to consider loss of load transient without thermal stratification
0411.8	Transient Type Selection (Load 8)	1	-	Option to consider partial loss of flow transient without thermal stratification
0411.9	Transient Type Selection (Load 9)	1	-	Option to consider reactor trip transient without thermal stratification

Global ID	Name	Value / Distribution Parameters	Units	Basis
0411.10	Transient Type Selection (Load 10)	3	-	Option to consider operating basis earthquake transient
0501	Crack Initiation Type Choice	3	-	Option to consider fatigue initiation consistent with case description
0601	Crack Growth Type Choice	1	-	Option to consider fatigue growth consistent with case description
1201	Fatigue Initial Flaw Full-Length (*)	Lognormal (0, 8.61, 4.849)	mm	Based on Case 3, Scenario 10, input set from [50]
1202	Multiplier Fatigue Initial Full-Length	1 Constant	-	Based on Case 3, Scenario 10, input set from [50]
1203	Fatigue Initial Flaw Depth (*)	Lognormal (0, 3, 0.05)	mm	Based on Case 3, Scenario 10, input set from [50]
1204	Multiplier Fatigue Initial Depth	1 Constant	-	Based on Case 3, Scenario 10, input set from [50]
3001	Flow Rate	0.18 Constant	m/s	From [55]

Global ID	Name	Value / Distribution Parameters	Units	Basis
3103	Dissolved Oxygen	40 Constant	ppm	Based on Case 3, Scenario 10, input set from [50]
9001	Fatigue Growth CKTH	Lognormal (1, 1, 1.149, 0, 4.559)	-	Based on Case 3, Scenario 10, input set from [50]
Correlation 2525-2528	Strain Threshold, STH Co	1	-	Value imposed by the xLPR code
Transient Definitions Tab	Points, Times, Delta Ts, and Delta Ps for Transient 1	1, 0, -287.78, -1.34E7 2, 20880, -32.24, 0	-, s, Cdeg, Pa	Plant heatup transient from Table 4-2 of [54]
Transient Definitions Tab	Points, Times, Delta Ts, and Delta Ps for Transient 2	1, 0, 0, 0 2, 20880, -323.89, -1.54E7	-, s, Cdeg, Pa	Plant cooldown transient from Table 4-2 of [54]
Transient Definitions Tab	Points, Times, Delta Ts, and Delta Ps for Transient 3	1, 0, 0, 0 2, 50, 0, 0 3, 50.1, 0, 4.14E5 4, 1120, 0, 4.14E5 5, 1120.1, 0, 4.14E5	-, s, Cdeg, Pa	Plant loading transient from Table 4-2 of [54]
Transient Definitions Tab	Points, Times, Delta Ts, and Delta Ps for Transient 4	1, 0, 0, -6.89E4 2, 0.1, 0, -6.89E4 3, 30, 0, 0 4, 30.1, 0, 0 5, 200, 0, -1.86E6 6, 1100, 0, -3.45E5 7, 1100.1, 0, -3.45E5 8, 1200, 0, 4.83E5	-, s, Cdeg, Pa	Plant unloading transient from Table 4-2 of [54]

Global ID	Name	Value / Distribution Parameters	Units	Basis
Transient Definitions Tab	Points, Times, Delta Ts, and Delta Ps for Transient 5	1, 0, 0, 0 2, 10, 0, 0 3, 10.1, 0, 0 4, 140, 0, 6.21E5 5, 140.1, 0, 6.21E5 6, 350, 0, 0 7, 350.1, 0, 0	-, s, Cdeg, Pa	Plant step load increase transient from Table 4-2 of [54]
Transient Definitions Tab	Points, Times, Delta Ts, and Delta Ps for Transient 6	1, 0, 0, 6.89E4 2, 0.1, 0, 1.93E5 3, 10, 0, 2E5 4, 10.1, 0, 2E5 5, 150, 0, 2.07E5 6, 150.1, 0, -4.83E5 7, 350, 0, -4.83E5 8, 350.1, 0, -4.83E5	-, s, Cdeg, Pa	Plant step load decrease transient from Table 4-2 of [54]
Transient Definitions Tab	Points, Times, Delta Ts, and Delta Ps for Transient 7	1, 0, 0, 0 2, 2, 0, 0 3, 2.1, 0, 0 4, 13, 0, 0, 1.03E6 5, 13.1, 0, 1.03E6 6, 60, -20.56, -3.38E6 7, 120, -20.56, -3.65E6 8, 120.1, -20.56, -3.65E6	-, s, Cdeg, Pa	Plant loss of load transient from Table 4-2 of [54]
Transient Definitions Tab	Points, Times, Delta Ts, and Delta Ps for Transient 8	1, 0, 0, 0 2, 2, 0, 0 3, 2.1, 0, 0 4, 13, 0, 0, 1.03E6 5, 13.1, 0, 1.03E6 6, 60, -20.56, -3.38E6 7, 120, -20.56, -3.65E6 8, 120.1, -20.56, -3.65E6	-, s, Cdeg, Pa	Plant partial loss of flow transient from Table 4-2 of [54]

Global ID	Name	Value / Distribution Parameters	Units	Basis
Transient Definitions Tab	Points, Times, Delta Ts, and Delta Ps for Transient 9	1, 0, 0, 0 2, 2, 0, 0 3, 2.1, 0, 0 4, 13, 0, 0, 1.03E6 5, 13.1, 0, 1.03E6 6, 60, -20.56, -3.38E6 7, 120, -20.56, -3.65E6 8, 120.1, -20.56, -3.65E6	-, s, Cdeg, Pa	Plant reactor trip transient from Table 4-2 of [54]
Type 2 Transient Inputs on TIFFANY Inputs Worksheet, Transient 1	+/- Membrane Stress, +/- Bending Stress, Start Month, End Month, Front-Back Loading, Frequency, # of Cycles per Event	2.08, 73.73, 0, 960, 0.5, 8.33, 1	MPa, MPa, mon, mon, -, 1/yr, -	Heatup transient loading from Table 4 of [55], and frequency from Table 4-2 of [54]
Type 2 Transient Inputs on TIFFANY Inputs Worksheet, Transient 2	+/- Membrane Stress, +/- Bending Stress, Start Month, End Month, Front-Back Loading, Frequency, # of Cycles per Event	2.08, 73.73, 0, 960, 0.5, 8.33, 1	Mpa, MPa, mon, mon, -, 1/yr, -	Cooldown transient loading from Table 4 of [55], and frequency from Table 4-2 of [54]
Type 1 Transient Inputs on TIFFANY Inputs Worksheet, Transient 3	Start Month, End Month, Front-Back Loading, Frequency, # of Cycles per Event	0, 960, 0.5, 250, 1	mon, mon, -, 1/yr, -	Plant loading transient frequency from Table 4-2 of [54]

Global ID	Name	Value / Distribution Parameters	Units	Basis
Type 1 Transient Inputs on TIFFANY Inputs Worksheet, Transient 4	Start Month, End Month, Front-Back Loading, Frequency, # of Cycles per Event	0, 960, 0.5, 250, 1	mon, mon, -, 1/yr, -	Plant unloading transient frequency from Table 4-2 of [54]
Type 1 Transient Inputs on TIFFANY Inputs Worksheet, Transient 5	Start Month, End Month, Front-Back Loading, Frequency, # of Cycles per Event	0, 960, 0.5, 33.33, 1	mon, mon, -, 1/yr, -	Step load increase transient frequency from Table 4-2 of [54]
Type 1 Transient Inputs on TIFFANY Inputs Worksheet, Transient 6	Start Month, End Month, Front-Back Loading, Frequency, # of Cycles per Event	0, 960, 0.5, 33.33, 1	mon, mon, -, 1/yr, -	Step load decrease transient frequency from Table 4-2 of [54]
Type 1 Transient Inputs on TIFFANY Inputs Worksheet, Transient 7	Start Month, End Month, Front-Back Loading, Frequency, # of Cycles per Event	0, 960, 0.5, 1.33, 1	mon, mon, -, 1/yr, -	Loss of load transient frequency from Table 4-2 of [54]
Type 1 Transient Inputs on TIFFANY Inputs Worksheet, Transient 8	Start Month, End Month, Front-Back Loading, Frequency, # of Cycles per Event	0, 960, 0.5, 1.33, 1	mon, mon, -, 1/yr, -	Partial loss of flow transient frequency from Table 4-2 of [54]

Global ID	Name	Value / Distribution Parameters	Units	Basis
Type 1 Transient Inputs on TIFFANY Inputs Worksheet, Transient 9	Start Month, End Month, Front-Back Loading, Frequency, # of Cycles per Event	0, 960, 0.5, 10.33, 1	mon, mon, -, 1/yr, -	Reactor trip transient frequency from Table 4-2 of [54]
Type 3 Transient Inputs on TIFFANY Inputs Worksheet, Transient 10	+/- Membrane Stress, +/- Bending Stress, Start Month, End Month, Front-Back Loading, Frequency, # of Cycles per Event, Rise Time	4.52, 60.61, 0, 960, 0.5, 0.1, 10, 1	Mpa, MPa, mon, mon, -, 1/yr, - , s	Loading from Table 4 of [55]; frequency, # cycles, and rise time based on Case 3, Scenario 10, input set from [50]
Uncertainty on TIFFANY Inputs Worksheet	Transients 1 through 10	Epistemic Lognormal (1, 0.5, 1.4142, 0.25, 1)	-	Based on Case 3, Scenario 10, input set from [50]

B9 Case 2.1.5

Case 2.1.5 was a sensitivity study of Case 2.1.0 considering MSIP® mitigation for Westinghouse pressurizer surge line nozzle DMWs.

The random seeds used for the Case 2.1.5 analyses were as follow:

Simulation Description	Replicate Simulation No.	Epistemic Random Seed	Aleatory Random Seed
100,000-realization composite simulation using the epistemic (outer) loop	1	1515	13118
	2	1974	713705
	3	2002	1503
	4	2004	909
	5	2010	907
	6	3131	131521
	7	4512	1685
	8	5121	919
	9	41520	2025
	10	1415	23118

The other inputs were developed using Case 2.1.0 input set as a template with the following modifications:

Global ID	Name	Value / Distribution Parameters	Units	Basis
-	Case Description	2.1.05		Based on case description
0301	Mitigation Type Choice	1	-	Based on case description
0305	Stress Mitigation Choice	1	-	Based on case description

Global ID	Name	Value / Distribution Parameters	Units	Basis
0306	Stress Mitigation Time	144	mon	Equivalent to 12 years, which is the latest time of MSIP® application for the welds represented by bin
0806	Post-MSIP® Trunc Meas Error	1	-	Based on case description
0807	Post-MSIP® Eval Length Effects	0	-	Default value
0813	Post-Mitigation Inspection Freq	0.1	1/yr	Annual frequency set to one inspection every 10 years
0816	Post-MSIP® Ligament Flag	0	-	Default value
4351	Hoop WRS post-mitigation	Epistemic	MPa	Uncertainty applied to the post-mitigation WRS profile
4353	Axial WRS post-mitigation	Epistemic	MPa	Uncertainty applied to the post-mitigation WRS profile
5201	Depth repair threshold, x_TH (during)	0 Constant	-	Set equal to the pre-mitigation inspection property values because no applicable values for MSIP®

Global ID	Name	Value / Distribution Parameters	Units	Basis
5202	Depth repair threshold, x_TH (post)	0 Constant	-	Set equal to the pre-mitigation inspection property values because no applicable values for MSIP®
5401-5412	Post-MSIP® Inspection Properties	beta_0 (circ): Normal (2.71, 0.21) beta_1 (circ): Normal (0.31, 0.45) beta_0 (axial): Normal (-0.8, 0.38) beta_1 (axial): Normal (8.3, 1.45) a (circ): Normal (0.034, 0.006) b (circ): Normal (0.955, 0.013) a (axial): Normal (0.041, 0.011) b (axial): Normal (0.88, 0.029) Sigma_depth (circ): 0.072 Sigma_depth (axial): 0.078	-	Set equal to the pre-mitigation inspection property values because no applicable values for MSIP®
Correlation 5401-5402	Intercept, B0 (circ) Slope, B1 (circ)	-0.86	-	Set equal to the pre-mitigation inspection property values because no applicable values for MSIP®
Correlation 5403-5404	Intercept, B0 (axial) Slope, B1 (axial)	-0.93	-	Set equal to the pre-mitigation inspection property values because no applicable values for MSIP®
Correlation 5405-5406	a (circ) b (circ)	-0.867	-	Set equal to the pre-mitigation inspection property values because no applicable values for MSIP®

Global ID	Name	Value / Distribution Parameters	Units	Basis
Correlation 5407-5408	a (axial) b (axial)	-0.87	-	Set equal to the pre-mitigation inspection property values because no applicable values for MSIP®
N/A	Post-Mitigation Hoop WRS	Mean / Std. Dev. -284.704 / 76.7 -231.14 / 76.7 -190.27 / 76.7 -175.22 / 76.7 -154.94 / 76.7 -135.48 / 76.7 -110.86 / 76.7 -128.48 / 76.7 -131.74 / 76.7 -136.54 / 76.7 -155.86 / 76.7 -205.61 / 76.7 -251.17 / 76.7 -270.11 / 76.7 -270.19 / 76.7 -233.49 / 76.7 -183.50 / 76.7 -132.96 / 76.7 -79.09 / 76.7 -40.05 / 76.7 0.20 / 76.7 30.48 / 76.7 55.26 / 76.7 39.35 / 76.7 18.44 / 76.7 7.46 / 76.7	MPa	MSIP® mitigation rules from [47] applied to the unmitigated mean WRS profile. Standard deviation set equal to the unmitigated WRS profile standard deviation.

Global ID	Name	Value / Distribution Parameters		Units	Basis
N/A	Post-Mitigation Axial WRS	Mean	Std. Dev.	MPa	MSIP® mitigation rules from [47] applied to the unmitigated mean WRS profile. Standard deviation set equal to the unmitigated WRS profile standard deviation.
		-294.48	57.9		
		-269.15	57.9		
		-244.64	57.9		
		-227.18	57.9		
		-207.89	57.9		
		-201.87	57.9		
		-182.16	57.9		
		-163.81	57.9		
		-156.48	57.9		
		-158.81	57.9		
		-176.67	57.9		
		-200.07	57.9		
		-207.16	57.9		
		-191.58	57.9		
		-147.28	57.9		
		-90.34	57.9		
		-13.31	57.9		
		72.42	57.9		
		156.94	57.9		
		239.93	57.9		
		313.26	57.9		
		385.70	57.9		
		445.19	57.9		
		446.96	57.9		
		439.00	57.9		
		438.37	57.9		

B10 Case 3.1.0

The objective of Case 3.1.0 was to assess the base likelihood of failure caused by PWSCC initiation and growth without mechanical mitigation for CE and B&W RCP nozzle DMWs. The effects of leak detection, ISI, and SSE were also assessed.

The random seeds used for the Case 3.1.0 analyses were as follow:

Simulation Description	Replicate Simulation No.	Epistemic Random Seed	Aleatory Random Seed
100,000-realization composite simulation using the epistemic (outer) loop	1	1515	13118
	2	1974	713705
	3	2002	1503
	4	2004	909
	5	2010	907
	6	3131	131521
	7	4512	1685
	8	5121	919
	9	41520	2025
	10	1415	23118

The other inputs were developed using the Case 2, Scenario 3, input set from the xLPR Inputs Group report [53] as a template with the following modifications:

Global ID	Name	Value / Distribution Parameters	Units	Basis
N/A	Case Description	3.1.00	-	Based on case description
0001	Plant Operation Time	960	mon	Based on case description
0402	Period End Time (Op Period #1)	961	mon	Based on case description
0403	Input Type Choice (Op Period #1)	2	-	Based on case description

Global ID	Name	Value / Distribution Parameters	Units	Basis
0405	Period End Time (Op Period #2)	962	mon	Based on case description
0808-0808.10	Inspection Month	N/A	mon	Inspection defined as an annual frequency
0811	Inspection schedule input type	1	-	Inspection defined as an annual frequency
0812	Pre-mitigation inspection freq	0.1	1/yr	Annual frequency set to one inspection every 10 years
0820	Number of cracks detected	1	-	Based on case description
0904	Max time between 2 check - single TWC - CC	1	mon	Based on case description
All uncertain variables, except Global ID 2528	Data Source	Epistemic	-	Outer loop preserves LHS structure
1001	Effective Full Power Years (EFPY)	80 Constant	yr	Based on case description
1101	Pipe Outer Diameter	0.8509 Constant	m	B&W geometry from Appendix E of [50]; Section 3.1, Table 4-1, of [79]; and Table 2.2 of [7]
1102 1104	Pipe Wall Thickness Weld Material Thickness	0.06985 Constant	m	B&W geometry from Appendix E of [50]; Section 3.1, Table 4-1, of [79]; and Table 2.2 of [7]
1103	Weld Width	0.01905 Constant	m	B&W geometry from Appendix E of [50]

Global ID	Name	Value / Distribution Parameters	Units	Basis
3002	Unmitigated H2 Level	25	cc/kg	Bounds the operating experience of PWRs as reported in [48]
3101	Operating Pressure	15.51 Constant	MPa	Operating pressure for CE plants from [7], which is higher than 14.82 MPa operating pressure for B&W plants from [6]
3102	Operating Temperature	293 Constant	°C	Maximum temperature reported for B&W plants in Appendix G of [50]
4001	Earthquake Probability	0.001 Constant	1/yr	Same value as used for analyses of other cases in this study (e.g., Case 2.1.0)
4002	Earthquake Δ Total Membrane	0.13 Constant	MPa	Appendix F of [50]
4003	Earthquake Δ Inertial Bending	0 Constant	MPa	All bending stresses captured in Global ID 4004
4004	Earthquake Δ Anchor Bending	44.35 Constant	MPa	Appendix F of [50]
4005	Sigma_SSa	0 Constant	MPa	Based on case description
4006	Sigma_SSh	0 Constant	MPa	Based on case description
4101	Fx (Dead Weight)	0 Constant	kN	Set to 0 because all loads input as stresses instead of forces and moments
4102	Mx (Dead Weight)	0 Constant	kN-m	Set to 0 because all loads input as stresses instead of forces and moments
4103	My (Dead Weight)	0 Constant	kN-m	Set to 0 because all loads input as stresses instead of forces and moments

Global ID	Name	Value / Distribution Parameters	Units	Basis
4104	Mz (Dead Weight)	0 Constant	kN-m	Set to 0 because all loads input as stresses instead of forces and moments
4105	Fx (Thermal Expansion)	0 Constant	kN	Set to 0 because all loads input as stresses instead of forces and moments
4106	Mx (Thermal Expansion)	0 Constant	kN-m	Set to 0 because all loads input as stresses instead of forces and moments
4107	My (Thermal Expansion)	0 Constant	kN-m	Set to 0 because all loads input as stresses instead of forces and moments
4108	Mz (Thermal Expansion)	0 Constant	kN-m	Set to 0 because all loads input as stresses instead of forces and moments
4121	Membrane Stress (DW)	0.07 Constant	MPa	Same as reference case
4122	Maximum Bending Stress (DW)	0.35 Constant	MPa	Same as reference case
4123	Membrane Stress (Thermal)	4.72 Constant	MPa	Same as reference case
4124	Bending Stress (Thermal)	120.5 Constant	MPa	Same as reference case
N/A	Hoop WRS Pre-Mitigation	Unchanged from reference case	MPa	No-repair hoop WRS profile
N/A	Axial WRS Pre-Mitigation	Unchanged from reference case	MPa	No-repair axial WRS profile
5004	Lower bound POD (POD_0)	0 Constant	-	Even though it is not used, the default 0.999 value would lead to 99.9 percent probability of detection for a crack of zero depth

Global ID	Name	Value / Distribution Parameters	Units	Basis
5001-5510	Inspection Properties	Unchanged from reference case	-	RVON inspection parameters are used following the recommendations in [61]
9003	TW Crack Distance Rule Modifier	Unchanged from reference case	mm	Assumed same as RVON based on similar geometries

B11 Case 3.1.1

The objective of Case 3.1.1 was to assess the base likelihood of failure with pre-existing flaws and subsequent PWSCC growth of circumferential and axial cracks without mechanical mitigation for CE and B&W RCP nozzle DMWs. The effects of leak detection, ISI, and SSE were also assessed.

The random seeds used for the Case 3.1.1 analyses were as follow:

Simulation Description	Epistemic Random Seed	Aleatory Random Seed
5000-realization simulation using the epistemic (outer) loop	6128	369

The other inputs were developed using the Case 3.1.0 input set as a template with the following modifications:

Global ID	Name	Value / Distribution Parameters	Units	Basis
N/A	Case Description	3.1.01	-	Based on case description
0501	Crack Initiation Type Choice	0	-	Based on case description
1209	Number of Flaws (Circ)	1 Constant	-	Considers the impact of one circumferential crack and one axial crack because the likelihood of multiple cracks is low enough to not affect the results as demonstrated in [2]
1210	Initial Flaw Full-Length (Circ) (*)	Lognormal (1, 4.3E-3, 2.226)	m	Based on PWSCC initial flaw sizes
1211	Multiplier Starting Full-Length (Circ)	1 Constant	-	Based on PWSCC initial flaw sizes

Global ID	Name	Value / Distribution Parameters	Units	Basis
1212	Initial Flaw Depth (Circ) (*)	Lognormal (1, 1.5E-3, 1.419, min=5E-4, max=0.0663)	m	Based on PWSCC initial flaw sizes
1213	Multiplier Starting Depth (Circ)	1 Constant	-	Based on PWSCC initial flaw sizes
1214	Number of Flaws (Axial)	1 Constant	-	Considers the impact of one circumferential crack and one axial crack because the likelihood of multiple cracks is low enough to not affect the results as demonstrated in [2]
1215	Initial Flaw Full-Length (Axial) (*)	Lognormal (1, 4.3E-3, 2.226)	m	Based on PWSCC initial flaw sizes
1216	Multiplier Starting Full-Length (Axial)	1 Constant	-	Based on PWSCC initial flaw sizes
1217	Initial Flaw Depth (Axial) (*)	Lognormal (1, 1.5E-3, 1.419, min=5E-4, max=0.0663)	m	Based on PWSCC initial flaw sizes
1218	Multiplier Starting Depth (Axial)	1 Constant	-	Based on PWSCC initial flaw sizes

B12 Case 3.1.2

Case 3.1.2 was a sensitivity study of Case 3.1.0 considering a more severe WRS profile for CE and B&W RCP nozzle DMWs.

The random seeds used for the Case 3.1.2 analyses were as follow:

Simulation Description	Replicate Simulation No.	Epistemic Random Seed	Aleatory Random Seed
100,000-realization composite simulation using the epistemic (outer) loop	1	1515	13118
	2	1974	713705
	3	2002	1503
	4	2004	909
	5	2010	907
	6	3131	131521
	7	4512	1685
	8	5121	919
	9	41520	2025
	10	1415	23118

The other inputs were developed using the Case 3.1.0 input set as a template with the following modifications:

Global ID	Name	Value / Distribution Parameters	Units	Basis
-	Case Description	3.1.02		Based on case description

Global ID	Name	Value / Distribution Parameters	Units	Basis
-	Hoop WRS Pre-Mitigation	Mean / Std. Dev. -139.48 / 50.4 -93.80 / 50.4 72.51 / 50.4 170.81 / 50.4 141.69 / 50.4 112.08 / 50.4 -32.80 / 50.4 -154.57 / 50.4 -166.86 / 50.4 -153.04 / 50.4 -132.55 / 50.4 -87.83 / 50.4 -49.64 / 50.4 -65.32 / 50.4 45.86 / 50.4 38.11 / 50.4 128.27 / 50.4 205.25 / 50.4 194.06 / 50.4 250.03 / 50.4 257.42 / 50.4 254.42 / 50.4 225.10 / 50.4 196.58 / 50.4 167.43 / 50.4 144.17 / 50.4	MPa	More severe hoop WRS profile estimated from FEA results for the weld butter as discussed in Section C3.2

Global ID	Name	Value / Distribution Parameters	Units	Basis
N/A	Axial WRS Pre-Mitigation	Mean: -145.06, -123.38, -29.33, 1.87, -20.60, -106.75, -256.09, -337.07, -313.15, -276.01, -251.71, -192.52, -156.08, -122.04, -92.61, -58.29, 13.87, 90.03, 156.95, 214.69, 277.74, 338.45, 355.12, 332.82, 314.71, 298.81 Std. Dev.: 28.3 (all)	MPa	More severe axial WRS profile estimated from FEA results for the weld butter as discussed in Section C3.2

B13 Case 4.1.0

The objective of Case 4.1.0 was to assess the base likelihood of failure caused by PWSCC initiation and growth with inlay mitigation for Westinghouse steam generator nozzle DMWs. The effects of leak detection, ISI, and SSE were also assessed.

The random seeds used for the Case 4.1.0 analyses were as follow:

Simulation Description	Replicate Simulation No.	Epistemic Random Seed	Aleatory Random Seed
100,000-realization composite simulation using the epistemic (outer) loop	1	1515	13118
	2	1974	713705
	3	2002	1503
	4	2004	909
	5	2010	907
	6	3131	131521
	7	4512	1685
	8	5121	919
	9	41520	2025
	10	1415	23118

The other inputs were developed using the Case 3, Scenario 9, input set from the xLPR Inputs Group Report [53] as a template with the following modifications:

Global ID	Name	Value / Distribution Parameters	Units	Basis
-	Case Description	4.1.00	-	Based on case description
0001	Plant Operation Time	960	mon	Based on case description
0306	Stress Mitigation Time	1	mon	Based on case description
0402	Period End Time (Op Period #1)	961	mon	Based on case description
0403	Input Type Choice (Op Period #1)	2	-	Based on case description

Global ID	Name	Value / Distribution Parameters	Units	Basis
0405	Period End Time (Op Period #2)	962	mon	Based on case description
0808-0808.10	Inspection Month (Pre-Mitigation)	N/A	mon	Inspection defined as an annual frequency
0809-0809.10	Inspection Month (Post-Mitigation)	N/A	mon	Inspection defined as an annual frequency
0811	Inspection Schedule Input Type	1	-	Inspection defined as an annual frequency
0812	Pre-Mitigation Inspection Freq	0.1	1/yr	Annual frequency set to one inspection every 10 years
0813	Post-Mitigation Inspection Freq	0.1	1/yr	Annual frequency set to one inspection every 10 years
0820	Number of cracks detected	1	-	Based on case description
0904	Max time between 2 check - single TWC - CC	1	mon	Based on case description
All uncertain variables, except Global ID 2528	Data Source	Epistemic	-	Outer loop preserves LHS structure
1001	Effective Full Power Years (EFPY)	80 Constant	yr	Based on case description
1101	Pipe Outer Diameter	1.03266 Constant	m	Outside diameter for North Anna, Units 1 and 2 steam generator welds from [80], which bounds

Global ID	Name	Value / Distribution Parameters	Units	Basis
				welds represented by bin
1102	Pipe Wall Thickness	0.12225 Constant	m	Thickness for North Anna, Units 1 and 2 steam generator welds from [80], which bounds welds represented by bin
1103	Weld Width	0.04064 Constant	m	Weld width for North Anna, Units 1 and 2 steam generator welds from [80], which bounds welds represented by bin
1104	Weld Material Thickness	0.12225 Constant	m	Set to same value as Global ID 1102
1106	Inlay Thickness	0.0033 Constant	m	Figure 7 from [56]
3002	Unmitigated H2 Level	25 Constant	cc/kg	Bounds the operating experience of PWRs as reported in [48]
3101	Operating Pressure	15.51 Constant	MPa	Maximum operating pressure for V.C. Summer, Unit 1 from [80], which bounds welds represented by bin
3102	Operating Temperature	328 Constant	°C	Maximum operating temperature for North-Anna, Units 1 and 2 from [80], which bounds welds represented by bin
3103	Dissolved Oxygen	40	ppm	Based on Case 3, Scenario 10, input set from [50]
4001	Earthquake Probability	0.001	1/yr	Same value as used for analyses of other cases in this study (e.g., Case 2.1.0)

Global ID	Name	Value / Distribution Parameters	Units	Basis
4002	Earthquake Δ Total Membrane	0	MPa	All SSE stresses captured in Global ID 4004
4003	Earthquake Δ Inertial Bending	0 Constant	MPa	All SSE stresses captured in Global ID 4004
4004	Earthquake Δ Anchor Bending	161.9 Constant	MPa	Maximum SSE stress for North Anna, Unit 1 from Tables 3-1 through 3-4 in [80], which bounds welds represented by bin
4005	Sigma_SSa	0 Constant	MPa	Based on case description
4006	Sigma_SSh	0 Constant	MPa	Based on case description
4101	Fx (Dead Weight)	0 Constant	kN	Set to 0 because all loads input as stresses instead of forces and moments
4102	Mx (Dead Weight)	0 Constant	kN-m	Set to 0 because all loads input as stresses instead of forces and moments
4103	My (Dead Weight)	0 Constant	kN-m	Set to 0 because all loads input as stresses instead of forces and moments
4104	Mz (Dead Weight)	0 Constant	kN-m	Set to 0 because all loads input as stresses instead of forces and moments
4105	Fx (Thermal Expansion)	0 Constant	kN	Set to 0 because all loads input as stresses instead of forces and moments
4106	Mx (Thermal Expansion)	0 Constant	kN-m	Set to 0 because all loads input as stresses instead of forces and moments

Global ID	Name	Value / Distribution Parameters	Units	Basis
4107	My (Thermal Expansion)	0 Constant	kN-m	Set to 0 because all loads input as stresses instead of forces and moments
4108	Mz (Thermal Expansion)	0 Constant	kN-m	Set to 0 because all loads input as stresses instead of forces and moments
4121	Membrane Stress (DW)	0 Constant	MPa	Reference [80] makes no distinction between membrane and bending stresses, so this input is set to 0, and Global ID 4124 contains the DW contribution
4122	Maximum Bending Stress (DW)	0 Constant	MPa	Reference [80] makes no distinction between membrane and bending stresses, so this input is set to 0, and Global ID 4124 contains the DW contribution
4123	Membrane Stress (Thermal)	0 Constant	MPa	Reference [80] makes no distinction between membrane and bending stresses, so this input is set to 0, and Global ID 4124 contains the thermal membrane stress contribution
4124	Bending Stress (Thermal)	92 Constant	MPa	Maximum stress for North Anna, Unit 2 from Tables 3-1 through 3-4 in [80], which bounds welds represented by bin
N/A	Hoop WRS Pre-mitigation	Same as hoop WRS post-mitigation	MPa	Set for consistency throughout the simulation

Global ID	Name	Value / Distribution Parameters	Units	Basis
N/A	Axial WRS Pre-mitigation	Same as axial WRS post-mitigation	MPa	Set for consistency throughout the simulation
N/A	Hoop WRS Post-mitigation	Mean: 188.73, 289.19, 269.03, 296.16, 295.05, 308.65, 328.51, 309.94, 165.39, -43.41, -68.83, 67.31, 182.84, 169.10, 139.86, 181.21, 228.36, 261.16, 304.80, 305.55, 302.81, 283.76, 272.20, 281.17, 241.45, 261.87 Std. Dev.: 67	MPa	Mean hoop WRS profile developed as discussed in Section 1.1.1.1.1A1.1. The standard deviation is based on the maximum standard deviation from [47].
N/A	Axial WRS Post-mitigation	Mean: 52.15, 120.65, 96.01, 100.73, 65.89, 60.41, 75.84, 33.72, -137.24, -317.64 Std. Dev.: 67	MPa	Axial hoop WRS profile developed as discussed in Section 1.1.1.1.1A1.1. The standard deviation is based on the maximum standard deviation from [47].

Global ID	Name	Value / Distribution Parameters	Units	Basis
		-323.08 67 -216.92 67 -142.67 67 -112.86 67 -104.57 67 -67.69 67 -11.59 67 -22.16 67 23.99 67 48.60 67 74.25 67 111.38 67 132.88 67 197.13 67 170.55 67 134.40 67		
5004	Lower bound POD, POD_0	0 Constant	-	Even though it is not used, the default 0.999 value would lead to 99.9 percent probability of detection for a crack of zero depth
2743	Multiplier Proport. Const. A (DM1)	Lognormal (0.0417, 17.99)	-	Based on minimum FOI of 24 from Pacific Northwest National Laboratories test data on Alloy 52/152 crack initiation and using a similar method as in [78]. The Alloy 82/182 distribution median from the xLPR Inputs Group report [53] was divided by this FOI.
2788	Power Law Constant, Alpha	2.01E-12 Constant	(m/s)(MPa-m1/2)^(-beta)	Set equal to the Alloy 82/182 power law constant because the FOI is applied in Global ID 2796

Global ID	Name	Value / Distribution Parameters	Units	Basis
2796	Factor of Improvement IF	324 Constant	-	Represents 75th percentile FOI from [52]

B14 Case 4.1.1

The objective of Case 4.1.1 was to assess the base likelihood of failure with pre-existing flaws and subsequent PWSCC growth of circumferential and axial cracks with inlay mitigation for Westinghouse steam generator nozzle DMWs. The effects of leak detection, ISI, and SSE were also assessed.

The random seeds used for the Case 4.1.1 analyses were as follow:

Simulation Description	Epistemic Random Seed	Aleatory Random Seed
5000-realization simulation using the epistemic (outer) loop	6128	369

The other inputs were developed using the Case 4.1.0 input set as a template with the following modifications:

Global ID	Name	Value / Distribution Parameters	Units	Basis
N/A	Case Description	4.1.01	-	Based on case description
0501	Crack Initiation Type Choice	0	-	Based on case description
1209	Number of Flaws (Circ)	1 Constant	-	Considers the impact of one circumferential crack and one axial crack because the likelihood of multiple cracks is low enough to not affect the results as demonstrated in [2]
1210	Initial Flaw Full-Length (Circ) (*)	Lognormal (1, 4.3E-3, 2.226)	m	Based on PWSCC initial flaw sizes
1211	Multiplier Starting Full-Length (Circ)	1 Constant	-	Based on PWSCC initial flaw sizes

Global ID	Name	Value / Distribution Parameters	Units	Basis
1212	Initial Flaw Depth (Circ) (*)	Lognormal (1, 1.5E-3, 1.419, min=5E-4, max=0.0663)	m	Based on PWSCC initial flaw sizes
1213	Multiplier Starting Depth (Circ)	1 Constant	-	Based on PWSCC initial flaw sizes
1214	Number of Flaws (Axial)	1 Constant	-	Considers the impact of one circumferential crack and one axial crack because the likelihood of multiple cracks is low enough to not affect the results as demonstrated in [2]
1215	Initial Flaw Full-Length (Axial) (*)	Lognormal (1, 4.3E-3, 2.226)	m	Based on PWSCC initial flaw sizes
1216	Multiplier Starting Full-Length (Axial)	1 Constant	-	Based on PWSCC initial flaw sizes
1217	Initial Flaw Depth (Axial) (*)	Lognormal (1, 1.5E-3, 1.419, min=5E-4, max=0.0663)	m	Based on PWSCC initial flaw sizes
1218	Multiplier Starting Depth (Axial)	1 Constant	-	Based on PWSCC initial flaw sizes

B15 Case 4.1.2

Case 4.1.2 was a sensitivity study of Case 4.1.0 considering a more severe WRS profile for Westinghouse steam generator nozzle DMWs.

The random seeds used for the Case 4.1.2 analyses were as follow:

Simulation Description	Replicate Simulation No.	Epistemic Random Seed	Aleatory Random Seed
100,000-realization composite simulation using the epistemic (outer) loop	1	1515	13118
	2	1974	713705
	3	2002	1503
	4	2004	909
	5	2010	907
	6	3131	131521
	7	4512	1685
	8	5121	919
	9	41520	2025
	10	1415	23118

The other inputs were developed using the Case 4.1.0 input set as a template with the following modifications:

Global ID	Name	Value / Distribution Parameters	Units	Basis
N/A	Case Description	4.1.02	-	Based on case description

Global ID	Name	Value / Distribution Parameters	Units	Basis
N/A	Hoop WRS Post-Mitigation	Mean / Std. Dev. 250.13 67 134.75 67 55.27 67 14.51 67 -2.01 67 -21.50 67 -81.53 67 -141.06 67 -177.72 67 -195.79 67 -183.49 67 -165.58 67 -139.10 67 -108.05 67 -90.13 67 -72.45 67 -65.47 67 -62.11 67 -47.94 67 -36.58 67 -22.76 67 -4.85 67 24.51 67 92.47 67 202.39 67 250.13 67	MPa	More severe hoop WRS profile estimated from FEA results for the weld butter as discussed in Section C4.3
N/A	Hoop WRS Pre-Mitigation	Same as hoop WRS post-mitigation	MPa	Set for consistency throughout the simulation

Global ID	Name	Value / Distribution Parameters	Units	Basis
N/A	Axial WRS Post-Mitigation	Mean Std. Dev. 247.82 67 191.42 67 98.57 67 46.10 67 30.31 67 10.36 67 -56.05 67 -127.90 67 -183.04 67 -213.67 67 -219.63 67 -201.55 67 -150.39 67 -99.58 67 -60.25 67 -33.63 67 -19.39 67 -10.82 67 8.82 67 30.82 67 56.92 67 90.43 67 122.54 67 154.68 67 221.83 67 254.66 67	MPa	More severe axial WRS profile estimated from FEA results for the weld butter as discussed in Section C4.3
N/A	Axial WRS Pre-Mitigation	Same as axial WRS post-mitigation	MPa	Set for consistency throughout the simulation

B16 Case 4.1.3

Case 4.1.3 was a sensitivity study of Case 4.1.0 considering overlay instead of inlay mitigation.

The random seeds used for the Case 4.1.3 analyses were as follow:

Simulation Description	Replicate Simulation No.	Epistemic Random Seed	Aleatory Random Seed
100,000-realization composite simulation using the epistemic (outer) loop	1	1515	13118
	2	1974	713705
	3	2002	1503
	4	2004	909
	5	2010	907
	6	3131	131521
	7	4512	1685
	8	5121	919
	9	41520	2025
	10	1415	23118

The other inputs were developed using the Case 4.1.0 input set as a template with the following modifications:

Global ID	Name	Value / Distribution Parameters	Units	Basis
N/A	Case Description	4.1.03	-	Based on case description
0305	Stress Mitigation Choice	2	-	Setting for weld overlay
0306	Stress mitigation time	240	mon	The steam generators represented by this case had overlays applied after 17 years of service, which was bounded in the analysis by applying the overlay at 20 EFPY (i.e., 240 months)

Global ID	Name	Value / Distribution Parameters	Units	Basis
0803	Post-Overlay Trunc Meas Error	1		Consistent with pre-mitigation approach default value
0804	Post-Overlay Eval Length Effects	0		Default value
0805	Full Structural WOL	1		Overlay represented is a full structural weld overlay
0815	Post-Overlay Ligament Flag	0		Default value
1105	Weld overlay thickness	0.04075 Constant	m	Weld thickness is 0.12225 m. Overlay thickness set to one third that value, which is the minimum acceptable thickness for a full structural weld overlay as stated in [59]
5201	Depth repair threshold x_TH (during)	0 Constant	-	Set to pre-mitigation value because no applicable values for overlays
5202	Depth repair threshold x_TH (post)	0 Constant	-	Set to pre-mitigation value because no applicable values for overlays
5301-5312	Post-Overlay Inspection Properties	beta_0 (circ): Normal (5.41, 3.64) beta_1 (circ): Normal (0.86, 6.02, min=0, max=14.86) beta_0 (axial): Normal (3.07, 2.07) beta_1 (axial): Normal (0.64, 4.46, min=0, max=11.02) a (circ): Normal (0.018, 0.017) b (circ): Normal (0.971, 0.029) a (axial): Normal (0.018, 0.017) b (axial): Normal (0.971, 0.029) Sigma_depth (circ): 0.04 Sigma_depth (axial): 0.04	-	Set equal to the pre-mitigation inspection property values because no applicable values for overlays

Global ID	Name	Value / Distribution Parameters	Units	Basis
		x_small: 0.1 x_LB: 0		
Correlation 5301-5302	Intercept, B0 (circ) Slope, B1 (circ)	-0.92	-	Set equal to the pre-mitigation inspection property values because no applicable values for overlays
Correlation 5303-5304	Intercept, B0 (axial) Slope, B1 (axial)	-0.92	-	Set equal to the pre-mitigation inspection property values because no applicable values for overlays
Correlation 5305-5306	a (circ) b (circ)	-0.94	-	Set equal to the pre-mitigation inspection property values because no applicable values for overlays
Correlation 5307-5308	a (axial) b (axial)	-0.94	-	Set equal to the pre-mitigation inspection property values because no applicable values for overlays

Global ID	Name	Value / Distribution Parameters		Units	Basis
N/A	Hoop WRS Pre-Mitigation	Mean	Std. Dev.	MPa	Same as hoop WRS profile used for Case 4.1.0 due to similar double-vee groove welding sequences and temperature-dependent weld material stress-strain curves
		188.73	67		
		289.19	67		
		269.03	67		
		296.16	67		
		295.05	67		
		308.65	67		
		328.51	67		
		309.94	67		
		165.39	67		
		-43.41	67		
		-68.83	67		
		67.31	67		
		182.84	67		
		169.10	67		
		139.86	67		
		181.21	67		
		228.36	67		
		261.16	67		
		304.80	67		
		305.55	67		
		302.81	67		
		283.76	67		
		272.20	67		
		281.17	67		
		241.45	67		
		261.87	67		

Global ID	Name	Value / Distribution Parameters		Units	Basis
N/A	Axial WRS Pre-Mitigation	Mean	stdev	MPa	Same as axial WRS profile used for Case 4.1.0 due to similar double-vee groove welding sequences and temperature-dependent weld material stress-strain curves
		52.15	67		
		120.65	67		
		96.01	67		
		100.73	67		
		65.89	67		
		60.41	67		
		75.84	67		
		33.72	67		
		-137.24	67		
		-317.64	67		
		-323.08	67		
		-216.92	67		
		-142.67	67		
		-112.86	67		
		-104.57	67		
		-67.69	67		
		-11.59	67		
		-22.16	67		
		23.99	67		
		48.60	67		
		74.25	67		
		111.38	67		
		132.88	67		
		197.13	67		
		170.55	67		
		134.40	67		

Global ID	Name	Value / Distribution Parameters		Units	Basis
N/A	Hoop WRS Post-Mitigation	Mean	Std. Dev.	MPa	Overlay mitigation rules from xLPR WRS Subgroup report [47] applied to pre-mitigation mean hoop WRS profile
		-11.27	67		
		97.19	67		
		85.03	67		
		120.16	67		
		127.05	67		
		148.65	67		
		176.51	67		
		165.94	67		
		29.39	67		
		-171.41	67		
		-188.83	67		
		-44.69	67		
		78.84	67		
		73.10	67		
		51.86	67		
		101.21	67		
		156.36	67		
		197.16	67		
		248.80	67		
		257.55	67		
		262.81	67		
		251.76	67		
		248.20	67		
		265.17	67		
		233.45	67		
		261.87	67		

Global ID	Name	Value / Distribution Parameters		Units	Basis
N/A	Axial WRS Post-Mitigation	Mean	Std. Dev.	MPa	Overlay mitigation rules from xLPR WRS Subgroup report [47] applied to pre-mitigation mean axial WRS profile
		-43.72	67		
		24.78	67		
		0.14	67		
		4.86	67		
		-29.98	67		
		-35.46	67		
		4.89	67		
		-14.69	67		
		-165.47	67		
		-328.06	67		
		-318.05	67		
		-198.83	67		
		-113.87	67		
		-75.72	67		
		-61.47	67		
		-20.98	67		
		36.35	67		
		25.77	67		
		71.92	67		
		96.54	67		
		122.18	67		
		159.32	67		
		180.81	67		
		245.07	67		
		218.48	67		
		182.33	67		

B17 Case 4.1.4

Case 4.1.4 was a sensitivity study of Case 4.1.0 without mechanical mitigation.

The random seeds used for the Case 4.1.4 analyses were as follow:

Simulation Description	Replicate Simulation No.	Epistemic Random Seed	Aleatory Random Seed
100,000-realization composite simulation using the epistemic (outer) loop	1	1515	13118
	2	1974	713705
	3	2002	1503
	4	2004	909
	5	2010	907
	6	3131	131521
	7	4512	1685
	8	5121	919
	9	41520	2025
	10	1415	23118

The other inputs were developed using the Case 4.1.0 input set as a template with the following modifications:

Global ID	Name	Value / Distribution Parameters	Units	Basis
N/A	Case Description	4.1.04	-	Case number for reference
0301	Mitigation type choice	0	-	Setting for no mitigation
3101	Operating Pressure	15.59 Constant	MPa	Same operating pressure as Case 4.1.0
3102	Operating Temperature	296 Constant	°C	Cold leg temperature corresponding with location of the steam generator outlet nozzles

Global ID	Name	Value / Distribution Parameters	Units	Basis
4001	Earthquake probability	0.001 Constant	-	Same value as used for analyses of other cases in this study (e.g., Case 2.1.0)
4002	Earthquake Δ Total Membrane	0 Constant	MPa	All SSE membrane stresses captured in Global ID 4004
4003	Earthquake Δ Inertial Bending	0 Constant	MPa	All SSE bending stresses captured in Global ID 4004
4004	Earthquake Δ Anchor Bending	161.9 Constant	MPa	Maximum SSE stress for North Anna, Unit 1 from Tables 3-1 through 3-4 in [80], which bounds welds represented by bin
4121	Membrane stress (DW)	0 Constant	MPa	Reference [80] makes no distinction between membrane and bending stresses, so this input is set to 0, and Global ID 4124 contains the DW contribution
4122	Maximum Bending Stress (DW)	0 Constant	MPa	Reference [80] makes no distinction between membrane and bending stresses, so this input is set to 0, and Global ID 4124 contains the DW contribution
4123	Membrane Stress (Thermal)	0 Constant	MPa	Reference [80] makes no distinction between membrane and bending stresses, so this input is set to 0, and Global ID 4124 contains the thermal membrane stress contribution

Global ID	Name	Value / Distribution Parameters	Units	Basis
4124	Bending Stress (Thermal)	92 Constant	MPa	Reference [80] makes no distinction between membrane and bending stresses, so this input is set to 0, and Global ID 4124 contains the DW contribution

Global ID	Name	Value / Distribution Parameters		Units	Basis
N/A	Hoop WRS Pre-Mitigation	Mean	Std. Dev.	MPa	Same as hoop WRS profile used for Case 4.1.0 due to similar double-vee groove welding sequences and temperature-dependent weld material stress-strain curves
		188.73	67		
		289.19	67		
		269.03	67		
		296.16	67		
		295.05	67		
		308.65	67		
		328.51	67		
		309.94	67		
		165.39	67		
		-43.41	67		
		-68.83	67		
		67.31	67		
		182.84	67		
		169.10	67		
		139.86	67		
		181.21	67		
		228.36	67		
		261.16	67		
		304.80	67		
		305.55	67		
		302.81	67		
		283.76	67		
		272.20	67		
		281.17	67		
		241.45	67		
		261.87	67		

Global ID	Name	Value / Distribution Parameters		Units	Basis
N/A	Axial WRS Pre-Mitigation	Mean	stdev	MPa	Same as axial WRS profile used for Case 4.1.0 due to similar double-vee groove welding sequences and temperature-dependent weld material stress-strain curves
		52.15	67		
		120.65	67		
		96.01	67		
		100.73	67		
		65.89	67		
		60.41	67		
		75.84	67		
		33.72	67		
		-137.24	67		
		-317.64	67		
		-323.08	67		
		-216.92	67		
		-142.67	67		
		-112.86	67		
		-104.57	67		
		-67.69	67		
		-11.59	67		
		-22.16	67		
		23.99	67		
		48.60	67		
		74.25	67		
		111.38	67		
		132.88	67		
		197.13	67		
		170.55	67		
		134.40	67		
N/A	Hoop WRS Post-Mitigation	Same as hoop WRS pre-mitigation		MPa	Not used in the simulation but filled for completeness
N/A	Axial WRS Post-Mitigation	Same as axial WRS pre-mitigation		MPa	Not used in the simulation but filled for completeness

B18 Case 5.1.0

The objective of Case 5.1.0 was to assess the base likelihood of failure caused by PWSCC initiation and growth without mechanical mitigation for CE hot leg branch line nozzle DMWs. The effects of leak detection, ISI, and SSE were also assessed.

The random seeds used for the Case 5.1.0 analyses were as follow:

Simulation Description	Replicate Simulation No.	Epistemic Random Seed	Aleatory Random Seed
100,000-realization composite simulation using the epistemic (outer) loop	1	1515	13118
	2	1974	713705
	3	2002	1503
	4	2004	909
	5	2010	907
	6	3131	131521
	7	4512	1685
	8	5121	919
	9	41520	2025
	10	1415	23118

The other inputs were developed using Case 2.1.0 input set as a template with the following modifications:

Global ID	Name	Value / Distribution Parameters	Units	Basis
-	Case Description	5.1.00	-	Based on case description
-	Weld Type Choice	CE HL Branch DMW	-	Based on case description
0808-0808.10	Inspection Month	N/A	mon	Inspection defined as an annual frequency
0811	Inspection Schedule Input Type	1	-	Inspection defined as an annual frequency

Global ID	Name	Value / Distribution Parameters	Units	Basis
0812	Pre-Mitigation Inspection Freq	0.1	1/yr	Annual frequency set to one inspection every 10 years
All uncertain variables, except Global ID 2528	Data Source	Epistemic	-	Outer loop preserves LHS structure
1101	Pipe Outer Diameter	0.324 Constant	m	Typical shutdown cooling system pipe outside diameter from [22]
1102	Pipe Wall Thickness	0.036 Constant	m	Typical shutdown cooling system pipe wall thickness from [22]
1103	Weld Width	0.036 Constant	m	Outside diameter weld width from generic CE branch line weld configuration
1104	Weld Material Thickness	0.036 Constant	m	Set to same value as Global ID 1102
2101	Yield Strength, Sigy	Lognormal (179.5, 26.87, min=128, max=269)	MPa	Mean from Table 4-2 of [22] and distribution developed using the coefficient of variation (COV) from Case 2.1.0, Global ID 2101

Global ID	Name	Value / Distribution Parameters	Units	Basis
2102	Ultimate Strength, Sigu	Lognormal (461.2, 60.72, min=359, max=700)	MPa	Mean from Table 4-2 of [22] and distribution developed using the COV from Case 2.1.0, Global ID 2102
2105	Elastic Modulus, E	Normal (179270, 26800, min=148716, max=201204)	MPa	Mean from Table 4-2 of [22] and distribution developed using the COV from Case 2.1.0, Global ID 2105
2106	Material Init J-Resistance, Jic	Normal (105.076, 58.6, min=10, max=254.1)	N/mm	Mean from Table 4-2 of [22] and distribution developed using the COV from Case 2.1.0, Global ID 2106
2107	Material Init J-Resist Coef, C	Normal (448.85, 138, min=91.6, max=615.9)	N/mm	Mean from Table 4-2 of [22] and distribution developed using the COV from Case 2.1.0, Global ID 2107
2108	Material Init J-Resist Exponent, m	Normal (0.274, 0.0317, min=0.1, max=1)	-	Mean from Table 4-2 of [22] and distribution developed using the COV from Case 2.1.0, Global ID 2108
2301	Yield Strength, Sigy	Lognormal (201, 22.42, min=154, max=253)	MPa	Distribution developed based on data from [81]
2302	Ultimate Strength, Sigu	Lognormal (360, 54.01, min=235, max=485)	MPa	Distribution developed based on data from [81]

Global ID	Name	Value / Distribution Parameters	Units	Basis
2305	Elastic Modulus, E	Normal (179959.5, 27000, min=150212, max=203228)	MPa	Mean value from [23]
2306	Material Init J-Resistance, Jic	Normal (106.6, 65, min=7, max=211)	N/mm	Distribution developed based on [23] and [82]
2307	Material Init J-Resist Coef, C	Normal (216, 135, min=44, max=467)	N/mm	Distribution developed based on [23] and [82]
2308	Material Init J-Resist Exponent, m	Normal (0.44, 0.09, min=0.21, max=0.56)	-	Distribution developed based on [23] and [82]
3002	Unmitigated H2 Level	25 Constant	cc/kg	Bounds the operating experience of PWRs as reported in [48]
3102	Operating Temperature	318 Constant	°C	Typical operating temperature for shutdown cooling system as reported in [22] and pressurizer surge line as reported in [21]
4001	Earthquake Probability	0.001 Constant	1/yr	From Section E.3.1 of [60], the maximum earthquake probability is 1E-3
4002	Earthquake Δ Total Membrane	16.43 Constant	MPa	Maximum SSE stress from Table 4-6 [22] is combined membrane and bending stress
4003	Earthquake Δ Inertial Bending	0 Constant	MPa	SSE bending stresses captured in Global ID 4002

Global ID	Name	Value / Distribution Parameters	Units	Basis
4004	Earthquake Δ Anchor Bending	0 Constant	MPa	SSE bending stresses captured in Global ID 4002
4121	Membrane Stress (DW)	0 Constant	MPa	Stress from [22] is combined DW and thermal, so this input is set to 0, and Global ID 4124 contains the DW contribution
4122	Maximum Bending Stress (DW)	0 Constant	MPa	Stress from [22] is combined DW and thermal, so this input is set to 0, and Global ID 4124 contains the DW contribution
4123	Membrane Stress (Thermal)	0 Constant	MPa	Stress from [22] is combined DW and thermal, so this input is set to 0, and Global ID 4124 contains the thermal contribution
4124	Bending Stress (Thermal)	21.51 Constant	MPa	Stress from Table 4-5 of [22] is combined DW and thermal; used the limiting thermal maximum

Global ID	Name	Value / Distribution Parameters		Units	Basis
N/A	Hoop WRS Pre-Mitigation	Mean	Std. Dev.	MPa	Mean hoop WRS profile and standard deviation based on analysis for generic CE branch line geometry as documented in Section C5.2
		91.43	76.7		
		136.17	76.7		
		173.20	76.7		
		223.04	76.7		
		321.41	76.7		
		353.55	76.7		
		323.67	76.7		
		279.46	76.7		
		229.43	76.7		
		159.52	76.7		
		114.54	76.7		
		72.28	76.7		
		71.63	76.7		
		77.13	76.7		
		136.84	76.7		
		110.97	76.7		
		163.95	76.7		
		229.93	76.7		
		209.21	76.7		
		218.51	76.7		
		250.47	76.7		
		261.70	76.7		
		243.47	76.7		
		234.81	76.7		
		248.73	76.7		
		252.10	76.7		

Global ID	Name	Value / Distribution Parameters	Units	Basis
N/A	Axial WRS Pre-Mitigation	Mean / Std. Dev. -152.59 / 57.9 -100.70 / 57.9 -45.09 / 57.9 1.38 / 57.9 75.69 / 57.9 97.53 / 57.9 64.70 / 57.9 22.01 / 57.9 -76.55 / 57.9 -129.83 / 57.9 -145.23 / 57.9 -215.12 / 57.9 -214.80 / 57.9 -204.85 / 57.9 -179.97 / 57.9 -136.36 / 57.9 -69.80 / 57.9 12.75 / 57.9 47.64 / 57.9 108.06 / 57.9 156.35 / 57.9 187.73 / 57.9 185.37 / 57.9 194.95 / 57.9 210.02 / 57.9 205.36 / 57.9	MPa	Mean axial WRS profile and standard deviation based on analysis for generic CE branch line geometry as documented in Section C5.2
5004	Lower bound POD, POD_0	0 Constant	-	Even though it is not used, the default 0.999 value would lead to 99.9 percent probability of detection for a crack of zero depth

Global ID	Name	Value / Distribution Parameters	Units	Basis
5101-5110	Pre-Mitigation Inspection Properties	beta_0 (circ): Normal (2.71, 0.21) beta_1 (circ): Normal (0.31, 0.45) beta_0 (axial): Normal (-0.8, 0.38) beta_1 (axial): Normal (8.3, 1.45) a (circ): Normal (0.034, 0.006) b (circ): Normal (0.955, 0.013) a (axial): Normal (0.041, 0.011) b (axial): Normal (0.88, 0.029) Sigma_depth (circ): 0.072 Sigma_depth (axial): 0.078	-	Uses values for the pressurizer surge line per the recommendations in [61]
Correlation 5101-5102	Intercept, B0 (circ) Intercept, B1 (circ)	-0.86	-	Uses values for the pressurizer surge line per the recommendations in [61]
Correlation 5103-5104	Intercept, B0 (axial) Intercept, B1 (axial)	-0.93	-	Uses values for the pressurizer surge line per the recommendations in [61]
Correlation 5105-5106	a (circ) b (circ)	-0.867	-	Uses values for the pressurizer surge line per the recommendations in [61]
Correlation 5107-5108	a (axial) b (axial)	-0.87	-	Uses values for the pressurizer surge line per the recommendations in [61]
9003	TW Crack Distance Rule Modifier	Uniform (0, 508)	mm	The circumference of the shutdown cooling system piping is similar enough to the pressurizer surge line to use the same upper bound from Case 2.1.0

B19 Case 5.1.1

The objective of Case 5.1.1 was to assess the base likelihood of failure with pre-existing flaws and subsequent PWSCC growth of circumferential and axial cracks without mechanical mitigation for CE hot leg branch line nozzle DMWs. The effects of leak detection, ISI, and SSE were also assessed.

The random seeds used for the Case 5.1.1 analyses were as follow:

Simulation Description	Epistemic Random Seed	Aleatory Random Seed
5000-realization simulation using the epistemic (outer) loop	6128	369

The other inputs were developed using the Case 5.1.0 input set as a template with the following modifications:

Global ID	Name	Value / Distribution Parameters	Units	Basis
N/A	Case Description	5.1.01	-	Based on case description
0501	Crack Initiation Type Choice	0	-	Based on case description
1209	Number of Flaws (Circ)	1 Constant	-	Considers the impact of one circumferential crack and one axial crack because the likelihood of multiple cracks is low enough to not affect the results as demonstrated in [2]
1210	Initial Flaw Full-Length (Circ) (*)	Lognormal (1, 4.3E-3, 2.226)	m	Based on PWSCC initial flaw sizes
1211	Multiplier Starting Full-Length (Circ)	1 Constant	-	Based on PWSCC initial flaw sizes

Global ID	Name	Value / Distribution Parameters	Units	Basis
1212	Initial Flaw Depth (Circ) (*)	Lognormal (1, 1.5E-3, 1.419, min=5E-4, max=0.0663)	m	Based on PWSCC initial flaw sizes
1213	Multiplier Starting Depth (Circ)	1 Constant	-	Based on PWSCC initial flaw sizes
1214	Number of Flaws (Axial)	1 Constant	-	Considers the impact of one circumferential crack and one axial crack because the likelihood of multiple cracks is low enough to not affect the results as demonstrated in [2]
1215	Initial Flaw Full-Length (Axial) (*)	Lognormal (1, 4.3E-3, 2.226)	m	Based on PWSCC initial flaw sizes
1216	Multiplier Starting Full-Length (Axial)	1 Constant	-	Based on PWSCC initial flaw sizes
1217	Initial Flaw Depth (Axial) (*)	Lognormal (1, 1.5E-3, 1.419, min=5E-4, max=0.0663)	m	Based on PWSCC initial flaw sizes
1218	Multiplier Starting Depth (Axial)	1 Constant	-	Based on PWSCC initial flaw sizes

B20 Case 5.1.2

Case 5.1.2 was a sensitivity study of Case 5.1.0 considering a more severe WRS profile for CE hot leg branch line nozzle DMWs.

The random seeds used for the Case 5.1.2 analyses were as follow:

Simulation Description	Replicate Simulation No.	Epistemic Random Seed	Aleatory Random Seed
100,000-realization composite simulation using the epistemic (outer) loop	1	1515	13118
	2	1974	713705
	3	2002	1503
	4	2004	909
	5	2010	907
	6	3131	131521
	7	4512	1685
	8	5121	919
	9	41520	2025
	10	1415	23118

The other inputs were developed using the Case 5.1.0 input set as a template with the following modifications:

Global ID	Name	Value / Distribution Parameters	Units	Basis
N/A	Case Description	5.1.02	-	Based on case description

Global ID	Name	Value / Distribution Parameters		Units	Basis
N/A	Hoop WRS Pre-Mitigation	Mean	Std. Dev.	MPa	More severe hoop WRS profile estimated from FEA results for the weld butter as discussed in Section C5.3
		135.82	76.7		
		177.92	76.7		
		209.02	76.7		
		251.85	76.7		
		340.89	76.7		
		369.79	76.7		
		339.69	76.7		
		295.63	76.7		
		248.33	76.7		
		178.62	76.7		
		131.49	76.7		
		91.90	76.7		
		89.13	76.7		
		85.42	76.7		
		144.50	76.7		
		119.70	76.7		
		165.50	76.7		
		228.94	76.7		
		208.52	76.7		
		221.96	76.7		
		257.46	76.7		
		268.67	76.7		
		250.29	76.7		
		242.98	76.7		
		257.83	76.7		
		260.38	76.7		

Global ID	Name	Value / Distribution Parameters		Units	Basis
N/A	Axial WRS Pre-Mitigation	Mean	Std. Dev.	MPa	More severe axial WRS profile estimated from FEA results for the weld butter as discussed in Section C5.3
		-105.58	57.9		
		-47.70	57.9		
		8.75	57.9		
		50.80	57.9		
		117.52	57.9		
		132.72	57.9		
		94.79	57.9		
		47.29	57.9		
		-55.16	57.9		
		-112.78	57.9		
		-131.67	57.9		
		-202.11	57.9		
		-203.49	57.9		
		-201.05	57.9		
		-180.28	57.9		
		-141.19	57.9		
		-82.63	57.9		
		-9.57	57.9		
		19.61	57.9		
		72.45	57.9		
		118.34	57.9		
		147.84	57.9		
		144.86	57.9		
		152.16	57.9		
		163.89	57.9		
		160.22	57.9		

B21 Case 5.2.0

The objective of Case 5.2.0 was to assess the base likelihood of failure caused by PWSCC initiation and growth without mechanical mitigation for CE cold leg branch line nozzle DMWs. The effects of leak detection, ISI, and SSE were also assessed.

The random seeds used for the Case 5.2.0 analyses were as follow:

Simulation Description	Replicate Simulation No.	Epistemic Random Seed	Aleatory Random Seed
100,000-realization composite simulation using the epistemic (outer) loop	1	1515	13118
	2	1974	713705
	3	2002	1503
	4	2004	909
	5	2010	907
	6	3131	131521
	7	4512	1685
	8	5121	919
	9	41520	2025
	10	1415	23118

The other inputs were developed using Case 5.1.0 input set as a template with the following modifications:

Global ID	Name	Value / Distribution Parameters	Units	Basis
N/A	Case Description	5.2.00	-	Based on case description
N/A	Weld Type Choice	CE CL Branch DMW	-	Based on case description
0808-0808.10	Inspection Month	N/A	mon	Inspection defined as an annual frequency
0811	Inspection Schedule Input Type	1	-	Inspection defined as an annual frequency

Global ID	Name	Value / Distribution Parameters	Units	Basis
0812	Pre-Mitigation Inspection Freq	0.1	1/yr	Annual frequency set to one inspection every 10 years
All uncertain variables, except Global ID 2528	Data Source	Epistemic	-	Outer loop preserves LHS structure
1101	Pipe Outer Diameter	0.32385 Constant	m	Typical safety injection system pipe outside diameter from [23]
1102	Pipe Wall Thickness	0.0361947 Constant	m	Typical safety injection system pipe wall thickness from [23]
1103	Weld Width	0.0355 Constant	m	Outside diameter weld width from generic CE branch line weld configuration
1104	Weld Material Thickness	0.0361947 Constant	m	Set to same value as Global ID 1102
2101	Yield Strength, Sigy	Lognormal (179.5, 26.87, min=128, max=269)	MPa	Mean from Table 4-2 of [22] and distribution developed using the COV from Case 2.1.0, Global ID 2101

Global ID	Name	Value / Distribution Parameters	Units	Basis
2102	Ultimate Strength, Sigu	Lognormal (461.2, 60.72, min=359, max=700)	MPa	Mean from Table 4-2 of [22] and distribution developed using the COV from Case 2.1.0, Global ID 2102
2105	Elastic Modulus, E	Normal (179270, 26800, min=148716, max=201204)	MPa	Mean from Table 4-2 of [22] and distribution developed using the COV from Case 2.1.0, Global ID 2105
2106	Material Init J-Resistance, Jic	Normal (105.076, 58.6, min=10, max=254.1)	N/mm	Mean from Table 4-2 of [22] and distribution developed using the COV from Case 2.1.0, Global ID 2106
2107	Material Init J-Resist Coef, C	Normal (448.85, 138, min=91.6, max=615.9)	N/mm	Mean from Table 4-2 of [22] and distribution developed using the COV from Case 2.1.0, Global ID 2107
2108	Material Init J-Resist Exponent, m	Normal (0.274, 0.0317, min=0.1, max=1)	-	Mean from Table 4-2 of [22] and distribution developed using the COV from Case 2.1.0, Global ID 2108
2301	Yield Strength, Sigy	Lognormal (201, 22.42, min=154, max=253)	MPa	Distribution developed based on data from [81]
2302	Ultimate Strength, Sigu	Lognormal (360, 54.01, min=235, max=485)	MPa	Distribution developed based on data from [81]

Global ID	Name	Value / Distribution Parameters	Units	Basis
2305	Elastic Modulus, E	Normal (179959.5, 27000, min=150212, max=203228)	MPa	Mean from [23]
2306	Material Init J-Resistance, Jic	Normal (106.6, 65, min=7, max=211)	N/mm	Distribution developed based on [22] and [82]
2307	Material Init J-Resist Coef, C	Normal (216, 135, min=44, max=467)	N/mm	Distribution developed based on [22] and [82]
2308	Material Init J-Resist Exponent, m	Normal (0.44, 0.09, min=0.21, max=0.56)	-	Distribution developed based on [22] and [82]
3002	Unmitigated H2 Level	25 Constant	cc/kg	Bounds the operating experience of PWRs as reported in [48]
3102	Operating Temperature	288 Constant	°C	Typical operating temperature for the safety injection system from [23]
4001	Earthquake Probability	0.001 Constant	1/yr	From Section E.3.1 of [60], the maximum earthquake probability is 1E-3
4002	Earthquake Δ Total Membrane	29.71 Constant	MPa	Maximum SSE stress from Table 4-6 [23] is combined membrane and bending stress
4003	Earthquake Δ Inertial Bending	0 Constant	MPa	SSE bending stresses captured in Global ID 4002
4004	Earthquake Δ Anchor Bending	0 Constant	MPa	SSE bending stresses captured in Global ID 4002

Global ID	Name	Value / Distribution Parameters	Units	Basis
4121	Membrane Stress (DW)	0 Constant	MPa	Stress from [23] is combined DW and thermal, so this input is set to 0, and Global ID 4124 contains the DW contribution
4122	Maximum Bending Stress (DW)	0 Constant	MPa	Stress from [23] is combined DW and thermal, so this input is set to 0, and Global ID 4124 contains the DW contribution
4123	Membrane Stress (Thermal)	0 Constant	MPa	Stress from [23] is combined DW and thermal, so this input is set to 0, and Global ID 4124 contains the thermal contribution
4124	Bending Stress (Thermal)	74.38 Constant	MPa	Stress from [23] is combined DW and thermal; used the limiting thermal maximum

Global ID	Name	Value / Distribution Parameters		Units	Basis
N/A	Hoop WRS Pre-Mitigation	Mean	Std. Dev.	MPa	Mean hoop WRS profile and standard deviation based on analysis for generic CE branch line geometry as documented in Section C5.2
		91.43	76.7		
		136.17	76.7		
		173.20	76.7		
		223.04	76.7		
		321.41	76.7		
		353.55	76.7		
		323.67	76.7		
		279.46	76.7		
		229.43	76.7		
		159.52	76.7		
		114.54	76.7		
		72.28	76.7		
		71.63	76.7		
		77.13	76.7		
		136.84	76.7		
		110.97	76.7		
		163.95	76.7		
		229.93	76.7		
		209.21	76.7		
		218.51	76.7		
		250.47	76.7		
		261.70	76.7		
		243.47	76.7		
		234.81	76.7		
		248.73	76.7		
		252.10	76.7		

Global ID	Name	Value / Distribution Parameters	Units	Basis
N/A	Axial WRS Pre-Mitigation	Mean Std. Dev. -152.59 57.9 -100.70 57.9 -45.09 57.9 1.38 57.9 75.69 57.9 97.53 57.9 64.70 57.9 22.01 57.9 -76.55 57.9 -129.83 57.9 -145.23 57.9 -215.12 57.9 -214.80 57.9 -204.85 57.9 -179.97 57.9 -136.36 57.9 -69.80 57.9 12.75 57.9 47.64 57.9 108.06 57.9 156.35 57.9 187.73 57.9 185.37 57.9 194.95 57.9 210.02 57.9 205.36 57.9	MPa	Mean axial WRS profile and standard deviation based on analysis for generic CE branch line geometry as documented in Section C5.2
5101-5110	Pre-Mitigation Inspection Properties	beta_0 (circ): Normal (2.71, 0.21) beta_1 (circ): Normal (0.31, 0.45) beta_0 (axial): Normal (-0.8, 0.38) beta_1 (axial): Normal (8.3, 1.45) a (circ): Normal (0.034, 0.006) b (circ): Normal (0.955, 0.013) a (axial): Normal (0.041, 0.011) b (axial): Normal (0.88, 0.029) Sigma_depth (circ): 0.072 Sigma_depth (axial): 0.078	-	Uses values for the pressurizer surge line per the recommendations in [61]

Global ID	Name	Value / Distribution Parameters	Units	Basis
Correlation 5101-5102	Intercept, B0 (circ) Intercept, B1 (circ)	-0.86	-	Uses values for the pressurizer surge line per the recommendations in [61]
Correlation 5103-5104	Intercept, B0 (axial) Intercept, B1 (axial)	-0.93	-	Uses values for the pressurizer surge line per the recommendations in [61]
Correlation 5105-5106	a (circ) b (circ)	-0.867	-	Uses values for the pressurizer surge line per the recommendations in [61]
Correlation 5107-5108	a (axial) b (axial)	-0.87	-	Uses values for the pressurizer surge line per the recommendations in [61]
9003	TW Crack Distance Rule Modifier	Uniform (0, 508)	mm	The circumference of the shutdown cooling system piping is similar enough to the pressurizer surge line to use the same upper bound from Case 2.1.0

B22 Case 5.2.1

The objective of Case 5.2.1 was to assess the base likelihood of failure with pre-existing flaws and subsequent PWSCC growth of circumferential and axial cracks without mechanical mitigation for CE cold leg branch line nozzle DMWs. The effects of leak detection, ISI, and SSE were also assessed.

The random seeds used for the Case 5.2.1 analyses were as follow:

Simulation Description	Epistemic Random Seed	Aleatory Random Seed
5000-realization simulation using the epistemic (outer) loop	6128	369

The other inputs were developed using the Case 5.2.0 input set as a template with the following modifications:

Global ID	Name	Value / Distribution Parameters	Units	Basis
N/A	Case Description	5.2.01	-	Based on case description
0501	Crack Initiation Type Choice	0	-	Based on case description
1209	Number of Flaws (Circ)	1 Constant	-	Considers the impact of one circumferential crack and one axial crack because the likelihood of multiple cracks is low enough to not affect the results as demonstrated in [2]
1210	Initial Flaw Full-Length (Circ) (*)	Lognormal (1, 4.3E-3, 2.226)	m	Based on PWSCC initial flaw sizes
1211	Multiplier Starting Full-Length (Circ)	1 Constant	-	Based on PWSCC initial flaw sizes

Global ID	Name	Value / Distribution Parameters	Units	Basis
1212	Initial Flaw Depth (Circ) (*)	Lognormal (1, 1.5E-3, 1.419, min=5E-4, max=0.0663)	m	Based on PWSCC initial flaw sizes
1213	Multiplier Starting Depth (Circ)	1 Constant	-	Based on PWSCC initial flaw sizes
1214	Number of Flaws (Axial)	1 Constant	-	Considers the impact of one circumferential crack and one axial crack because the likelihood of multiple cracks is low enough to not affect the results as demonstrated in [2]
1215	Initial Flaw Full-Length (Axial) (*)	Lognormal (1, 4.3E-3, 2.226)	m	Based on PWSCC initial flaw sizes
1216	Multiplier Starting Full-Length (Axial)	1 Constant	-	Based on PWSCC initial flaw sizes
1217	Initial Flaw Depth (Axial) (*)	Lognormal (1, 1.5E-3, 1.419, min=5E-4, max=0.0663)	m	Based on PWSCC initial flaw sizes
1218	Multiplier Starting Depth (Axial)	1 Constant	-	Based on PWSCC initial flaw sizes

B23 Case 1.3.0

The objective of Case 1.3.0 was to assess the base likelihood of failure caused by PWSCC initiation and growth without mechanical mitigation for Westinghouse two- and three-loop RVON and RVIN DMWs. The effects of leak detection, ISI, and SSE were also assessed.

The random seeds used for the Case 1.3.0 analyses were as follow:

Simulation Description	Replicate Simulation No.	Epistemic Random Seed	Aleatory Random Seed
100,000-realization composite simulation using the epistemic (outer) loop	1	1515	13118
	2	1974	713705
	3	2002	1503
	4	2004	909
	5	2010	907
	6	3131	131521
	7	4512	1685
	8	5121	919
	9	41520	2025
	10	1415	23118

The other inputs were developed using the Case 1.1.0 inputs set from the prior study [2] as a template with the following modifications:

Global ID	Name	Value / Distribution Parameters	Units	Basis
N/A	Case Description	1.3.00	-	Based on case description
003	Crack Orientation	3	-	Option to include both circumferential and axial cracks
0808-0808.10	Inspection Month	N/A	-	Inspection defined as an annual frequency

Global ID	Name	Value / Distribution Parameters	Units	Basis
0811	Inspection Schedule Input Type	1	-	Inspection defined as an annual frequency
0812	Pre-Mitigation Inspection Freq	0.1	1/yr	Annual frequency set to one inspection every 10 years
0820	Number of cracks detected	1	-	All cracks detected independently per case description
0904	Max time between 2 check - single TWC - CC	1	mon	For post-processing purposes per case description
All uncertain variables, except Global ID 2528	Data Source	Epistemic	-	Outer loop preserves LHS structure
1101	Pipe Outer Diameter	0.863 Constant	m	Largest diameter for the plants represented by bin
1102	Pipe Wall Thickness	0.056 Constant	m	Smallest thickness for the plants represented by bin
1104	Weld Material Thickness	0.056 Constant	m	Set to same value as Global ID 1102

Global ID	Name	Value / Distribution Parameters	Units	Basis
3002	Unmitigated H2 Level	25 Constant	cc/kg	Bounds the operating experience of PWRs as reported in [48]
3101	Operating Pressure	15.51 Constant	MPa	Highest operating pressure for the plants represented by bin
3102	Operating Temperature	326 Constant	°C	Highest operating temperature for the plants represented by bin
4001	Earthquake Probability	0.001 Constant	1/yr	Same value as used for analyses of other cases in this study (e.g., Case 2.1.0)
4002	Earthquake Δ Total Membrane	7.6 Constant	MPa	Largest SSE membrane stress for the plants represented by bin
4003	Earthquake Δ Inertial Bending	29.8 Constant	MPa	Largest SSE bending stress for the plants represented by bin
4004	Earthquake Δ Anchor Bending	0 Constant	MPa	All SSE bending stresses captured in Global ID 4003

Global ID	Name	Value / Distribution Parameters	Units	Basis
4101	Fx (Dead Weight)	0 Constant	kN	Set to 0 because all loads input as stresses instead of forces and moments
4102	Mx (Dead Weight)	0 Constant	kN-m	Set to 0 because all loads input as stresses instead of forces and moments
4103	My (Dead Weight)	0 Constant	kN-m	Set to 0 because all loads input as stresses instead of forces and moments
4104	Mz (Dead Weight)	0 Constant	kN-m	Set to 0 because all loads input as stresses instead of forces and moments
4105	Fx (Thermal Expansion)	0 Constant	kN	Set to 0 because all loads input as stresses instead of forces and moments
4106	Mx (Thermal Expansion)	0 Constant	kN-m	Set to 0 because all loads input as stresses instead of forces and moments

Global ID	Name	Value / Distribution Parameters	Units	Basis
4107	My (Thermal Expansion)	0 Constant	kN-m	Set to 0 because all loads input as stresses instead of forces and moments
4108	Mz (Thermal Expansion)	0 Constant	kN-m	Set to 0 because all loads input as stresses instead of forces and moments
4121	Membrane Stress (DW)	0 Constant	MPa	All membrane stresses captured in Global ID 4123
4122	Maximum Bending Stress (DW)	0 Constant	MPa	All bending stresses captured in Global ID 4124
4123	Membrane Stress (Thermal)	1.69 Constant	MPa	Largest membrane stress for the plants represented by bin
4124	Bending Stress (Thermal)	100.92 Constant	MPa	Largest bending stress for the plants represented by bin
N/A	Hoop WRS Pre-mitigation	Unchanged from reference case	MPa	No-repair hoop WRS profile
N/A	Axial WRS Pre-mitigation	Unchanged from reference case	MPa	No-repair axial WRS profile

Global ID	Name	Value / Distribution Parameters	Units	Basis
5004	Lower bound POD, POD_0	0 Constant	-	Even though it is not used, the default 0.999 value would lead to 99.9 percent probability of detection for a crack of zero depth

B24 Case 1.3.1

The objective of Case 1.3.1 was to assess the base likelihood of failure with pre-existing flaws and subsequent PWSCC growth of circumferential and axial cracks without mechanical mitigation for Westinghouse 2- and 3-loop RVON and RVIN DMWs. The effects of leak detection, ISI, and SSE were also assessed.

The random seeds used for the Case 1.3.1 analyses were as follow:

Simulation Description	Epistemic Random Seed	Aleatory Random Seed
5000-realization simulation using the epistemic (outer) loop	6128	369

The other inputs were developed using the Case 1.3.0 input set as a template with the following modifications:

Global ID	Name	Value / Distribution Parameters	Units	Basis
N/A	Case Description	1.3.01	-	Based on case description
0501	Crack Initiation Type Choice	0	-	Based on case description
1209	Number of Flaws (Circ)	1 Constant	-	Considers the impact of one circumferential crack and one axial crack because the likelihood of multiple cracks is low enough to not affect the results as demonstrated in [2]
1210	Initial Flaw Full-Length (Circ) (*)	Lognormal (1, 4.3E-3, 2.226)	m	Based on PWSCC initial flaw sizes
1211	Multiplier Starting Full-Length (Circ)	1 Constant	-	Based on PWSCC initial flaw sizes

Global ID	Name	Value / Distribution Parameters	Units	Basis
1212	Initial Flaw Depth (Circ) (*)	Lognormal (1, 1.5E-3, 1.419, min=5E-4, max=0.0663)	m	Based on PWSCC initial flaw sizes
1213	Multiplier Starting Depth (Circ)	1 Constant	-	Based on PWSCC initial flaw sizes
1214	Number of Flaws (Axial)	1 Constant	-	Considers the impact of one circumferential crack and one axial crack because the likelihood of multiple cracks is low enough to not affect the results as demonstrated in [2]
1215	Initial Flaw Full-Length (Axial) (*)	Lognormal (1, 4.3E-3, 2.226)	m	Based on PWSCC initial flaw sizes
1216	Multiplier Starting Full-Length (Axial)	1 Constant	-	Based on PWSCC initial flaw sizes
1217	Initial Flaw Depth (Axial) (*)	Lognormal (1, 1.5E-3, 1.419, min=5E-4, max=0.0663)	m	Based on PWSCC initial flaw sizes
1218	Multiplier Starting Depth (Axial)	1 Constant	-	Based on PWSCC initial flaw sizes

APPENDIX C
WELDING RESIDUAL STRESS PROFILE DEVELOPMENT

C1 Introduction to Weld Residual Stress Profile Development

Welding is the preferred method for connecting many components in nuclear power plants. Welds are used for vessel fabrication, piping and nozzle connections, reactor and piping supports, vessel head and bottom penetration connections, along with many other component fabrications. The welding process consists of applying a heat source and often weld filler metal along the weld path. Shrinkage of the weld beads during cooling leads to the development of WRS in components. The WRS profiles may have stress components greater than the yield stress because the stress state is multiaxial and, at locations where the mean stress is high, the component stresses can be quite high. Material hardening also plays a role. Moreover, in many applications, especially nuclear components, weld repairs are often necessary to remove defects. The WRS profiles caused by the repair welds are often more severe (i.e., produce higher tensile WRS that promotes crack growth) as compared with the original WRS state. Also, WRS profiles are often self-equilibrating. For instance, the axial WRS profiles produced from the nozzle-to-piping dissimilar metal butt-welds considered in this study are typically close to self-equilibrating while the hoop WRS profiles are not. However, it is noted that repair welds have repair lengths only partway around the circumference of the weld. Therefore, the WRS profile near the start and stop locations of the repair are often quite different from those at the midpoint as reported by Brust and others [83].

A physical perspective for the development of WRS profiles is provided in Chapter 7, “Residual Stress and Distortion,” of the 2019 *Welding Handbook* [84], which describes weld bead shrinkage and geometry effects of residual stress development, among other factors. For complex geometries, the development of the WRS profile can be more involved and requires a nonlinear finite element solution of the welding process where the deposition of each pass is modeled. The history behind the development of computational weld models is summarized in many of the references cited in the *Welding Handbook*.

C1.1 Existing Library of WRS Profiles

A series of WRS profiles were developed for use in xLPR code simulations for several different nozzle geometries as documented in the xLPR WRS Subgroup report [47]. Hoop and axial WRS profiles were developed for three typical PWR nozzle geometries: (i) hot and cold leg nozzles, (ii) steam generator inlet and outlet nozzles, and (iii) RCP inlet and outlet nozzles. These nozzles are representative of many of the nozzles of interest for LBB assessment using the xLPR code. The factors that affect the WRS include the number of weld and butter passes, nozzle geometry (e.g., thickness, diameter, and taper), heat input, weld groove geometry, distance between the DMW and the SS closure weld, and weld repair depth, among others. For each nozzle geometry, the xLPR WRS Subgroup developed no-repair WRS profiles and WRS

profiles considering repair depths of 15 and 50 percent. A separate procedure summarized in the WRS essential parameters and profile selection document [85] was developed for use by the NRC and EPRI project teams for the purposes of this study to determine which, if any, of the existing library of WRS solutions were applicable to the geometries of interest in the present study. If it was determined following this procedure that a particular geometry was not sufficiently represented by an existing solution, then a new solution was developed.

The WRS profiles in the xLPR WRS Subgroup report [47] were developed so that uncertainties could be calculated for use in the xLPR code simulations. These uncertainties were developed by having four experienced modelers develop solutions for each of the geometries considered. Each modeler developed solutions using both isotropic and nonlinear kinematic hardening (NLKH) laws because these laws strongly influence the magnitude of the predicted results. The average of the isotropic and NLKH solutions for each modeler was used because it provides the best estimate of the WRS profiles as described in [47]. The modeling efforts provided a series of WRS profiles for each geometry and repair depth and the WRS uncertainty was assessed as discussed in [47] and then used as an input to the xLPR code.

The standard deviation was estimated at each point through the weld thickness in [47]. An average standard deviation over all 26 points was then recommended to represent uncertainties. This averaging approach produced a more stable estimate of the standard deviation because it was based on 504 data points (i.e., 4 WRS profiles times 26 through-thickness data points per profile) versus only 4 data points at each through-thickness location. This approach was validated as discussed in [47], and the same approach was applied for the WRS profiles developed for this study.

C1.2 Mechanical Mitigation

The two types of mechanical mitigation against PWSCC most often used in PWR nuclear power plants that affect the WRS profile are weld overlay and MSIP®. Both overlays and MSIP® reduce the inside diameter WRS profile, often making the magnitude compressive. A third type of mitigation is an inlay. It consists of depositing a layer of PWSCC-resistant Alloy 52 weld metal on the inside diameter. It was beyond the scope of the xLPR WRS Subgroup to develop mechanically mitigated WRS profiles directly from FEA solutions, so instead, they were estimated by applying a series of rules for each mechanical mitigation type that can be applied to the base, unmitigated WRS profile of interest. The rationale behind the development of these rules is discussed in [47].

C1.3 Overview of the WRS Profiles Used for the Generalization Study

The WRS profiles for each nozzle DMW considered in the present study are summarized in the Sections C2 through C6. For each DMW, it was first determined if any of the WRS profiles from the existing library of solutions in [47] would apply, and justifications for applicability of these solutions are provided. Summaries are provided for cases where new WRS profiles were developed. In the WRS essential parameters and profile selection document [85], rules were developed to identify the closest match between a selected weld type and the library of existing

WRS solutions in [47]. These rules were used as guidance to select the appropriate weld geometry for the FEA solutions presented in Sections C2 through C6.

Section C2 describes the Westinghouse pressurizer surge line nozzle DMW solutions for the base case and the more severe WRS profile that were developed for this study. Note that the base case uses a no-repair WRS profile. The more severe WRS profile was defined as one that results in a higher tensile stress at the weld inside diameter to favor more crack initiations. For the base case, the WRS profile was developed from the weld centerline as described in Section C2.1. For the more severe WRS case, it was developed from a path defined through the butter region as described in Section C2.2.

Section C3 describes the WRS profiles used for the CE and B&W RCP nozzle DMW analyses. For the base case, the WRS profile from the existing library of solutions described in [47] was selected for the reasons provided in Section C2.1. A no-repair WRS profile was used. Section C2.2 describes the more severe WRS profile developed from a path defined through the butter region.

Section C4 describes the WRS profiles used for the Westinghouse steam generator nozzle DMW analyses. Reference [47] provides the WRS profiles for a conventional, single-vee groove geometry. Section C4.1 describes the geometry and welding sequence for the double-vee groove replacement stream generator case. Section 1.1.1.1.1A1.1 describes the base case WRS profiles. Section C4.3 describes the more severe WRS profiles, which were again developed from a path defined through the butter region. As discussed in [47], the inlay WRS profiles were estimated by developing rules based on inlay solutions in the literature, because it was beyond the scope of the xLPR WRS Subgroup to develop mechanical mitigation WRS profiles directly from FEA solutions.

Section C5 summarizes the WRS profiles developed for the CE hot and cold leg branch line nozzle DMWs. Section C5.1 describes the geometries and welding sequences. Section C5.2 describes the base case WRS profiles, which are no-repair. The more severe WRS profile is summarized in Section C5.3. This profile was developed for a closure weld that was farther from the DMW as compared to the base case.

Finally, Section C6 describes the WRS profiles used for the Westinghouse two- and three-loop RVON and RVIN DMW analyses. These WRS profiles come from the existing library of solutions in [47]. The baseline WRS profiles are summarized in Section C6.1. They are for the no-repair case. The more severe WRS profiles are summarized in Section C6.2. These profiles were developed from a different PWR RVON weld geometry.

C2 Westinghouse Pressurizer Surge Line Nozzle DMWs

The pressurizer surge line connection to the pressurizer is a geometry that does not fit into the categories of WRS profiles summarized in [47]. The nozzle geometry is unique because it has a fill-in weld, which is shown in Figure C-1. During the fabrication process, the fill-in weld is applied prior to the SS weld. A Westinghouse fill-in type pressurizer surge nozzle weld was chosen to develop the WRS profile because it is the most prevalent type. Of note, the fill-in

weld tends to produce higher tensile WRS fields. The NRC/EPRI Phase 2b round robin mockup problem was used to obtain the WRS profiles for Case 2.1.0 assuming no repairs. The mockup description, model geometry, dimensions, material properties, and WRS solution results for ten independent modelers are summarized in NUREG-2162, "Weld Residual Stress Finite Element Analysis Validation: Part 1 – Data Development Effort," issued March 2014 [86], NUREG-2228, "Weld Residual Stress Finite Element Analysis Validation, Part II – Proposed Validation Procedure, Final Report," issued July 2020 [87], the Phase 2b finite element round robin results technical letter report, issued December 2015 [75], and by Rathburn and others [88]. The geometry and weld definition are illustrated in Figure C-1.

The welding procedure for this geometry consists of the following steps:

1. add butter
2. apply post-weld heat treatment (PWHT)
3. machine the butter in preparation for the DMW
4. add DMW beads
5. add fill-in weld on the inside diameter
6. add SS closure safe-end-to-pipe weld

There was no repair weld considered for this case. Each of the 10 participants provided their WRS profiles along the weld centerline path, which is illustrated in Figure C-1, as the average of the isotropic and NLKH results. These data were then compiled so that the uncertainty in the participants' results could be used to define the uncertainty in the WRS profile.

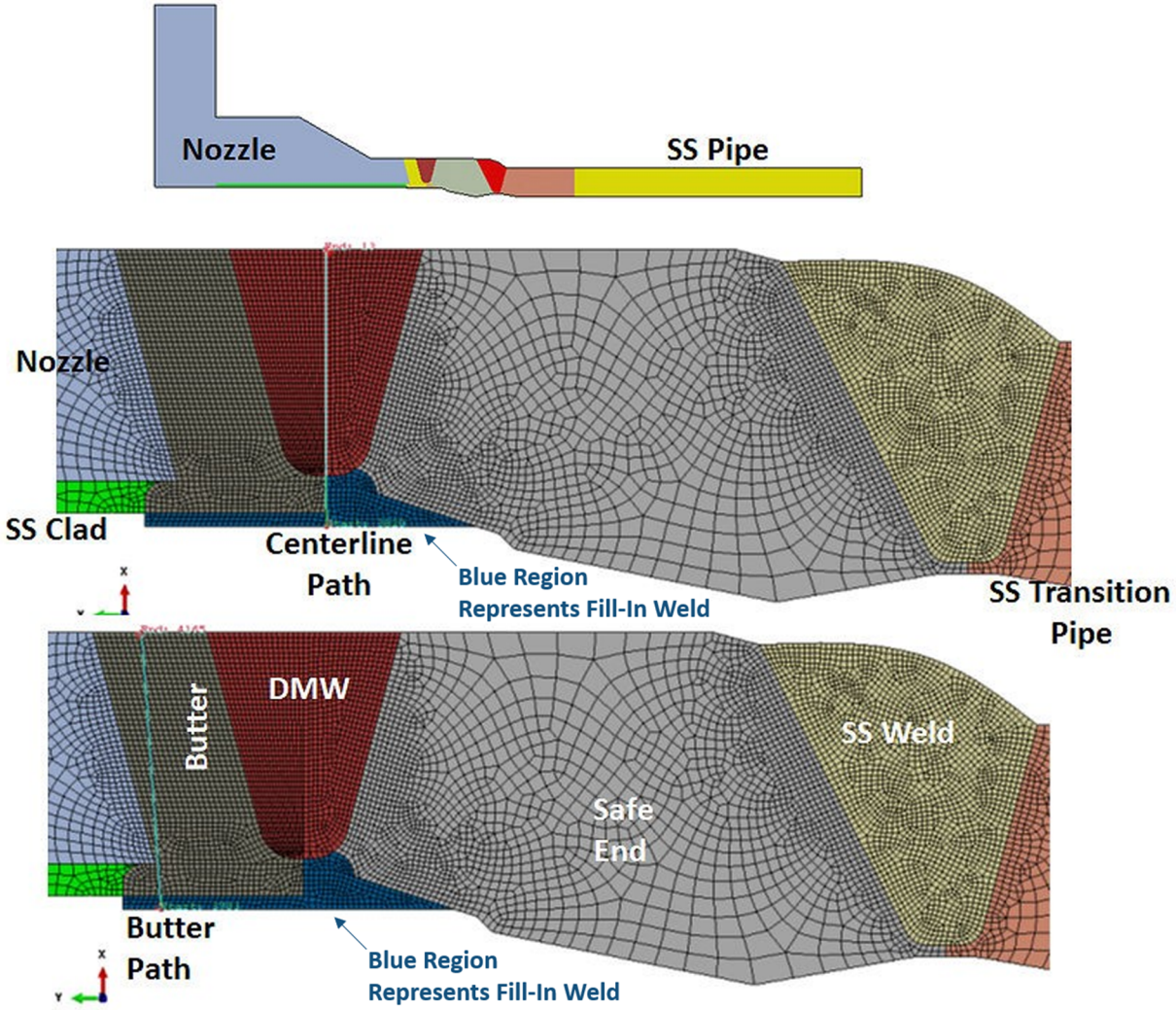

Figure C-1 FEA model for pressurizer surge line nozzle with fill-in weld used for WRS profile development

C2.1 Baseline and Mitigated WRS Profiles

The axial and hoop WRS profiles plotted through the center of the pressurizer surge line nozzle weld are illustrated in Figure C-2 and Figure C-3, respectively. There is some variation among the WRS modelers, but in general the trends are quite similar. There were also WRS measurements made on this mock-up as discussed in the Phase 2b finite element round robin results technical letter report [75], and those measurements also exhibit some scatter. In general, the measurements reasonably validated the modelers' analytical predications.

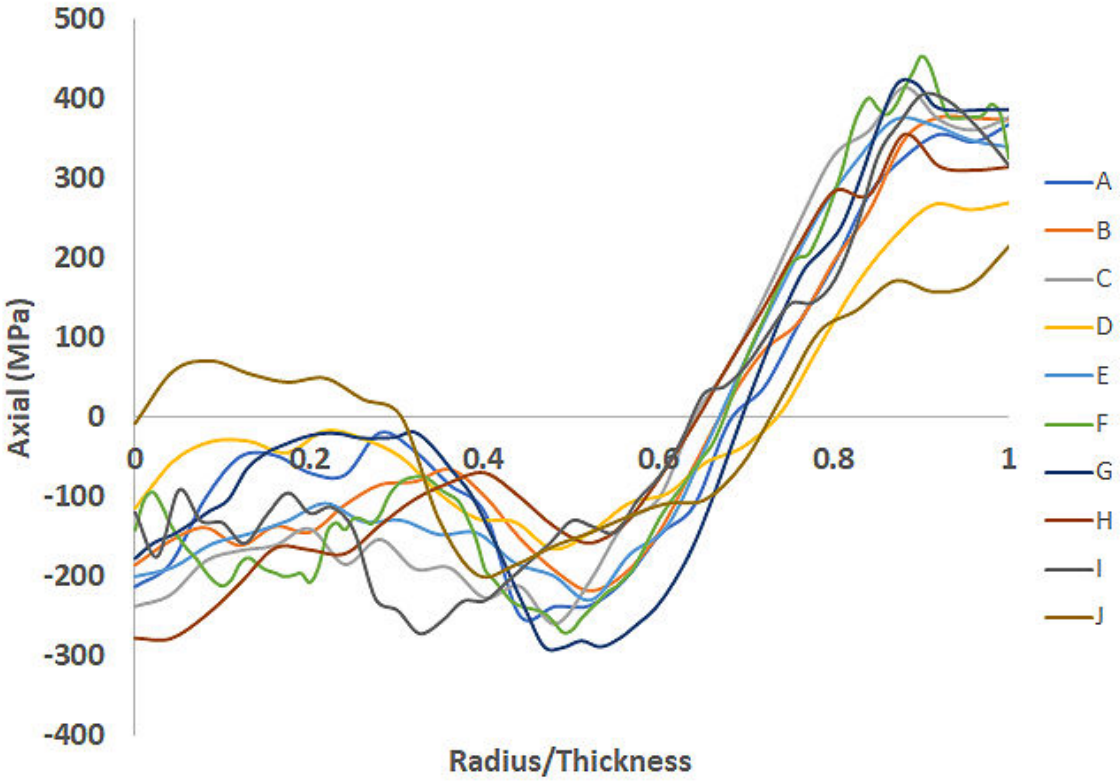

Figure C-2 Pressurizer surge line nozzle axial WRS profiles through the weld centerline from 10 modelers

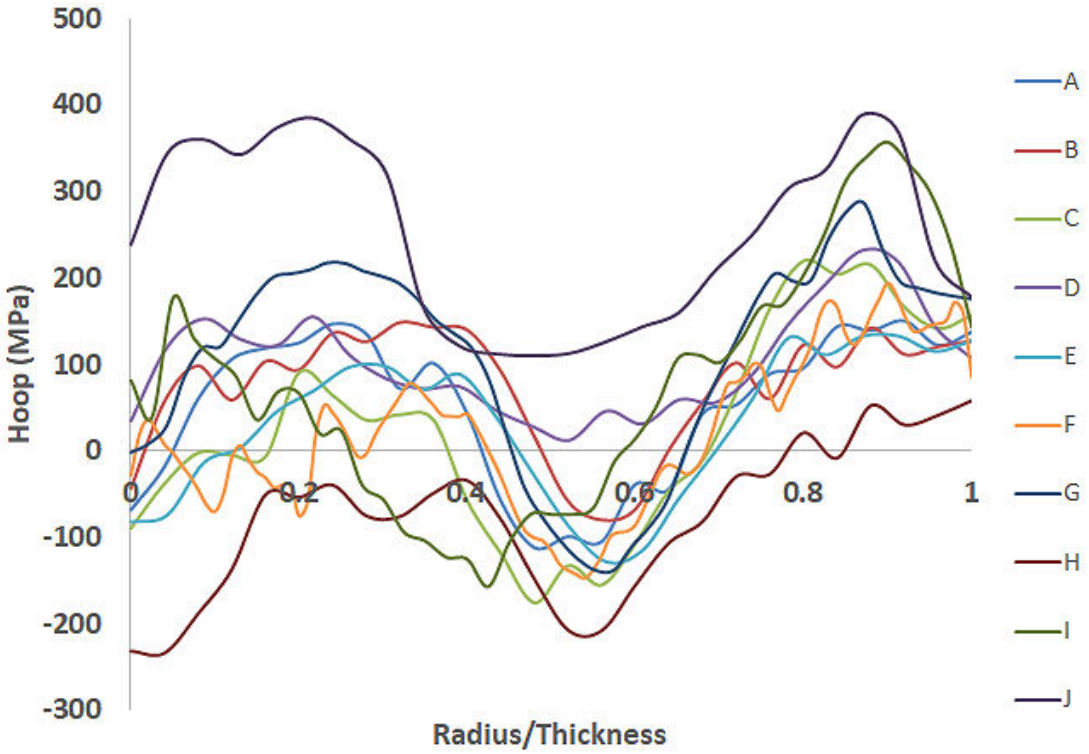

Figure C-3 Pressurizer surge line nozzle hoop WRS profiles through the weld centerline from 10 modelers

The average axial and hoop WRS profiles for the pressurizer surge line weld analyses are shown in Figure C-4 and Figure C-5, respectively. The WRS uncertainty parameters were determined using the same procedure as outlined in the xLPR WRS Subgroup report [47]. Following this procedure, a weighted mean and weighted standard deviation were calculated to reduce the impact of an outlier profile. Following this approach, the outlier solutions from Figure C-2 and Figure C-3 were given less weight in determining the mean and standard deviation values.

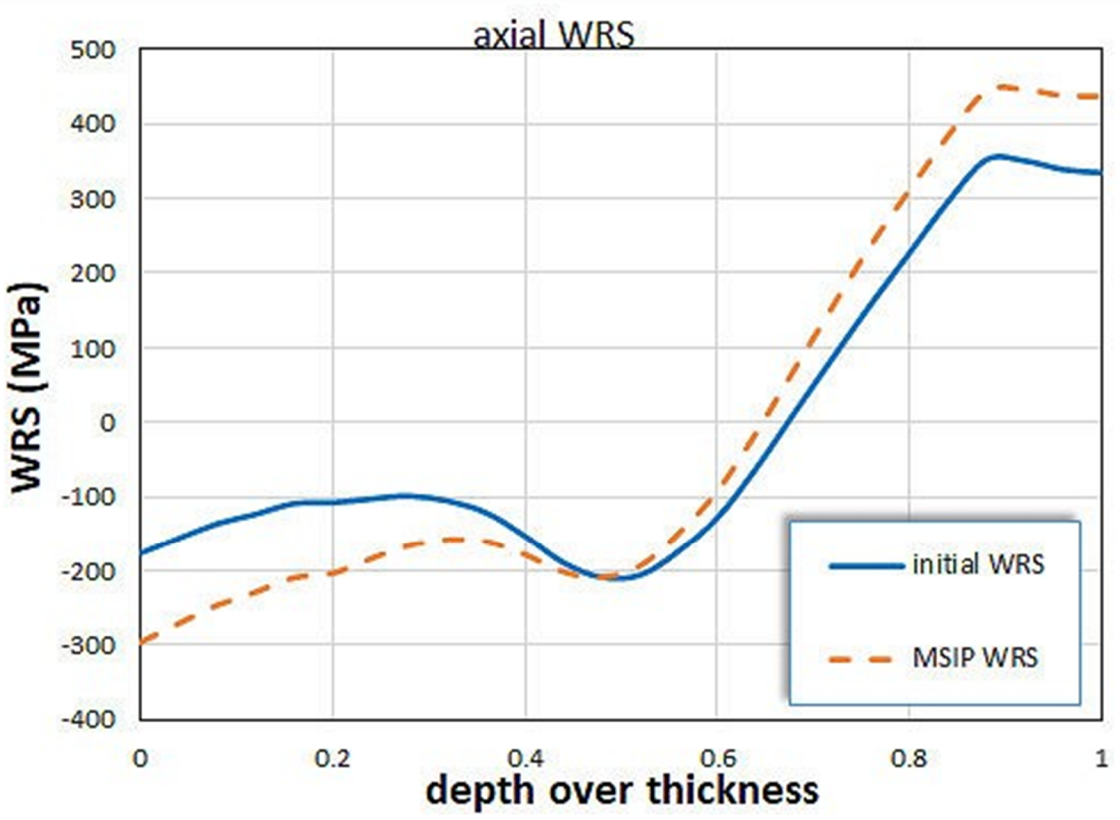

Figure C-4 Pressurizer surge line nozzle average axial WRS profiles through the weld centerline

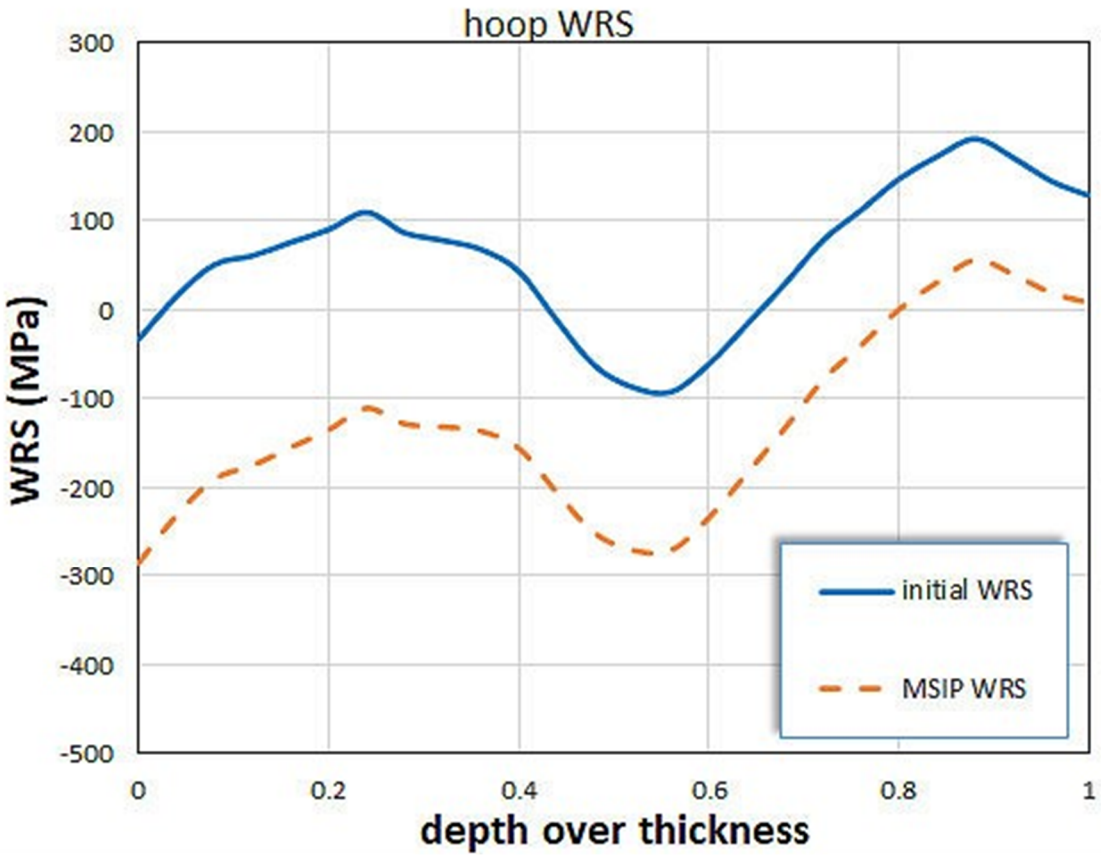

Figure C-5 Pressurizer surge line nozzle average hoop WRS profiles through the weld centerline

From the case descriptions, mechanical mitigation of the pressurizer surge line nozzle DMWs was also considered. For Case 2.1.3, the WRS profiles were obtained using the rules in [47] for overlay mitigation as shown in Figure 3-31. The main effect of the overlay is to reduce the inside diameter residual hoop stress, thereby reducing the probability of axial PWSCC initiation. The overlay slightly increases the inside diameter residual axial stress. For Case 2.1.5, the rules in [47] for MSIP® mitigation were applied to the mean pre-mitigation WRS profiles. The results are shown in Figure 3-43. The effect of MSIP® is to reduce the inside diameter residual stress, thereby reducing the probability of both axial and circumferential PWSCC initiation.

C2.2 More Severe WRS Profile

Case 2.1.2 was analyzed using a more severe WRS profile. For this case, an off-center location was selected. From the WRS contour plots shown in Figure C-6, a location in the Alloy 182 butter was chosen. The WRS at the inside diameter in the butter region is less compressive than at the weld centerline (i.e., -210 MPa versus -280 MPa). This figure shows the WRS generated using the isotropic hardening law; however, the same effect is seen with NLKH. Because the participants in the round robin study only extracted WRS results at the weld centerline, only the Emc^2 solution was used to develop the more severe WRS profile. Figure C-7 shows line plots for the Emc^2 results in the butter. They provide a higher axial WRS

at the inside diameter as compared to the Emc^2 weld centerline results. The average of the 10 participants' results for the weld centerline are shown for reference in the figure. The differences between the Emc^2 weld centerline results and the 10 participants' weld centerline results were used to adjust the Emc^2 butter results so that it would be more representative of a solution as if it were based on data from all 10 participants.

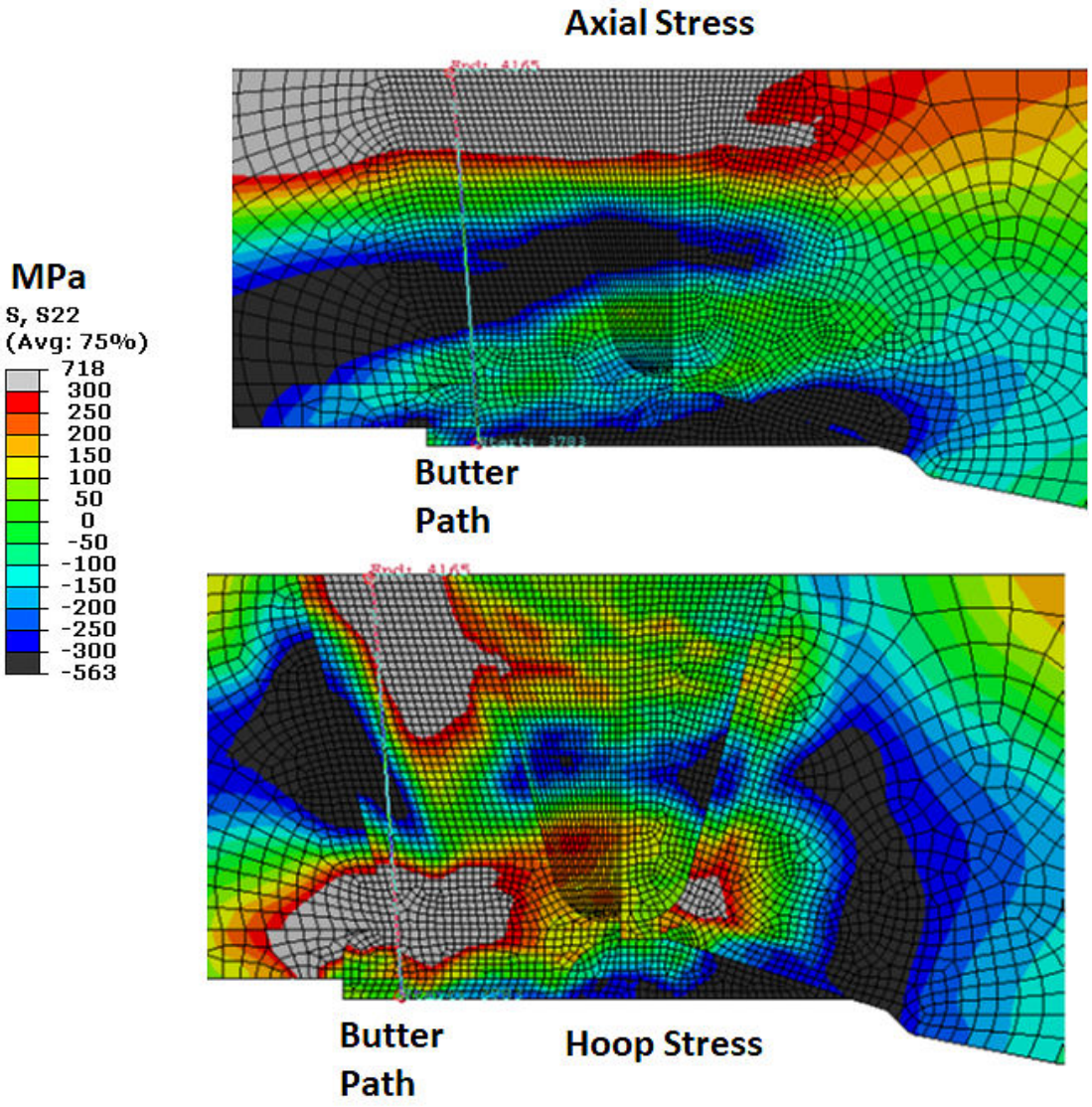

Figure C-6 Pressurizer surge line nozzle axial and hoop WRS contour plots generated from FEA with isotropic hardening law

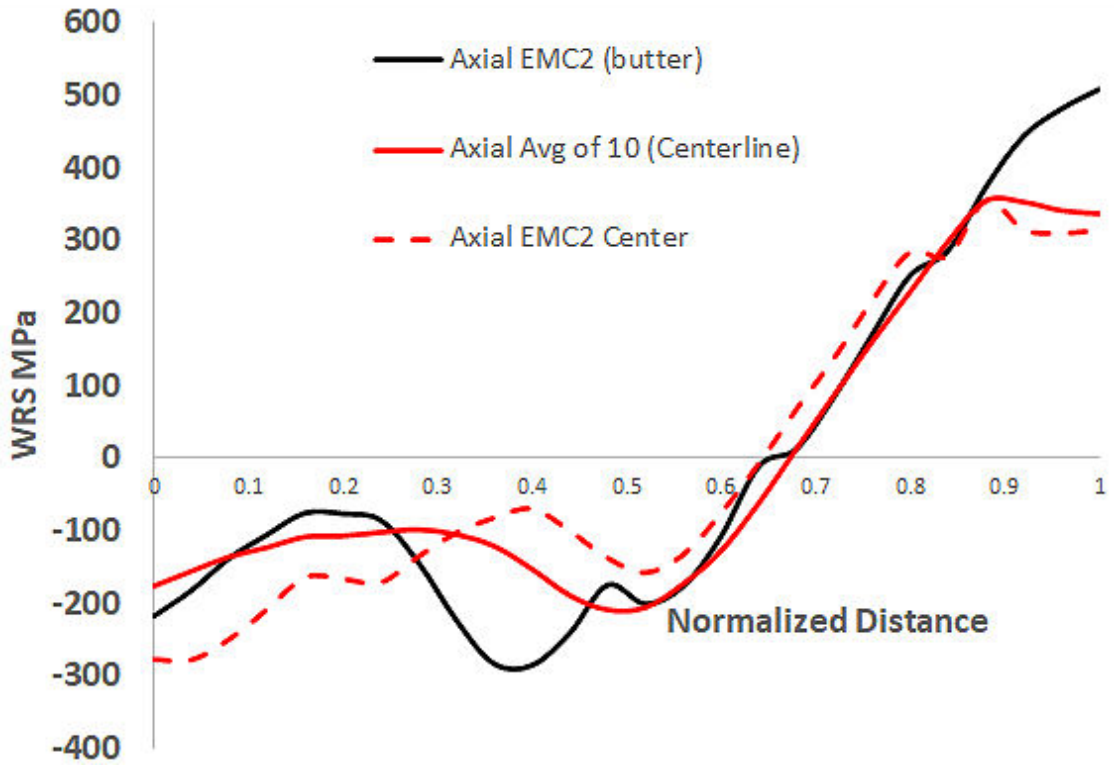

Figure C-7 Pressurizer surge line nozzle axial WRS profiles through the weld centerline and butter using the average of the isotropic and NLKH solutions

C3 CE and B&W RCP Nozzle DMWs

C3.1 Baseline WRS Profiles

B&W RCP WRS profiles are available in the xLPR WRS Subgroup report [47]. The only dissimilar metal butt-welds in the reactor coolant system main loop piping in a B&W plant are at the piping connections to the RCP at the lower cold leg and the upper cold leg locations. Of note, a B&W plant has two steam generators with two RCPs per generator; therefore, a total of eight DMWs are present within the system. The nozzle weld geometry and materials are shown in Figure C-8, and a more complete description of the FEA model and results is provided in [47]. For the RCP, the no-repair WRS profile was used because it has the highest mean stress on the inside diameter. For completeness, the mean profile is shown in in Figure C-9 along with results from the four modelers.

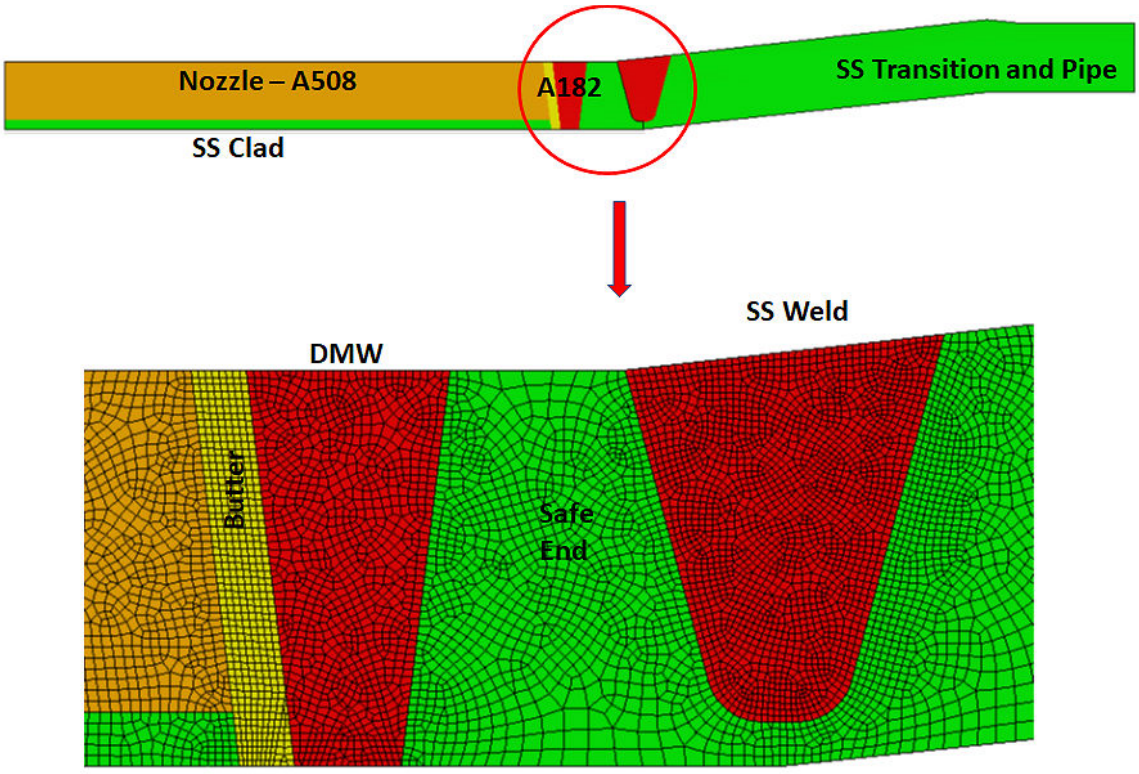

Figure C-8 FEA model used for RCP nozzle WRS profile development

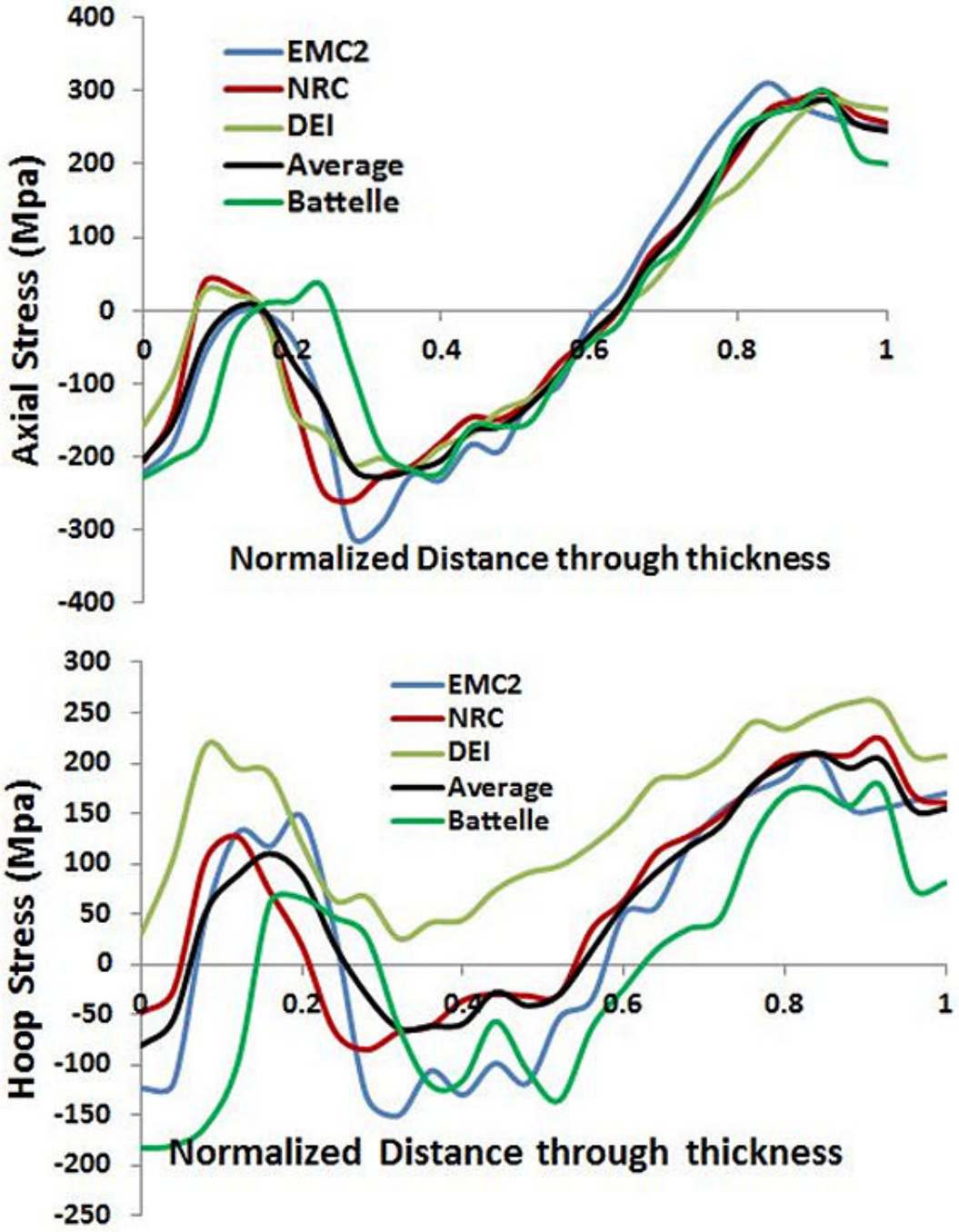

Figure C-9 RCP nozzle axial and hoop WRS profiles through the weld centerline

C3.2 More Severe WRS Profile

For the RCP, the more severe WRS profile was developed by finding a region in the DMW where the inside diameter residual stresses were the highest. Figure C- 10 shows contour plots from the Emc^2 FEA solution (the only available) using the isotropic hardening law. The upper

illustration shows the WRS around the weld centerline, and the lower illustration shows the WRS around the butter where the higher stresses exist at the inside diameter.

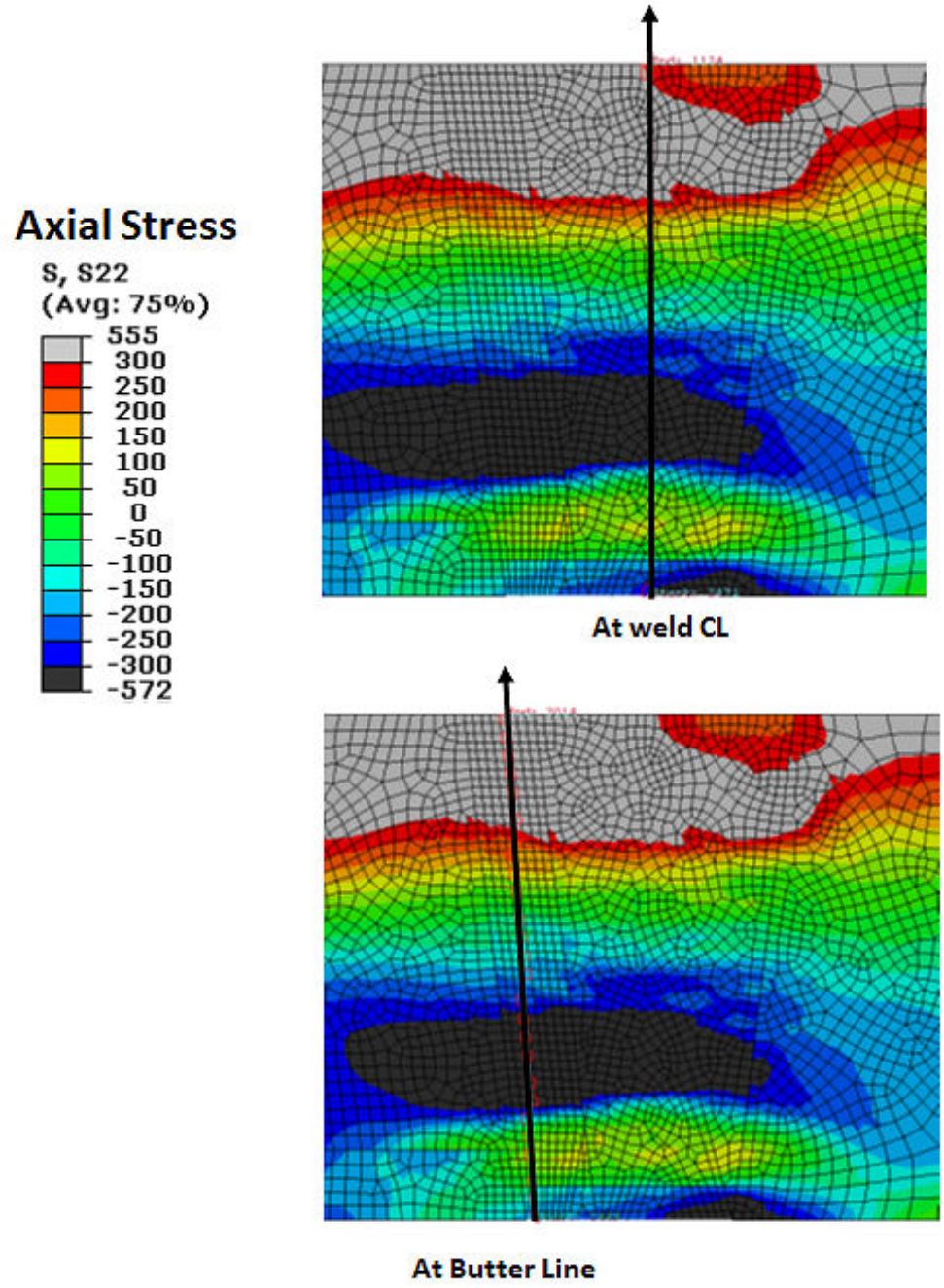

Figure C- 10 RCP nozzle axial WRS contour plots generated from FEA with isotropic hardening law

Figure C-11 shows the weld centerline axial WRS profile plots for all four analysts along with the mean. These WRS profiles are discussed in detail in [47]. Also shown is the WRS profile in the butter from the Emc^2 analysis. The differences between the Emc^2 centerline profile and the 4

participants' centerline profiles were used to adjust the Emc^2 butter results so that they would be more representative of a solution as if it were based on data from all 4 modelers. Figure C-12 shows a comparison of the axial WRS profiles though the weld centerline and butter, the latter of which represents the more severe case.

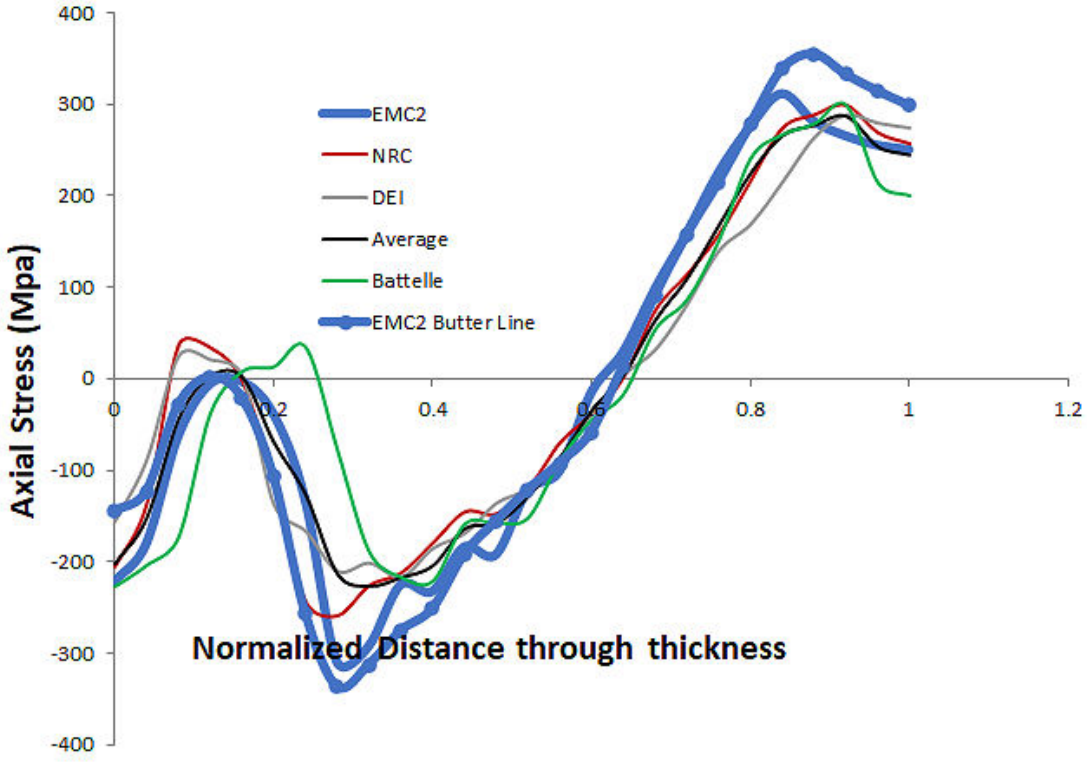

Figure C-11 RCP nozzle axial WRS profiles through the weld centerline and butter from four modelers

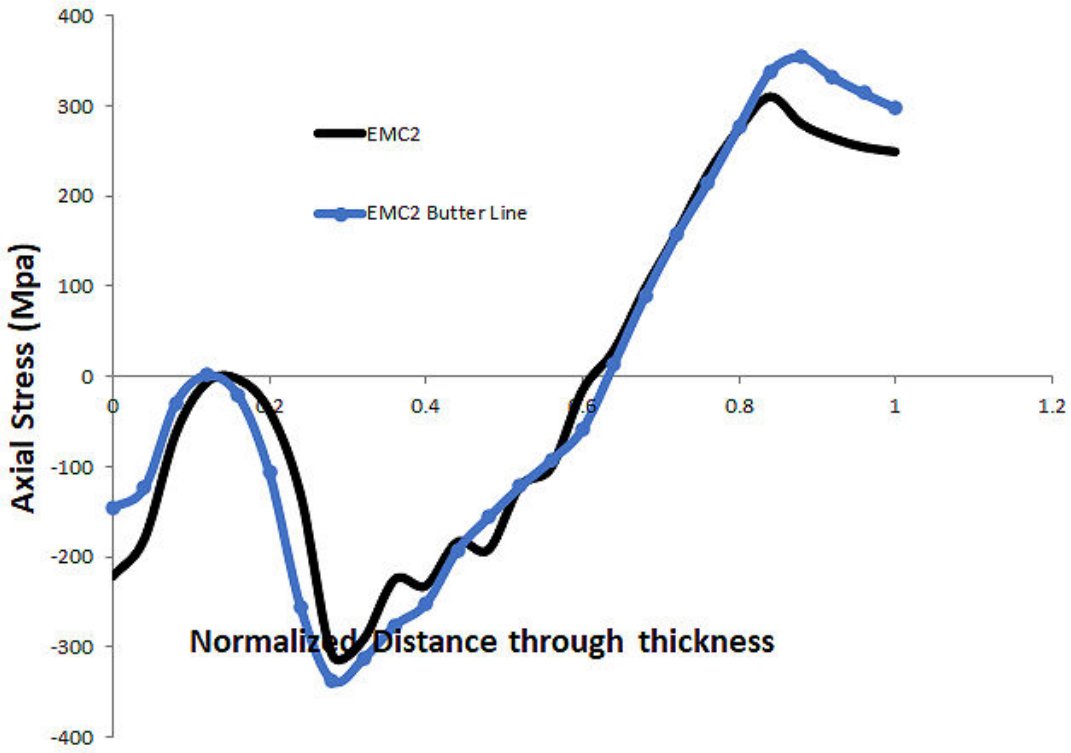

Figure C-12 RCP nozzle axial WRS profiles through the weld centerline and butter from Emc^2

C4 Westinghouse Steam Generator Nozzle DMWs

Westinghouse steam generator nozzle WRS profiles are available in the xLPR WRS Subgroup report [47] for no-repair and 15 percent and 50 percent repair depths. These solutions were also presented in detail by Brust and others [89], where PWSCC growth was also modeled as driven by the WRS profiles. These solutions are for the more typical single-vee groove geometry. However, some steam generators have been replaced with a double-vee groove geometry with an Alloy 52 inlay. These steam generators include the ones at Peach Bottom Atomic Power Station, Unit 2; North Anna Power Station, Units 1 and 2; and Virgil C. Summer Nuclear Station, Unit 1.

C4.1 Replacement Steam Generator Nozzle Geometry and Welding Sequence

The geometry, dimensions, and materials for the replacement steam generator double-vee groove weld are shown in Figure C-13. The nozzle is tapered with a 122.33 mm thickness along the weld centerline. The safe end is 177 mm from the DMW. At such a distance, the closure weld is unlikely to reduce the WRS profiles at the DMW inside diameter. Based on experience modeling other nozzles, 100 mm or less is typically required to see such an effect. The dimensions and other details regarding the weld were obtained from the April 22, 2013, letter from E. S. Grecheck, Vice President – Nuclear Engineering and Development, Virginia Electric and Power Company, to the NRC Document Control Desk [56].

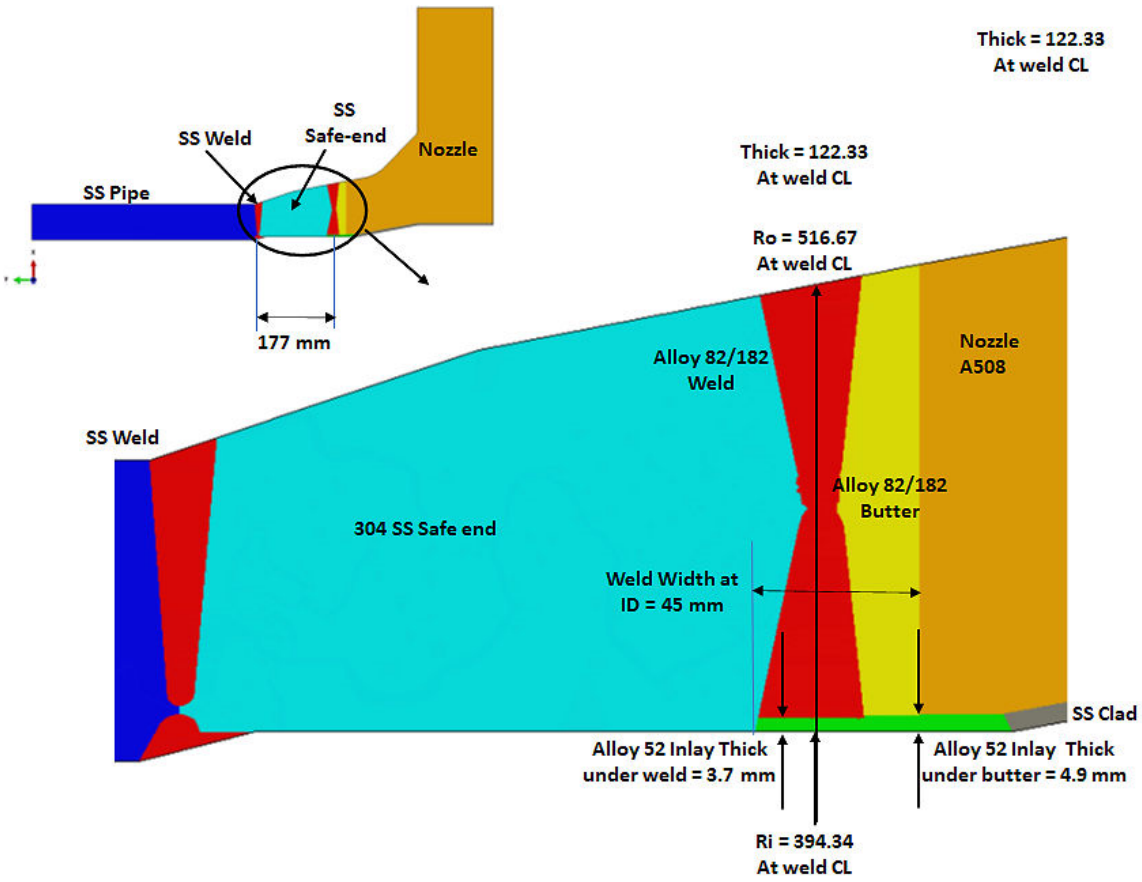

Figure C-14 Replacement steam generator nozzle geometry, dimensions, and materials

The FEA model is presented in Figure C-15. The welding sequence and modeling procedure is summarized in the following steps. As applicable, references to region numbers in these steps refer to the numbered areas in the figure.

1. Model butter application, PWHT, and machining of the butter (neglected here)
2. Model the Alloy 152 tie in Region 1 (5.6 mm thick)
3. Model the inner Region 2 vee partial groove welds
4. Model back gouge below Region 3 and add back gouge passes
5. Model the outer vee Region 3 weld passes
6. Model the inner vee Region 4 weld passes
7. Model Alloy 152 inlay in Region 5 (3.4 mm thick)
8. Model the SS closure weld
9. Model the application of the hydrotest and removal
10. Apply operating temperature of 300°C

The DMW has a double-vee groove. The butter was first applied to the nozzle, subjected to PWHT, and then machined to facilitate the double-vee groove weld. The butter and PWHT process was not included in this WRS model because, from experience, when the PWHT is applied after the butter, the effect of neglecting the PWHT is small on the final WRS field. Next, the Alloy 152 inlay tie-in (shown as Region 1 in the figure) was deposited, which was followed by the inner vee weld (Region 2). Then the back-gouge removal was modeled, and the Region 3 Alloy 182 weld was deposited followed by completion of the inside diameter weld (Region 4). Finally, the Alloy 152 inlay (shown as Region 5 in the figure) was modeled and then the SS closure weld. As is the case with all the xLPR WRS Subgroup solutions [47], afterwards a hydrostatic test was modeled and then three cycles of service load (pressure and end cap stresses only), which can help to shake down (i.e., reduce) the WRS profile to some extent. Finally, all results are presented at the operating temperature of 300°C.

An inlay performed in the field consists of removing Alloy 82/182 material under the DMW and then adding Alloy 52/152, PWSCC resistant material as discussed in detail in the xLPR WRS Subgroup report [47]. The inlay feature shown in Figure C-15 was actually applied during the steam generator replacement process and was added to enhance the DMW's resistance to PWSCC. The temperature-dependent material stress-strain curve for Alloy 82/182 and Alloy 52/152 are nearly identical. Therefore, the WRS profiles shown in Figure C-16 and Figure C-17 are the same regardless of whether Alloy 82/182 or Alloy 52/152 is deposited. Therefore, analyses can be made using this WRS field for either material.

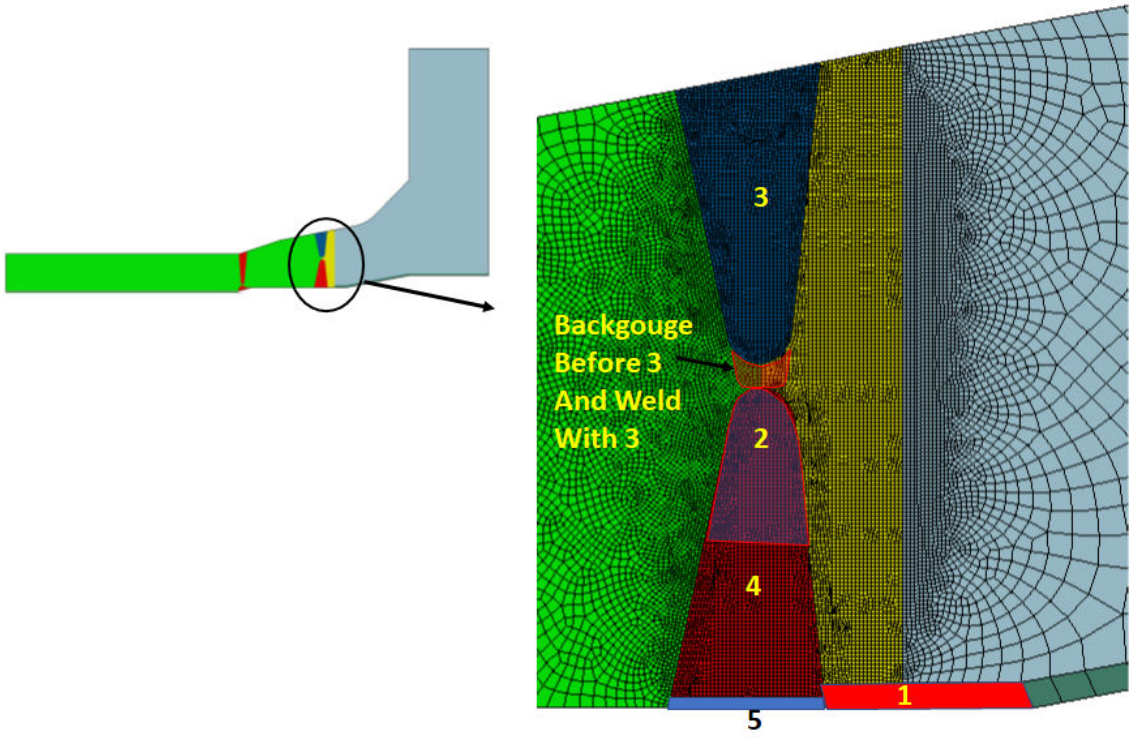

Figure C-15 FEA model used for replacement steam generator nozzle WRS profile development

C4.2 Baseline and Mitigated WRS Profiles

As described above, the replacement steam generator weld is a unique geometry because it includes an inlay of PWSCC-resistant Alloy 152 material, but the inlay was deposited during the original fabrication sequence rather than during an outage.

Figure C-16 and Figure C-17 provide the axial and hoop WRS profiles, respectively, for isotropic and NLKH laws, and the average stresses through the weld centerline. The average WRS profile is used for Cases 4.1.0, 4.1.1, and 4.1.2. The uncertainty in the WRS profile was assumed to be similar as in [47]. Because the Alloy 152 inlay was deposited at the end of the weld sequence, and the closure weld had little effect, the inside diameter axial stresses are tensile.

Overlay mitigation was also considered for the steam generator nozzle DMWs in Case 4.1.3. The WRS profiles for this case were obtained using the rules from [47] and are shown in Figure **3-69**.

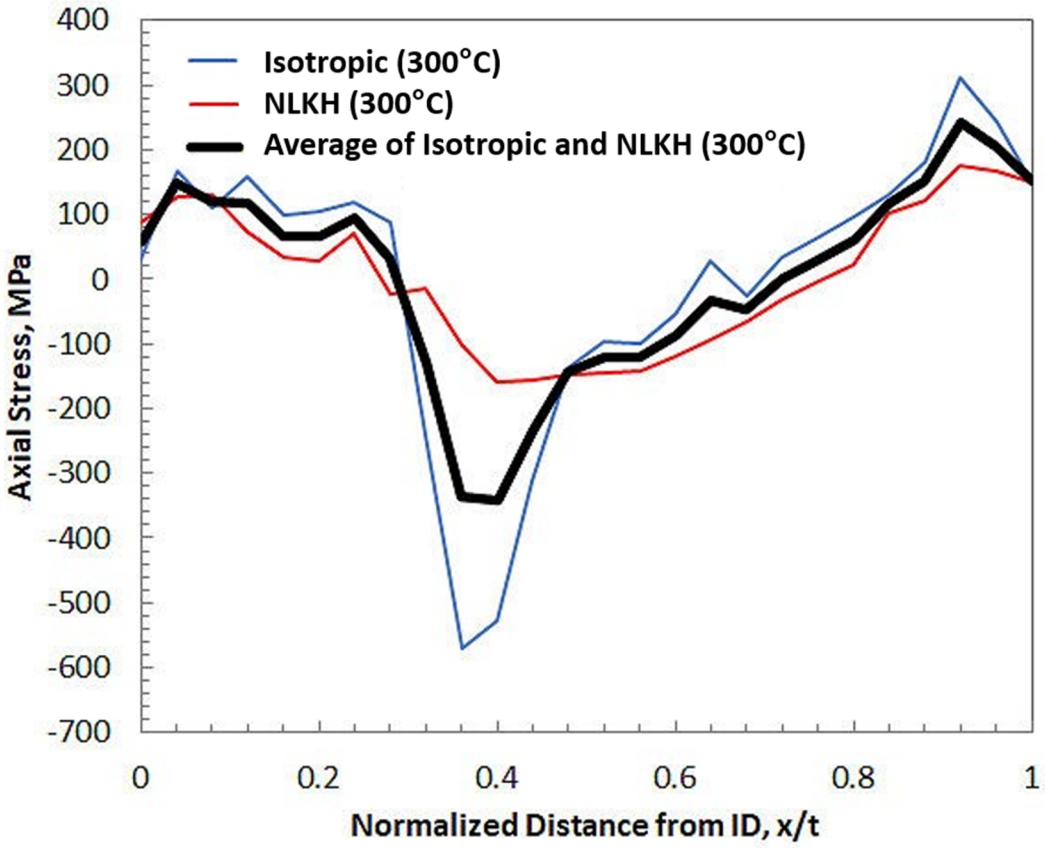

Figure C-16 Replacement steam generator nozzle axial WRS profiles

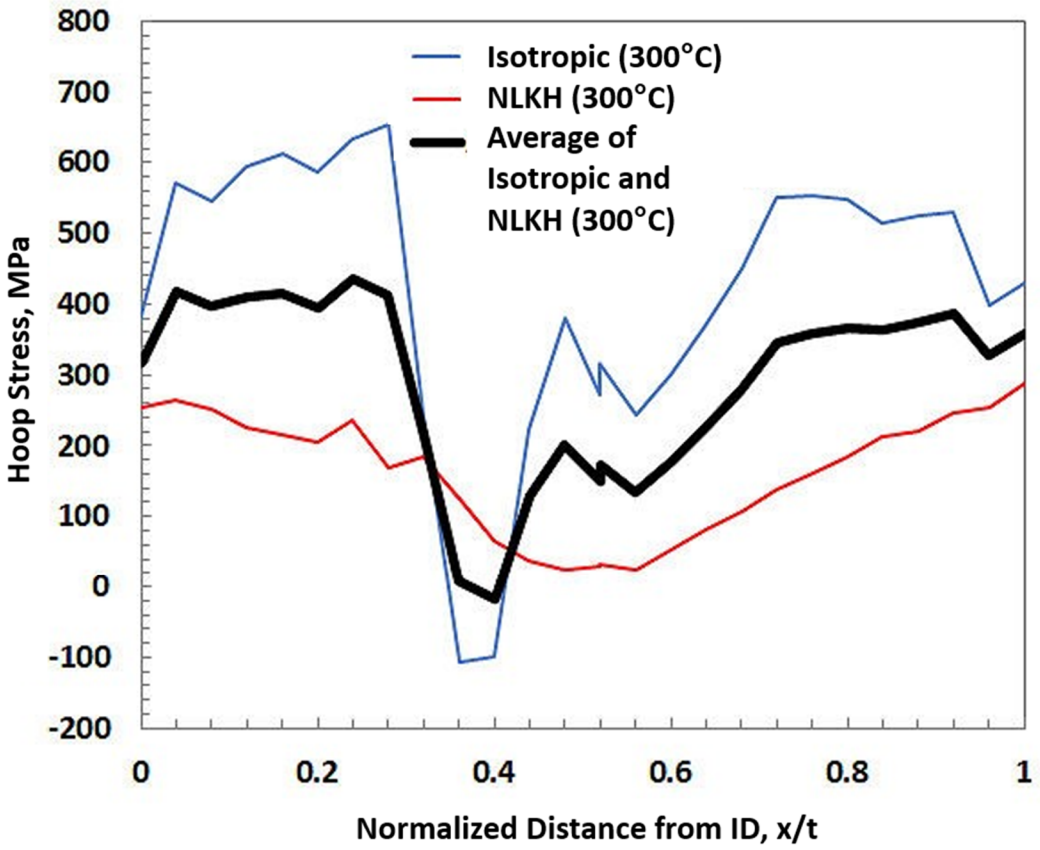

Figure C-17 Replacement steam generator nozzle hoop WRS profiles

C4.3 More Severe WRS Profile

The more severe WRS profile was determined from a location within the steam generator weld or butter where the axial stresses at the inside diameter were the highest because these conditions promote PWSCC initiation. Figure C-18 and Figure C-19 provide contour plots of the axial and hoop WRS, respectively. A path in the butter region was chosen to obtain the more severe WRS profile. Figure C-20 and Figure C-21 show the average axial and hoop WRS profiles, respectively. The weld centerline stresses are shown for comparison. Figure C-20 shows that the axial WRS profile in the butter is higher at the inside diameter as compared to the weld centerline; however, the hoop stresses are lower in the butter as shown in Figure C-21.

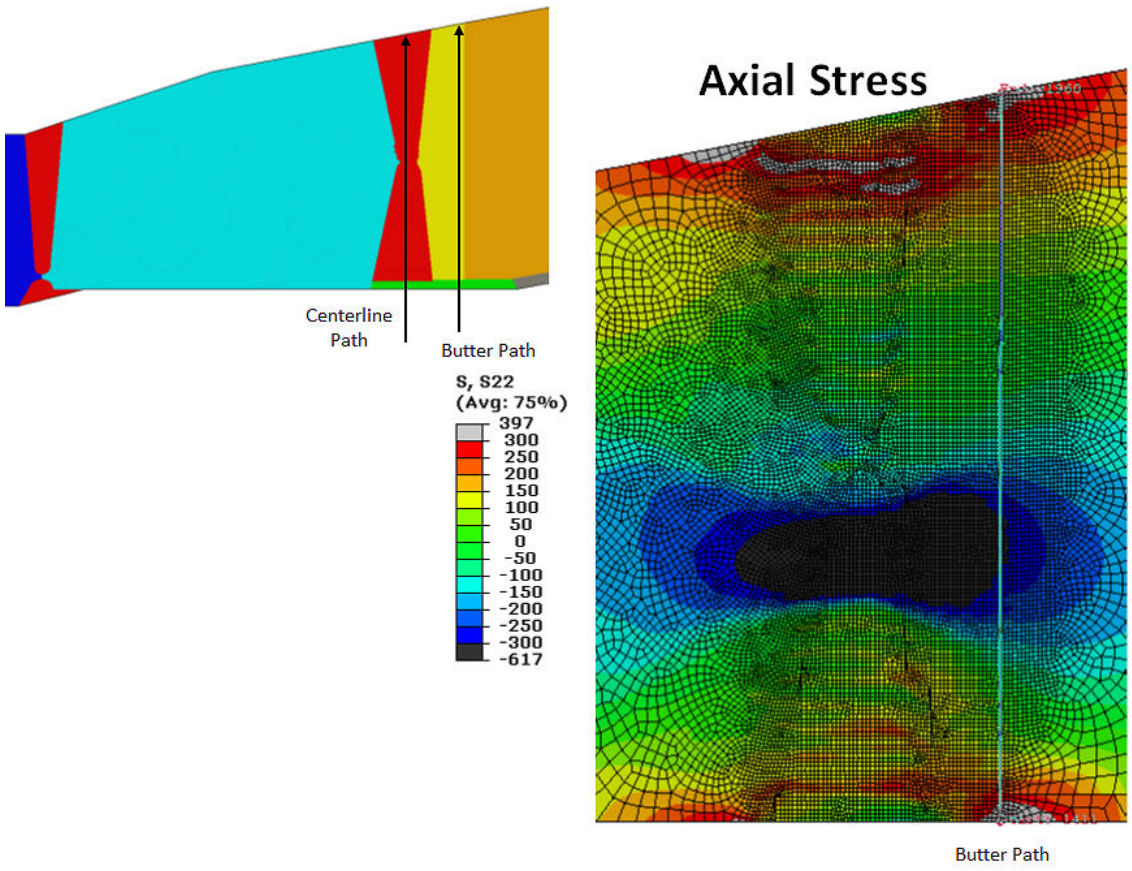

Figure C-18 Replacement steam generator nozzle baseline axial WRS contour plot generated from FEA

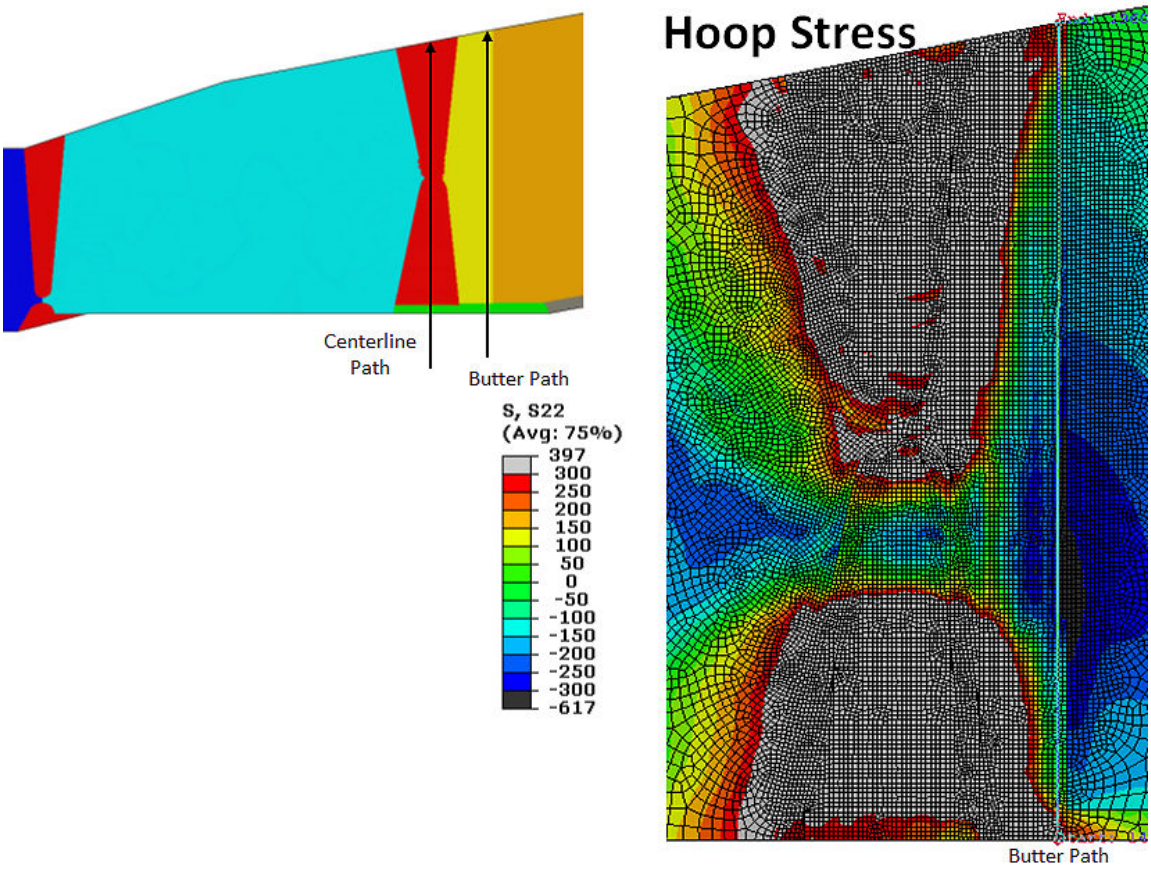

Figure C-19 Replacement steam generator nozzle hoop WRS contour plot generated from FEA

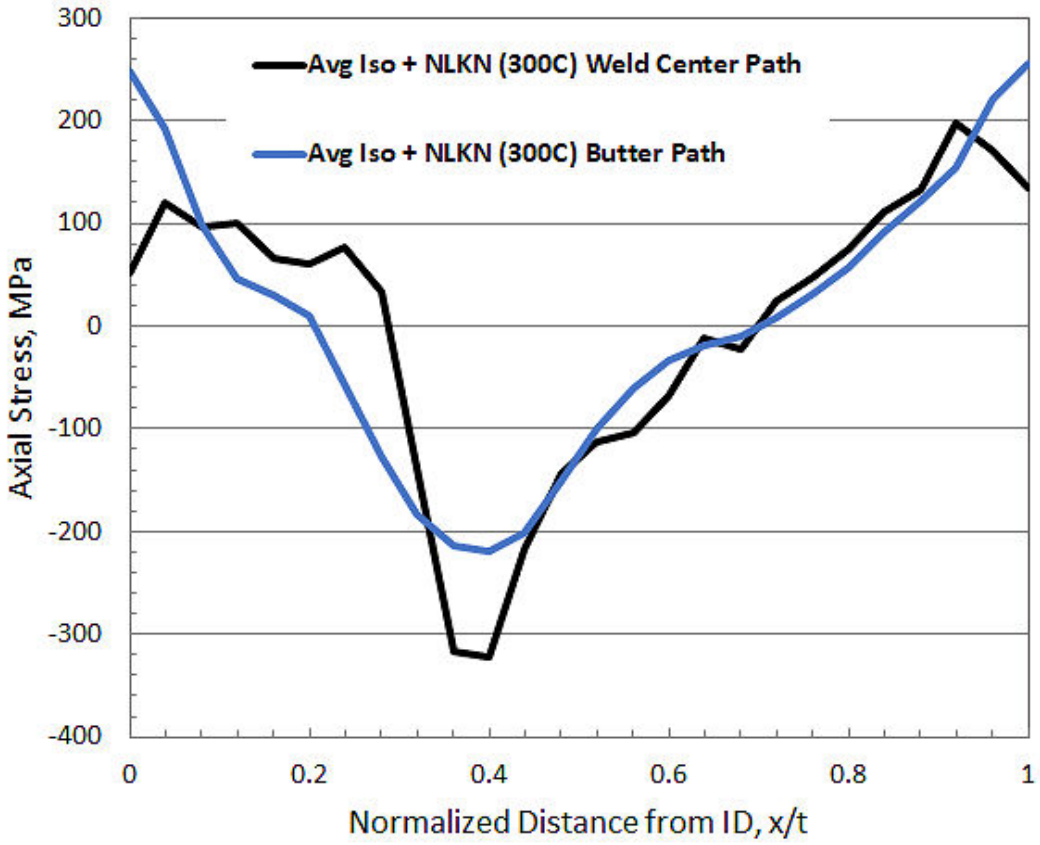

Figure C-20 Comparison of replacement steam generator nozzle baseline and more severe axial WRS profiles

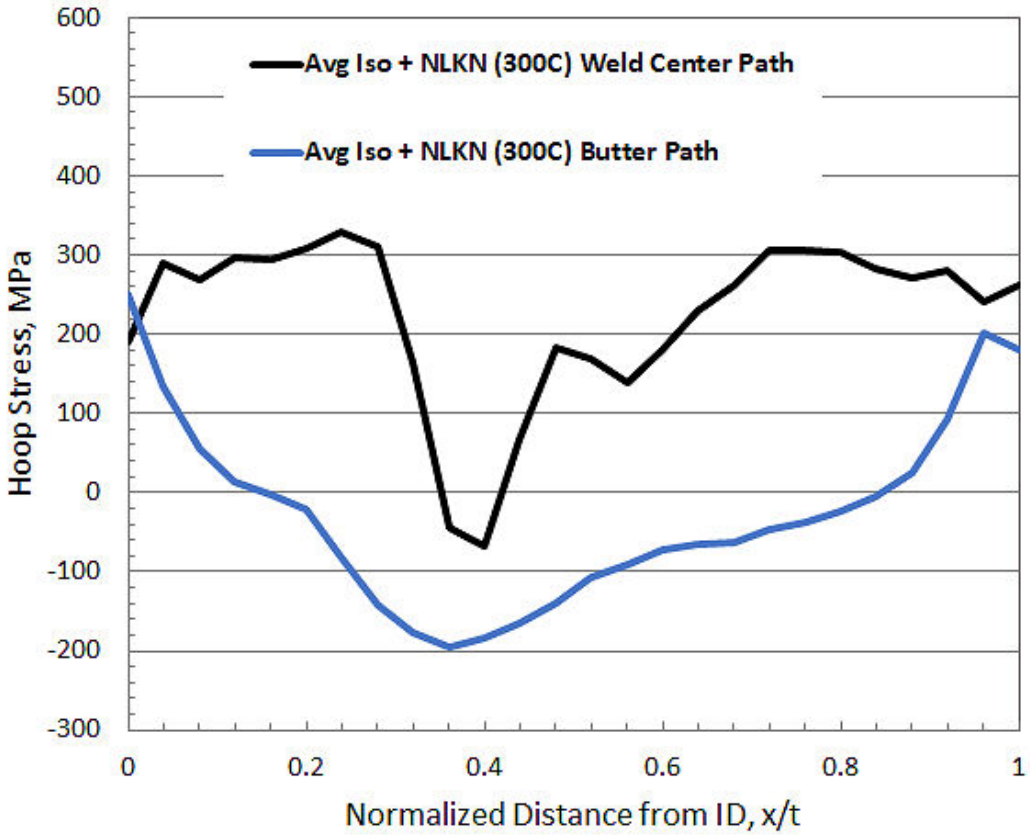

Figure C-21 Comparison of replacement steam generator nozzle and more severe hoop WRS profiles

C5 CE Hot and Cold Leg Branch Line Nozzle DMWs

The CE plants have DMWs for some of the hot leg and cold leg branch line connections. This includes a DMW from the surge line to the hot leg and to the pressurizer, which is different from Westinghouse plants where the DMW is only to the pressurizer. The geometry and welding process for these lines are proprietary, so they were estimated for this study based on field measurements and other documents provided by EPRI. The generic geometry is applicable for the hot leg to surge weld and other lines, including shutdown cooling and high-pressure injection. It is noted that this geometry does not fall within the guidelines of the xLPR WRS Subgroup report [47] or the WRS essential parameters and profile selection document [85], so a new WRS profile was developed for this study.

C5.1 Geometry and Welding Sequence

A representative geometry for the CE branch lines is shown in Figure C-22. The distance between the DMW and SS weld is 95.25 mm (3.75 inches), which is the average distance for all the nozzles. The maximum distance was 107.95 mm (4.25 inches), and this distance was used to obtain the more severe WRS profile as discussed in Section C5.3.

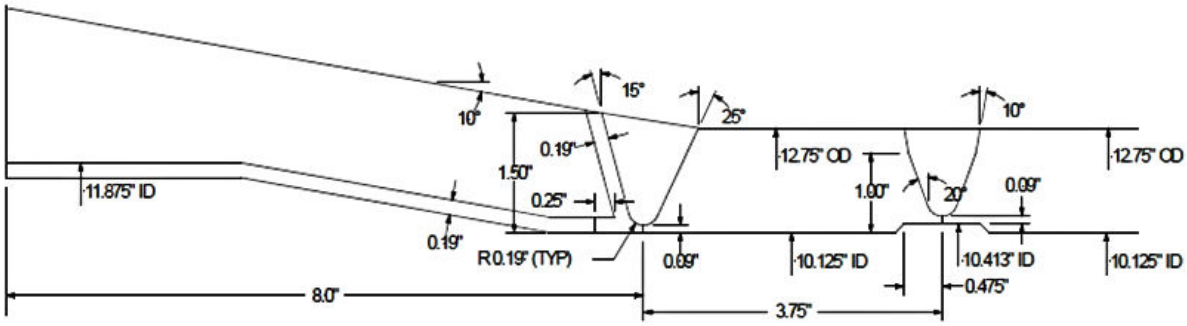

Figure C-22 Representative CE branch line nozzle geometry and dimensions

The FEA model and materials for the CE branch line are shown in Figure C-23 and Figure C-24. The weld has a single-vee groove geometry. The weld sequence is shown in Figure C-25. The DMW was modeled with 36 weld bead passes and the SS weld with 24 passes. The different colors in Figure C-23 and Figure C-25 illustrate the weld passes. As in the approach used to develop the xLPR WRS Subgroup solutions [47], a hydrostatic test was modeled, and then three cycles of service load (pressure and end cap stress only), which can help to shake down the WRS profile to some extent. Finally, all results are presented at an operating temperature of 300°C.

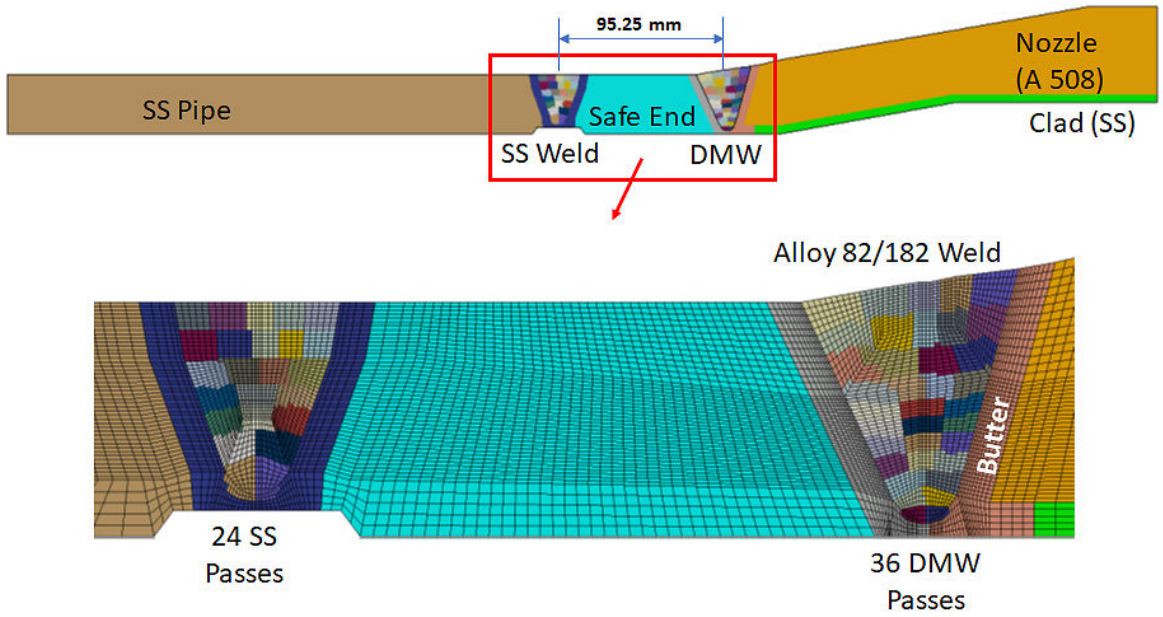

Figure C-23 FEA model used for CE branch line nozzle WRS profile development

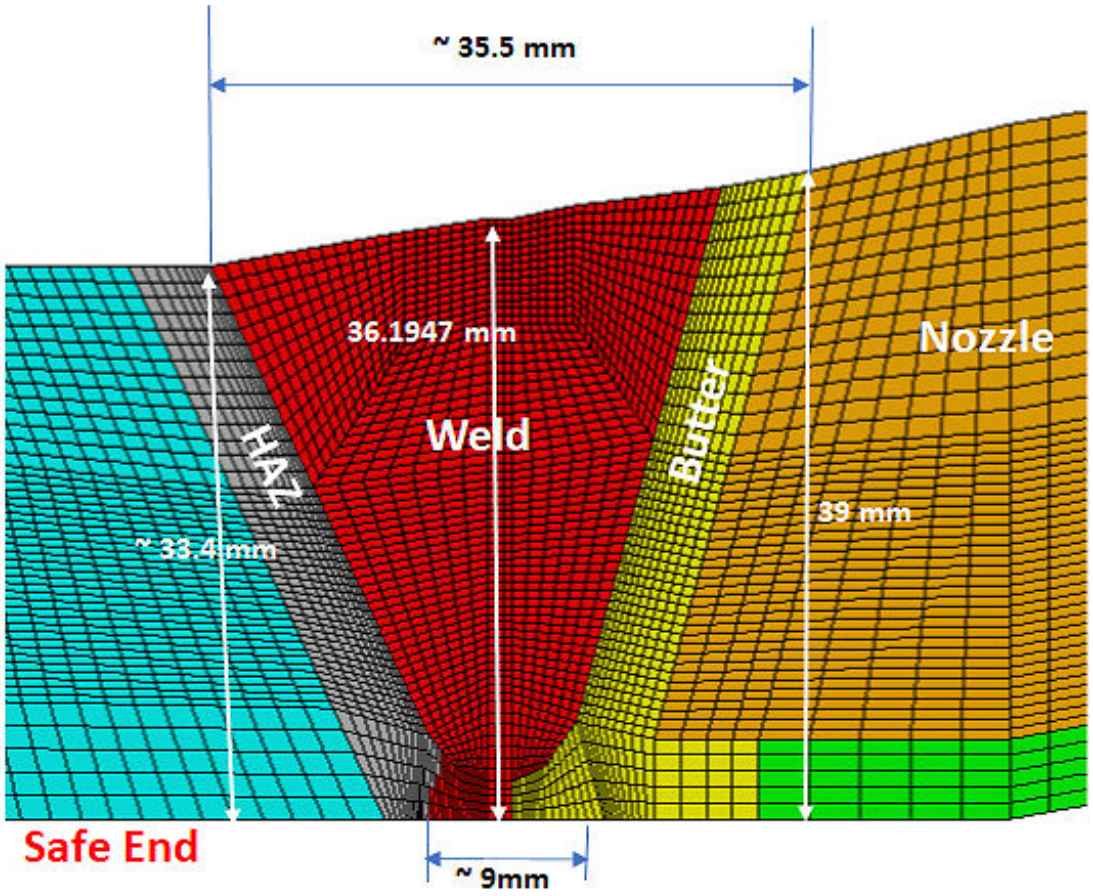

Figure C-24 Details of FEA model used for CE branch line nozzle WRS profile development

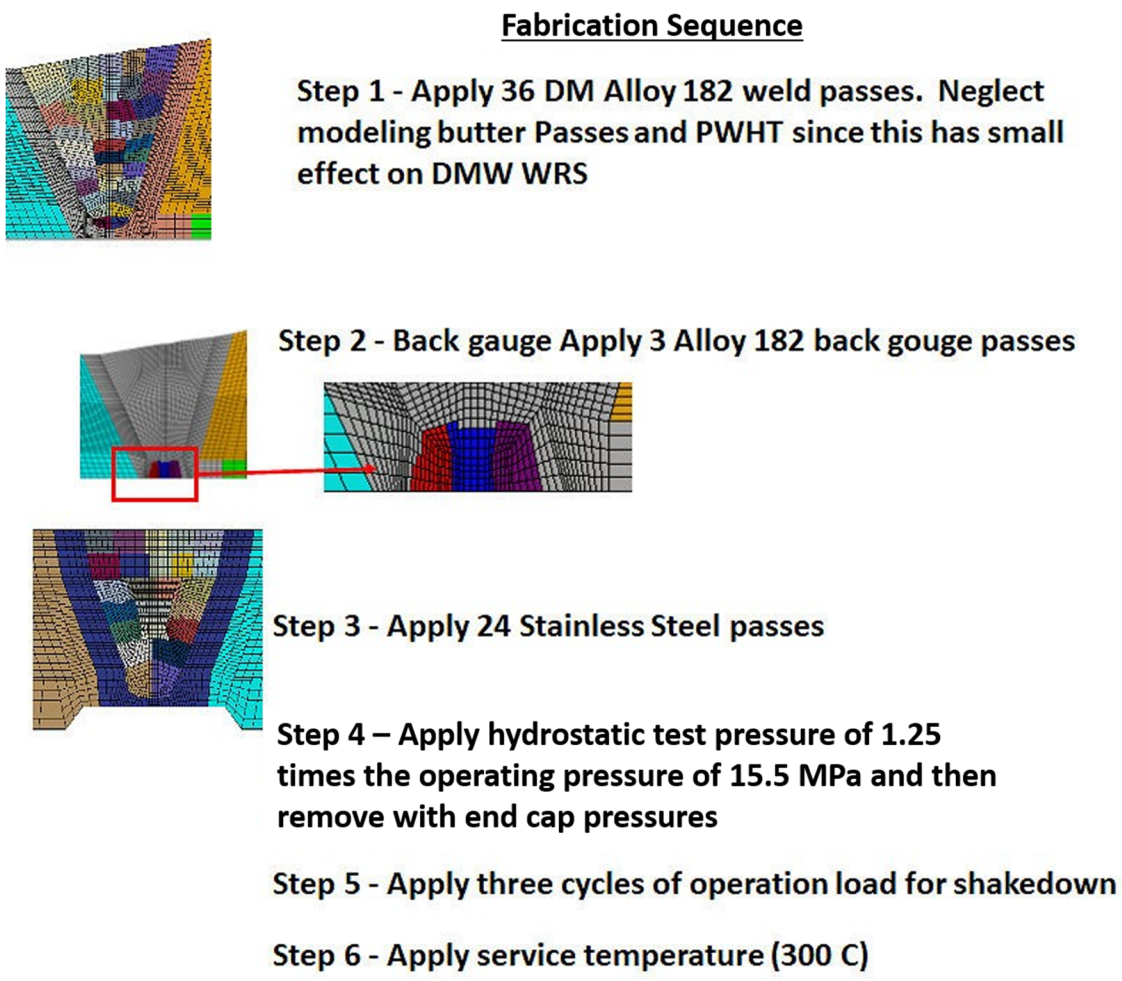

Figure C-25 Fabrication sequence used for CE branch line nozzle WRS profile development

C5.2 Baseline WRS Profiles

Contour plots of the axial and hoop WRS for the CE branch line weld are shown in Figure C-26. The corresponding axial and hoop WRS profiles are shown in Figure C-27 and Figure C-28. The average of the isotropic and NLKH law results was used. Since only one analysis was performed, the uncertainty was defined by assuming similar uncertainty to that shown in [47] for the hot leg.

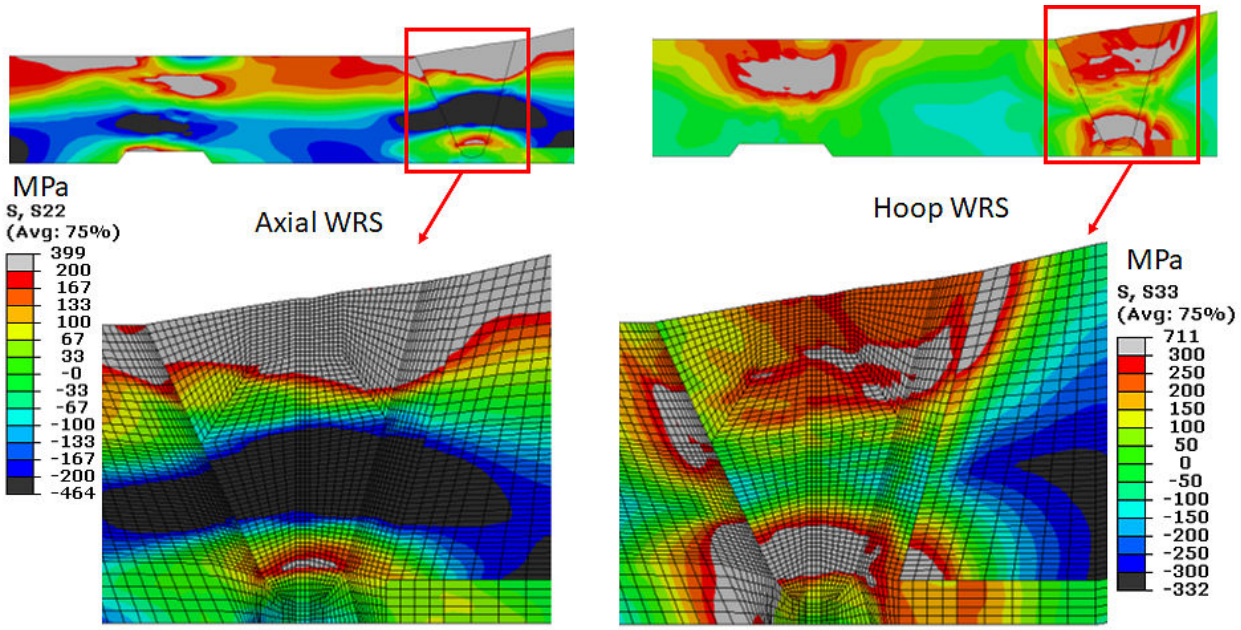

Figure C-26 CE branch line nozzle axial (left) and hoop (right) WRS contour plots generated from FEA at 300°C

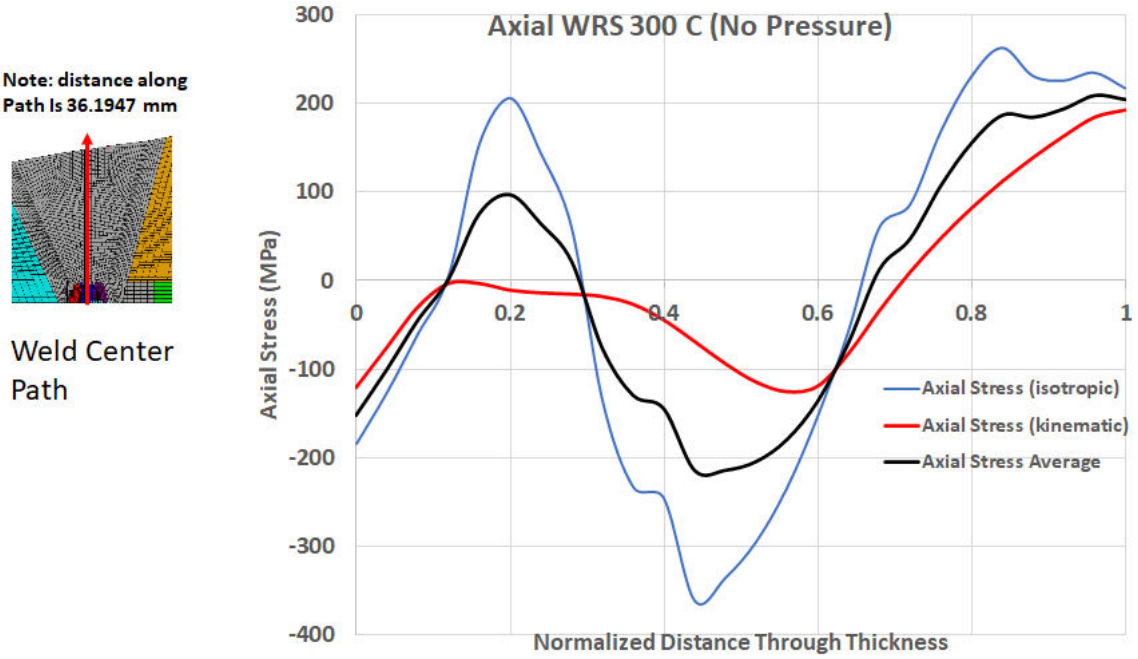

Figure C-27 CE branch line nozzle axial WRS profiles through the weld centerline

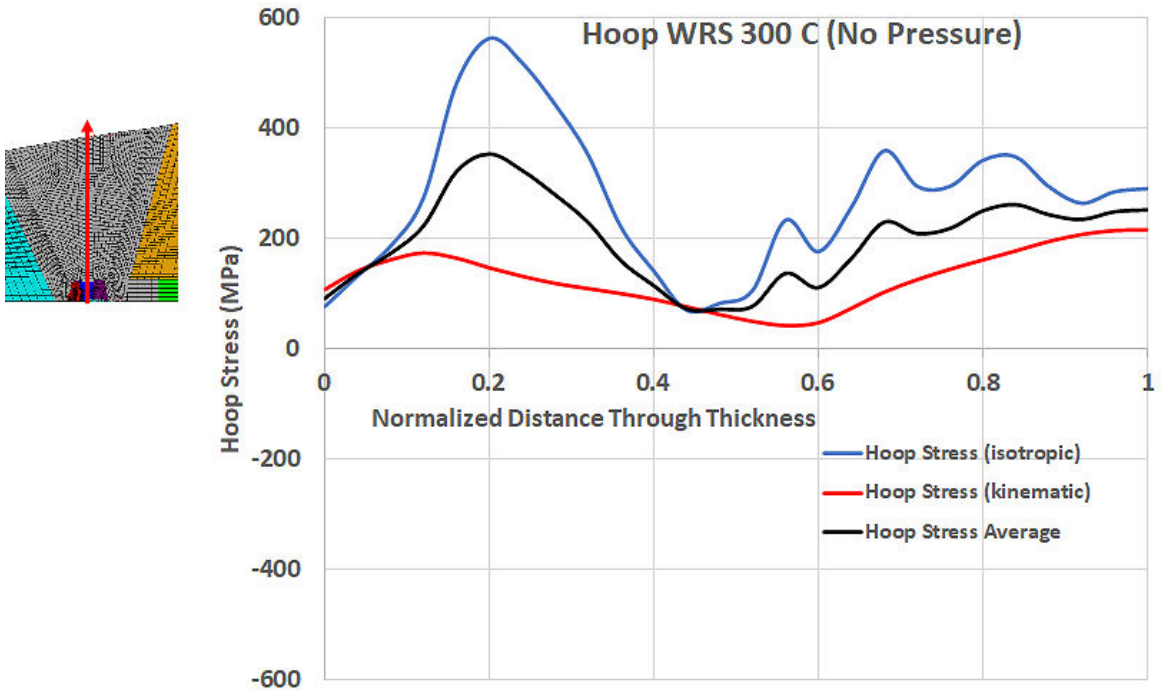

Figure C-28 CE branch line nozzle hoop WRS profiles through the weld centerline

C5.3 More Severe WRS Profile

There is 95.25 mm between the DMW and the SS weld in the typical CE branch line as shown in Figure C-29(a). This distance is the average of all the CE branch lines based on information provided by EPRI. The greatest distance was 107.95 mm as shown in Figure C-29(b). In general, if this distance is greater, the WRS profile will be more tensile at the inside diameter, because the SS closure weld applies a ring shrinkage load to the pipe. This load affects the WRS field in the DMW, and the farther this weld is from the DMW, the less the WRS field is reduced. As such, this greater distance was used to develop the more severe WRS profile.

Figure C-30 and Figure C-31 show the axial and hoop WRS profiles through the weld centerline for different DMW to SS closure weld distances. The axial WRS profile is higher by about 50 MPa at the inside diameter, and the tensile stress has a higher maximum of about 40 MPa at a depth of about 20 percent of the wall thickness. In addition, the compressive stress in the middle of the nozzle is about the same. The more severe WRS profile will thus lead to more crack initiations and a greater chance for axial crack leakage. From Figure C-31, there is also an increase in the hoop WRS profile for the greater DMW to SS closure weld distance.

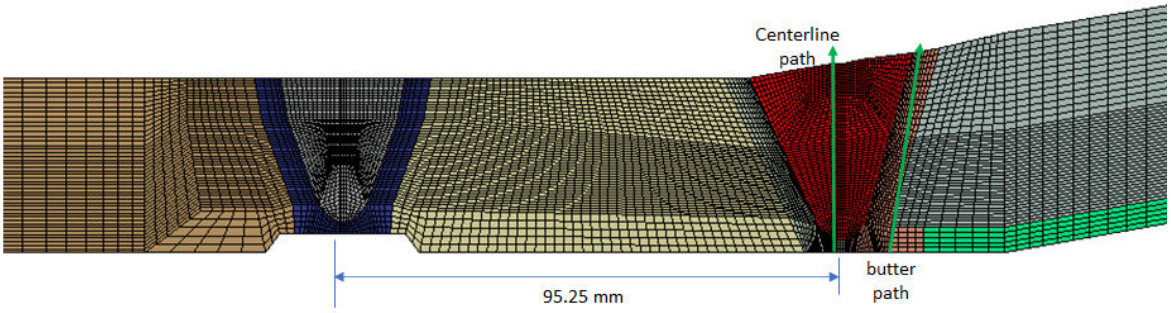

(a)

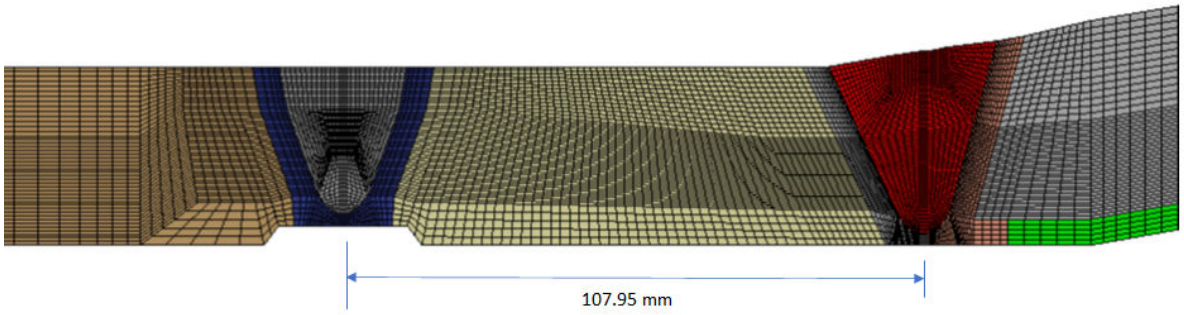

(b)

Figure C-29 CE branch line nozzle DMW to SS closure weld distances of (a) 95.25 mm and (b) 107.95 mm as shown on the FEA models

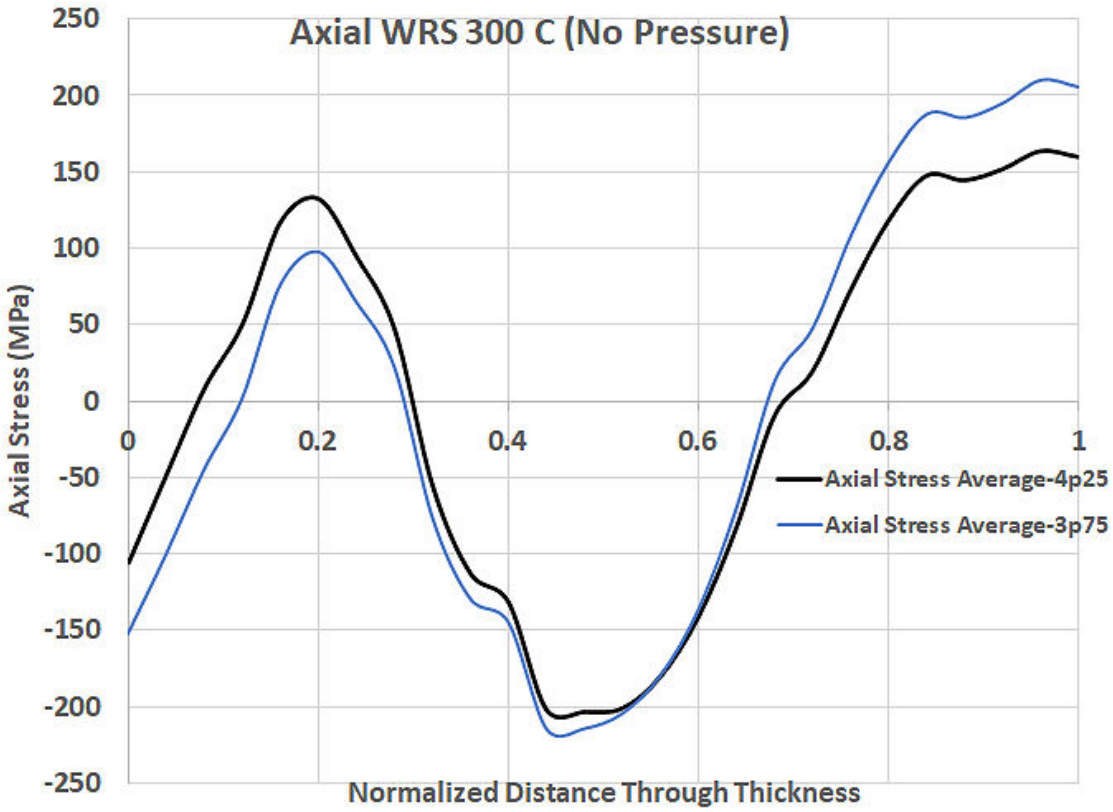

Figure C-30 CE branch line nozzle axial WRS profiles for different DMW to SS closure weld distances

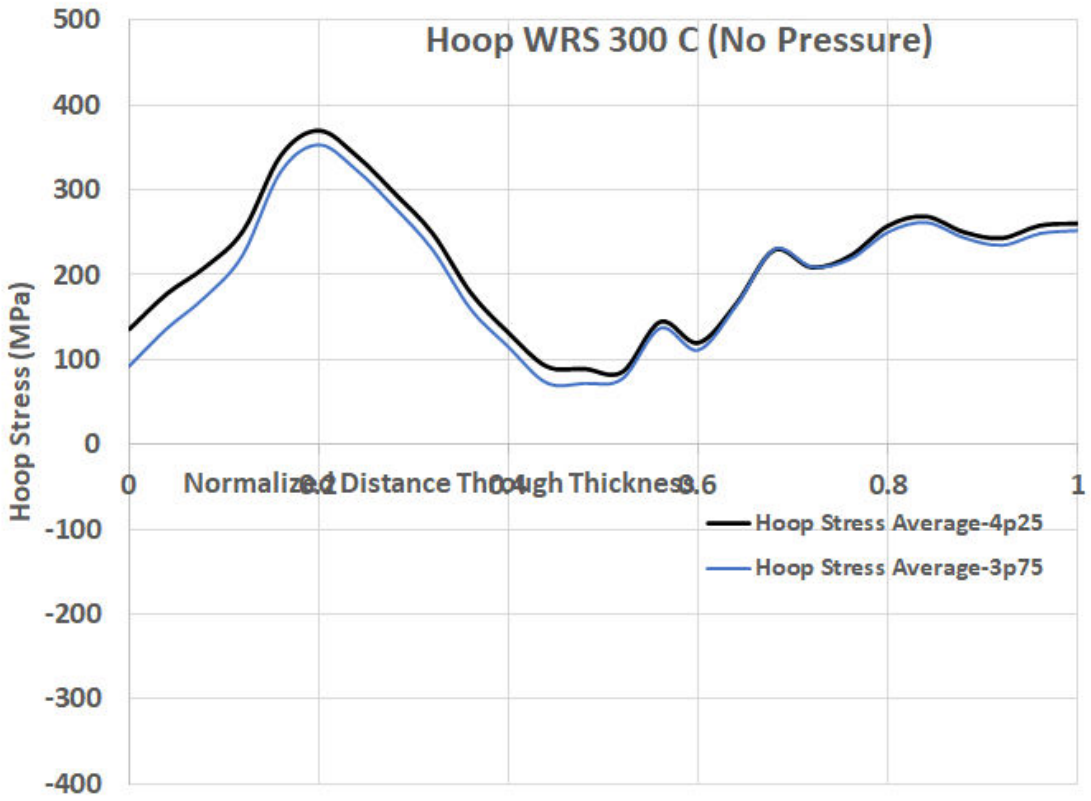

Figure C-31 CE branch line nozzle hoop WRS profiles for different DMW to SS closure weld distances

Finally, the butter location provides the higher axial WRS profile as compared to the weld centerline location for the larger DMW to SS closure weld distance. This location was thus chosen to extract the more severe WRS profile for the CE branch line weld. Comparisons of the weld centerline and butter WRS profiles are shown in Figure C-32 and Figure C-33 for axial and hoop stresses, respectively. As shown in these figures, the butter region for the DMW to SS closure weld distance of 107.95 mm represents the more severe WRS profile for the CE branch line nozzles.

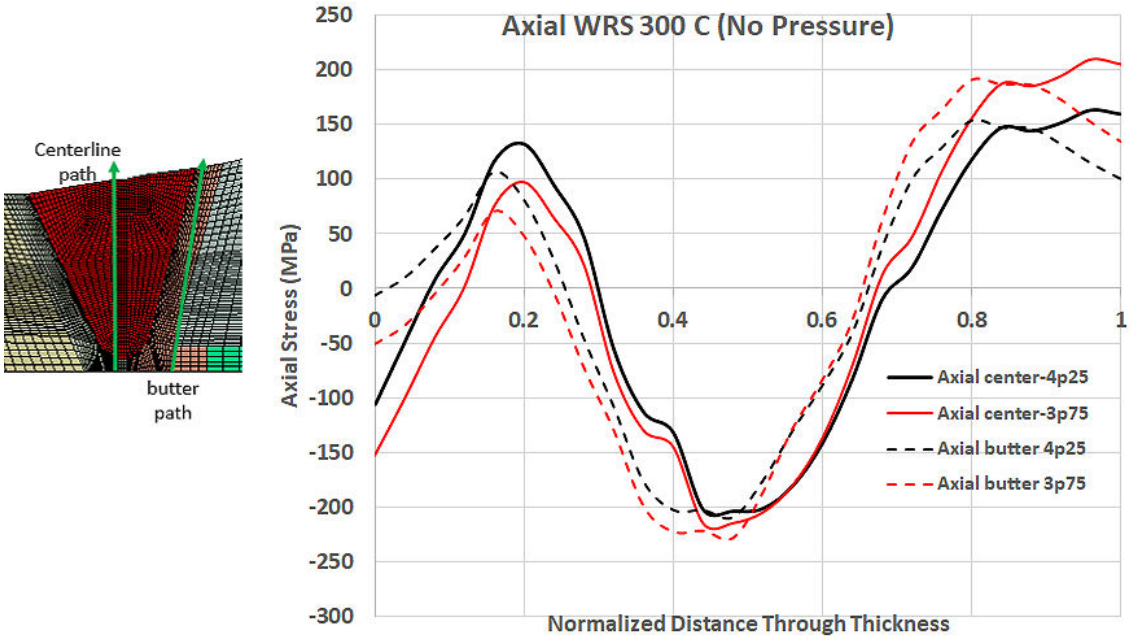

Figure C-32 Comparison of CE branch line nozzle axial WRS profiles through weld centerline and butter

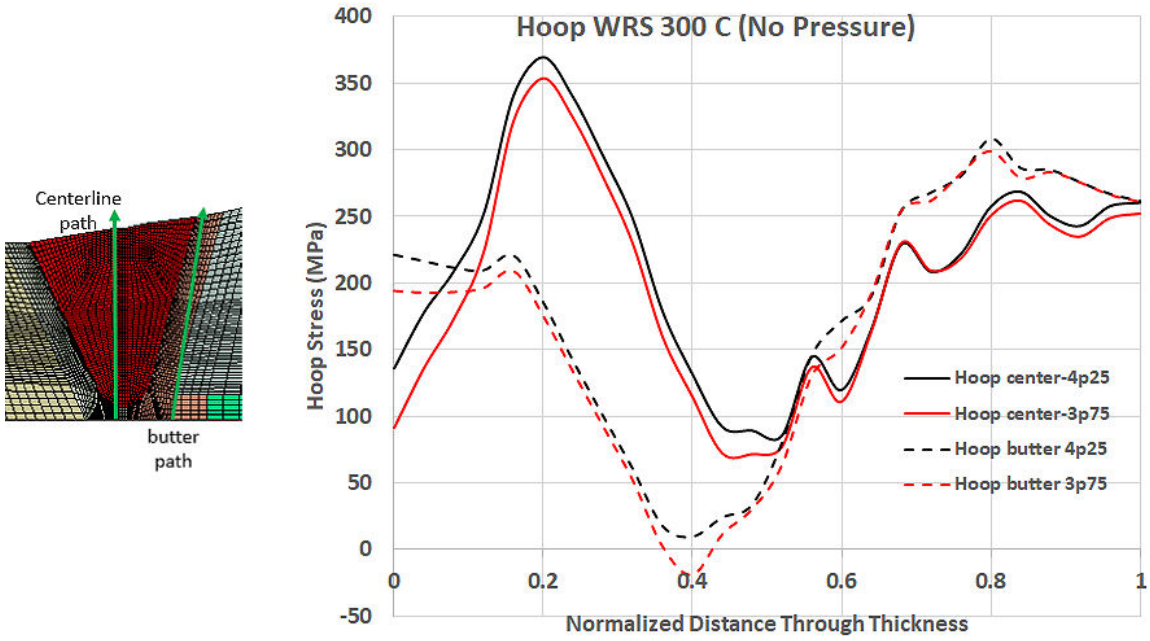

Figure C-33 Comparison of CE branch line nozzle hoop WRS profiles through the weld centerline and butter

C5.4 DMW to SS Weld Distance Study

One of the main drivers of the WRS in DMWs is the distance between the DMW and the SS closure weld. If the closure weld is within about 100 mm from the DMW, the shrinkage of the

SS weld acts like a shrink fit clamp ring that modifies the WRS profile in both the DMW and the SS weld. There are several factors that make the DMW WRS profile more compressive. These factors include the distance between the two welds, the thickness of both the DMW and the SS safe end, and the SS weld groove size, which control the amount of weld shrinkage and hence the clamping force caused by the SS weld.

One of the challenges in developing WRS profiles for use in xLPR code simulations is that there are several variables that affect the final DMW WRS profile, especially the distance between the DMW and SS closure weld. There has been no systematic study of this effect to develop rules for modifying the existing library of WRS profiles. The effect of mechanical mitigation had been implemented in [47] through rules that can be applied to modify the WRS profile for mechanical mitigation (i.e., overlay, MSIP®, and inlay). A companion study was thus undertaken to examine the effect of the distance between the DMW and SS closure weld to develop rules to extend the existing library of WRS profiles. This study only considered the geometry of the CE surge line nozzle; however, similar studies of other, thicker nozzle geometries could be similarly performed.

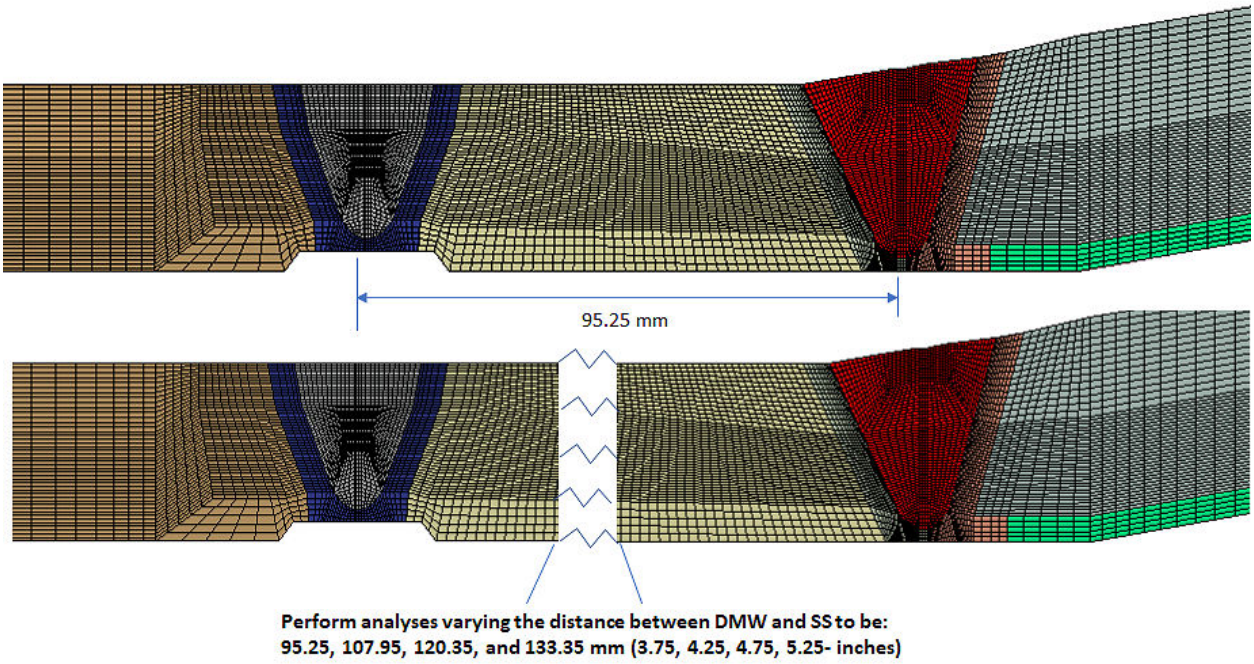

Figure C-34 FEA mesh for DMW to SS closure weld distance

Figure C-34 illustrates the concept. The top mesh was used to develop the CE branch line WRS profiles. The distance between the DMW and the SS closure weld is 95.25 mm, which represents the average of all the different CE branch lines. To obtain the more severe WRS profile, a second analysis was performed by setting this distance to 107.95 mm, which was the largest distance among all the CE branch line welds. As seen in the bottom illustration of Figure C-34, this latter case can be modeled by simply adding 12.7 mm (0.5 inches) to the mesh length. Meshes with distances of 120.35 and 133.35 mm were generated along with a case where there was no SS closure weld, which represented an infinite distance. By adding the

additional elements in the region between the DMW and SS closure weld and beginning with node and element numbering range larger than the original mesh (95.25 mm distance), there was no need to modify the weld pass numbering or any other mesh parameters necessary to perform the analysis. This made rerunning of the analyses quick and straightforward. The case with no SS closure weld represents the limit of the solution.

Figure C-35 shows the effect of the DMW to SS closure weld distance on the axial WRS profile. The stresses increase at the inside diameter as the distances between the DMW and SS closure weld increase until there is no closure weld. The inside diameter stresses increase as the outside diameter stresses decrease because of the axisymmetric nature of the solution. Figure C-36 shows a similar trend for the hoop stresses. These results could be used to develop rules to account for this important variable for use in xLPR code simulations. These results are for a thinner nozzle geometry, but by generating results for a few thicker nozzle geometries (e.g., RVON and steam generator), the effect of this parameter could be quantified to expand the existing set of WRS solutions. The rules would be developed as a function of a normalized distance through the weld thickness.

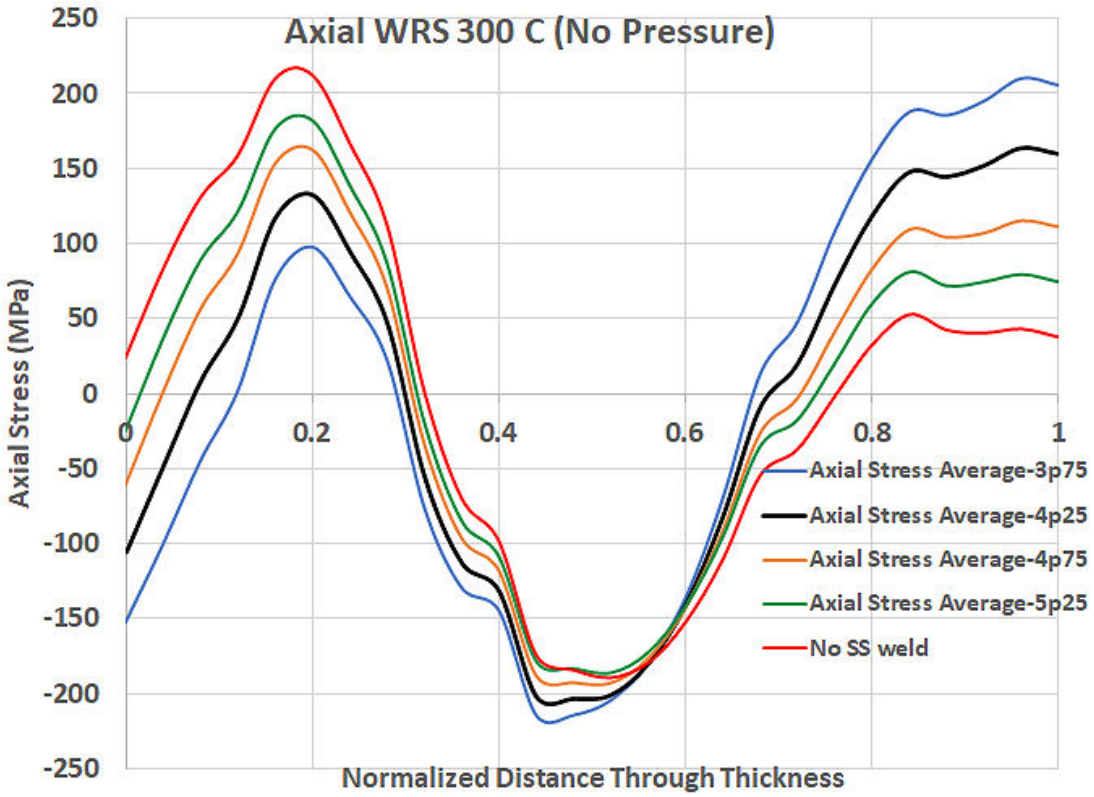

Figure C-35 Axial WRS profiles for CE branch line considering different DMW to SS closure weld distances

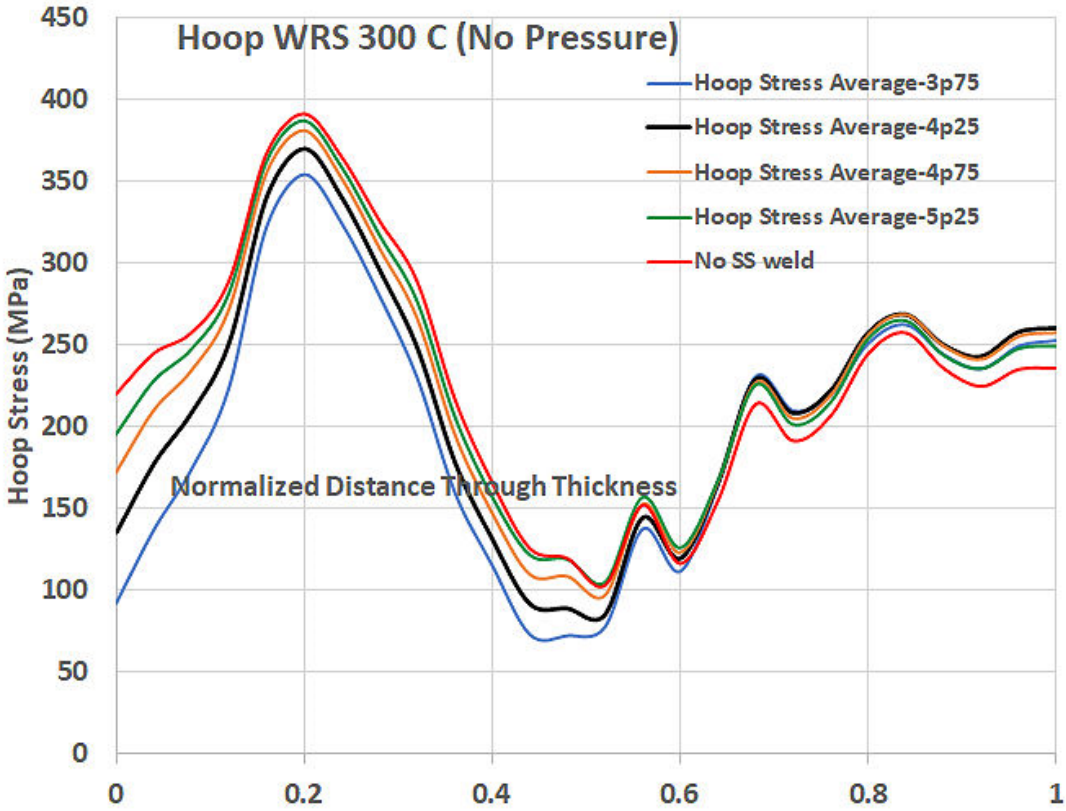

Figure C-36 **Hoop WRS profiles for CE branch line considering different DMW to SS closure weld distances**

C6 Westinghouse Two- and Three-Loop RVON and RVIN DMWs

The RVON and RVIN DMWs for Westinghouse four-loop plants were analyzed in the prior study. The Westinghouse two- and three-loop DMWs are examined here. The nozzle geometries, materials, and welding sequences are similar among the two-, three- and four-loop designs. Therefore, the WRS profile used for the four-loop designs was also used for the two- and three-loop analyses.

C6.1 Baseline WRS Profiles

The no-repair WRS profile was used because the inside diameter stresses are higher as compared to the 15 and 50 percent repair cases. The closure weld is close to the DMW, so the WRS profile is compressive. A more complete description of the RVON geometry, fabrication process, and WRS results is available in [47]. For completeness, the axial and hoop WRS profiles are shown in Figure C-37.

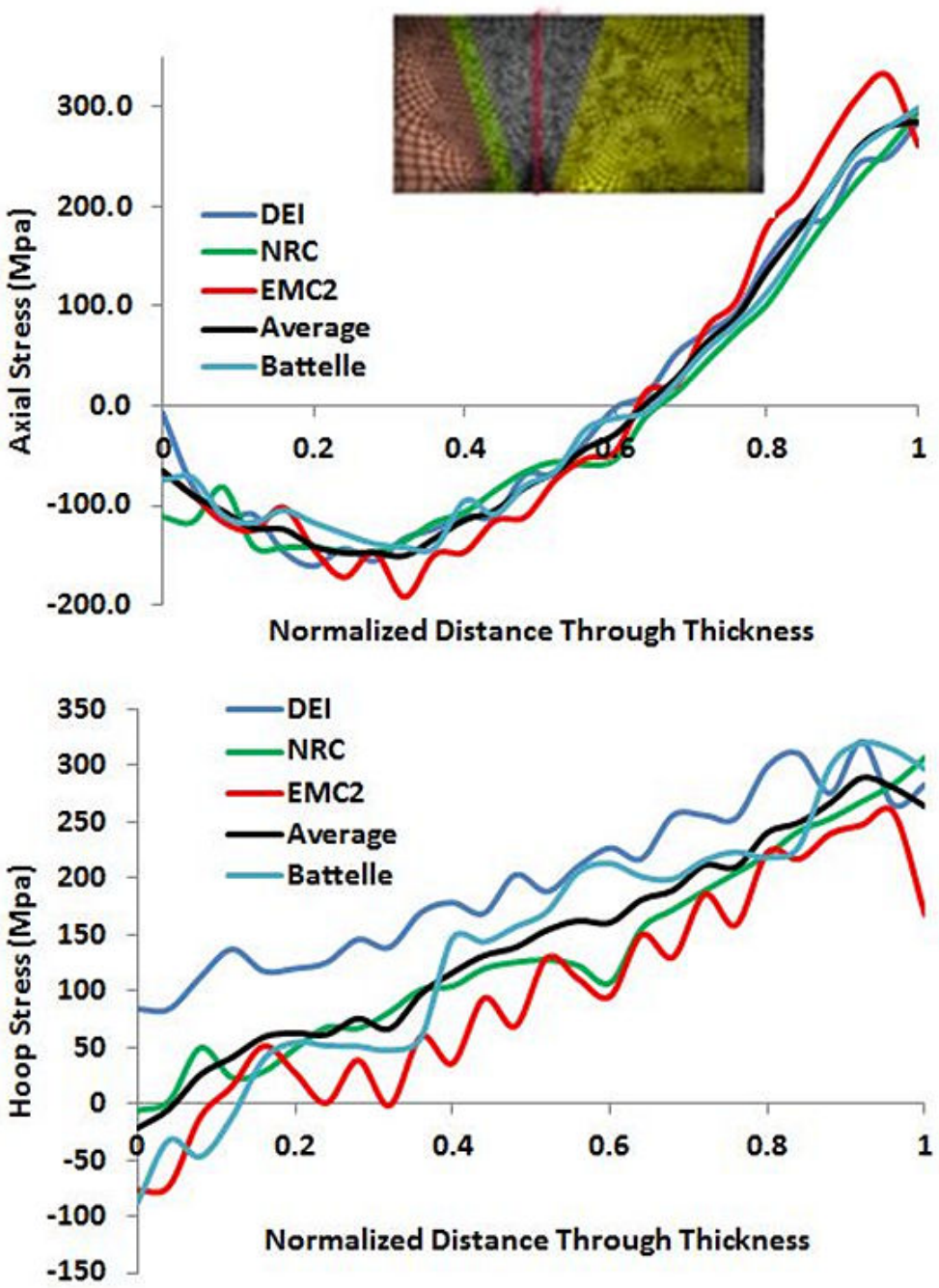

Figure C-37 Axial and hoop WRS profiles for Westinghouse three- and four-loop RVONs

C6.2 More Severe WRS Profile

The more severe WRS profiles for the Westinghouse RVON cases were developed from a nozzle with a different geometry [47]. The geometries considered for this case are described in the evaluation of the inlay process as a mitigation strategy for PWSCC [57] along with the

welding processes and fabrication sequence. Since that evaluation was performed in 2010, the model was used to redevelop the WRS profiles using the xLPR WRS Subgroup approach [47]. The WRS profiles were generated from an average of the isotropic and NLKH law results. The model is shown in Figure C-38. The geometry is different from that used in [47] with the distance from the DMW to SS closure weld set to 93.1 mm. The mesh near the inside diameter is quite fine, because this region is where the small temper bead inlay passes were deposited for the evaluation in [57]. However, for the present analysis no inlay was modeled and only deposition of the Alloy 82/182 weld material was included. The fabrication modeling process consisted of the following steps:

1. add butter passes and corresponding PWHT
2. deposit the DMW passes
3. add the SS closure weld
4. hydrotest modeling
5. apply three loading cycles including temperature application, pressure, and removal
6. heat to operating temperature of 300°C

It is noted that further details of the WRS profile calculations and PWSCC growth predictions in the inlay can be found in [57] and the publications by Brust and others [90] and Rudland and others [58]. The natural PWSCC growth predictions lead to a bubble-shape after the crack grows through the Alloy 52 material and enters the Alloy 182 material. Such a shape causes the leak rate to be constrained by the small crack size in the inlay, and thus the crack may not be easily detected in the simulation, even if a large crack exists outside the inlay.

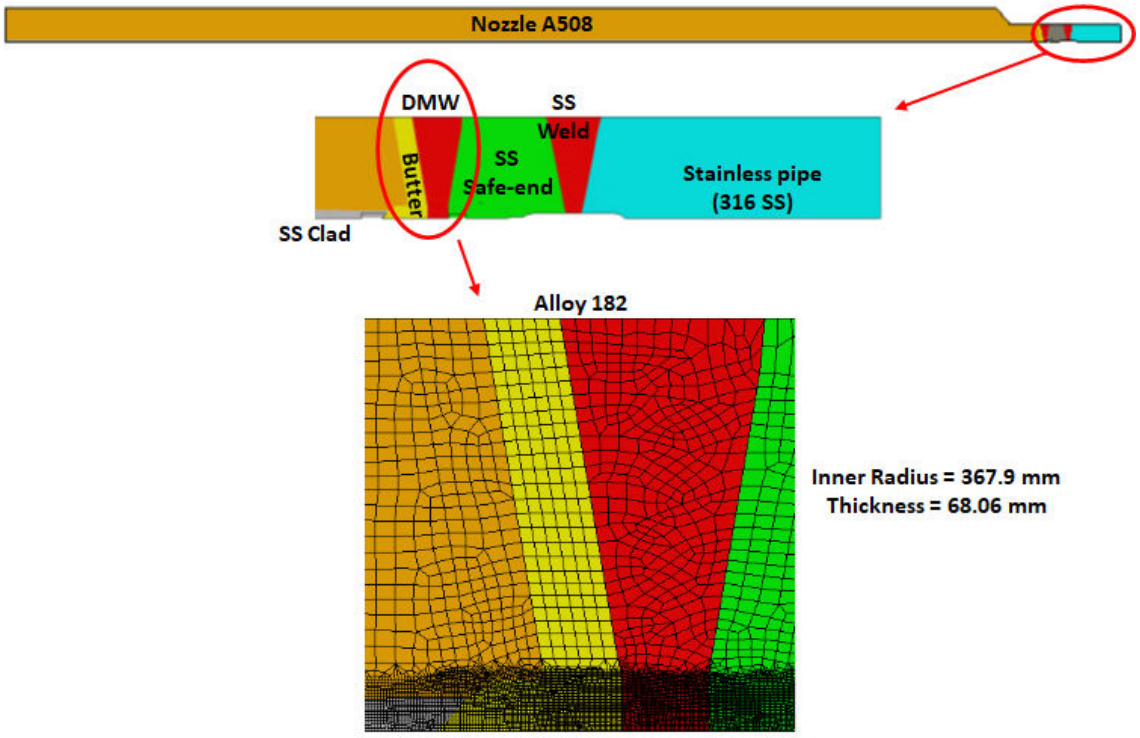

Figure C-38 RVON nozzle model for more severe WRS profile

A contour plot of the axial WRS profiles, showing the butter and weld outlines, is shown in Figure C-39 for the isotropic hardening law case. The axial and hoop WRS profiles at the weld centerline are shown in Figure C-40. The average WRS profiles were used for the RVON analyses. Finally, the axial WRS profile and more severe WRS profile are shown in Figure C-41. These profiles were used for the Case 1.3.0 and 1.3.1 analyses.

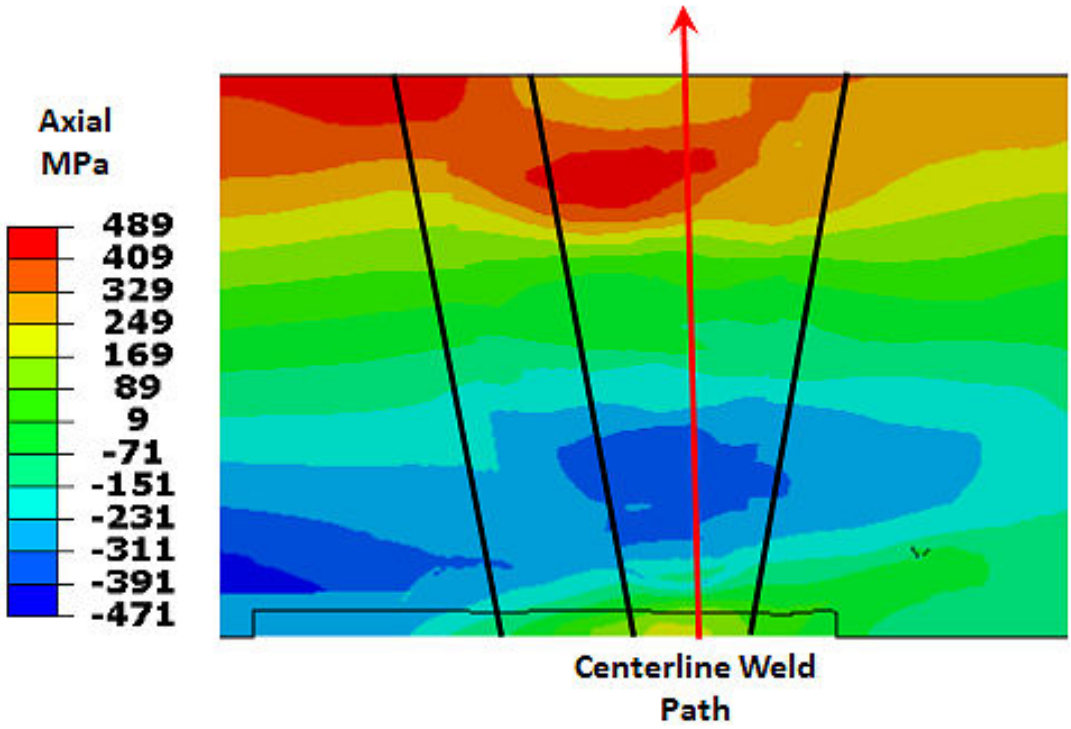

Figure C-39 More severe axial WRS contour plot for the RVON weld

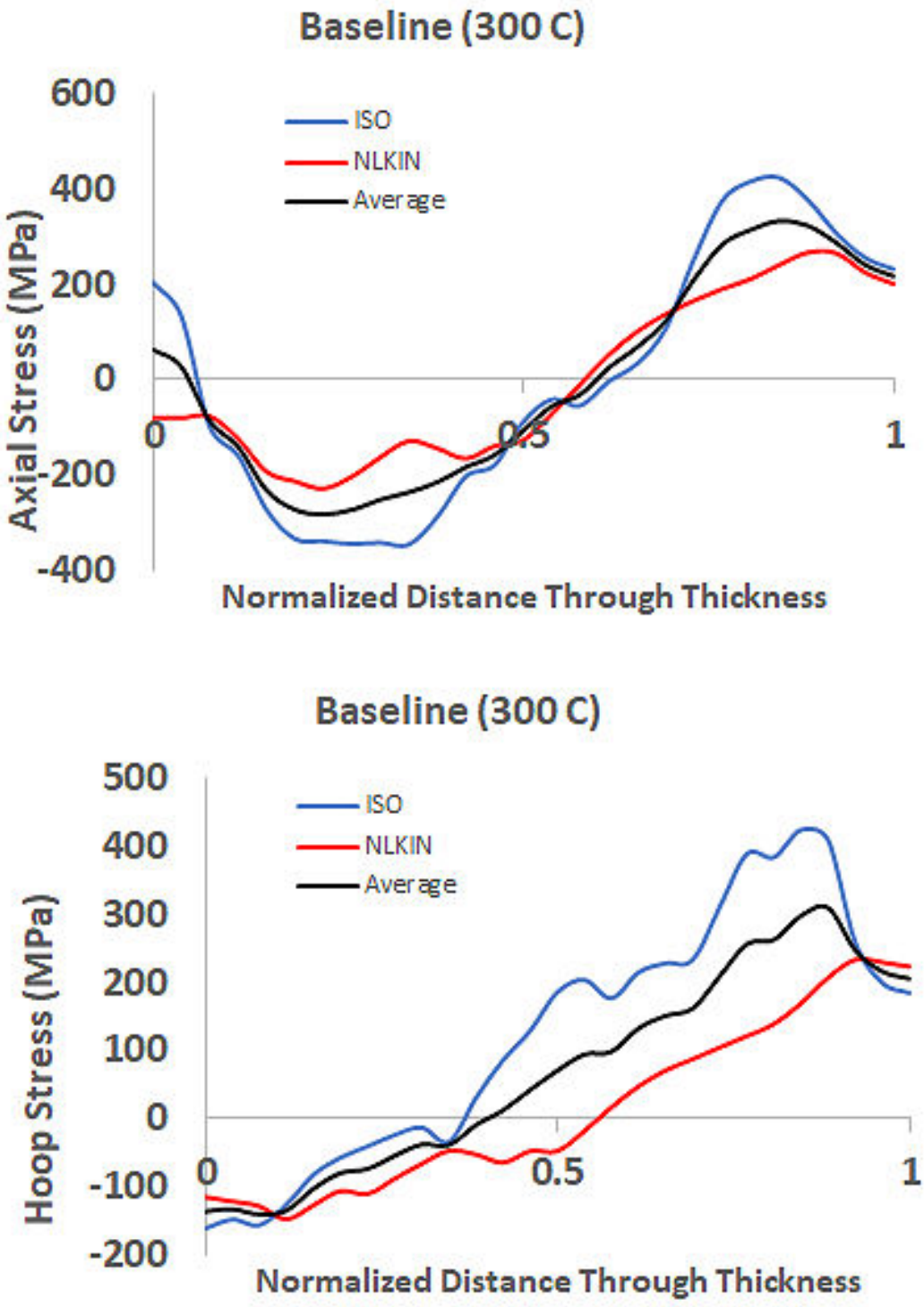

Figure C-40 More severe axial and hoop WRS profiles for the RVON weld

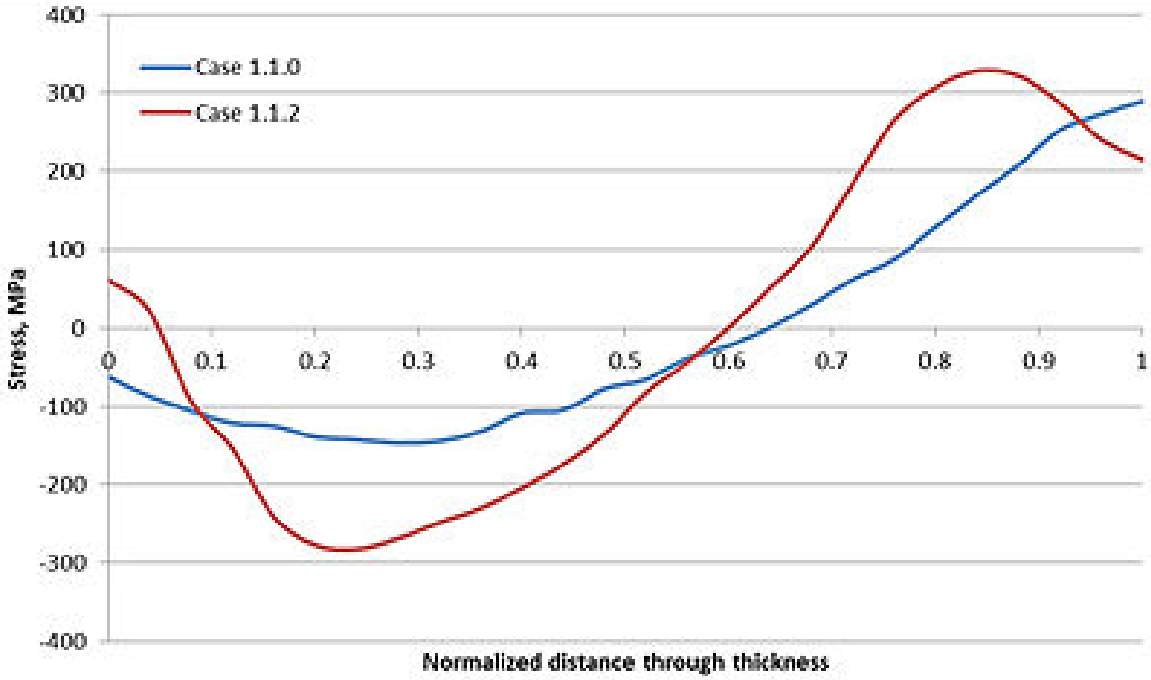

Figure C-41 Comparison of more severe and axial WRS profiles for the RVON weld